Identification of early molecular changes associated with Fumonisin B_1-induced carcinogenesis *in vivo* and *in vitro*

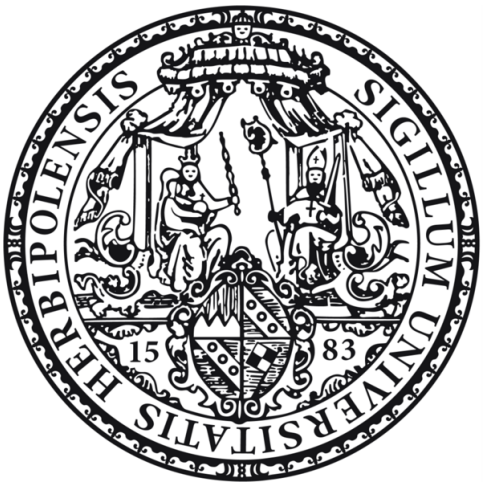

Dissertation

zur Erlangung
des naturwissenschaftlichen Doktorgrades
der Julius-Maximilians-Universität Würzburg

vorgelegt von
Stephanie Müller
aus Themar

Würzburg 2012

Eingereicht am:
bei der Fakultät für Chemie und Pharmazie

1. Gutachter: ……..

2. Gutachter: ……..

der Dissertation

1. Prüfer: ……

2. Prüfer: ……

3. Prüfer: ……

des Öffentlichen Promotionskolloquiums

Tag des Öffentlichen Promotionskolloquiums: …….

Doktorurkunde ausgehändigt am: ……..

Meiner Familie & Bastian

Danksagung

An erster Stelle möchte ich Frau PD Dr. Angela Mally und Herrn Prof. Dr. Wolfgang Dekant für die Überlassung des interessanten Themas und die Möglichkeit, in Ihrer Arbeitsgruppe zu promovieren, danken. Ein besonderer Dank gilt dabei PD Dr. Angela Mally für die engagierte Betreuung und das Vertrauen, das sie mir während der Erstellung dieser Arbeit entgegengebracht hat.

Frau Prof. Dr. Leane Lehmann vom Institut für Lebensmittelchemie der Universität Würzburg möchte recht herzlich für die Übernahme der externen Betreuung meiner Doktorarbeit danken.

Ein herzlicher Dank gilt meinen lieben Arbeitskreiskolleginnen Dana, Susi, Melli und Sabrina, mit denen ich während meiner Promotion in Würzburg eine sehr schöne Zeit verbracht habe und die stets ein offenes Ohr für sämtliche Belange des beruflichen wie auch privaten Alltags hatten.

Allen weiteren Kollegen und Doktoranden des Instituts für Toxikologie möchte ich für die stets gute Zusammenarbeit und angenehme Arbeitsatmosphäre danken. Ein besonderes Dankeschön geht dabei an Micha, Ursula, Marion, Elisabeth, Miriam und Nataly, die mit ihrer tatkräftigen Unterstützung im Labor wesentlich zum Gelingen dieser Arbeit beigetragen haben. Für ihre Mitarbeit im Rahmen ihrer Master– bzw. Bachelorarbeit möchte ich mich ganz herzlich bei Fausto und Florian bedanken.

Nicht zuletzt gilt ein großes Dankeschön meiner Familie, meinen Freunden und Bastian, die mich mit ihrer liebevollen Art stets unterstützt, gefördert, und immer an mich geglaubt haben.

Table of contents

Abbreviations

ABC	ATP-binding cassette
AC	adenylate cyclase
ACTB	beta-Actin
AKT (AKT1)	v-akt thymoma viral proto-oncogene 1, protein kinase B
ALP	alkaline phosphatase
ALAT	alanine aminotransferase
ANOVA	analysis of variance
AP	aminopentol
AP-1	activator protein 1
ARF	alternate open frame
ASAT	aspartate aminotransferase
aSMase	acid spingomyelinase
BAD	Bcl2-associated death promoter
BAX	Bcl2-associated X protein
BCL2	B-cell leukemia/lymphoma 2
BrdU	5-bromo-2-deoxyuridine
BSA	bovine serum albumin
bw	body weight
CalS	calibration standard
CAPP	ceramide-activated protein phosphatase
caspase	cysteine-aspartic protease
CDK	cyclin-dependent kinase
cDNA	complementary DNA
Cer	ceramide
CerK	ceramide kinase
CK	creatine kinase
CoA	coenzyme A
C_p	crossing point
CRS	cerebrosidase
CS	ceramide synthase
CYP	cytochrome P450 superfamiliy
d	days
DAB	3,3'-diaminobenzidine
DAG	diacylglycerol

DEPC	diethylpyrocarbonate
DES	dihydroceramide desaturase
DMEM	Dulbecco's modified Eagle's medium
DMSO	dimethylsulfoxide
DNA	deoxyribonucleic acid
dNTP	deoxynucleoside triphosphate
E	efficiency
ECL	enhanced chemiluminescence
ECM	extracellular matrix
EDTA	ethylenediaminetetraacetic acid
e.g.	*exempli gratia* (for example)
EGF	epidermal growth factor
ERK	extracellular regulated kinase
ESI	electron spray ionization
et al.	*et alii* (and others)
ETS	v-ets erythroblastosis virus E26 oncogene homolog
FAK	focal adhesion kinase
FCS	fetal calf serum
FB	fumonisin B
FB_1	fumonisin B_1
FW	forward
GAP	GTPase-activating protein
GCS	glucosylceramide synthase
gDNA	genomic DNA
GEF	guanine nucleotide exchange factor
GGT	gamma-glutamyl transferase
GLDH	glutamate dehydrogenase
GPCR	G protein-coupled receptor
GSH	glutathione
GSK-3b	glycogen synthase kinase-3 beta
HCl	hydrochloric acid
HDAC	histone deacetylase
H&E	hematoxylin and eosin
HEK	human embryonal kidney
HFB_1	hydrolyzed FB_1
HGF	hepatocyte growth factor
HKG	housekeeping gene

HPLC	high pressure liquid chromatography
HRP	horseradish peroxidase
HSC	hepatic stellate cell
HUVEC	human umbilical vein endothelial cell
IHKE	immortalized human kidney cells
i.e.	*id est* (that is)
IEG	immediate early gene
i.p.	*intraperitoneal*
IKK	IκB kinase
IL	interleukin
INF	interferon
iNOS	inducible nitric oxide synthase
IS	internal standard
JNK	c-Jun N-terminal kinase
KSR	kinase suppressor of Ras
LC	liquid chromatography
LDH	lactate dehydrogenase
LRP	low density lipoprotein receptor
MAPK	mitogen activated protein kinase
MMP	matrix metalloproteinase
MOPS	3-(N-morpholino)propanesulfonic acid
MRM	multiple reaction monitoring
mRNA	messenger RNA
MS	mass spectrometry
MS/MS	tandem mass spectrometry
MTA	metastasis-associated antigen
MTT	(3-(4,5-Dimethylthiazol-2-yl)-2,5-diphenyl-tetrazolium bromide
MYC	myelocytomatosis viral oncogene homolog
m/z	mass-to-charge
NADH	nicotinamide adenine dinucleotide
NADPH	nicotinamide adenine dinucleotide phosphate
NTP	National Toxicology Program
n.d.	not detectable
NEC	no enzyme control
NFκB	nuclear factor 'kappa-light-chain-enhancer' of activated B-cells

NOEL	no observed effect level
NRK-52E	normal rat kidney epithelial
NTD	neural tube defect
NuRD	nucleosome remodeling and histone deacetylation
OAT	organic anion transporter
OSOM	outer stripe of the outer medulla
8-oxodG	8-oxo-7,8-dihydro-2'-deoxyguanosine
PA	polyacrylamide
PAGE	polyacrylamide gel electrophoresis
PAI-1	Plasminogen activator inhibitor-1
PAP	phosphatidic acid phosphatase
PBS	phosphate buffered saline
PC	phosphatidylcholine
PCNA	proliferating cell nuclear antigen
PCR	polymerase chain reaction
PI3K	phosphatidylinositol 3-kinase
PKC	protein kinase C
PLC	phospholipase C
PMTDI	provisional maximum tolerable daily intake
ppm	parts per million
PIC	protease inhibitor cocktail
PTX	pertussis toxin
RAC	Ras-related C3 botulinum toxin substrate
RAS	rat sarcoma
RCC	renal cell carcinoma
RHO	Ras homolog gene family
RIE	rat intestinal epithelial
RIPA	radio immune precipitation assay
RNA	ribonucleic acid
RNase	ribonuclease
rRNA	ribosomale RNA
ROS	reactive oxygen species
RK	rabbit kidney
RT	room temperature
RTK	receptor tyrosine kinase
RT-PCR	reverse transcriptase PCR
qRT-PCR	quantitative real-time PCR

RV	reverse
Sa	sphinganine
Sa1P	sphinganine 1-phosphate
SAPK	stress-activated protein kinase
SD	standard deviation
SDS	sodium dodecyl sulfate
SDS-PAGE	sodium dodecyl sulfate-polyacrylamide gel electrophoresis
SEC	sinusoidal endothelial cell
SMase	spingomyelinase
SMB	somatomedin B
SMS	sphingomyelin synthase
So	sphingosine
So1P	sphingosine 1-phosphate
SPHK	sphingosine kinase
SPL	sphingosine 1-phosphate lyase
$S1P_{1-5}$	sphingosine 1-phosphate receptor 1-5
S1PP	S1P phosphatase
S1PR	sphingosine 1-phosphate receptor
SPT	serine palmitoyl transferase
TBE	tris-borate-EDTA
TBS	tris buffered saline
TBST	TBS-Tween®
TdT	terminal deoxynucleotidyl transferase
TEMED	N,N,N',N'-tetramethyl-ethane-1,2-diamine
TIC	total ion current
TGF	transforming growth factor
T_m	melting point
TNF	tumor necrosis factor
TNFR	tumor necrosis factor receptor
Tris	tris(hydroxymethyl)aminomethane
TUNEL	TdT-mediated dUTP-biotin nick end labeling
uPA	urokinase-type plasmino-gen activator
uPAR	urokinase-type plasminogen receptor
VLDLR	very low density lipoprotein receptors
VN	vitronectin
z.B.	zum Beispiel

Gene and protein nomenclature:

Gene symbols are italicized with the first letter in uppercase and the rest letters in lowercase (e.g. *Thbs1*), whereas protein symbols are not italicized with all letters in uppercase (THBS1).

1 Introduction

Exposure to mycotoxins - secondary metabolites produced by molds - *via* contaminated food may present a serious risk to human health. While acute adverse health effects in humans are generally not expected, irreversible effects such as reproductive toxicity and carcinogenicity resulting from chronic exposure are a matter of great concern.

In rodent bioassays conducted by the National Toxicology Program (NTP), nephrotoxicity and renal carcinogenicity were identified as the most sensitive endpoints of fumonisin B_1 (FB_1) toxicity (NTP, 2001), which is a widespread mycotoxin and food contaminant produced by various *Fusarium* species. The carcinomas induced by FB_1 showed an exceptionally aggressive growth and high potential to metastasize, which is rarely seen in chemically induced renal carcinogenesis in rats. Although numerous studies aimed at elucidating the mechanisms of FB_1 carcinogenicity, a detailed understanding of the molecular events leading to FB_1-induced renal tumor formation and malignant progression is still lacking.

Environmental factors (*e.g.* tobacco smoke, diet, infections) are estimated to account for about 80 to 90% of all cancers (Perera, 1996; Schulte-Hermann and Parzefall, 2004). However, the susceptibility to cancer is also dependent on individual factors such as genetics, age, ethnicity and immune function (Perera, 1996). Chemical carcinogenesis is described a multistep process that involves a mutational event leading to irreversible genetic alterations and selective growth advantage (initiation), followed by clonal expansion and genomic instability of initiated cells to form (pre)-neoplastic lesions (promotion). Finally, these lesions may develop to malignant tumors with invasive growth characteristics and potential of metastatic spread (progression). In general, chemical carcinogens are distinguished to act either *via* genotoxic or non-genotoxic mechanisms. Genotoxic carcinogens directly or indirectly interact with DNA to cause damage in the form of base modifications, adduct formation, deletion and strand breaks, which results in the alteration of genetic information and induction of DNA repair mechanisms (Schulte-Hermann and Parzefall, 2004). Incomplete or incorrect DNA repair combined with enhanced DNA replication may then manifest as mutations that are inherited after every DNA replication (Schulte-Hermann and Parzefall, 2004). The balance between cell replication and death can be influenced by chemicals in various ways and is crucial for the formation of tumors. Non-genotoxic agents

frequently induce acute or chronic injury, leading to cell death and subsequent regenerative proliferation. However, there are also non-genotoxic carcinogens, which act as mitogens and influence cell proliferation by direct interference with growth signaling pathways (Schulte-Hermann *et al.*, 1999). If the rate of cell replication then exceeds those of cell death, spontaneously initiated or predisposed cells, which would normally be eliminated from the tissue, may survive and continue to divide, thereby stimulating tumorigenesis (Goldsworthy *et al.*, 1996; Schulte-Hermann *et al.*, 1999). In recent years, epigenetic regulation of gene expression has gained increasing attention as a non-genotoxic mechanism for carcinogenesis (Goodman and Watson, 2002). Initiation of carcinogenesis may not only be restricted to mutagenesis, which involves alterations in DNA base sequence, but may also involve epigenetic modifications of promoter regions that influence the transcriptional activity of cancer-related genes (Goodman and Watson, 2002).

With respect to human risk assessment, carcinogens can be classified into genotoxic and non-genotoxic (Roberts *et al.*, 2003). For many non-genotoxic carcinogens, a threshold of toxicity below which no adverse effects are expected to occur (no observed adverse effect level (NOAEL)) can be defined. To estimate human exposure levels that are regarded to be safe, a tolerable daily intake level is derived from the NOAEL and the inclusion of uncertainty factors (USEPA, 2005). In contrast, carcinogens acting through a genotoxic or unknown mode of action are generally assumed to operate by a non-threshold mechanism.

To minimize human exposure to genotoxic and carcinogenic contaminants *via* food, maximum levels in food stuffs are set at a level, which is as low as reasonably achievable (ALARA) by good manufacturing and agriculture practice (EC, 2006). However, the ALARA principle represents only a tool for risk management, but does not consider human exposure. The alternative approach for risk assessment and management of genotoxic and carcinogenic substances in food recommended by European Food Safety Authority (EFSA) is the margin of exposure (MOE) principle (EFSA, 2005; Benford *et al.*, 2010). It is defined as the ratio of the point of departure (POD) on the observed dose range for carcinogenicity to the estimated dietary exposure in humans (MOE = POD/Exposure) (Barlow and Schlatter, 2010; Benford *et al.*, 2010). For genotoxic carcinogens, a MOE of ≥ 10,000 is considered to be of “low concern” and “low priority for risk management actions” (EFSA, 2005).

2 State of knowledge

2.1 Human exposure to fumonisin B_1

Fumonisins are a group of structurally related mycotoxins produced by *Fusarium verticillioides* and several other *Fusarium* species (Gelderblom *et al.*, 1988; Marasas, 1996) that grow on crops, particularly maize worldwide. FB_1, the most abundant homologue among these secondary fungal metabolites, is a common and thus economically important contaminant of maize and maize-based food stuffs. Fungal infestation of crops and subsequent contamination with FB_1 can occur during different stages of cultivation, including crop growth, harvesting or storage, and is influenced by temperature and humidity. Accordingly, human exposure to FB_1 varies widely around the world depending on climate, processing technologies and consumption of maize-based diet (Turner *et al.*, 1999).

Table 1: Estimated human exposure to FB_1 or total fumonisins (FB) in different areas of the world from maize-based food

Continent Country *Region*	**Mean FB concentration in food [mg/kg] (or mean range)**	**Mean food consumption [g/d] (or mean range)**	**Mean FB intake [µg/kg bw per day] (or mean range)**	**Ref.**
Europe				
Germany	0.013	6	0.01[a]	(Zimmer *et al.*, 2008)
North America				
United States[b]	n.s.	n.s.	0.08	(Humphreys *et al.*, 2001)
South America				
Guatemala				
rural	3.55	454	15.6	(Torres *et al.*, 2007)
urban	3.55	102	3.5	
Asia				
China				
home-grown corn[b]	0.08 – 41	100 –750	0.4 – 740	(Qiu and Liu, 2001)
Africa				
South Africa				
rural (moldy corn)[b]	54.0	460	354.9	(Marasas, 2001)
rural (healthy corn)[b]	7.1	460	46.6	
urban[b]	0.3	276	1.2	

[a] calculated from an assumed body weight (bw) of 70 kg for adults ; [b] FB_1 only; n.s. = not specified

Industrialized food production appears to constitute an effective means for preventing and mitigating food contamination by FB_1 and thus concentrations of FB_1 in maize-based food are generally low in the western world, *e.g.* Germany (Table 1).

Combined with a fairly modest consumption of maize-based food in Europe and North America, estimated dietary human exposures to FB_1 range from 0.01 µg/kg bodyweight (bw) per day in Germany to 0.08 µg/kg bw per day in the USA (Table 1) (Humphreys *et al.*, 2001; Zimmer *et al.*, 2008). In contrast, maize grown in South America, the Far East and Africa is more frequently infected by fumonisin-producing fungi due to unfavorable climate as well as inappropriate cultivation and storage conditions, resulting in high levels of FB_1 in food (Table 1) (Dutton, 2009). In addition, maize cultivated in rural regions has been shown to contain significantly higher amounts of FB_1 than maize produced in urban areas of the same country. For instance, in South Africa mean concentrations of FB_1 in healthy or moldy unprocessed maize from rural regions were reported to be 7.1 and 54 mg/kg FB_1, respectively, while in urban regions the mean level of contamination of maize was more than an order of magnitude lower (0.3 mg/kg FB_1). Since maize-based food presents a significant part of the traditional African diet (Turner *et al.*, 1999), dietary intakes of FB_1 in rural areas may be as high as 354.9 µg/kg bw per day. This compares to FB_1 intakes of 1.2 µg/kg bw per day in urban regions of South Africa, which is still considerably above exposure estimates in Europe and North America (Table 1) (Marasas, 2001). High levels of contamination of maize with FB_1 have also been observed in rural parts of China (up to 41 mg/kg), in which maize is traditionally consumed and represents a substantial part of the staple diet, resulting in mean FB_1 intakes of up to 740 µg/kg bw per day (Table 1) (Qiu and Liu, 2001).

2.2 Toxicity and carcinogenicity of fumonisin B_1

FB_1, a diester of propane-1,2,3-tricarballylic acid and 2*S*-amino-12*S*,16*R*-dimethyl-3*S*,5*R*,10*R*,14*S*,15*R*-pentahydroxyeicosane (CAS 116355-83-0) is composed of a long-chain aminopentol (AP) backbone with two of the hydroxyl groups esterfied to tricarballylic acid (Figure 1) (Marasas, 2001).

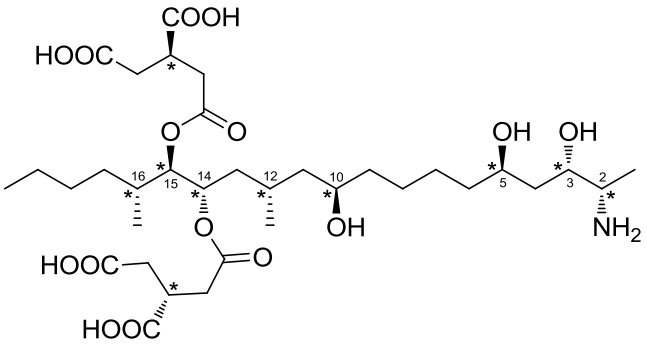

Figure 1: Chemical structure of fumonisin B_1 (FB_1)

Toxic effects of FB_1 in the form of leukoencephalomalacia in horses (Marasas *et al.*, 1988; Kellerman *et al.*, 1990) and pulmonary edema in pigs (Harrison *et al.*, 1990) were first observed in farm animals fed contaminated moldy feed. Subsequent studies in laboratory animals showed a relationship between FB_1 intake and hepatotoxicity, nephrotoxicity, carcinogenicity as well as developmental and reproductive toxicity (Riley *et al.*, 1994; Voss *et al.*, 1995a; Gelderblom *et al.*, 2001a; NTP, 2001; Marasas *et al.*, 2004).

While acute toxicity of FB_1 appears to be low (JECFA, 2001), repeated dose toxicity studies in rodents revealed the kidney and the liver as the main target organs of FB_1 toxicity, with marked sex-, strain- and species-dependent differences in target organ susceptibility.

Gender-specific differences in FB_1 toxicity were first observed in male and female Sprague Dawley rats receiving FB_1 at concentrations of 15, 50 and 150 ppm in the diet, equivalent to 1.4, 4.7 and 13.6 mg/kg bw per day, for 4 weeks (Table 2) (Voss *et al.*, 1993). At the high dose, nephrotoxic changes and mild hepatotoxicity were noted in both male and female rats. At lower doses, kidney lesions consisting of tubular epithelial basophilia and single cell degeneration within the proximal convoluted tubules were observed, with males being more susceptible than females. From this study, a no observed effect level (NOEL) of < 1.4 mg/kg bw per day based on the nephrotoxic effects of FB_1 in male Sprague Dawley rats was derived.

In a 28-day toxicity study in male and female F344N rats conducted by the NTP, oral administration of FB_1 at 0, 99, 163, 234 and 484 ppm in the diet (corresponding to 12, 20, 28 and 56 mg/kg bw per day) resulted in kidney and liver lesions characterized by decreased absolute and relative organ weights and

significantly increased incidences of apoptosis and degeneration (NTP, 2001). Consistent with findings in Sprague Dawley rats, males were found to be more sensitive to FB_1-mediated tubular epithelial cell apoptosis and degeneration than females, and a NOEL for renal toxicity of < 12 mg/kg bw per day was derived (Table 2). However, hepatocellular apoptosis and subsequent mitotic alterations occurred at lower doses in females than in males (NTP, 2001).

In contrast to rats, kidney lesions were not reported to occur in $B6C3F_1$/Nctr BR mice fed diets containing FB_1 in the same concentration range for 28 days (NTP, 2001). In mice, exposure to FB_1 resulted in hepatocellular necrosis, periportal hypertrophy, and centrilobular hyperplasia, as well as hyperplasia of the bile canaliculi and Kupffer cells, accompanied by elevated activities of alanine aminotranferase (ALAT) and alkaline phosphatase (ALP). Similar to rats, however, female mice were significantly more sensitive to the hepatotoxic effects of FB_1 than male mice, with histopathological and clinical chemistry changes indicative of hepatotoxicity occurring at dietary FB_1 concentrations of ≤ 99 ppm in females vs. 484 ppm in males (NTP, 2001).

Interestingly, male BDIX rats were also found to be more sensitive to FB_1-mediated hepatotoxicity than nephrotoxicity, which contrasts findings in F344N and Sprague Dawley rats. In a subacute toxicity study, Gelderblom *et al.* demonstrated that male BDIX rats receiving FB_1 in the diet at a dose of 70 mg/kg bw per day for 33 days developed degenerative, proliferative and fibrotic changes in the hepatobiliary tract, whereas only slight changes in the proximal tubules of the kidney were reported to occur (Table 2) (Gelderblom *et al.*, 1988).

Subchronic feeding of male and female F344N rats with doses of FB_1 ranging from 0.1 to 6.4 mg/kg bw per day for 90 days confirmed the kidney as the most sensitive target organ of FB_1 toxicity in F344N rats and the greater susceptibility of males as compared to females (Table 2) (Voss *et al.*, 1995a). Nephropathy was found to involve the outer stripe of the outer medulla (OSOM) and was characterized by single cell necrosis, necrotic or degenerated tubule epithelial cells, eosinophilic cytoplasm and sloughing of tubule epithelial cells. In males, these changes were recorded at FB_1 doses ≥ 0.6 mg/kg bw per day, whereas in females renal toxicity did not occur at doses below 5.7 mg/kg bw per day. Consequently, the NOEL for renal toxicity in male rats as the most sensitive endpoint for FB_1 toxicity was defined at 0.2 mg/kg bw per day (Voss *et al.*, 1995a).

Table 2: Strain and gender-dependent toxicity in rats fed with FB_1-contaminated diets

Strain/ Animal number/ Duration		Dietary concentration of FB_1 [mg/kg diet]	FB_1 intake [mg/kg bw per day]	Main target organs/pathological lesions		Ref.
				Liver	Kidney	
Subacute studies						
Fischer 344N/ n = 100/ 28 days	♂ ♀	99 160 230 480	12 20 28 56	minimal to mild apoptosis, disorganization of the sinusoidal structure (hepatocellular degeneration) as result of apoptosis, and increased hepatocellular mitosis; bile duct hyperplasia, ♀ more susceptible than ♂; **NOEL: < 20** mg/kg bw per day (♀)	decreased kidney weights; tubular epithelial cell apoptosis in the cortico-medullary area; tubule cell proliferation at the cortico-medullary junction; ♂ more sensitive than ♀; **NOEL: < 12** mg/kg bw per day (♂)	(NTP, 2001)
Sprague Dawley/ n = 24/ 28 days	♂ ♀	15 50 150	1.4 4.7 13.6	single cell necrosis, hepatocellular cytoplasmic vacuolation	decreased kidney weights; cortical (proximal) tubular epithelial basophilia, hyperplasia; single cell necrosis or pyknosis; ♂ more susceptible than ♀ **NOEL: ≤ 1.4** mg/kg bw per day (♂); **1.4** mg/kg bw per day (♀)	(Voss *et al.*, 1993)
BDIX/ n = 18/ 33 days	♂	1000	70	chronic toxic hepatitis; bile duct hyperplasia and fibrosis; hyperplastic nodules; presence of numerous (also abnormal) mitotic figures	fatty changes and scant necrosis in the proximal tubules	(Gelderblom *et al.*, 1988)
Subchronic studies						
Fischer 344N/ n = 180/ 90 days	♂ ♀	1 3 9 27 81	0.1 0.2 0.6 1.9 5.7	no lesions observed	decreased kidney weights; nephropathy: degeneration or necrosis of tubular cells; presence of mitotic figures; ♂ more sensitive than ♀ **NOEL: 0.2** mg/kg bw per day (♂); **< 5.7** mg/kg bw per day (♀)	(Voss *et al.*, 1995a)
Chronic studies/Carcinogenicity studies						
BDIX/ n = 50/ 2 years	♂	50	1.6	micro- and macronodular cirrhosis; cholangiofibrosis at the hilus of the liver; fatty changes, necrosis, hemorrhage; primary hepatocellular carcinoma with metastases to the heart, lungs or kidneys; cholangiocarcinoma	chronic interstitial nephritis; fibrosis, scattered lymphocytic interstitial infiltrate, retention cysts, hyaline casts, hydropic and hyaline droplet degeneration and scant necrosis of the proximal tubular epithelium	(Gelderblom *et al.*, 1991)
Fischer 344N/ n = 464/ 2 years	♂ ♀	5 15 50 150	0.22 0.67 2.2 6.6	Reduced liver weights; non-neoplastic focal cellular alterations consisting of clusters of hepatocytes with basophilic, clear cell, eosinophilic or mixed cell cytoplasm	adenomas and carcinomas with metastasis to lung and lymph nodes (♂); renal tubular hyperplasia (♂ more sensitive than ♀) **NOEL: 0.22** mg/kg bw per day (♂ toxicity); **0.67** mg/kg bw per day (♂ tumors)	(NTP, 2001)
BDIX/ n = 80/ 2 years	♂	1 10 25	0.03 0.3 0.8	Apoptosis, proliferation of bile duct epithelial cells; early signs of fibrosis and bile duct hyperplasia; hepatocyte nodules **NOEL: 0.03** mg/kg bw per day (♂ toxicity); **0.8** mg/kg bw per day (♂ tumors)	granular casts, necrosis, apoptosis, calcification, regenerative foci within the tubular epithelium **NOEL: 0.03** mg/kg bw per day (♂ toxicity)	(Gelderblom *et al.*, 2001a)

A 2-year carcinogenicity study, in which male and female F344N rats were administered FB_1 at dietary concentrations of 5, 15, 50, or 150 ppm equivalent to mean doses of 0.22, 0.67, 2.2 and 6.6 mg/kg bw per day (males) showed clear evidence for renal carcinogenicity in male rats (Table 2) (NTP, 2001). At 50 and 150 ppm FB_1 in the diet significant increases in the incidence of renal tubular adenomas and carcinomas were reported (Table 3).

Table 3: Renal tumor incidences in male and female F344 rats following chronic exposure to FB_1 (NTP, 2001). Data are shown as number of animals affected by renal tumors per group with respective tumor rates in brackets.

		FB_1 [ppm in the diet]				
		0	**5**	**15**	**50**	**150**
Adenoma	♂	0/48 (0%)	0/40 (0%)	0/48 (0%)	4/48 (8%)	6/48 (13%)
	♀	0/48 (0%)	0/40 (0%)	0/48 (0%)	0/48 (0%)	0/48 (0%)
Carcinoma	♂	0/48 (0%)	0/40 (0%)	0/48 (0%)	8/48 (17%)	10/48 (21%)
	♀	0/48 (0%)	0/40 (0%)	0/48 (0%)	1/48 (2%)	1/48 (2%)
Total	♂	0/48 (0%)	0/40 (0%)	0/48 (0%)	12/48 (25%)	16/48 (33%)
	♀	0/48 (0%)	0/40 (0%)	0/48 (0%)	1/48 (2%)	1/48 (2%)

At the same doses a significant rise in the number of preneoplastic proliferative lesions (atypical tubule hyperplasia) was observed (Hard *et al.*, 2001; NTP, 2001). Non-neoplastic changes included single-cell death, basophilia, simple tubule hyperplasia and regeneration within proximal tubules of the deep cortex and OSOM. Single-cell death involving loss of cell anchorage to the basement membrane and detachment of cells into the tubule lumen was observed at ≥ 15 ppm FB_1 in the diet. Importantly, FB_1-induced renal tubular carcinomas were characterized by an unusually rare and highly malignant anaplastic phenotype with marked pleomorphism, a high mitotic rate and invasive growth (Hard *et al.*, 2001). The potential to metastasize to the lung was observed in 25 and 50% of the rats with renal carcinomas in the 50 and 150 ppm dose group (metastasis rates in the lung not shown in Table 3) (NTP, 2001).

Based on the induction of tumors, a NOEL at 0.67 mg/kg bw per day in male rats was defined, whereas the NOEL for renal toxicity in males was set at 0.22 mg/kg bw per day (Howard *et al.*, 2001a; NTP, 2001). In the same study, increased incidences of hepatocellular neoplasms accompanied by non-neoplastic lesions were observed in female B6C3F_1/Nctr BR mice fed diets containing FB_1 at 50 and 80 ppm, supporting the greater susceptibility of female mice to FB_1 hepatotoxicity.

The apparent differences in the subacute toxicity of FB_1 in selected rat strains (Sprague Dawley, Fischer 344N and BDIX) were also confirmed by chronic feeding studies. While Fischer 344N rats were more susceptible to the formation of renal tumors (NTP, 2001), BDIX rats revealed increased incidences of hepatocyte nodules and hepatocellular carcinomas (Gelderblom *et al.*, 1991; Gelderblom *et al.*, 2001a) (Table 2).

In humans, epidemiological studies revealed an association between intake of FB_1-contaminated food and high incidences of esophageal cancer in the Transkei region of Southern Africa (Sydenham *et al.*, 1990; Rheeder *et al.*, 1992) and in China (Yang, 1980; Yoshizawa *et al.*, 1994). However, a causal relationship between FB_1 and human cancer has not yet been established, and other factors may play a role in the etiology of the disease. For instance, low socioeconomic status, tobacco smoking and alcohol consumption were identified as risk factors for the development of esophageal tumors in black South Africans (Pacella-Norman *et al.*, 2002). In addition, long-term residence in the Transkei region significantly increased the risk for esophageal cancer, particularly in women, and this is thought to be related to nutritional deficiencies in minerals and vitamins resulting from diets predominantly based on maize in these areas (Pacella-Norman *et al.*, 2002).

2.3 Toxicokinetics and biotransformation of fumonisin B_1

After oral administration of 10 mg/kg bw to male Wistar rats by gavage, less than 4% of the administered FB_1 dose was recovered in plasma and tissues, demonstrating low oral bioavailability (Martinez-Larranaga *et al.*, 1999). Following absorption, FB_1 was subjected to rapid distribution and elimination. Furthermore, oral doses of 10 mg/kg bw resulted in maximum plasma concentrations of 0.18 µg/ml FB_1 (corresponding to ~ 0.25 µM FB_1) within 1 h and a plasma half-life of 3.5 h. FB_1 was

distributed to most tissues with liver and kidney retaining highest levels of FB_1 in male Wistar rats (Martinez-Larranaga *et al.*, 1999). Riley *et al.* reported that FB_1 accumulated 10-fold more in kidneys than in livers of male Sprague Dawley rats consuming FB_1-contaminated diets for 10 days (1.1, 13.5, and 88.6 ppm of total fumonisins, corresponding to 0.7, 8.7 and 57.2 mg/kg FB_1). After 5 days of treatment, maximum mean concentrations in the kidney of male rats from the high dose group (88.6 ppm total FB, 57.2 mg/kg FB_1) were 201 pmol/g (estimated 251 nM = 0.25 µM) FB_1, whereas concentrations in liver reached 19 pmol/g (estimated 24 nM = 0.02 µM). FB_1 concentrations in kidneys correlated with the moderate renal lesions observed in this study. These high tissue levels, compared to low maximum serum concentration of 1 ng/ml (1.4 nM) FB_1 (Riley and Voss, 2006), provide support for the accumulation of FB_1 in the target organs of FB_1 toxicity.

Biotransformation experiments in rat liver microsomes indicated that FB_1 is not metabolized by cytochrome P450 enzymes (CYPs) (Merrill *et al.*, 1999). However, there is evidence that FB_1 can selectively inhibit the activity of CYP2C11 and to a lesser extent CYP1A2 as a consequence of FB_1 mediated alterations in sphingolipid metabolism (Spotti *et al.*, 2000). The inhibitory effects of FB_1 on CYP activities are thought to be related to suppression of protein kinase C (PKC) activity as a result of increased cellular concentrations of free sphingoid bases and subsequent regulation of organ specific expression of different CYPs (Spotti *et al.*, 2000).

After oral application, excretion of FB_1 primarily occurs *via* feces. It is either excreted in form of the parent compound or after microbial deesterfication of one or both tricarballylic acid moieties, producing partially or totally hydrolyzed FB_1s (HFB_1s) as metabolites (Shephard *et al.*, 1994b; Shephard *et al.*, 1995). Loss of tricarballylic residues converts HFB_1 into a substrate for ceramide synthase, thus generating acylated HFB_1 (Merrill *et al.*, 1993; Humpf *et al.*, 1998), which was found to be more toxic than FB_1 or HFB_1 in intestinal HT29 cells (Humpf *et al.*, 1998) but not in human epithelial kidney cells (IHKE) (Seefelder *et al.*, 2003). Although *intraperitoneal* administration of pure HFB_1 to rats confirmed the formation of N-acylated metabolites in kidney *in vivo,* intestinal absorption of HFB_1s and thus the contribution of these metabolites to FB_1 toxicity remain to be established (Seiferlein *et al.*, 2007).

2.4 Consideration of different modes of action for fumonisin B_1 carcinogenicity in rat kidney

2.4.1 Genotoxicity

Results from a range of *in vitro* and *in vivo* studies indicate that FB_1 is not a genotoxic carcinogen. Mutagenicity tests in *Salmonella typhimurium* with or without metabolic activation consistently showed negative results (Gelderblom and Snyman, 1991; Knasmueller *et al.*, 1997; Aranda *et al.*, 2000). These were also confirmed by tests for gene mutation and deoxyribonucleic acid (DNA) repair in *Escherichia coli* (Knasmueller *et al.*, 1997). Moreover, FB_1 did not induce unscheduled DNA synthesis in rat hepatocytes *in vitro* and *in vivo* (Gelderblom *et al.*, 1992; Norred *et al.*, 1992).

However, increased micronucleus frequencies and DNA strand breaks as assessed by the comet assay were observed in a range of mammalian cell lines (human derived hepatoma cells, human fibroblasts, rat astrocytes) (Ehrlich *et al.*, 2002; Galvano *et al.*, 2002a; Galvano *et al.*, 2002b). Consistent with the *in vitro* data, the comet assay revealed a significant increase in DNA damage in kidneys of male Wistar rats treated with FB_1 at oral doses ranging from 0.2 µg/kg bw up to 500 µg/kg bw for 5 days (Domijan *et al.*, 2006). Further *in vivo* studies confirmed the DNA-damaging potential of FB_1 in both liver and kidney of rats by detecting DNA lesions using the comet assay (Atroshi *et al.*, 1999; Domijan *et al.*, 2007b; Domijan *et al.*, 2008). However, considering the lack of DNA reactivity of FB_1, it is generally concluded that these effects are likely to be mediated by oxidative stress rather than being indicative of a direct genotoxic potential of FB_1 (JECFA, 2001).

2.4.2 Oxidative stress

Oxidative stress, resulting from increased production of reactive oxygen species (ROS) or impaired antioxidant defense mechanisms, is well established to contribute to renal toxicity and carcinogenicity. ROS can cause damage to proteins, lipids and DNA and has thus been suspected to play a causative role in FB_1 induced DNA damage (Abel and Gelderblom, 1998; Atroshi *et al.*, 1999; Mobio *et al.*, 2000; Stockmann-Juvala *et al.*, 2004; Kouadio *et al.*, 2007; Domijan *et al.*, 2008). In support of this, results from selected studies, which are summarized in the following section, demonstrate that FB_1 induces lipid peroxidation and oxidative DNA damage.

In a recent study in male Wistar rats, treatment with FB_1 at 0.2, 50 and 500 µg/kg bw by oral gavage for 5 days resulted in a dose-dependent increase in DNA damage in the kidney as assessed by single-cell gel electrophoresis in the presence of formamidopyrimidine-glycosylase, which converts oxidative DNA base modifications, particularly 8-oxo-7,8-dihydro-2´-deoxyguanosine (8-oxodG), to strand breaks (Domijan *et al.*, 2006). DNA lesions in rat kidney were also accompanied by a significant rise in protein carbonyls and malondialdehyde, further indicating that FB_1 causes oxidative stress in the target tissue of FB_1 carcinogenicity (Domijan *et al.*, 2007a).

Consistent with these results, *in vitro* studies demonstrated a rise in 8-oxodG in a rat glioma cell line (Mobio *et al.*, 2003) and increased production of malondialdehyde in porcine and monkey kidney cells treated with FB_1 (Abado-Becognee *et al.*, 1998; Klaric *et al.*, 2007; Meca *et al.*, 2010). Rumora *et al.* analyzed cellular redox state and signal transduction in kidneys of male Wistar rats treated with 0.5 mg FB_1/kg (*i.p.*) bw for up to 7 days (Rumora *et al.*, 2007). Determination of total intracellular glutathione (GSH) levels showed a significant decrease in GSH levels (27%) in kidneys of rats treated with FB_1 as compared to controls, suggesting depletion of cellular GSH stores. These changes were associated with activation of the redox-sensitive mitogen-activated protein kinase (MAPK) pathway (Bondy *et al.*, 1995; Atroshi *et al.*, 1999; He *et al.*, 2006b; Rumora *et al.*, 2007). Collectively, these data demonstrate that FB_1 toxicity is associated with altered redox balance and oxidative damage to cellular macromolecules, including DNA, which may contribute to FB_1 carcinogenicity.

However, it is still unknown how FB_1 functions to induce conditions of oxidative stress, and some evidence suggest that ROS production may be a consequence of FB_1 toxicity rather than its cause. In this regard, Abel and Gelderblom demonstrated that addition of the antioxidant α-tocopherol to primary hepatocyte cultures completely abolished the FB_1-mediated increase in thiobarbituric acid reactive substances, but provided only partial protection from FB_1 cytotoxicity, indicating that lipid peroxidation may occur secondary to FB_1 cytotoxicity (Abel and Gelderblom, 1998).

2.4.3 Modulation of cell death and cell proliferation

Tissue homeostasis is maintained through a tightly controlled balance between cell death and cell proliferation. A common feature of carcinogens operating by a non-genotoxic mechanism is their ability to disturb homeostatic control through promotion of cell growth and/or suppression of apoptosis. Conversely, persistent cell loss by either apoptosis or necrosis may stimulate regenerative processes including cell proliferation. If the rate of cell replication exceeds the rate of cell death, spontaneously initiated or predisposed cells, which would normally be eliminated from the tissue, may survive and continue to divide, thereby stimulating tumorigenesis (Goldsworthy *et al.*, 1996; Schulte-Hermann *et al.*, 1999). There is a large body of evidence from both *in vitro* (Tolleson *et al.*, 1996; Jones *et al.*, 2001a; Rumora *et al.*, 2002; Gopee *et al.*, 2003; Seefelder *et al.*, 2003; Klaric *et al.*, 2008) and *in vivo* studies (Tolleson *et al.*, 1996; Gelderblom *et al.*, 2001b; NTP, 2001) to show that FB_1 is a potent inducer of apoptosis.

Tolleson *et al.* first reported that FB_1 causes apoptosis in human cells *in vitro* (Tolleson *et al.*, 1996). Based on the morphological detection of features characteristic of apoptosis (cell shrinkage, chromatin condensation, apoptotic bodies), Rumora *et al.* found that cytotoxicity of FB_1 in rabbit kidney (RK13) cells was at least in part due to apoptosis, although DNA ladder formation was not observed (Rumora *et al.*, 2002). However, a subsequent study in RK13 cells confirmed FB_1-mediated induction of apoptosis by demonstrating increased activity of cysteine-aspartic protease (caspase)-3 in response to FB_1 treatment (Klaric *et al.*, 2008). Seefelder *et al.* investigated the potential of a range of fumonisin derivatives to induce apoptosis in a human proximal tubule cell line, and found that treatment with FB_1 (10 µM), but not FB_2, FB_3 or hydrolyzed FB_1 resulted in caspase-3 activation, chromatin condensation and DNA ladder formation (Seefelder *et al.*, 2003).

Consistent with the induction of apoptosis by FB_1 *in vitro*, cell loss by apoptosis and oncotic necrosis accompanied by sustained regenerative cell proliferation in the target tissues of FB_1 toxicity has been recognized as a key event in the mechanism of FB_1 carcinogenicity (Dragan *et al.*, 2001; Howard *et al.*, 2001a; Howard *et al.*, 2001b). In F344N rats fed diets containing 0, 99, 163, 234, and 484 ppm FB_1 for 28 consecutive days, increased incidences of hepatocyte and renal tubule epithelial cell apoptosis as determined by morphological evaluation were paralleled by a significant, dose-

dependent increase in cells in S-phase in both organs (Howard *et al.*, 2001b; NTP, 2001). At the lower doses (99 and 163 ppm), the effects of FB_1 on renal cell apoptosis and cell proliferation to compensate for the cell loss were more pronounced in males than in females, consistent with the formation of renal tubule adenomas and carcinomas in male but not in female F344N rats in this dose-range (Howard *et al.*, 2001b). Similarly, renal tubule cell apoptosis accompanied by increased cell proliferation within proximal tubules of the deep cortex and outer stripe of the outer medulla as determined by PCNA expression and 5-bromo-2-deoxyuridine (BrdU) incorporation was consistently observed in male F344N rats treated for 6, 10, 14 and 26 weeks under conditions of carcinogenicity, *i.e.* at 50 and 150 ppm (NTP, 2001). In contrast, male and female rat liver did not appear to be a target for FB_1-induced carcinogenicity (NTP, 2001), further supporting the importance of sustained toxicity and regeneration in FB_1 carcinogenicity in kidney of male rats. As opposed to the effects on kidney seen in male F344 rats, studies in BDIX rats showed that treatment with FB_1 (70 mg/kg bw per day for 33 days) induced liver toxicity, which was characterized by hepatocellular necrosis and accompanied by abnormal mitotic figures, karyomegaly, bile duct hyperplasia, and the formation of hyperplastic nodules in the liver, indicative of excessive regenerative processes in response to the FB_1-mediated hepatotoxic effects (Gelderblom *et al.*, 1988). Severe hepatotoxicity in form of liver cirrhosis was found in a 2-year carcinogenicity study in BDIX rats receiving 1.6 mg/kg bw/d FB_1 in the diet (Gelderblom *et al.*, 1991). As a result of marked hepatotoxicity, regenerative hepatic nodules were present from 6 months of exposure onwards, and paralleled the induction of hepatocellular carcinomas after 20 months of treatment (Gelderblom *et al.*, 1991). Less severe effects were observed after chronic exposure of BDIX rats to considerably lower doses of FB_1 (0.8 mg/kg bw per day), which led to mild apoptosis and proliferation of bile duct epithelial cells and hepatocytes, resulting in the formation of liver tumors (hepatocyte nodules) between 18 and 24 months of exposure (Gelderblom *et al.*, 2001b).

In summary, these results show that even though target organs of FB_1 toxicity are described to be different between F344N and BDIX rats, similar FB_1-mediated responses in form of cell death and subsequent sustained regenerative proliferation, which are thought to be prerequisite for the induction of renal and hepatic tumors, may occur in both kidney and liver.

The precise mechanism as to how FB_1 functions to induce apoptosis is still not fully understood. However, it is suggested that apoptosis occurs as a consequence of FB_1-mediated perturbation of sphingolipid metabolism, resulting in accumulation of pro-apoptotic sphingoid bases and loss of complex sphingolipids, which participate in the regulation of cell adhesion (see chapter 2.4.4.2). In this regard, it is interesting to note that degenerate cells in kidneys of FB_1-treated rats were frequently detached from the basement membrane and free in the tubule lumen, suggesting that FB_1-mediated cell death may represent anoikis, a special form of apoptosis that occurs as a consequence of loss of cell anchorage (Hard *et al.*, 2001). Although no direct proof has been obtained, this hypothesis is consistent with results from an *in vitro* study, demonstrating altered integrin-mediated cell-matrix adhesion in a mouse melanoma cell line in the presence of FB_1 (Pelagalli *et al.*, 1999).

So far, only a few mediators of apoptosis have been identified to be involved in FB_1-mediated toxicity *in vitro* and *in vivo*.

Several *in vitro* studies showed that FB_1 triggers cell death by interaction with pathways involving tumor necrosis factor (TNF) alpha, protein kinase C (PKC), nuclear factor 'kappa-light-chain-enhancer' of activated B-cells (NFκB) and caspase-3 (Gopee *et al.*, 2003; Johnson *et al.*, 2003; Gopee Neera and Sharma Raghubir, 2004; Gopee and Sharma, 2004; Rentz *et al.*, 2005). Consistent with the *in vitro* findings, studies in mice confirmed that TNF-alpha might be related to FB_1-induced hepato- or nephrotoxicity (Sharma *et al.*, 2000; Sharma *et al.*, 2001; Bhandari and Sharma, 2002a; Sharma *et al.*, 2003; Voss *et al.*, 2006). Treatment with FB_1 also induced an increase in the expression of anti-apoptotic and proliferative molecules (*e.g.* B-cell leukemia /lymphoma 2 (*Bcl2*) and myelocytomatosis viral oncogene homolog (*Myc*)), which were associated with hepatocyte proliferation in livers of rats and mice (Lemmer *et al.*, 1999; Bhandari and Sharma, 2002b). However, the precise mechanism leading to the induction of apoptosis (and sustained regenerative cell proliferation) in rat kidney as most sensitive target organ of FB_1 toxicity is still poorly understood. Since the observed *in vivo* and *in vitro* effects in liver and kidney were frequently reported to correlate with an increase in deregulated sphingolipids, it is very likely that modulation of cell death and proliferation occurs as a response of the FB_1-induced disruption of sphingolipid metabolism (Riley *et al.*, 2001).

2.4.4 Disruption of sphingolipid metabolism, cellular function of sphingolipids and biological consequences of altered sphingolipid metabolism

2.4.4.1 Disruption of sphingolipid metabolism

It is well established that FB_1 interferes with sphingolipid metabolism and consequently, sphingolipid-mediated cell signaling and function. In particular, FB_1 inhibits sphinganine N-acetyltransferase (ceramide synthase, CS) (Figure 2), an enzyme that catalyzes acylation of the sphingoid base sphinganine to generate dihydroceramide during *de novo* sphingolipid synthesis, as well as reacylation of sphingosine to ceramide (Wang *et al.*, 1991; Merrill *et al.*, 2001; Riley *et al.*, 2001; Desai *et al.*, 2002).The ability of FB_1 to inhibit ceramide synthase is due to the structural similarity between the ceramide precursor sphinganine (Figure 3) and FB_1 (Figure 1) (Gopee Neera and Sharma Raghubir, 2004), whereby the AP backbone of FB_1 appears to compete for binding of the sphingoid base substrate and the anionic tricarballylic acids of FB_1 interfere with binding of the fatty acyl coenzyme A (CoA) (Merrill *et al.*, 2001). Inhibition of ceramide synthase by FB_1 may result in complex alterations in sphingolipid metabolism, including elevation of free sphingoid bases (sphinganine and sphingosine) and their corresponding sphingoid base 1-phosphates, a decrease in ceramide, and depletion of complex sphingolipids (*e.g.* sphingomyelins and glycosphingolipids), which are important components of biological membranes (Riley *et al.*, 2001).

The first evidence for FB_1-mediated alterations in sphingolipid metabolism *in vivo* was reported by Wang *et al.*, demonstrating an increase in serum sphinganine and sphingosine and a decrease in complex sphingolipids in ponies exposed to FB_1 *via* contaminated feed (Wang *et al.*, 1992). A subsequent study in pigs fed diets containing fumonisins confirmed altered levels of free sphingoid bases in serum (Riley *et al.*, 1993). In addition, a significant increase in the ceramide precursor sphinganine – and to a lesser extent sphingosine – was observed in liver, lung, and kidney tissue of FB_1-exposed pigs (Riley *et al.*, 1993).

Further *in vivo* and *in vitro* studies support an association between FB_1-induced toxicity and carcinogenicity and the disturbance of sphingolipid metabolism.

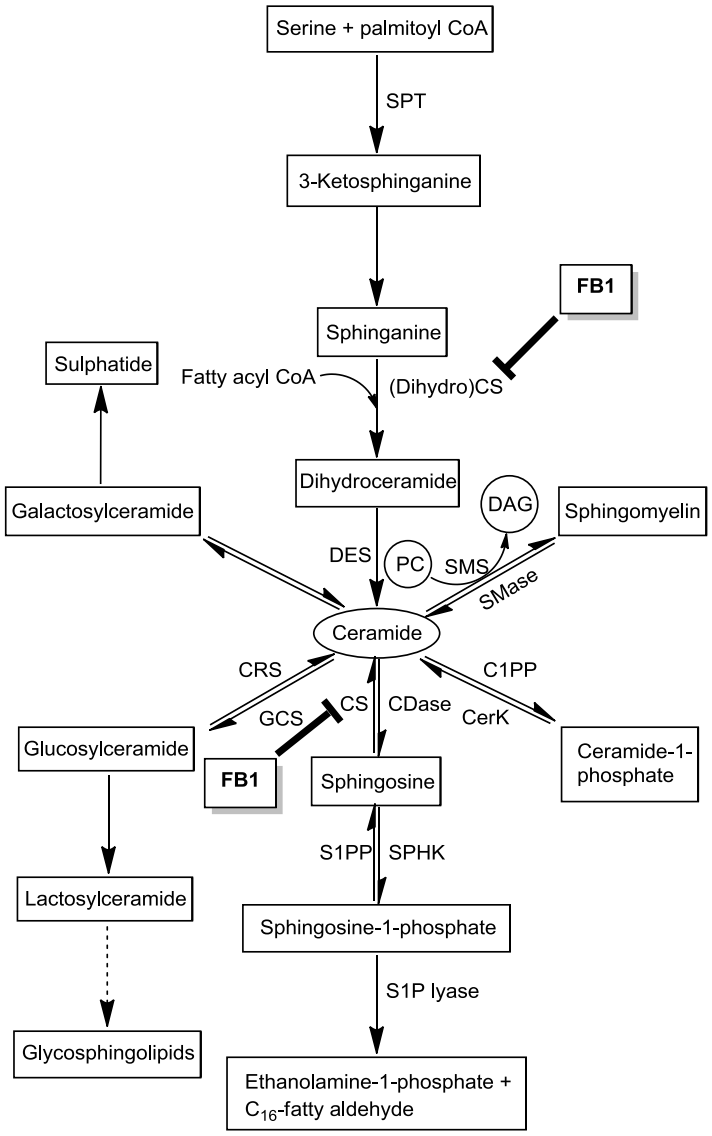

Figure 2: FB_1-mediated disruption of sphingolipid metabolism by inhibition of ceramide synthase (CS) (modified from (Ogretmen and Hannun, 2004)). **CRS** = cerebrosidase**; CerK** = ceramide kinase; **CS** = ceramide synthase; **DAG** = diacylglycerol; **DES** = dihydroceramide desaturase; **GCS** = glucosylceramide synthase; **PC** = phosphatidylcholine; **S1PP** = S1P phosphatase; **SMS =** sphingomyelin synthase; **SMase** = spingomyelinase; **SPHK** = sphingosine kinase; **SPT** = serine palmitoyl transferase;

Studies in rodents revealed a clear dose-response relationship between biochemical alterations in sphingolipid metabolism and FB_1 exposure and close correlation with the extent and severity of FB_1-mediated histopathological changes in the target tissues of FB_1 toxicity and carcinogenicity (Riley *et al.*, 1994; Gelderblom *et al.*, 1996; Gelderblom *et al.*, 1997; NTP, 2001). In Sprague Dawley rats administered FB_1 *via* feed, concentrations of free sphingoid bases were found to be significantly higher in the kidney as compared to the liver, consistent with the greater susceptibility of the

kidney to FB_1 toxicity in this rat strain (Riley *et al.*, 1994). Similarly, the degree of FB_1-mediated disruption of sphingolipid metabolism in the kidney was somewhat lower in females than in males, thus correlating with the increased sensitivity of male rat kidney as compared to females (Riley *et al.*, 1994). Importantly, dose-dependent changes in free sphingoid bases or the sphinganine/sphingosine ratio were detected before or concurrent with the onset of toxicity, suggesting a mechanistic link between biochemical alterations in sphingolipid metabolism and FB_1 toxicity (Riley *et al.*, 1994). More recent studies suggest that determination of free sphingoid bases alone may underestimate the overall effects of FB_1 on sphingolipid metabolism (Riley and Voss, 2006). To counterbalance the increase in free sphingoid bases, cells may initiate regulatory mechanisms to reduce the levels of pro-apoptotic sphinganine and sphingosine by kinase-dependent phosphorylation to sphinganine 1-phosphate or sphingosine 1-phosphate and subsequent degradation to ethanolamine 1-phosphate and the corresponding fatty aldehyde (Hannun and Obeid, 2008). Indeed, work by Riley and Voss showed that accumulation of free sphinganine in serum and tissues is accompanied by a marked increase in sphinganine 1-phosphate in the kidney but not liver of FB_1 treated male Sprague Dawley rats, suggesting that organ-specific differences in sphingoid base metabolism may contribute to the relative sensitivity of the kidney to FB_1 toxicity (Riley and Voss, 2006).

In vitro, inhibition of *de novo* sphingolipid biosynthesis by FB_1 was also shown to cause rapid and dramatic elevations in sphinganine, sometimes accompanied by minor changes in sphingosine (Ciacci-Zanella *et al.*, 1998; Schmelz *et al.*, 1998; Tolleson *et al.*, 1999; He *et al.*, 2002; Seefelder *et al.*, 2003). Since both intermediates are known to exert cytotoxic, growth inhibitory and pro-apoptotic functions when added to cells exogenously, accumulation of free sphingoid bases has been suspected of being responsible for the induction of apoptosis in response to FB_1 treatment. In support of this, co-treatment of cultured human keratinocytes with N-acetylsphingosine or beta-chloroalanine, which blocked sphinganine accumulation, provided partial protection from FB_1-induced apoptosis (Tolleson *et al.*, 1996). In contrast, a study by He *et al.* demonstrated that FB_1-mediated alterations in the expression of TNF-alpha, which is thought to play a key role in FB_1 toxicity, were independent of sphingoid base accumulation in LLC-PK_1 treated with FB_1 (He *et al.*, 2001). Similarly, Seefelder *et al.* (Seefelder *et al.*, 2003) reported that FB_1 and several

of its structural analogues caused a significant increase in sphinganine in IHKE cells, whereas apoptosis was only seen in response to FB_1. Based on the poor correlation between sphinganine levels and induction of apoptosis in their study, the authors concluded that accumulation of sphinganine alone may not account for the cytotoxic effects of FB_1. This suggests that additional alterations may be involved in determining the overall cellular response to FB_1. Indeed, several studies demonstrate that accumulation of sphinganine in cells exposed to FB_1 is accompanied by depletion of ceramide and more complex sphingolipids (Yoo *et al.*, 1996; Tolleson *et al.*, 1999) Considering the key role of ceramide in the initiation and execution of apoptosis, it would appear that reduction of intracellular ceramide through exposure to FB_1 may confer resistance to stress-induced cell death rather than inducing apoptosis. However, depletion of complex sphingolipids, which correlates with inhibition of cell-adhesion, loss of epithelial cell morphology and reduced cell growth, may contribute to the mechanism of FB_1-mediated cell death. Consistent with *in vivo* studies, FB_1 treatment was also shown to cause formation of phosphorylated sphingoid bases in a variety of mammalian cell lines (Smith and Merrill, 1995; Min *et al.*, 2002; Tani *et al.*, 2005; Berdyshev *et al.*, 2009; Zitomer *et al.*, 2009). Zitomer *et al.*, demonstrated that treatment with FB_1 (50 µM for 48 h) significantly increased the formation of sphinganine 1-phosphate (~ 15 pmol/mg protein) in LLC-PK_1, whereas elevation in sphinganine was less pronounced (~ 6 pmol/mg protein) (Zitomer *et al.*, 2009). This was suggested to be due to a high metabolic conversion of accumulated sphinganine to its respective 1-phosphate by activated sphingosine kinase. Similar results were obtained after treatment of immortalized human keratinocyte cells with FB_1 (20 µM for 12, 24 and 48 h), which resulted in a time-dependent increase of sphinganine, sphingosine and their phosphorylated metabolites sphinganine- and sphingosine 1-phosphate (Min *et al.*, 2002). Consistent with the results by Zitomer *et al.*, levels of sphinganine 1-phosphate markedly exceeded those of sphinganine after 48 h incubation with FB_1 (~ 1500-fold increase in sphinganine 1-phosphate vs. ~ 14-fold in sphinganine compared to controls) in contrast to earlier time points (Zitomer *et al.*, 2009). Thus, accumulation of sphinganine in response to treatment with FB_1 seems to initiate metabolic conversion to the phosphorylated metabolite to counterbalance the FB_1-induced changes in sphingolipid metabolism. Importantly, an increase in the concentrations of sphingoid base 1-phosphates may confer resistance to FB_1-mediated apoptosis. This is supported by a study in human embryonal kidney cells

(HEK-293), demonstrating increased sensitivity to FB_1-mediated apoptosis in the presence of DL-*threo*-dihydrosphingosine, an inhibitor of sphingosine kinase (Sharma *et al.*, 2004). Importantly, co-incubation with sphingosine 1-phosphate abrogated DL-*threo*-dihydrosphingosine-mediated potentiation of FB_1 toxicity, supporting the fact that metabolic conversion of sphingoid bases into their corresponding phosphorylated metabolites by sphingosine kinase may promote cell survival (Sharma *et al.*, 2004).

Besides the sphingoid bases sphinganine, sphingosine and their metabolites, Zitomer *et al.* recently identified 1-deoxy-sphinganine and 1-deoxy-dihydroceramides as being elevated in cells and animals treated with FB_1 (Zitomer *et al.*, 2009). 1-Deoxy-sphinganine and 1-deoxy-dihydroceramides are bioactive sphingolipids, which lack the 1-hydroxyl group of sphinganine and originate from *de novo* synthesis of sphingolipids utilizing palmitoyl-CoA and L-alanine instead of L-serine, presumably as a result of serine depletion (Zitomer *et al.*, 2009). In contrast to sphinganine/sphingosine, accumulation of 1-deoxy-sphinganine did not result in the formation of phosphorylated metabolites, since it lacks the hydroxyl group in position 1, which is the target for sphingosine kinase-dependent phosphorylation. Compared to sphinganine, 1-deoxy-sphinganine was shown to be equally potent in inhibition of cell growth and induction of cell death, suggesting a potential role of this novel metabolite in FB_1 toxicity. This suggestion is further confirmed by the detection of 1-deoxy-sphinganine in the target organs (liver and kidney) of FB_1 toxicity (Zitomer *et al.*, 2009). Furthermore, higher accumulation of 1-deoxy-sphinganine was also found in murine liver as compared to kidney, which correlated with the higher susceptibility of mice to FB_1-induced hepatotoxicity (Zitomer *et al.*, 2009). Accordingly, a recent study by Voss *et al.* demonstrated markedly elevated levels of 1-deoxy-sphinganine in livers of female rats after *i.p.* treatment with 10 mg/kg bw per day FB_1 (Voss *et al.*, 2009). Furthermore, a putative novel sphingoid base was tentatively identified as 1-deoxy-sphingosine, which was shown to be transiently elevated in murine liver after FB_1 treatment. However, the role of this novel sphingoid base in contributing to FB_1 toxicity remains to be determined (Voss *et al.*, 2009).

2.4.4.2 Cellular functions of sphingolipids and sphingosine 1-phosphate receptors

A growing body of evidence demonstrates that sphingolipids are not merely structural components of biological membranes, but also bioactive lipids with multiple roles in

cell signaling, including regulation of the cell cycle, apoptosis, cytoskeletal organization, intracellular trafficking, cell adhesion, migration, and angiogenesis (Hait *et al.*, 2006; Hannun and Obeid, 2008). There are more than 300 different sphingolipids, which are predominantly located in plasma membranes, Golgi membranes and lysosomes (Hannun and Obeid, 2008). Levels of individual sphingolipids and their metabolic interconversion are tightly regulated both spatially and temporally. Besides the complexity of sphingolipid biochemistry, different sphingolipids may exert opposing effects on cell signaling, suggesting that the relative balance between individual sphingolipids may be a critical determinant of cell fate. Thus, the biological consequences of FB_1-mediated disruption of sphingolipid metabolism are still poorly understood. In the following, the cellular functions of sphingolipids and their precursors are summarized.

Sphinganine and sphingosine (Figure 3) are sphingoid bases, which belong to a diverse class of long chain APs, and comprise the structural backbones of the key intermediate ceramide (see Figure 4) and more complex sphingolipids (see Figure 7). Sphinganine (dihydrosphingosine) is one of the major sphingoid bases found in many organisms. It is generated during *de novo* biosynthesis of sphingolipids by the condensation of serine and palmitoyl-CoA through catalytic activity of serine palmitoyltransferase (Brady and Koval, 1958; Pruett *et al.*, 2008).

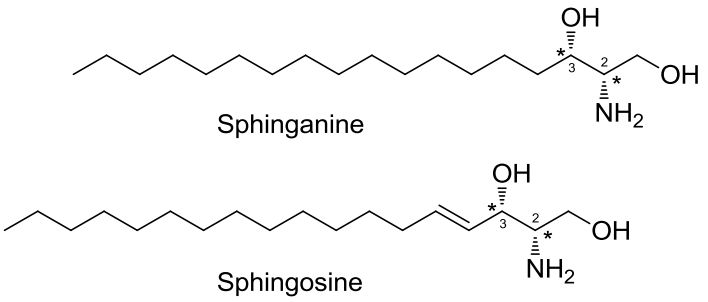

Figure 3: Chemical structures of the sphingoid bases sphinganine and sphingosine

In contrast, sphingosine is not directly synthesized in the *de novo* pathway, but results from the enzymatic turnover of ceramide or more complex sphingolipids during sphingolipid metabolism (Figure 2) (Merrill, 2002). Physiologically, free sphingoid

bases are only present at very low cellular concentrations, as they are rapidly transformed into (dihydro) ceramide by ceramide synthase.

Sphingosine is a potent inducer of apoptosis and growth arrest *in vitro*. This has been demonstrated in several studies by increasing the levels of endogenous sphingosine, *e.g.* in response to chemical treatment or serum deprivation, whereas blocking the formation of sphingosine attenuated the induction of apoptosis (reviewed in (Mao and Obeid, 2008)). Similarly, exogenous treatment with sphingosine was able to induce apoptosis in various cell lines (reviewed in (Mao and Obeid, 2008)), indicating a prevalent pro-apoptotic function of sphingosine. Mechanisms of induction of apoptosis by free sphingoid bases involve inhibition of PKC and phosphatidic acid phosphatase (PAP) activity (Hannun *et al.*, 1986; Perry *et al.*, 1992; Smith *et al.*, 2000). PAP is a key enzyme in the regulation of signaling lipids, since it generates the second messenger diacylglycerol (DAG) that is important for PKC activation (Carman and Han, 2009). PKC has a central role in signal transduction and regulation of complex downstream signaling pathways, including cell proliferation, differentiation and programmed death. In this context, sphingoid bases have been shown to counteract PKC-mediated proliferation and survival signals by induction of growth arrest, differentiation and apoptosis (Merrill, 1991; Solomon *et al.*, 2003). Besides PKC, sphingosine also inhibits various other protein kinases involved in proliferation and cell survival, *e.g.* Src tyrosine kinase, Ca^{2+}/calmodulin-dependent protein kinase, MAPK, extracellular regulated kinase (ERK1/2) and protein kinase B (v-akt thymoma viral proto-oncogene 1 (Akt1)) (Mao and Obeid, 2008). This supports sphingosine as a second messenger lipid involved in the induction of pro-apoptotic signals. Alternatively, sphingosine has also been proposed to initiate apoptosis by acting as a lysomotropic detergent, which alters the integrity of intracellular membranes and increases the permeability of lysosomes and mitochondria, resulting in the release of pro-apoptotic mediators such as cathepsin B, D or L and cytochrome c (Cuvillier *et al.*, 2001; Kagedal *et al.*, 2001). It is interesting to note that sphingosine has been demonstrated to inhibit the formation of glycosylated β1-integrin, which is an important component of cell-cell or cell-matrix adhesion (Hu *et al.*, 2005; Mao and Obeid, 2008). Inhibition occurred *via* fragmentation of the Golgi apparatus, an important cellular compartment involved in post-translational modifications (e.g. glycosylation) and trafficking of proteins. The sphingosine-mediated perturbation of

integrin glycosylation and functionality (*e.g.* in Hela cells) resulted in the disruption of cell adhesion and the loss of cell contact with the extracellular matrix (ECM), leading to detachment-induced apoptosis, also known as anoikis (Hu *et al.*, 2005; Mao and Obeid, 2008).

In vivo, sphingosine has been demonstrated to be an anti-tumor agent, since it efficiently induced apoptosis in transformed cells and tissues (Schmelz *et al.*, 2001; Kohno *et al.*, 2006). Studies by Schmelz *et al.* showed that feeding with sphingolipid-enriched diets reduced tumorigenesis in $Apc^{Min/+}$ mice, a transgenic model of heritable colon cancer (Schmelz *et al.*, 2001). In this context, sphingosine has been identified as a main digestion product of complex sphingolipids in intestinal segments with reduced number of tumors. Further investigations in this mice model showed that a deficiency in sphingosine kinase 1 protein (SPHK1) activity generated by gene deletion of *Sphk1* markedly increased the formation of sphingosine in intestinal adenomas. As a result, tumor size and cell proliferation were reduced in the intestines of $Apc^{Min/+}$ $Sphk1^{-/-}$ mice, whereas apoptosis was slightly increased (Kohno *et al.*, 2006). In compliance with the findings *in vivo,* treatment of immortalized non-transformed rat intestinal epithelial (RIE) cells with sphingosine resulted in marked suppression of cell proliferation, which was confirmed by the reduction in proteins of cell cycle progression such as cyclin-dependent kinase (CDK) 4 and decreased phosphorylation of the retinoblastoma protein (Kohno *et al.*, 2006).

Collectively, these studies provide evidence that sphingosine inhibits tumor cell growth *in vivo via* its ability to initiate apoptotic processes.

Ceramides (Figure 4) are the key intermediates of sphingolipid metabolism and major precursors of complex sphingolipids such as sphingomyelin (Figure 7) and glycosphingolipids.

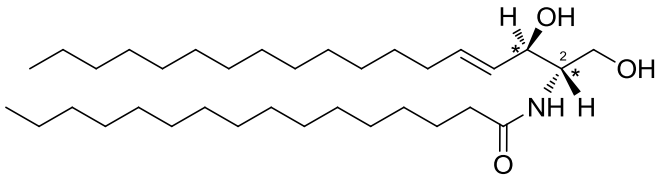

C16-Ceramide (d18:1/16:0)

Figure 4: Chemical structure of C16-Ceramide, a representative sphingolipid composed of the sphingosine backbone (d18:1), which is N-acylated with palmitic acid (C16:0) at the amino group in position 2.

They are generated *via* N-acylation of sphinganine or sphingosine by the enzyme ceramide synthase in the course of *de novo* sphingolipid synthesis or during sphingolipid metabolism, respectively (see Figure 2). Among the bioactive sphingolipids, ceramides are most abundant and constitute (together with DAG) between 0.1 and 1% of total membrane lipids (Hannun and Obeid, 2008; Bartke and Hannun, 2009).

In response to various stress stimuli (*e.g.* TNF-alpha), increased levels of ceramide are rapidly generated as a result of the enzymatic degradation of complex sphingolipds, *e.g.* by activation of sphingomyelinases (SMases) (see Figure 2). Ceramides have been demonstrated to exert a pivotal role as second messengers in cell-stress response, apoptosis, differentiation and growth control. Some of these effects are thought to be mediated through activation of ceramide-activated protein phosphatases (CAPPs), which in turn cause dephosphorylation of a range of proteins involved in the regulation of growth control and cell death, including the retinoblastoma gene product, PKC-alpha, AKT and BAX (Xin and Deng, 2006; Hannun and Obeid, 2008). In addition, ceramide has been proposed to interact with PKC-zeta and MAPK signaling and may bind to cathepsin D, consequently leading to activation of effector caspases and initiation of apoptosis (Shayman, 2000; Hannun and Obeid, 2008).

In compliance with the role of sphingosine in cancer, ceramides have been considered to act as ‘tumor-suppressor lipids’, since they exert remarkable anti-proliferative and pro-apoptotic functions in various cancer types (Taha *et al.*, 2006).
A crucial role for ceramide in cancer has emerged from a number of studies, where total amounts of ceramides in tumors were significantly decreased compared to normal tissues (Rylova *et al.*, 1998). In contrast, SPHK1 has been shown to be frequently overexpressed in cancer, suggesting that augmented levels of So1P counteracted the levels and functionality of ceramide, probably by accelerating its metabolism *via* activation of degradation enzymes (Ogretmen and Hannun, 2004). Ceramide-induced apoptosis of cancer cells in response to diverse death stimuli has gained an important role in the development of anti-cancer treatments. Many of these death-inducing agents were capable of accumulating ceramide through its enforced generation, which is frequently mediated by increased activation of acid

sphingomyelinase (aSMase) (Ogretmen and Hannun, 2004). In contrast, mice deficient in aSMase loose their ability to accumulate ceramide and become resistance to radiation-induced apoptosis (Santana *et al.*, 1996). Modulation of ceramide levels in cancer cells may also be obtained by the inhibition of ceramide-metabolizing enzymes, *e.g.* ceramidases and glucosylceramide synthase (GCS). In particular, GCS has been related to the phenomenon of multi-drug resistance in response to many chemotherapeutic drugs (Ogretmen and Hannun, 2004). For instance, inhibition of GCS enhanced the sensitivity to anti-cancer drugs in multi-drug resistant MCF-7/Adr breast cancer cells by increasing the levels of ceramide (Liu *et al.*, 2001). Tumor-suppressing functions of ceramide have also been linked to the induction of senescence by inhibiting the activity of telomerase in cancer cells (Ogretmen *et al.*, 2001). Sustained telomerase activity is important for cancer cells to overcome biological aging and become immortal by ongoing elongation of telomers, which increase the stability of chromosomes and permit continued cycles of cell division without quiescence of the cell (Ogretmen and Hannun, 2004).

In summary, there is strong evidence for the pro-apoptotic and anti-proliferative function of ceramide, which is associated with the activation of proteins that enhance the susceptibility of cells to undergo programmed cell death and growth arrest.

Sphingoid base 1-phosphates (Figure 5) are sphingolipid metabolites formed by SPHK1 mediated phosphorylation of intracellular or membrane-bound sphinganine and sphingosine (Alvarez *et al.*, 2007).

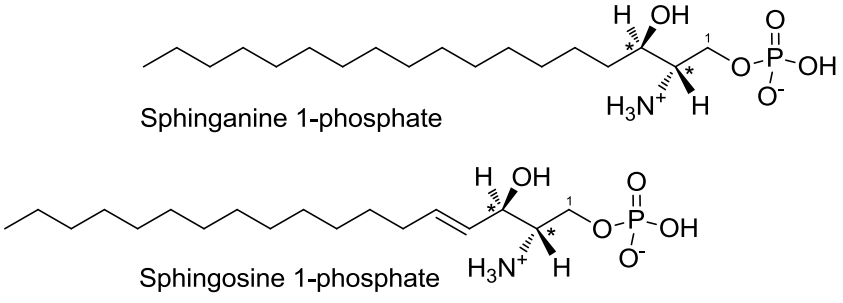

Figure 5: Chemical structures of sphinganine- and sphingosine 1-phosphate

The role of sphingosine 1-phosphate (So1P) as a key second messenger in sphingolipid metabolism has been well established over the last years, whereas data

on the biological role of sphinganine 1-phosphate (Sa1P) are less comprehensive. However, comparative studies revealed that Sa1P acts in a similar mode to So1P and has equivalent or little less signaling potential than So1P (Kimura *et al.*, 2000; Katsuma *et al.*, 2002). Many growth factors and cytokines have been shown to activate Sphk1, which leads to transient increases in intracellular sphingoid base 1-phosphate levels (Ogretmen and Hannun, 2004). Under physiological conditions, sphingoid base 1-phosphate levels are tightly regulated by the balance between kinase-dependent formation and lyase- or phosphatase-dependent degradation (see Figure 2) (Ogretmen and Hannun, 2004).

So1P is involved in many pathways mediating cell survival, proliferation, migration, and invasion and may either act *via* intracellular or extracellular signaling mechanisms ('inside-out signaling') (Spiegel and Milstien, 2003). The major biological functions of So1P are summarized in Figure 6 and explained in the following section.

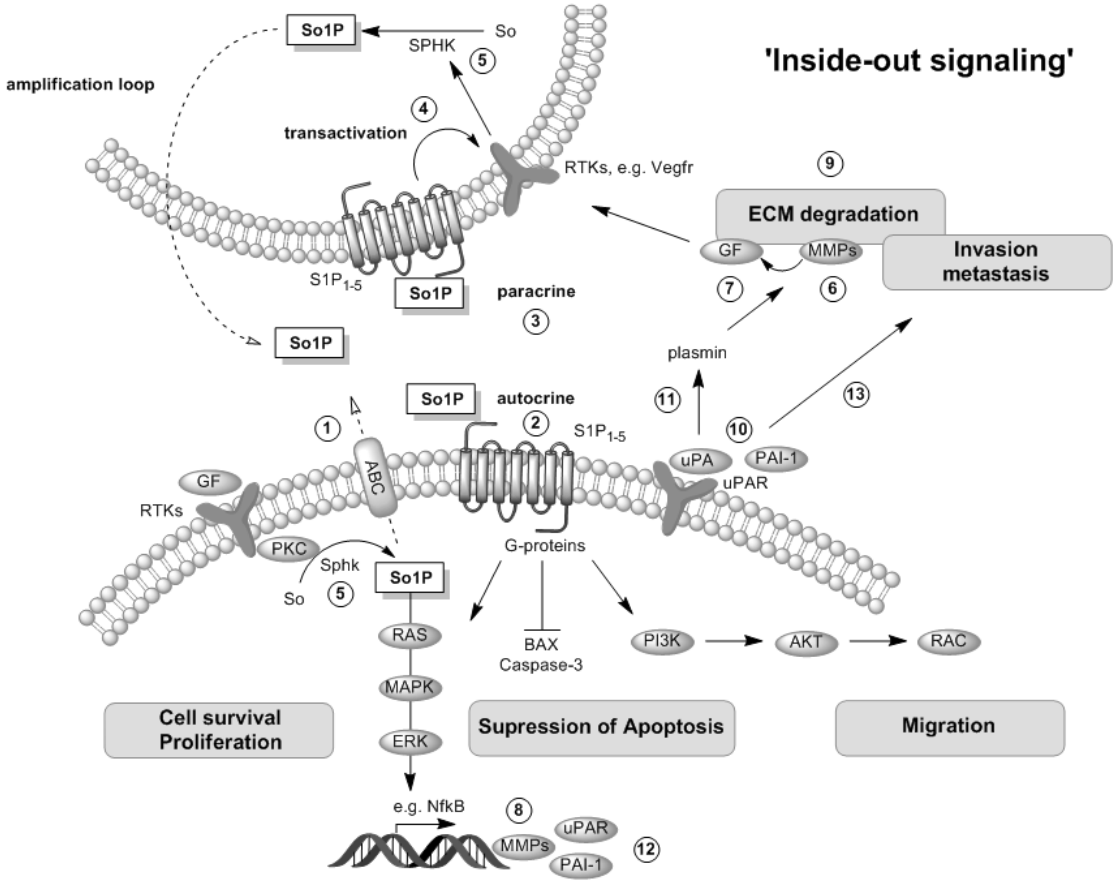

Figure 6: Pathways involved in sphingosine 1-phosphate (So1P)-mediated cell survival, proliferation, migration, invasion and metastasis.

To exert extracellular functions, intracellular generated So1P has to be actively transported to receptors on the cell surface (**1**). Studies in activated mast cells and breast carcinoma cells demonstrated that ATP-binding cassette (ABC) transporters are involved in the export of So1P (Mitra *et al.*, 2006; Takabe *et al.*, 2010).

After secretion to the ECM, sphingoid base 1-phosphates may activate downstream pathways through specific interactions with their transmembrane-associated high-affinity G protein-coupled receptors, termed sphingosine 1-phosphate receptors 1-5 ($S1P_{1-5}$) (**2**), resulting in the activation of signaling cascades related to cell survival, proliferation and migration. Interaction of So1P with its receptors occurs either in an autocrine or paracrine manner by activation of S1P receptors on the same cell or nearby cells (**3**), respectively. Intracellular actions of So1P, which are not mediated through the activation of S1P receptors, may lead to increased cell proliferation and suppressed apoptosis (Alvarez *et al.*, 2007).

In addition, binding of So1P to $S1P_{1-5}$ can lead to transactivation of growth factor receptor tyrosine kinases (RTKs) (**4**) and subsequent modulation of downstream signaling pathways such as rat sarcoma (RAS), ERK1/2, NFκB and phosphatidylinositol 3-kinase (PI3K)/AKT, which promote cell growth, vascular remodeling and angiogenesis. Activation of RTKs by growth factors can in turn cause production of sphingoid 1-phosphates through upregulation and stimulation of SPHK1 (**5**), resulting in amplification of growth signals (Milstien and Spiegel, 2006).

Interestingly, receptor transactivation by So1P has also been associated with the activation of matrix metalloproteinases (MMPs) (**6**). MMPs are enzymes that degrade proteins of the ECM, thereby causing release of latent growth factors (**7**) such as epidermal growth factor (EGF), which may result in the activation of respective growth factor receptors and subsequent signaling pathways (Alvarez *et al.*, 2007).

Deregulated proteolysis of the ECM and cell migration both constitute important processes in tumor invasion and metastasis and overexpression of MMPs is frequently observed in various cancer tissues (Wu *et al.*, 2005). MMPs are not merely enzymes that degrade ECM proteins, but also act on other proteinases, cell surface receptors and cell-cell adhesion molecules (Bjorklund and Koivunen, 2005). In endothelial cells, So1P has been shown to increase the expression and activity of MMP2 (**8**) *via* activation of MAPK/ERK, NFκB and calcium influx-dependent pathways, which resulted in MMP2-dependent cell invasion (**9**) (Wu *et al.*, 2005).

Furthermore, Bu *et al.* demonstrated that elevated Sa1P levels induced MMP1 gene expression through activation of ERK1/2 and v-ets erythroblastosis virus E26 oncogene homolog (ETS) 1 pathways (Bu *et al.*, 2006). These results implicate that deregulation of sphingoid base 1-phosphate levels and subsequent alterations in MMP expression might contribute to pathological processes including tumorigenesis and metastasis, which are characterized by abnormal ECM remodeling (Bu *et al.*, 2006). Since SPHK1, the important enzyme for the formation of bioactive phosphorylated sphingoid bases, is frequently overexpressed in tumors, it is considered to act as oncogene (Shida *et al.*, 2008).

Besides its impact on MMPs, So1P seems to influence the regulation of the plasminogen activator system, which also exerts proteolytic activity on ECM proteins and mediates migration and invasion of cells (Blasi and Carmeliet, 2002). The plasminogen activator system consists of various components, such as plasminogen activators (*e.g.* urokinase-type plasminogen activator (uPA)), inhibitors (*e.g.* plasminogen activator inhibitor 1 (PAI-1)) and a specific receptor for uPA (uPAR) (**10**). The uPA protein mediates proteolytic activity through binding to uPAR on the cell surface, which results in subsequent activation of the protease plasmin (**11**) and the activation of several signaling pathways *via* uPAR. Upregulation of uPA, uPAR and PAI-1 has been correlated with the invasiveness and migration of various cancer cell lines (Blasi and Carmeliet, 2002; Croucher *et al.*, 2008). For instance, Bryan *et al.* have shown that exogenous treatment with So1P resulted in the activation of MAPK/ERK1/2 signaling, leading to the upregulation of uPAR and PAI-1 (**12**) and increased invasiveness of glioblastoma cells (**13**) (Bryan *et al.*, 2008).

In vivo, the role of intracellular formed So1P in tumor progression has been clearly demonstrated in transgenic $Apc^{Min/+}$ mice additionally depleted in *Sphk1*, which showed reduced tumor size and dramatic decrease in cell proliferation of intestinal tumors due to the increase of growth-inhibitory sphingosine over mitogenic So1P (Kohno *et al.*, 2006). Thus, increased SPHK1 activity seems to be pivotal in determining cell fate by clearing pro-apoptotic sphingosine through increased metabolic conversion into pro-survival So1P (Cuvillier, 2002).

Complex sphingolipids (Figure 7) are structural components of cell membranes and composed of ceramide and a polar head group, such as phosphorylcholin or sugar residues, forming sphingomyelins or glycosphingolipids, respectively. They are involved in binding of cytoskeletal proteins, cell-cell communication and cell-substratum interactions (Riley *et al.*, 2001).

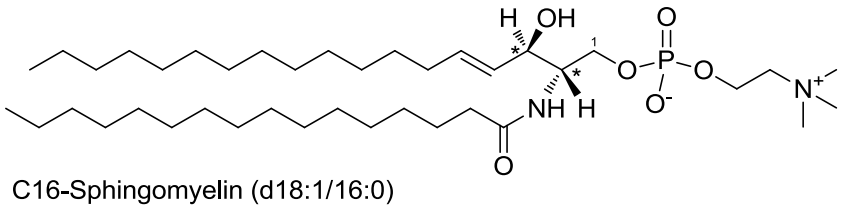

Figure 7: Chemical structure of C16-sphingomeylin, a representative complex sphingolipid composed of C16-Ceramide (d18:1/C16:0) and the polar head group phosphorylcholin attached to position 1.

In membranes, complex sphingolipids are often clustered in specialized microdomains enriched in cholesterol, which are called lipid rafts and have emerged as important centers for cell signaling and motility. Since various signaling molecules, for example SRC family tyrosine kinases and glycosylinositolphosphate-anchored proteins, are associated with lipid rafts, disruption of these domains may crucially affect cellular responses. It is thought that recruitment and organization of receptors and signaling molecules into lipid rafts is a critical event in the regulation of G protein-coupled receptor (GPCR) and growth factor receptor signaling (Ohanian and Ohanian, 2001). Concerning the domain stability, relative proportions of both sphingomyelin and cholesterol appear to be critical (Hoekstra *et al.*, 2003).

Sphingosine 1-phosphate receptors are high affinity G-protein-coupled receptors (GPCRs) for sphingoid base 1-phosphates and located on the surface of various mammalian cells (reviewed in (Young and Van Brocklyn, 2006)). Among the five known sphingosine 1-phosphate receptors, $S1P_{1-3}$ are the most ubiquitous and predominantly expressed receptors subtypes, which mainly exert effects on cell proliferation, survival and migration (Meyer zu Heringdorf and Jakobs, 2007). Several studies on the receptor affinity of sphingoid base 1-phosphates demonstrated that sphingosine- and sphinganine 1-phosphate showed equal affinity for binding to $S1P_{1-3}$, resulting in similar biological effects (Kimura *et al.*, 2000; Sato *et al.*, 2000; Tamama *et al.*, 2001; Katsuma *et al.*, 2002). Depending on the cell type-specific S1PR

repertoire, a complex network of signaling pathways may be initiated by the interaction of sphingoid bases 1-phosphates with their specific receptors (Taha *et al.*, 2004). This complexity results from the activation of different G-proteins (G_i, G_q and $G_{12/13}$) coupled to their respective receptors as shown for the major S1PR subtypes $S1P_{1-3}$ illustrated in Figure 8.

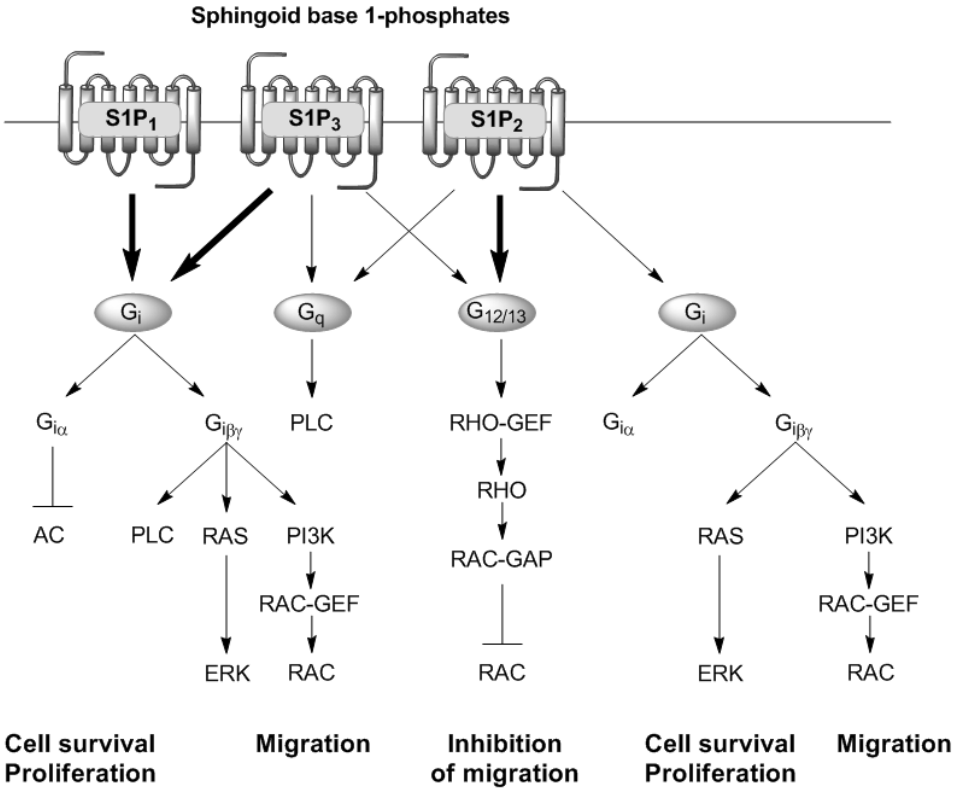

Figure 8: Major sphingoid base 1-phosphate receptors $S1P_{1-3}$ and their main signaling pathways involved in cell survival, proliferation and migration (modified from (Taha *et al.*, 2004)). Thick arrows indicate receptor coupling to the preferred G-protein partners, leading to the predominant activation of specific signaling pathways. **AC** = adenylate cyclase; **GEF** = guanine nucleotide exchange factor; **GAP** = GTPase-activating protein.

Principally, $S1P_1$ exclusively binds and activates G_i-proteins ($G_{i\alpha}$ or $G_{i\beta\gamma}$), resulting in the inhibition of adenylate cyclase (AC) and activation of PLC, RAS and PI3K-signaling, which promote cell survival, proliferation and migration (reviewed in (Taha *et al.*, 2004)). In a similar manner, $S1P_3$ preferably activates G_i-protein signaling, but may also couple to the proteins G_q (also activating PLC) and $G_{12/13}$ (reviewed in (Taha *et al.*, 2004). In contrast to $S1P_1$ and $S1P_3$, studies on $S1P_2$ revealed that this receptor subtype prefers binding to $G_{12/13}$, which initiates RHO-dependent inactivation of RAC *via* stimulation of GTPase-activating protein (GAP) for RAC and thus inhibits

cell migration (reviewed in (Taha *et al.*, 2004). In this regard, $S1P_2$ seems to mediate negative regulation of cell migration by RHO-dependent activation of stress fiber formation and focal adhesion (Sugimoto *et al.*, 2003).

Consistent with their role in normal cells, $S1P_1$ and $S1P_3$ have also been shown to initiate cell migration and invasion in cancer cells, whereas $S1P_2$ rather inhibited these effects in most, but not all types of cancer cells (Pyne and Pyne, 2010). Furthermore, $S1P_1$ and $S1P_3$ were found to be critically involved in tumor proliferation, angiogenesis and interaction with growth factor receptor signaling (Pyne and Pyne, 2010). This suggests that the specific response to exogenous sphingoid base 1-phosphates is largely determined by the cell type-specific predominance of S1PR subtypes, which might mediate distinct signaling pathways involved in cancer (Pyne and Pyne, 2010).

2.5 Biological consequences of FB_1-mediated disruption of sphingolipid metabolism

The inhibition of ceramide synthase by FB_1 causes elevation in the sphingoid bases sphinganine and sphingosine, whereby sphinganine is responsible for approximately 95% of the increased concentration (Riley *et al.*, 2001). To counterbalance these increases, cells may initiate regulatory mechanisms to reduce the levels of free sphinganine and sphingosine by kinase-dependent phosphorylation to sphinganine 1-phosphate or sphingosine 1-phosphate and subsequent catabolic degradation to ethanolamine 1-phosphate and the corresponding fatty aldehyde (see Figure 2) (Hannun and Obeid, 2008).

Possible biological consequences of FB_1-mediated alterations in sphingolipid metabolism are summarized in Figure 9.

Cells with substantial SPHK1 activity and potentially lesser extent of sphingosine 1-phosphate phosphatase- and lyase activity are reported to develop growth stimulatory instead of pro-apoptotic effects by exposure to FB_1 (Menaldino *et al.*, 2003). Consistent with this, Sharma *et al.* have shown that increased activity of SPHK1 in HEK-293 cells conferred resistance to apoptosis despite significant accumulation of pro-apoptotic sphingoid bases (Sharma *et al.*, 2004). Competitive inhibition of SPHK1 activity with an unnatural analogue of sphingosine significantly decreased the viability

of HEK-293 cells by enhancing the levels of sphingoid bases in the presence of FB_1 (Sharma *et al.*, 2004). Addition of So1P in physiological amounts was able to prevent FB_1-induced apoptosis after inhibition of SPHK1 (Sharma *et al.*, 2004), demonstrating the anti-apoptotic role of So1P.

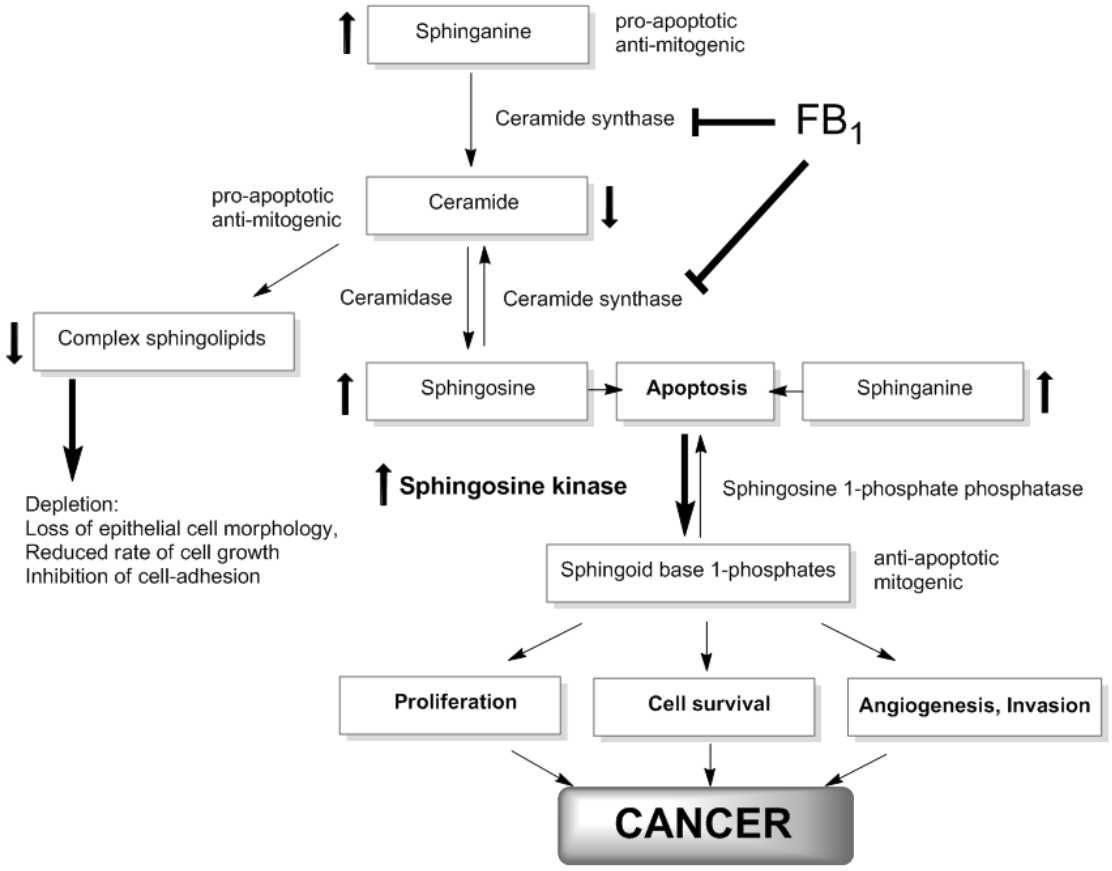

Figure 9: Possible biological consequences resulting from FB_1-induced alterations in sphingolipid metabolism.

The anti-apoptotic role of So1P was further demonstrated by Cuvillier *et al.*, who showed that SPHK1-dependent increase in So1P was sufficient to suppress ceramide-mediated apoptosis by TNF-alpha in human leukemia cells (Cuvillier *et al.*, 1996). In this context, increased So1P levels caused activation of PKC and stimulation of ERK pathways, which counteracted the ceramide-induced activation of stress-activated protein kinase JNK (Cuvillier *et al.*, 1996). Considering the fact that intracellular concentrations of sphingoid 1-phosphates are usually very low compared to free sphingoid bases, it has been estimated that phosphorylation of 1-3% of sphingosine may lead to a 2-fold increase in sphingosine 1-phosphate. Thus, even

minor changes in sphingoid base phosphorylation may have marked effects on sphingoid base 1-phosphate levels. As a result, profound biological consequences may occur, since sphingoid base 1-phosphates are very sensitively recognized by their high affinity receptors $S1P_{1-5}$ (Hannun and Obeid, 2008). A further consequence of FB_1-induced inhibition of *de novo* sphingolipid biosynthesis is reflected by the decrease in intracellular ceramide concentrations. Considering the key role of ceramide in the initiation and execution of apoptosis, it has been suggested that reduction of intracellular ceramide through exposure to FB_1 may lead to resistance to stress-induced cell death, thereby facilitating survival of initiated or preneoplastic cells and promoting tumorigenesis (Riley *et al.*, 2001). Moreover, ceramide synthase inhibition by FB_1 causes depletion of more complex sphingolipids, such as sphingomyelin and glycosphingolipids, which are involved in binding of cytoskeletal proteins, cell-cell communication and cell-substratum interactions. Degradation of complex sphingolipids has been shown to correlate with loss of epithelial cell morphology, reduced rate of cell growth and inhibition of cell-adhesion (Riley *et al.*, 2001; Desai *et al.*, 2002). Furthermore, increased rates in enzymatic turnover may lead to the release of ceramides from complex sphingolipids. Increased ceramidase activity may then result in the accumulation of pro-apoptotic sphingosine and initiate further metabolization to the respective phosphorylated forms *via* SPHK1 activity (Kitatani *et al.*, 2007). Since sphingolipid metabolites are interconvertible, their dynamic balance, the so-called ‘sphingolipid rheostat’ and their regulation of opposing signals can critically determine cell fate. Whereas sphingoid bases and ceramide have been associated with growth arrest and apoptosis, sphingoid base 1-phosphates are responsible for proliferation and survival of cells (Milstien and Spiegel, 2006). SPHK1 is considered to be a critical regulator of the ‘sphingolipid rheostat’, since it favors the formation of pro-survival So1P/Sa1P and therefore decreases the intracellular levels of pro-apoptotic sphingosine and sphinganine (Hait *et al.*, 2006). Thus, upregulation of this enzyme may ultimately act as a switch between apoptotic/growth inhibitory and mitogenic/pro-angiogenic signals, resulting in loss of growth control and subsequent tumor formation. Interestingly, treatment with FB_1 has been demonstrated to increase the activity of SPHK1 through the upregulation of both gene and protein levels in murine liver (He *et al.*, 2006a). Subsequent studies in mice demonstrated that the FB_1-mediated increase in the levels of SPHK1 was dependent the production of inducible nitric oxide synthase

(iNOS), which also exerted a protective effect on FB_1-induced hepatotoxicity (Suzuki *et al.*, 2007). The mitigation of FB_1-induced toxicity (apoptosis) in liver was associated with increased hepatocyte regeneration that seemed to be a result of iNOS/SPHK-dependent formation of proliferative and anti-apoptotic sphingoid base 1-phosphates (Suzuki *et al.*, 2007).

With regard to continuing exposure to FB_1, it is thus conceivable that overexpression of SPHK1 may occur either as a regulatory mechanism to decrease pro-apoptotic free sphingoid bases or through other signaling mechanisms required for compensatory cell proliferation in response to sustained cell loss.

2.6 Fumonisin B_1 risk assessment

Fusarium monoliforme causes worldwide contamination of maize by production of the mycotoxin FB_1. Highest amounts of FB_1 have been found in unprocessed moldy maize, since industrial procession of contaminated maize, *e.g.* in flour, grits, polenta and cornflakes, significantly reduces levels of FB_1 in the food. In particular, wet milling is an effective procedure to diminish levels of FB_1 in contaminated maize through aqueous extraction of the highly hydrophilic FB_1 from food. Hence, populations having only less processing procedures involved in food production, but a strong dependency on maize as staple diet, bear a greater risk for high intakes of FB_1 *via* contaminated food.

Based on food consumption data with respect to different FB_1 contents in regional diets of the world, an estimated mean intake of FB_1 ranging from 0.2 µg/kg bw per day in the European diet to 2.4 µg/kg bw per day in the African diet has been established (JECFA, 2001). The Joint FAO/WHO Expert Committee on Food Additives set a provisional maximum tolerable daily intake (PMTDI) for humans of 2 µg/kg bw per day for FB_1 alone or the combinations of all major fumonisins (FB_1 + FB_2 + FB_3), which is derived from the NOEL of 0.2 mg/kg bw per day for nephrotoxicity in rats as the most sensitive toxic effect of FB_1 and a safety factor of 100 (based on the lack of genotoxicity) (JECFA, 2001). Although European consumers have an average daily intake below the calculated PMTDI, it has to be emphasized that infants and children as well as populations with locally higher exposures to FB_1 need to be considered more strictly according to the risk assessment of diet-dependent FB_1 intake and possible health effects. Especially in populations of urban areas in South

Africa and China, very high mean FB_1 intakes may occur as a result of consuming homegrown and mold-infected maize as staple diet (see Table 1). In these regions, high consumers of maize may be exposed to an average of up to 354 and 740 µg/kg bw per day FB_1 in the diet, which is 177 and 370-fold above the PMTDI of 2 µg/kg bw per day, respectively. Moreover, a life-long intake of 740 µg/kg bw per day FB_1 would not only exceed the NOEL for nephrotoxicity, but also the NOEL of 0.67 mg/kg bw/d for renal cancer in rats. Under these conditions, food consumption may not longer be recognized as safe, but represents a serious risk to human health regarding the development of diet-related cancer by FB_1.

3 Objectives

Food contamination by mycotoxins represents a worldwide matter of toxicological concern, since many of these substances are considered to be potentially carcinogenic to humans. Among these, FB_1, a mycotoxin produced by molds of the *Fusarium* species, has been demonstrated to be both a nephro- and hepatotoxin in rodents, and a renal carcinogen in rats (NTP, 2001). Morphologically, these tumors showed a rare and highly malignant, anaplastic phenotype, characterized by marked cellular pleomorphism, high mitotic rate and invasive growth potential (Howard *et al.*, 2001a; NTP, 2001). Several standard testing methods demonstrated that FB_1 is not genotoxic and does not bind to DNA, suggesting that non-genotoxic mechanisms may play a crucial role in the carcinogenicity of FB_1. Up to now, the mechanisms underlying the FB_1-induced carcinogenesis in kidneys of male rats are still not clear. However, there is strong evidence that FB_1 carcinogenicity is associated with FB_1-mediated disruption of sphingolipid metabolism and formation of sphingoid base 1-phosphates. Over the last decades, these bioactive lipids have gained increasing attention in cancer research based on their role in pathways mediating tumor formation and progression.

The overall aim of the present study was to establish a hypothetical mode of action for FB_1-induced carcinogenicity in kidney, involving the identification of pathways linked to FB_1-mediated increases in bioactive sphingoid base 1-phosphates, which may mediate the initiation and exceptional aggressive growth characteristics of FB_1-induced renal tumors in rat. To achieve this aim, early alterations in gene expression and sphingo-lipid metabolism in response to FB_1 were analyzed *in vivo* and *in vitro*.

To identify FB_1-induced gene expression patterns in the kidney, which may be associated with sphingolipid-mediated signaling pathways in cancer, a short-term *i.p.* study with FB_1 in male Sprague Dawley rats was performed. The specific aims of this study were:

1. to detect early histopathological changes in kidney associated with apoptosis and regenerative cell proliferation in response to FB_1 using standard staining and (immuno)-histochemical techniques.

2. to link FB_1-induced alterations in renal histopathology (apoptosis and cell proliferation) to alterations in pro-apoptotic or proliferative sphingolipids in kidney, urine and serum using LC-MS/MS techniques.
3. to monitor early expression changes in 84 cancer-related genes by quantitative real-time polymerase chain reaction (qRT-PCR) and to correlate them to alterations in bioactive sphingolipids such as sphingoid base 1-phosphates.
4. to identify differences in the organ-specific susceptibility to tumor formation by comparing FB_1-mediated effects on histopathology, cell proliferation, sphingolipids, and selected cancer-related genes in kidney and liver.

To identify FB_1-induced alterations in genes and sphingolipid metabolism *in vitro*, a study in the normal rat kidney tubular epithelial cell line NRK52E was performed. The specific aims of this study were:

1. to compare FB_1-induced alterations in sphingolipid metabolism *in vitro* to those found after FB_1 treatment *in vivo* by LC-MS/MS analysis of intracellular sphingolipids in NRK-52E cells.
2. to identify genes commonly altered by FB_1 treatment *in vivo* and *in vitro* after qRT-PCR analysis of 84-cancer related genes and establish a link to changes in the amount of bioactive sphingolipids.
3. to analyze whether FB_1-induced expression of genes involved in tumor formation may have an impact on the cellular functions of NRK-52E cells by monitoring the invasion of cells through gelatin using a modified Boyden chamber.

4 Materials and methods

4.1 Materials

4.1.1 Equipment and laboratory consumables

Equipment	Provider
Accu-jet® pipette controller	Brand, Wertheim, Germany
AG245 Dual Range Analytical Balance	Mettler-Toledo, Giessen, Germany
Agilent Series 1100 LC quaternary pump	Agilent Technologies, Waldbronn, Germany
Agilent Series 1100 autosampler	Agilent Technologies, Waldbronn, Germany
Antair BSK 6 Laminar flow bench	Anthos, Siegburg, Germany
API 2000 QTRAP hybrid triple quadrupole linear ion trap tandem mass spectrometer equipped with Turbo Ion Spray source	Applied Biosystems, Darmstadt, Germany
Autoclave Type 28	MELAG, Berlin, Germany
Capsule Microcentrifuge HF-120	Tomy Seiko Co., Tokyo, Germany
Centrivac Vacuum centrifuge	Heraeus Instruments, Hanau, Germany
CH-2 Light microscope	Olympus, Hamburg, Germany
Dri-Block® Heater DB-2A	Techne, Burlington, USA
EPS 600 Electrophoresis Power Supply	Pharmacia Biotech, Freiburg, Germany
E-300 Digital single-lens reflex camera with MF-1 OM-Adapter	Olympus, Hamburg, Germany
Eppendorf Combitips plus, sterile (2.5, 5, 10, 25 and 50 ml volume)	Eppendorf, Hamburg, Germany
Eppendorf Microcentrifuge 5415 C	Eppendorf, Hamburg, Germany
Eppendorf Refrigerated Centrifuge 5403	Eppendorf, Hamburg, Germany
Gel Doc™ 2000 Gel Documentation System	Bio-Rad Laboratories, München, Germany
Glass homogenizer for tissue	VWR International, Darmstadt, Germany
Glassware	Schott, Mainz, Germany
HERAcell® CO_2-Incubator	Heraeus, Hanau, Germany
HyperClone™ C8 column with 150 x 2.0 mm dimension and 3 µm pore size	Phenomenex, Aschaffenburg, Germany
Julabo U3 Circulating water bath	Julabo, Seelbach, Germany
Julabo SW-20C Shaking water bath	Julabo, Seelbach, Germany
Leica Rotation Microtome RM 2165	Leica, Wetzlar, Germany

Equipment	Provider
Laboratory incubator BKE-30	Memmert, Schwabach, Germany
Labofuge GL	Heraeus Sepatech, Hanau, Germany
LightCycler® 480 qRT-PCR system	Roche, Mannheim, Germany
Magnetic stirrer IKA-Combimag RCO	Janke & Kunkel, Staufen, Germany
Makrolon® type-4 cages	Bayer Makrolon, Leverkusen, Germany
Microscope adapter LM Scope	MICRO TECH LAB, Graz, Austria
Mini-centrifuge/vortex Microspin FV-2400	Biosan, Riga, Latvia
Microwave MW 309	DeLonghi, Treviso, Italien
Multipette® Xstream	Eppendorf, Hamburg, Germany
Neubauer (Improved) Hemocytometer	Hartenstein, Würzburg, Germany
Nanodrop 2000C Spectralphotometer	Thermo Fisher Scientific, Dreieich, Germany
Owl Separation Systems Model B1 for horizontal electrophoresis	Thermo Fisher Scientific, Dreieich, Germany
PC 440 DeltaRange® Balance	Mettler, Giessen, Germany
pH meter pH 526	WTW, Weilheim, Germany
PowerPac 200/2.0 Power supply	Bio-Rad Laboratories, München, Germany
PTC-200™ Thermal cycler	MJ Research, Massachusetts, USA
SE 250 Mighty Small™ mini vertical electrophoresis unit	Hoefer, San Francisco, USA
SE 245 Mighty Small™ Dual Gel Caster	Hoefer, San Francisco, USA
Shaker KL-2	Edmund Bühler, Hechingen
Shaker Ika-Vibrax-VXR VX7	Janke & Kunkel, Staufen, Germany
Sonorex® RK 100 Ultrasonic bath	Bandelin, Berlin, Germany
Spacers for SE 250 Mini-Vertical Gel Units (8 cm × 1.50 mm)	GE Healthcare, München, Germany
SpectraMax® 340 Microplate reader	Molecular Devices, Ismaning, Germany
TE 22 Mighty Small Transfer Tank	Hoefer, San Francisco, USA
15-well Teflon Comb for SE 250 Mini-Vertical Gel Units (2.9 x 1.50 mm)	GE Healthcare, München, Germany
TMS Inverted light microscope	Nikon, Düsseldorf, Germany
Transferpette® Microliter pipettes	Brand, Wertheim, Germany
Transferpette® S -8 Multichannel pipette	Brand, Wertheim, Germany
Ultra-Turrax® T8 Disperser	IKA, Staufen, Germany
Ultrospec 2000 Spectralphotometer	Pharmacia Biotech, Cambridge, UK
Universal 320R Refrigerated Centrifuge	Hettich, Tuttlingen, Germany
Vortexer L-46	Hartenstein, Würzburg, Germany

Equipment	Provider
X-ray Film cassette	Hartenstein, Würzburg, Germany

Laboratory consumables	Provider
Cell culture plastic ware (24- and 96-well plates, 21-cm^2 dishes, 75-cm^2 flasks)	Greiner Bio-one, Frickenhausen, Germany
24-well cell culture inserts (8 µm translucent membranes)	Greiner Bio-one, Frickenhausen, Germany
Cell scrapers (25 cm)	Sarstedt, Nümbrecht; Germany
Cover slips	Carl Roth, Karlsruhe, Germany
Cryovials	Hartenstein, Würzburg, Germany
Filter tips SafeSeal-Tips® professional	Biozym, Hess. Oldendorf, Germany
HPLC Autosampler vials 2 ml	Brown, Wertheim, Germany
HPLC Conical insert (0.3 ml) for vials	Brown, Wertheim, Germany
HPLC Crimp seals with silicone/PTFE septa	Brown, Wertheim, Germany
Hyperfilm™ ECL High performance chemiluminescence film	GE Healthcare, München, Germany
LightCycler480® Multiwell Plate 96	Roche, Mannheim, Germany
LightCycler480® Sealing foil	Roche, Mannheim, Germany
Monovette® S for serum separation 2.7 ml	Sarstedt, Nümbrecht; Germany
Monovette® S (EDTA) for plasma separation 2.7 ml	Sarstedt, Nümbrecht; Germany
Monovette® S needle 20 gauge x 1 ½''	Sarstedt, Nümbrecht; Germany
Needle Sterican®, 26 gauge x 1'', Gr. 18 (Ø 0.45 x 25 mm)	Braun, Melsungen, Germany
Microscopy slides Elka (glass)	Hartenstein, Würzburg, Germany
Pelleted standard rat maintenance diet	SSNIFF, Soest, Germany
0.2-ml PCR tubes	Biozym, Hessisch Oldendorf, Germany
Pipette tips	Sarstedt, Nümbrecht, Germany
Polystyrene cuvettes (10 x 4 x 45 mm)	Sarstedt, Nümbrecht, Germany
Polypropylene microcentrifuge tubes (0.5 ml, 1.5 ml, 2.0 ml)	Sarstedt, Nümbrecht, Germany
Polypropylene conical tubes (5 ml, 10 ml, 15 ml, 50 ml)	Sarstedt, Nümbrecht, Germany
Protran™ nitrocellulose transfer membranes (0.45 µm pore size)	Whatman, Dassel, Germany

Laboratory consumables	Provider
Rotilabo® syringe filters (Ø 0.22 µm)	Carl Roth, Karlsruhe, Germany
Saran® foil	Dow, Schwalbach/Ts, Germany
Serological pipettes (2 ml, 5 ml, 10 ml, 25 ml)	Sarstedt, Nümbrecht, Germany
Scalpels	Braun, Melsungen, Germany
Syringe "INJECT" 2 ml	Braun, Melsungen, Germany

4.1.2 Chemicals and standards

Chemicals	Provider
Acetic acid	Carl Roth, Karlsruhe, Germany
Acrylamide 30%	Carl Roth, Karlsruhe, Germany
Agarose (Biozym LE Agarose)	Biozym, Hessisch Oldendorf, Germany
Albumin Fraction V	Carl Roth, Karlsruhe, Germany
Ammonium persulfate (APS) $(NH4)_2S_2O_8$	Carl Roth, Karlsruhe, Germany
Boric acid	Carl Roth, Karlsruhe, Germany
Bovine Serum Albumine (BSA)	PAA Laboratories, Cölbe, Germany
Bromphenol blue	Carl Roth, Karlsruhe, Germany
5-Bromo-2-deoxyuridine	Sigma-Aldrich, Taufkirchen, Germany
4-[[4-(4-Chlorophenyl)-2-thiazolyl]amino]-phenol (SKI II)	Cayman Chemicals, Ann Arbor, USA
Crystal violet	Serva, Heidelberg, Germany
Diethylpyrocarbonate (DEPC)	
DEPC-treated (DEPC) H_2O (autoclaved and sterile)	Carl Roth, Karlsruhe, Germany
Dimethylsulfoxide (DMSO)	Carl Roth, Karlsruhe, Germany
Disodium hydrogen phosphate dihydrate (Na_2HPO_4 x 2 H_2O)	Carl Roth, Karlsruhe, Germany
Dulbecco's modified Eagle's medium (DMEM) high glucose (4.5 g/l)	PAA Laboratories, Cölbe, Germany
Eosin G	Carl Roth, Karlsruhe, Germany
Ethanol	Carl Roth, Karlsruhe, Germany
Ethidium bromide	Sigma-Aldrich, Taufkirchen, Germany
Ethyl acetate	Carl Roth, Karlsruhe, Germany
Ethylenediaminetetraacetic acid (EDTA)	Sigma-Aldrich, Taufkirchen, Germany
Eukitt®	Sigma-Aldrich, Taufkirchen, Germany
Fetal Calf Serum (FCS)	PAA Laboratories, Cölbe, Germany

Chemicals	Provider
Formamide	Carl Roth, Karlsruhe, Germany
Formic acid	Sigma-Aldrich, Taufkirchen, Germany
Fumonisin B_1 (FB_1)	Cayman Chemicals, Ann Arbor, USA
Gelatin	USB, Cleveland, USA
L-Glutamine	PAA Laboratories, Cölbe, Germany
Glycerin	Carl Roth, Karlsruhe, Germany
Glycin	Carl Roth, Karlsruhe, Germany
Hemalum solution (according to Mayer)	Carl Roth, Karlsruhe, Germany
Hydrochloric acid (HCl) 37%	Carl Roth, Karlsruhe, Germany
HPLC Grade Water	Carl Roth, Karlsruhe, Germany
HPLC Grade Methanol	Carl Roth, Karlsruhe, Germany
Hydrogen peroxide 30%	Carl Roth, Karlsruhe, Germany
Isopropanol	Sigma-Aldrich, Taufkirchen, Germany
β-Mercaptoethanol	Sigma-Aldrich, Taufkirchen, Germany
Methanol	Carl Roth, Karlsruhe, Germany
3-(N-morpholino)propanesulfonic acid (MOPS)	Carl Roth, Karlsruhe, Germany
MTT tretrazolium salt (3-(4,5-Dimethylthiazol-2-yl)-2,5-diphenyl-tetrazolium bromide	Sigma-Aldrich, Taufkirchen, Germany
Non-essential amino acids (NEAA)	PAA Laboratories, Cölbe, Germany
Non-fat dried milk powder	Applichem, Darmstadt, Germany
Nonidet® P-40 Substitute	Fluka, Buchs, Switzerland
Penicillin/Streptomycin	PAA Laboratories, Cölbe, Germany
Ponceau S	Sigma-Aldrich, Taufkirchen, Germany
Potassium chloride KCl	Applichem, Darmstadt, Germany
Potassium dihydrogen phosphate	Carl Roth, Karlsruhe, Germany
Primers (forward and reverse)	Biomers, Ulm, Germany
Protease Inhibitor Cocktail (PIC)	Sigma-Aldrich, Taufkirchen, Germany
Roti®-Histol	Carl Roth, Karlsruhe, Germany
Saline (0.9% sodium chloride solution), sterile-filtered	Sigma-Aldrich, Taufkirchen, Germany
Sodium acetate trihydrate $Na(CH_3COO) \times 3\ H_2O$	Carl Roth, Karlsruhe, Germany
Sodium chloride NaCl	Carl Roth, Karlsruhe, Germany
Sodium desoxycholate	Carl Roth, Karlsruhe, Germany
Sodium dodecyl sulfate (SDS) Pellets	Carl Roth, Karlsruhe, Germany

Chemicals	Provider
Sodium fluoride	Sigma-Aldrich, Taufkirchen, Germany
Sodium hydroxide	Carl Roth, Karlsruhe, Germany
Sodium orthovanadate Na_3VO_4	Sigma-Aldrich, Taufkirchen, Germany
D-*erythro*-sphingosine 1-phosphate	Cayman Chemicals, Ann Arbor, USA
N,N,N',N'-tetramethyl-ethane-1,2-diamine (TEMED)	Sigma-Aldrich, Taufkirchen, Germany
Tris-HCl	Carl Roth, Karlsruhe, Germany
Tris (tris(hydroxymethyl)aminomethane) base	Carl Roth, Karlsruhe, Germany
Triton X-100	Sigma-Aldrich, Taufkirchen, Germany
0.4% Trypan blue solution (w/v), sterile-filtered	Sigma-Aldrich, Taufkirchen, Germany
Trypsin/EDTA (sterile)	Sigma-Aldrich, Taufkirchen, Germany
Tween® 20	Carl Roth, Karlsruhe, Germany

Standards	Provider
D-*erythro*-sphinganine (C17 base)	Avanti Polar Lipids, Alabaster, USA
D-*erythro*-sphinganine 1-phosphate	Avanti Polar Lipids, Alabaster, USA
D-*erythro*-sphinganine-1-phosphate (C17 base)	Avanti Polar Lipids, Alabaster, USA
D-*erythro*-sphingosine	Avanti Polar Lipids, Alabaster, USA
D-*erythro*-sphingosine (C17 base)	Avanti Polar Lipids, Alabaster, USA
D-*erythro*-sphingosine-1-phosphate	Avanti Polar Lipids, Alabaster, USA
D-*erythro*-sphingosine 1-phosphate (C17 base)	Avanti Polar Lipids, Alabaster, USA
N-heptadecanoyl-D-*erythro*-sphingosine (C17 Ceramide)	Avanti Polar Lipids, Alabaster, USA
N-oleoyl-D-*erythro*-sphingosine	Avanti Polar Lipids, Alabaster, USA
N-palmitoyl-D-*erythro*-sphingosine	Avanti Polar Lipids, Alabaster, USA
N-stearoyl-D-*erythro*-sphingosine	Avanti Polar Lipids, Alabaster, USA
Protein standard II (lyophilized BSA)	Bio-Rad Laboratories, München, Germany

4.1.3 Buffers and solutions

Buffers and solutions	Preparation
BrdU *i.p.* solution (10 mg/ml) for animal treatment	350 mg BrdU in 35 ml sterile saline; sterile-filtered
0.2% Crystal violet dye solution for invasion assay	40 mg crystal violet in 20 ml 2% aqueous ethanol
DAB (3,3'-diaminobenzidine) solution for BrdU In-Situ Detection Kit	1 drop DAB chromogen (Kit) per 1 ml DAB buffer
DAB solution for FragEL™ DNA Fragmentation Detection Kit	1 tablet of DAB chromogen (Kit) + 1 tablet of H_2O_2/Urea (Kit) per 1 ml water
DNAse I stock solution for RNA isolation (RNase-Free DNase Set)	Lyophilized DNAse I in 550 µl RNAse-free water (Kit)
DNAse I working solution for RNA isolation (RNase-Free DNase Set)	1:8-dilution of DNAse I stock solution in RDD buffer (Kit)
1% Eosin G dye solution for H&E staining	10 g Eosin G in 1000 ml deionized water
FB_1 stock solution (1mM) for cell culture treatment	1 mg FB_1 in 1.385 ml sterile, deionized H_2O
Freezing medium for NRK-52E cells	10% FCS (final 20%), 10% DMSO in NRK-52E medium (see Table 24)
2% Gelatin solution	1 g gelatin solution in 50 ml deionized water; autoclavation (30 min)
3% H_2O_2 solution	1:10-dilution of 30% H_2O_2 in 1x PBS
10x PBS (phosphate buffered saline)	26.8 mM KCl, 1.4 M NaCl, 32.1 mM Na_2HPO_4 x 2 H_2O, 14.7 mM KH_2PO_4 in deionized H_2O
1x PBS buffer	1:10 dilution of 10x PBS in deionized water; adjustment to pH 7.4 with HCl
10x MOPS buffer for RNA electrophoresis	200 mM MOPS, 50 mM sodium acetate, 10 mM EDTA in deionized H_2O; adjustment to pH 7.0 with HCl, treatment with 0.1% DEPC and autoclavation
5x and 1x MOPS buffer	1:2 and 1:10-dilution of 10x MOPS in DEPC-water
MTT solubilisation solution	Isopropanol:Triton X-100: 37% Hcl (89:10:1; v:v:v)
MTT stock solution (5 mg/ml)	25 mg MTT in 5 ml 1x PBS
Ponceau S dye for membrane staining	0.1% Ponceau S in 5% aqueous acetic acid
BSA standard for DC assay® (1.48 mg/ml) (Protein standard II)	14.8 mg lyophilized BSA in 10 ml deionized water

Buffers and solutions	Preparation
RIPA (radio immune-precipitation assay) lysis buffer	50 mM Tris-HCl, 150 mM NaCl, 1 mM EDTA, 0.25% sodium desoxycholate, 1% Nonidet P-40 Substitute in deionized H_2O; adjustment to pH 7.4 with HCl; working solution contains freshly added protease inhibitors (5 µg/ml of each PIC, 200 mM NaF and Na_3VO_4)
RLT working lysis buffer for RNA isolation (RNeasy® Mini Kit)	10 µl β-mercaptoethanol per 1 ml RLT buffer (Kit)
10x RNA loading buffer	50% glycerin, 0.25% Bromphenol blue, 1 mM EDTA in DEPC-water
Stripping buffer for membranes	62.5 mM Tris-HCl (pH 6.8), 2% SDS, 0.1 M β-mercaptoethanol in deionized water
5x TBE (Tris-Borate-EDTA) buffer for DNA electrophoresis	446 mM Tris base, 445 mM boric acid, 10 mM EDTA in deionized water; adjustment to pH 8.0 with NaOH
1x TBE buffer	1:5-dilution of 5x TBE in deionized water
10x TBS (Tris buffered saline)	500 mM Tris-HCl, 1.5 M NaCl in deionized H_2O, adjustment to pH 7.4 with HCl
1x TBS buffer	1:10 dilution of 10x TBS in deionized water
1x TBST (TBS-Tween®) buffer	0.1% Tween® 20 in 1x TBS buffer
Transfer buffer for Western Blotting	25 mM Tris base, 192 mM Glycin, 20% Methanol in deionized H_2O

4.1.4 Commercial kits and reagents

Product	Provider
BrdU *In-Situ* Detection Kit	BD Biosciences, Heidelberg, Germany
DC Assay®	Bio-Rad Laboratories, München, Germany
6x Orange G Loading Buffer (DNA)	PEQLAB, Erlangen, Germany
ECL Western Blotting Reagents	GE Healthcare, Freiburg, Germany
FastStart® PCR Master mix	Roche, Mannheim, Germany
FragEL™ DNA Fragmentation Detection Kit	Merck, Darmstadt, Germany
LightCycler® 480 SYBR Green I Master mix	Roche, Mannheim, Germany
PeqGOLD 50 bp DNA Ladder Orange G	PEQLAB, Erlangen, Germany
PeqGOLD Protein Marker IV	PEQLAB, Erlangen, Germany

Product	Provider
QIAshredder	Qiagen, Hilden, Germany
RNase-Free DNase Set	Qiagen, Hilden, Germany
RNeasy® Mini Kit	Qiagen, Hilden, Germany
Rat Cancer PathwayFinder™ RT² Profiler™ PCR Array	SABiosciences, Frederick, USA
RT² First Strand Kit	SABiosciences, Frederick, USA
2x RT² qPCR SYBR® Green Mastermix	SABiosciences, Frederick, USA
RT² RNA QC PCR Array (Rat)	SABiosciences, Frederick, USA
Sample Buffer, Laemmli 2x concentrate	Sigma-Aldrich, Taufkirchen, Germany
Verso™ cDNA Kit	Thermo Fisher Scientific, Dreieich, Germany

4.1.5 Oligonucleotides for polymerase chain reaction (PCR)

Gene	Description	Forward (FW) and reverse (RV) primer (5'-3') for quantitative Real-time PCR (qRT-PCR)	Reference
PAI-1	Plasminogen activator inhibitor-1	FW: GACTGACATCTTCAGCTCAACCC RV: TCACCTCGATCTTGACCTTTTGT	(Pereira *et al.*, 2006)
Thbs1	Thrombospondin-1	FW: AACGTGGATCAGAGGGACAC RV: GTCATCGTCATGGTCACAGG	(Zhou *et al.*, 2010)
Itga2	Integrin, alpha 2	FW: TTGCTGCATCAACTTTCCAG RV: GTGGGCACTTCTGCTTTCTC	(Leonardi-Essmann *et al.*, 2005)
Actb	Actin, beta	FW: GGGAAATCGTGCGTGACATT RV: GCGGCAGTGGCCATCTC	(Depreter *et al.*, 2002)
$S1P_1$	Sphingosine 1-phosphate receptor 1	FW: CTGACCTTCCGCAAGAACATCT RV: CTTCAGCAAGGCCAGAGACTTC	(Novgorodov *et al.*, 2007)
$S1P_2$	Sphingosine 1-phosphate receptor 2	FW:GCCTTGTACGTCCGAATCTACTTC RV: AGCGTCTGAGGACCAGCAA	(Novgorodov *et al.*, 2007)
$S1P_3$	Sphingosine 1-phosphate receptor 3	FW: ACGCGCGCATCTACTTCCT RV: TGGATCTCTCGGAGTTGTGGTT	(Novgorodov *et al.*, 2007)
Gene	**Description**	**Forward (FW) and reverse (RV) primer (5'-3') for reverse transcriptase PCR (RT-PCR)**	**Reference**
$S1P_1$	Sphingosine 1-phosphate receptor 1	FW: CTTCAGCCTCCTTGCTATCG RV: GCAGGCAATGAAGACGACACTCA	(Coste *et al.*, 2008)
$S1P_2$	Sphingosine 1-phosphate receptor 2	FW: TTCTGGTGCTAATCGCAGTG FV: GAGCAGAGAGTTGAGGGTGG	(Coste *et al.*, 2008)

Gene	Description	Forward (FW) and reverse (RV) primer (5'-3') for reverse transcriptase PCR (RT-PCR)	Reference
$S1P_3$	Sphingosine 1-phosphate receptor 3	FW: TCAGGGAGGGCAGTATGTTC RV: CTGACTCTTGAAGAGGATGG	(Coste *et al.*, 2008)

4.1.6 Software

Software	Provider
Analyst® software 1.4.2	Applied Biosystems, Darmstadt, Germany
BLAST®	http://blast.ncbi.nlm.nih.gov/Blast.cgi
ChemBioOffice 2010	CambridgeSoft, Cambridge, USA
EisenLab (Cluster 2.11 and TreeView 1.6)	http://www.eisenlab.org/eisen/?page_id=42
GraphPad Prism® 5	STATCON, Witzenhausen, Germany
Ingenuity® pathway analysis software	Ingenuity® Systems, Redwood City, USA
LightCycler®480 SW 1.5	Roche, Mannheim, Germany
Multi-analyst® software	Bio-Rad Laboratories, München, Germany
Nanodrop 2000 software	Thermo Fisher Scientific, Dreieich, Germany
SoftMax® Pro	Molecular Devices, Ismaning, Germany

4.1.7 Antibodies

Antibody [Western blot dilution]	Provider
Monoclonal mouse PCNA (PC-10) [1:500]	Santa Cruz, Heidelberg
Goat-anti mouse IgG-HRP [1:5000]	Santa Cruz, Heidelberg

4.2 Methods

4.2.1 Short-term toxicity study in male Sprague Dawley rats

A short-term toxicity study was designed to investigate the early time- and dose-dependent transcriptional response to FB_1 in kidney and livers of male Sprague Dawley rats following short-term *intraperitoneal* (*i.p.*) administration of 0.25 and 0.75 mg/kg bw/d FB_1 for 1 and 6 days. The expression of cancer-related genes (see chapter 4.2.3, Table 8) in kidneys and livers was analyzed to relate FB_1-mediated changes in the transcriptional profile to histopathological changes, particularly to apoptosis and regenerative cell proliferation. Furthermore, biochemical alterations in sphingolipids in kidney and liver were investigated to establish a link between the observed histopathological and transcriptional changes and the FB_1-induced imbalance in sphingolipids known to be involved in cell death and cell proliferation.

4.2.1.1 Study rational

Choice of strain (Sprague Dawley), selection of dose and dose regimen were based on short-term studies, demonstrating that *intraperitoneal* (*i.p*.) administration of FB_1 to male Sprague Dawley rats caused histopathological changes (Bondy *et al.*, 2000) and markedly increased levels of sphinganine and sphingosine in rat kidney (Domijan *et al.*, 2007b) comparable to those seen in FB_1-treated male Fischer F344N rats administered known carcinogenic doses *via* feed (NTP, 2001).

4.2.1.2 Animal housing

Male Sprague Dawley rats weighing 151-175 g were purchased from a commercial supplier (Harlan-Winkelmann GmbH, Borchen, Germany) and acclimatized for 1 week under standard laboratory conditions (temperature of 21-23 °C, relative humidity of 45-55%, 12-15 air changes per hour and a 12 hour light/dark cycle) in climate cabinets. Animals were housed in groups of 4 in Makrolon® type-4 cages with wire mesh tops and standard softwood bedding. Animals received pelleted standard rat maintenance diet (Ssniff, Spezialdiäten GmbH, Soest) and water *ad libitum*.

4.2.1.3 Animal treatment

A stock solution of FB_1 representing the high dose formulation (0.75 mg/ml) was prepared by dissolving FB_1 (15 mg) in 20 ml sterile saline (0.9% NaCl). The lower concentration (0.25 mg/ml) was obtained by diluting 5 ml of FB_1 stock solution (0.75 mg/ml) in 10 ml sterile saline to a total volume of 15 ml. The dosing solutions (0.75 mg/ml and 0.25 mg/ml) were sterile filtered, aliquoted in sterile 1.5-ml microcentrifuge tubes and stored at -20 °C until use. All dilution and aliquotation steps were conducted under a laminar flow clean bench to guarantee sterility of the treatment solutions.

At the beginning of each treatment day, respective aliquots of FB_1 dosing solutions were thawed and animals were weighed to calculate the volume of the dosing solutions required to obtain the desired FB_1 dose for each individual animal. In the morning, animals (n=4) were *i.p*. injected with the respective FB_1 dosing solutions corresponding to 0.25 or 0.75 mg/kg bw/d, while sterile saline (max. 280 µl) was injected as vehicle for animals (n=4) of the control group (Table 4).

Table 4: Treatment schedule for the short-term toxicity study with FB_1 in male Sprague Dawley (SD) rats.

Allocation		**FB_1 dose [mg/kg bw/d]**		
Male SD rats	Treatment time	0	0.25	0.75
A	1 day	1 – 4	5 – 8	9 – 12
B	6 days	13 – 16	17 – 20	21 – 24

A – Sacrifice after 1 day of treatment; B – Sacrifice after 6 days of treatment

On each treatment day, animals were observed for viability, mortality, and behavior. Clinical signs of toxicity, body weights and consumption of food and water were recorded daily. Before sacrifice, animals were fasted in metabolism cages for approximately 12 hours, but allowed access to water *ad libitum*. Urine samples were collected on ice during the 12 hours fasting period into specimen vials. Urine was weighed, aliquoted and frozen at -80 °C until further use.

4.2.1.4 Animal sacrifice and necropsy

On the day of sacrifice, a 10 mg/ml solution of BrdU in sterile saline was prepared and sterile filtered under a laminar flow bench. Two hours prior to sacrifice, animals

were *i.p.* administered a single dose of 100 mg/kg bw/d BrdU to allow assessment of cell proliferation *via* incorporation of BrdU into newly synthesized DNA.

At the end of each treatment period (after 1 or 6 days), animals were weighed and killed by CO_2 asphyxiation followed by cardiac puncture for blood collection. Blood for the preparation of serum was collected into a 2.7-ml serum tube (Sarstedt), containing a clotting activator. To obtain plasma, blood was collected into a 2.7-ml EDTA-tube (Sarstedt). Plasma samples collected in EDTA-tubes were immediately centrifuged for 10 min at 2500 x g to separate erythrocytes and plasma. Blood samples collected in serum tubes (Sarstedt) were allowed to clot at room temperature (approximately 1-2 h) and centrifuged at 2,000 x g and 4 °C for 10 minutes to separate the serum from the clotted plasma. Serum plasma samples were aliquoted and stores at -80 °C until further use.

At necropsy, all macroscopic abnormalities and organ weights of kidney and liver were recorded. Kidneys were cut longitudinally and ½ of the right kidney and an aliquot of the left liver lobe were fixed in 10% neutral buffered formalin for histological evaluation. The remaining kidney and liver tissue was aliquoted, flash frozen in liquid nitrogen and stored at -80 °C until further use.

4.2.1.5 Clinical chemistry of serum and urine

One aliquot of each serum (500 µl) and urine (1000 µl) sample was sent to the Laboratory of Clinical Chemistry (University of Würzburg) for analysis. The following clinical parameters were determined in serum:

- Glucose
- Urea
- Creatinine
- Bilirubin, total
- Cholesterol, total
- Triglycerides
- Aspartate aminotransferase
- Alanine aminotransferase
- Lactate dehydrogenase
- Glutamate dehydrogenase
- Creatine kinase
- Alkaline phosphatase
- Gamma-glutamyl-transferase
- Sodium
- Potassium
- Chloride
- Calcium
- Phosphorus inorganic
- Protein, total
- Albumin

In urine, the following parameters were analyzed:

- Volume (12 hours)
- Specific gravity (relative density)
- Osmolality
- Color
- Appearance
- pH
- Protein
- Phosphate
- Calcium
- Potassium
- Sodium
- Creatinine
- Glucose
- Ketones
- Urobilinogen
- Bilirubin
- Erythrocytes
- Leukocytes

Mean and standard deviation (SD) of analyzed data were calculated for each control and treatment group (n=4 animals per group). Statistical analysis was performed by one-way analysis of variance (ANOVA) and Dunnett's *post hoc* test using GraphPad Prism® 5 (STATCON) software to compare the mean ± SD of the control group to the mean of each treatment group. Statistically significant changes to controls are indicated by * $p < 0.05$, ** $p < 0.01$ and *** $p < 0.001$.

4.2.1.6 Histopathology

For the assessment of histopathological alterations, formalin fixed kidneys and livers were embedded in paraffin and tissue sections were cut at an approximate thickness of 2 µm using a Microtome (Leica) and placed on a glass microscopy slide (Elka). To structurally distinguish the different components of the cells, sections were stained with hematoxylin/eosin (H&E) dye. Whereas hematoxylin stains basophilic structures like cell nuclei or ribosomes of the rough endoplasmic reticulum with a blue color, counterstaining with eosin results in red or pink staining of eosinophilic structures, such as cytoplasm and connective tissue. Before staining with hematoxylin/eosin, paraffin was removed from the tissue sections by transferring the slides several times (3 x 4 min) in the limonene-containing Roti®Histol solution (Roth), which serves as substitute for xylol-based deparaffination. Afterwards, deparaffinized tissue sections were rehydrated in a descending series of alcohol concentrations (3 x 2 min 100% Ethanol and 1 x 2 min 70% Ethanol) and rinsed with deionized water (4 x 30 sec). For the staining procedure, tissue sections were first incubated in an alum hematoxylin

solution according to Mayer (Roth) for 1.5 min and then rinsed for 10 min in running tap water. Then, counterstaining was performed by transferring the slides into a 1% aqueous Eosin G solution for 30 sec and immediately rinsing in deionized water (3 x 30 sec). For dehydration of the tissue sections, slides were passed through an ascending series of alcohol concentrations (1 x 1 min 70% Ethanol and 4 x 2 min 100% Ethanol). Then, tissue sections were immersed in Roti®Histol (2x for 2 min) and embedded with 1 drop of the mounting medium Eukitt® and a cover slip.

Microscopic evaluation of tissue sections was performed at 200x and 400x magnification using a light microscope (Olympus CH-2).

4.2.1.7 Determination of apoptosis – TUNEL (TdT-mediated dUTP-biotin nick end labeling) assay

Apoptosis was assessed by using the TUNEL assay, which detects apoptosis-induced fragmentation of DNA caused by endonuclease activity. Apoptotic cells were visualized on formalin-fixed paraffin-embedded kidney sections by using the TdT-FragEl™ DNA Fragmentation Detection Kit (Merck Calbiochem, Darmstadt, Germany) according to the manufacturer's instructions (www.emdchemicals.com).
The recognition of apoptotic cells is based on the binding of terminal deoxynucleotidyl transferase (TdT) to the 3'-OH ends of apoptotic DNA fragments. Then, DNA-bound TdT enzymatically catalyzes the addition of biotin-labeled and unlabeled deoxynucleotides. After streptavidin-horseradish peroxidase (HRP) conjugate is bound to biotinylated nucleotides, the peroxidase substrate 3,3'-diaminobenzidine (DAB) is applied to generate an insoluble colored product at the site of DNA fragmentation of labeled samples.

For the TUNEL assay, kidney sections were deparaffinized by immersing the slides twice in Roti®Histol for 5 min. Then, a descending series of alcohol concentrations (2 x 5 min 100% Ethanol, 1 x 3 min 90% Ethanol, 1 x 3 min 80% Ethanol and 1 x 3 min 70% Ethanol) was used to dehydrate the kidney sections. After briefly washing the deparaffinized slides with 1x TBS, kidney sections were incubated with 100 µl proteinase K solution (20 µg/ml) for 20 min at RT to permeabilize cell membranes and to inactivate DNA-degrading nucleases. Then, slides were rinsed with 1x TBS and were incubated with 3% H_2O_2 for 5 min at RT to inactivate endogenous peroxidase activity, and rinsed again with 1x TBS. For labeling of apoptotic DNA fragments,

slides were incubated with 1x TdT equilibration buffer for 20 min at RT, followed by incubation of each slide with 80 µl of freshly prepared TdT labeling reaction mix (1:5 diluted with deionized water) for 1.5 h at 37 °C in a humidified chamber. To terminate the labeling reaction, kidney slides were washed with 1x TBS and incubated with 100 µl stop solution for 5 min at RT. Subsequently, slides were incubated with blocking buffer for 10 min at RT and the streptavidin-HRP conjugate was freshly prepared by 1:50 dilution in blocking buffer. To bind biotin-labeled apoptotic DNA fragments, kidney sections were incubated with strepatavidin-HRP for 30 min at RT in a humidified chamber. Then, slides were rinsed with 1x TBS and incubated with 100 µl freshly prepared DAB solution (containing H_2O_2 and urea, see 4.1.3) for 15 min at RT. In the presence of H_2O_2, the colorless DAB reacts with the streptavidin-coupled horseradish peroxidase to generate an insoluble brown chromagen at the site of DNA-labeling. To stop the DAB reaction after 15 min incubation, slides were briefly washed in deionized water. Finally, slides were stained with H&E dye, dehydrated and embedded in 1 drop of Eukitt® mounting medium (see section 4.2.1.6).

The apoptotic index in kidney was determined as the percentage of the number of tubular epithelial cells which acquired brown nuclear staining per total number of nuclei within the tubular epithelium per field counted at 400x magnification using a light microscope (OLYMPUS CH-2). Mean and SD of apoptotic indices were calculated for each control and treatment group (n=4 animals per group). Statistical analysis was performed by one-way analysis of variance (ANOVA) and Dunnett's *post hoc* test using GraphPad Prism® 5 (STATCON) software to compare the mean ± SD of the control group to the mean of each treatment group. Statistically significant changes to controls are indicated by * $p < 0.05$, ** $p < 0.01$ and *** $p < 0.001$.

4.2.1.8 Determination of cell proliferation – BrdU immunohistochemistry

Cell proliferation in kidneys was visualized using the BrdU technique. BrdU, which was *i.p*. administered to Sprague Dawley rats two hours before necropsy, is a synthetic base analogue of thymidine that becomes incorporated into newly synthesized DNA during S phase. Detection of BrdU-positive cell nuclei in kidney was performed on formalin-fixed paraffin-embedded tissue sections using the BrdU In-situ detection kit (BD Biosciences, Heidelberg, Germany) according to the manufacturer's instructions (www.bdbiosciences.com).

Deparaffinized kidney slides (see section 4.2.1.6) were briefly washed in deionized water several times and endogenous peroxidase activity was blocked by 20 min incubation with 3% H_2O_2 in 1x PBS. After repeatedly rinsing the slides in 1x PBS, they were placed in a coplin jar containing "Retrievagen A" buffer and heated for 10 minutes at 89 °C in the microwave to unmask the antigen epitope for antibody binding. The heated kidney slides in the coplin jar were then cooled down to RT for approximately 45 min and washed several times in 1x PBS. After the biotinylated anti-BrdU antibody was diluted 1:10 in the Diluent Buffer, 100 µl of this solution were carefully distributed on each kidney section and slides were incubated for 1 h at RT in a humidified chamber. The antibody-treated slides were repeatedly rinsed in 1x PBS and incubated with Streptavidin-HRP for 30 min at RT in a humidified chamber. In the next step, they were washed several times in 1x PBS and 600 µl of the freshly prepared DAB substrate solution (see 4.1.3) was applied to the kidney sections. Slides were incubated for 5 minutes or less until the desired color intensity developed. To stop the DAB staining, slides were briefly washed in deionized water. Finally, slides were stained with H&E dye, dehydrated and embedded in 1 drop of Eukitt® mounting medium (see section 4.2.1.6).

The mitotic index in kidney was determined as the percentage of the number of tubule epithelial cells which acquired brown nuclear staining per total number of nuclei within the tubular epithelium per field counted at 400x magnification using a light microscope (OLYMPUS CH-2). Mean and SD of apoptotic indices were calculated for each control and treatment group (n=4 animals per group). Statistical analysis was performed by one-way analysis of variance (ANOVA) and Dunnett's *post hoc* test using GraphPad Prism® 5 (STATCON) software. Statistically significant changes to controls are indicated by * $p < 0.05$, ** $p < 0.01$ and *** $p < 0.001$.

4.2.2 RNA isolation for gene expression analysis

RNA isolation was performed using the silica membrane column-based technology of the RNeasy® Mini Kit (Qiagen) according to the manufacturer's instructions (www.qiagen.com).

4.2.2.1 RNA extraction from tissue

100 mg of frozen tissue samples (kidney or liver) were weighed and homogenized using a manual tissue homogenizer with 2 ml RLT lysis buffer containing guanidinium-thiocyanate and β-mercaptoethanol for cell lysis and inactivation of RNAses. After homogenization, tissue lysates were transferred into autoclaved 2-ml microcentrifuge tubes, collected on ice and subsequently centrifuged at 8,000 rpm and 4 min for 10 min. 350 µl of each sample supernatant were placed in an autoclaved 1.5-ml microcentrifuge tube and homogenized with the same volume of 70% ethanol. Then, 700 µl of each sample lysate-ethanol mixture were applied to a RNeasy mini spin column inserted into a 2-ml collection tube and centrifuged at 11,000 rpm for 15 s. The flow-through was discarded.

RNeasy mini spin columns were washed with 350 µl RW1 buffer, which contains ethanol and guanidinium-thiocyanate, to remove any contaminants. Following centrifugation at 11,000 rpm for 15 s, the eluate was discarded and 80 µl of freshly prepared DNAse I solution was loaded onto the RNeasy mini spin column and incubated for 15 min at room temperature to digest genomic DNA (gDNA). To remove the digested DNA and the DNAse I from the RNA-binding membrane, columns were washed again with 350 µl RW1 buffer and centrifuged at 11,000 rpm for 15 s. Subsequently, columns were placed into fresh 2-ml collection tubes and washed with 500 µl RPE buffer, followed by centrifugation at 11,000 rpm for 15 s. The washing step was repeated and columns were centrifuged at 11,000 rpm for 2 min to dry the RNeasy spin column membrane. To avoid carry-over of ethanol from the washing procedure, columns were placed into new 2-ml collection tubes and were centrifuged at 14,000 rpm for 1 min. Again, collection tubes were discarded and columns were inserted into 1.5-ml microcentrifuge tubes. To eluate the RNA from the silica membrane, 30 µl of RNAse-free water was loaded onto the column membrane and columns were centrifuged at 11,000 rpm for 1 min. The eluation and centrifugation step was repeated to increase the yield of RNA from each sample. Long-term storage of RNA solutions was performed at -80 °C.

4.2.2.2 RNA quantification and determination of purity

The RNA samples were quantified using a Nanodrop 2000C UV-Vis spectrophotometer (Thermo Fisher Scientific) with patented sample retention technology according to the manufacturer's instructions (www.nanodrop.com).

2 µl of each RNA sample were placed onto the optical pedestal, and the nucleic acid concentration was automatically measured by the Nanodrop 2000C spectrophotometer. The Nanodrop 2000 software was used to calculate RNA concentrations after reading the absorbance of nucleic acids at 260 nm. The absorbance at 280 nm was recorded to identify contaminants such as protein. Generally, the ratio of the absorbances at 260 and 280 nm (A_{260}/A_{280}) should be in the range of 1.9–2.1 to ensure pure, contamination-free RNA.

4.2.2.3 RNA electrophoresis for RNA integrity control

RNA integrity is a further criterion for the quality of RNA samples. Using formaldehyde (denaturating) agarose gel electrophoresis, ribosomal RNA (rRNA) can be separated and visualized by ethidium bromide staining. Intact rRNA should appear as two sharp bands on the gel (ratio of 28S rRNA to 18S RNA should be approximately 2:1). If the bands of these subunits appear smeared, degradation of RNA can be assumed.

For RNA electrophoresis, a 1.2% agarose gel was prepared by dissolving 1.2 g agarose in 85 ml sterile, deionized water by carefully heating in the microwave. After cooling to approximately 60 °C, the agarose solution was mixed with 10 ml 10x MOPS buffer and 5 ml 37% formaldehyde. Then, the gel was poured in a horizontal gel cast with inserted 14-well gel comb. After polymerization at RT, the gel was transferred to the chamber of an Owl Separation Systems Model B1 (Thermo Fisher, Scientific) and overlaid with 1x MOPS electrophoresis buffer.

Sample preparation was performed on ice by diluting the RNA in DEPC-water in a sterile microcentrifuge tube to obtain a total amount of 2 µg RNA in 4.7 µl solution. Then, a mastermix for all samples was prepared, which contained formamide and formaldehyde to aid denaturation of RNA (Table 5).

Table 5: Composition of mastermix volume added per RNA sample

Components	Volume per RNA sample [µl]
5x MOPS	2.0
37% Formaldehyde	3.3
Formamide	10.0
Total volume	**15.3**

To each diluted RNA sample (4.7 µl = 2 µg RNA) 15.3 µl of mastermix were added to achieve a total volume of 20 µl per sample. Subsequently, samples were heated at 65 °C for 10 min in a heating block to denature RNA. Then, samples were briefly spun down and 2 µl of 10x RNA loading buffer containing bromphenol blue dye was added. After mixing, the gel combs were removed and the sample (22 µl) was loaded into the wells of the gel. Electrophoresis was performed at 80 V for ~ 1 h, until the bromphenol blue front had reached 2/3 of the gel length. Then, the gel was placed in 100 ml ethidium bromide solution (0.5 µg/ml in sterile, deionized water) and incubated for 15 min. Ethidium bromide intercalates with RNA to form UV-fluorescent complexes, which are visualized under UV light using the transilluminator of the gel documentation system Gel Doc™ 2000 (Biorad). Visual control of the appearing rRNA bands was performed based on the criteria described above. In Figure 10, a representative image of intact total RNA after denaturating agarose gel electrophoresis is shown with sharp bands and proper ratio of the respective RNA subunits.

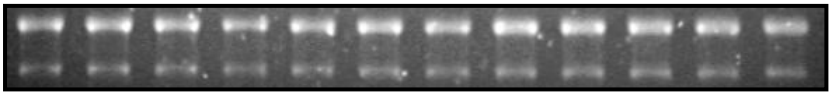

Figure 10: Representative image of intact total RNA after agarose gel electrophoresis. Bands of the ribosomal RNA (rRNA) subunits appear as sharp and distinct bands. The ratio of 28S rRNA to 18S rRNA is approximately 2:1.

4.2.3 Gene expression analysis of cancer-related genes using a quantitative real-time polymerase chain reaction (qRT-PCR) array

Gene expression was analyzed using real-time polymerase chain reaction (PCR), which is a fast and sensitive method to exponentially amplify the DNA sequence of a specific gene (template) during several cycles by using primers (oligonucleotides) complementary to the region in a target gene, and nucleotides (*i.e* deoxynucleoside triphosphates (dNTPs)) as building blocks for the elongation of DNA single strands by the enzyme DNA polymerase. Each PCR cycle consists of three individual temperature steps, mediating (1) the denaturation of double stranded into single stranded DNA, (2) the annealing of sequence-specific primers to the single DNA strand and (3) the enzymatic elongation of the single to double stranded DNA by a heat-stable Taq-polymerase, thereby generating a copy of the template DNA. Under ideal conditions, each DNA strand doubles during each PCR cycle, so that the amount of DNA template exponentially increases with the number of cycles. Thus, a single DNA copy may be amplified by several orders of magnitude during one PCR experiment, which is important for the successful detection of trace amounts of PCR product in a sample.

The relative amount of PCR product can be assessed by qRT-PCR, which is a technique to quantitatively measure a specific sequence amplified from a template (DNA, complementary DNA (cDNA) or RNA) during each PCR cycle of a PCR experiment. For the detection of the PCR product formed during qRT-PCR, SYBR green I fluorescence dye is commonly used, which intercalates between the helices of double stranded DNA, thereby emitting fluorescence of a defined wavelength. At the beginning of each PCR experiment, only weak fluorescence creating a baseline level is present, which subsequently increases with the number of cycles due to the exponential formation of the PCR product. In the exponential phase, fluorescence rapidly exceeds the baseline level until it reaches a plateau for the formation of the PCR product due to product inhibition and depletion of PCR reagents. Since the fluorescence is proportional to the amount of PCR product, quantification of the PCR product based on the emitted fluorescence signal can be performed. To accurately quantify the amount of PCR product from a target sequence, the PCR cycle generating a fluorescence signal exceeding the baseline level is set as the threshold cycle for quantification. The LightCycler® 480 Real-time PCR System, which was

used for qRT-PCR analysis in this work, calculated the threshold cycle based on the second derivative (crossing point, C_p) of the sigmoid curve generated as a function of the recorded fluorescence plotted against the individual PCR cycles of each experiment.

4.2.3.1 cDNA synthesis using the RT² First Strand Kit

The isolated RNA (kidney or cells) was transcribed into cDNA using the RT² First Strand Kit (SABiosciences) according to the manufacturer's instructions (www.sabiosciences.com). This kit is specifically designed for real-time PCR-based gene expression analysis with RT² Profiler™ PCR Arrays (SABioscience) and includes the following components (Table 6):

Table 6: Components of the RT² First Strand Kit

Kit components	Abbreviations	Total volumes
5x gDNA Elimination Buffer	GE	30 µl
5x Reverse Transcription Buffer 3	BC3	60 µl
RNase-free Water	H_2O	1 ml
Primer and External Control Mix	P2	18 µl
Reverse Transcriptase Enzyme Mix 3	RE3 RT mix	28 µl

The kit includes an additional gDNA elimination procedure and a built-in external RNA control to check reverse transcription efficiency and the presence of enzyme inhibitors when used together with a RT² RNA QC PCR Array or the RT² Profiler™ PCR Array.

Before starting cDNA synthesis, kit components were thawed and briefly spun down using a microcentrifuge. In the next step, volumes corresponding to 1 µg of experimental RNA were mixed with 2 µl of GE buffer in a nuclease-free PCR tube and added to a final volume of 10 µl with RNAse-free H_2O. The obtained gDNA elimination mix was carefully mixed with a pipette and incubated for 5 min at 42 °C in a thermocycler (PTC-200™ Programmable Thermal Controller MJ) to remove any gDNA in the samples, which might interfere with the analysis of mRNA (cDNA) expression of target genes. After incubation, samples were cooled down on ice for at least 1 min and the reverse transcription mix for cDNA synthesis was prepared for a total of 12 (+1) samples (Table 7).

Table 7: Reverse transcriptase mix for cDNA syntheses

Kit components	1 reaction [Volume in µl]	12 (+1) reactions [Volume in µl]
5x Buffer BC3	4	52
Control P2	1	13
RE3 RT mix	2	26
H_2O	3	39
Total volume	**10**	**130**

Then, 10 µl of the reverse transcription mix were added to each PCR tube containing 10 µl of gDNA elimination mix and gently resuspendend using a pipette. The cDNA synthesis mixture was placed in a thermocycler (PTC-200™ Programmable Thermal Controller MJ) and incubated at 42 °C for 15 min. Then, the thermocycler was immediately heated to 95 °C for 5 minutes to stop cDNA synthesis by inactivation of the reverse transcriptase and degradation of remaining RNA. After incubation, samples were chilled on ice and each 20 µl cDNA sample was diluted with 91 µl of DEPC-water to obtain a total volume of 111 µl cDNA. Samples were stored at -20 °C until further analysis.

4.2.3.2 qRT-PCR using the RT² Profiler™ PCR Array

Targeted qRT-PCR analysis of 84 genes critically involved in tumor formation and progression was performed to identify pathways possibly modulated by FB_1. Using the Rat Cancer PathwayFinder™ RT² Profiler™ PCR Array (SABiosciences), the expression of the following 84 genes representative of six biological pathways involved in transformation and tumorigenesis (Table 8) were investigated in kidneys of male Sprague Dawley rats and in NRK-52E cells treated with FB_1.

PCR analysis was carried out according to the manufacturer's instructions (www.sabiosciences.com), involving the steps described in the following section.

Table 8: Layout of the Rat Cancer PathwayFinder™ RT² Profiler™ PCR Array, divided into the 6 pathways and 84 representative genes involved in tumorigenesis. For normalization of gene expression and control of PCR quality, 5 housekeeping genes and 7 PCR controls were included in the array.

Cell cycle control and DNA damage repair			
Pos.	Accession no.	Gene Symbol	Gene description
A04	XM_236275	*Atm*	Ataxia telangiectasia mutated homolog (human)
A10	NM_012514	*Brca1*	Breast cancer 1
A12	NM_171992	*Ccnd1*	Cyclin D1
B01	XM_574426	*Ccne1*	Cyclin E
B02	NM_133571	*Cdc25a*	Cell division cycle 25 homolog A (S. pombe)
B04	NM_199501	*Cdk2*	Cyclin dependent kinase 2
B05	NM_053593	*Cdk4*	Cyclin-dependent kinase 4
B06	NM_080782	*Cdkn1a (p21)*	Cyclin-dependent kinase inhibitor 1A
B07	NM_031550	*Cdkn2a (p16)*	Cyclin-dependent kinase inhibitor 2A
B09	NM_053677	*Chek2*	CHK2 checkpoint homolog (S. pombe)
B12	XM_230765	*E2f1*	E2F transcription factor 1
D11	XM_235169	*Mdm2*	Transformed mouse 3T3 cell double minute 2
F04	NM_031606	*Pten*	Phosphatase and tensin homolog
F06	XM_344434	*Rb1*	Retinoblastoma 1
G08	NM_030989	*Tp53*	Tumor protein p53
Apoptosis and Cell Senescence			
Pos.	Accession no.	Gene Symbol	Gene description
A03	NM_023979	*Apaf1*	Apoptotic peptidase activating factor 1
A05	NM_022698	*Bad*	Bcl2-associated death promoter
A06	NM_017059	*Bax*	Bcl2-associated X protein
A07	NM_016993	*Bcl2*	B-cell leukemia/lymphoma 2
A08	NM_031535	*Bcl2l1 (Bcl-XL)*	Bcl2-like 1
A09	NM_022274	*Birc5*	Baculoviral IAP repeat-containing 5
A11	NM_022277	*Casp8*	Caspase 8
B08	NM_057138	*Cflar*	CASP8 and FADD-like apoptosis regulator
F11	NM_053423	*Tert*	Telomerase reverse transcriptase
G05	XM_344431	*Tnfrsf10b_pred*	Tumor necrosis factor receptor superfamily, member 10b (predicted)
G06	NM_013091	*Tnfrsf1a*	Tumor necrosis factor receptor superfamily, member 1a
G07	NM_139194	*Fas (Tnfrsf6)*	Fas (TNF receptor superfamily, member 6)
Signal transduction molecules and transcription factors			
Pos.	Accession no.	Gene Symbol	Gene description
A01	NM_033230	*Akt1*	v-akt thymoma viral proto-oncogene 1
B11	NM_053357	*Ctnnb1*	Catenin (cadherin associated protein), beta 1
C02	XM_239510	*Ets2*	V-ets erythroblastosis virus E26 oncogene homolog 2 (avian)
C06	NM_022197	*Fos*	FBJ murine osteosarcoma viral oncogene homolog
C07	NM_030846	*Grb2*	Growth factor receptor bound protein 2
D07	NM_021835	*Jun*	Jun oncogene
D09	NM_031643	*Map2k1*	Mitogen activated protein kinase kinase 1

Signal transduction molecules and transcription factors

Pos.	Accession no.	Gene Symbol	Gene description
E06	NM_012603	*Myc*	Myelocytomatosis viral oncogene homolog (avian)
E08	XM_342346	*Nfκb1*	Nuclear factor of kappa light chain gene enhancer in B-cells 1, p105
E09	XM_343065	*Nfκbia (IκBα)*	Nuclear factor of kappa light chain gene enhancer in B-cells inhibitor, alpha
F01	NM_013005	*Pik3r1*	Phosphatidylinositol 3-kinase, regulatory subunit, polypeptide 1
F05	NM_012639	*Raf1*	V-raf-1 murine leukemia viral oncogene homolog 1

Adhesion

Pos.	Accession no.	Gene Symbol	Gene description
B03	NM_031334	*Cdh1*	Cadherin 1
C09	NM_012967	*Icam1*	Intercellular adhesion molecule 1
D01	XM_345156	*Itga2*	Integrin, alpha 2
D02	XM_340884	*Itga3_pred*	Integrin alpha 3 (predicted)
D03	XM_230033	*Itga4*	Integrin alpha 4
D04	XM_230950	*Itgav_pred*	Integrin alpha V (predicted)
D05	NM_017022	*Itgb1*	Integrin beta 1 (fibronectin receptor beta)
D06	NM_153720	*Itgb3*	Integrin beta 3
D10	NM_023983	*Mcam*	Melanoma cell adhesion molecule
E07	NM_031521	*Ncam1*	Neural cell adhesion molecule 1

Angiogenesis

Pos.	Accession no.	Gene Symbol	Gene description
A02	NM_053546	*Angpt1*	Angiopoietin 1
B10	XM_241632	*Col18a1*	Procollagen, type XVIII, alpha 1
C01	NM_031507	*Egfr*	Epidermal growth factor receptor
C03	NM_012846	*Fgf1*	Fibroblast growth factor 1
C04	XM_341940	*Fgfr2*	Fibroblast growth factor receptor 2
C05	NM_031761	*Figf*	C-fos induced growth factor
C08	NM_017017	*Hgf*	Hepatocyte growth factor
C10	NM_001014786	*Ifna1*	Interferon-alpha 1
C11	NM_019127	*Ifnb1*	Interferon beta 1, fibroblast
C12	NM_178866	*Igf1*	Insulin-like growth factor 1
E11	NM_012801	*Pdgfa*	Platelet derived growth factor, alpha
E12	XM_343293	*Pdgfb*	Platelet derived growth factor, B polypeptide
F10	XM_342863	*Tek*	Endothelial-specific receptor tyrosine kinase
F12	NM_021578	*Tgfb1*	Transforming growth factor, beta 1
G01	NM_012775	*Tgfbr1*	Transforming growth factor, beta receptor 1
G02	NM_001013062	*Thbs1 (TSP-1)*	Thrombospondin 1
G04	NM_012675	*Tnf*	Tumor necrosis factor (TNF superfamily, member 2)
G10	NM_031836	*Vegfa*	Vascular endothelial growth factor A
G11	NM_053549	*Vegfb*	Vascular endothelial growth factor B
G12	NM_053653	*Vegfc*	Vascular endothelial growth factor C

Invasion and metastasis			
Pos.	Accession no.	Gene Symbol	Gene description
D08	NM_181692	*Kiss1*	KiSS-1 metastasis-suppressor
D12	NM_031517	*Met*	Met proto-oncogene
E01	NM_031054	*Mmp2*	Matrix metallopeptidase 2
E02	NM_031055	*Mmp9*	Matrix metallopeptidase 9
E03	NM_022588	*Mta1*	Metastasis associated 1
E04	XM_342015	*Mta2*	Metastasis-associated gene family, member 2
E05	XM_342281	*Muc1*	Mucin 1, transmembrane
E10	NM_138548	*Nme1*	Expressed in non-metastatic cells 1
F02	NM_013085	*Plau (uPA)*	Plasminogen activator, urokinase
F03	NM_017350	*Plaur (uPAR)*	Plasminogen activator, urokinase receptor
F07	NM_012618	*S100a4*	S100 calcium-binding protein A4
F08	NM_021696	*Serpinb2 (PAI-2)*	Serine (or cysteine) proteinase inhibitor, clade B, member 2
F09	NM_012620	*Serpine1 (PAI-1)*	Serine (or cysteine) peptidase inhibitor, clade E, member 1
G03	NM_053819	*Timp1*	Tissue inhibitor of metallopeptidase 1
G09	NM_053530	*Twist1*	Twist gene homolog 1 (Drosophila)
Housekeeping genes			
Pos.	Accession no.	Gene Symbol	Gene description
H01	NM_001007604	*Rplp1*	Ribosomal protein, large, P1
H02	NM_012583	*Hprt*	Hypoxanthine guanine phosphoribosyl transferase
H03	NM_173340	*Rpl13a*	Ribosomal protein L13A
H04	NM_017025	*Ldha*	Lactate dehydrogenase A
H05	NM_031144	*Actb*	Actin, beta
PCR quality controls			
Pos.	Accession no.	Gene Symbol	Gene description
H06	U26919	*RGDC*	Rat Genomic DNA Contamination
H07	SA_00104	*RTC*	Reverse Transcription Control
H08	SA_00104	*RTC*	Reverse Transcription Control
H09	SA_00104	*RTC*	Reverse Transcription Control
H10	SA_00103	*PPC*	Positive PCR Control
H11	SA_00103	*PPC*	Positive PCR Control
H12	SA_00103	*PPC*	Positive PCR Control

The ready-to-use 2x RT^2 qPCR SYBR® Green Mastermix (SABiosciences), containing HotStart *Taq* DNA polymerase, PCR buffer, dNTP mix (dATP, dCTP, dGTP, dTTP) and SYBR® Green dye, was thawed and briefly spun down using a microcentrifuge. Then, the PCR components mix was prepared in a sterile, nuclease-free conical 5-ml tube by gently dispensing the mastermix into the diluted First Strand cDNA sample (Table 9):

Table 9: Composition of the PCR components mix for each diluted cDNA sample

Components	Volume [µl]
2x RT^2 qPCR SYBR® Green Mastermix (1.4-ml vial)	1350
Diluted First Strand cDNA	102
DEPC-water	1248
Total volume	**2700**

Using a multipette® (Eppendorf) with a sterile, nuclease-free 5-ml dispenser tip, 25 µl of the PCR component mix was pipetted into the wells of the RT² Profiler™ PCR Array containing the pre-dispensed forward and reverse primers for each individual gene (see Table 8). After loading the wells, the array was carefully sealed with an optical adhesive film and liquids in the wells were briefly spun down at 2,000 rpm for 20 sec (Labofuge GL, Heraeus Sepatech). Then, plates were placed in a LightCycler® 480 Real-Time PCR instrument (Roche) and qRT-PCR reactions were performed using the following two-step cycling program:

Table 10: qRT-PCR program for the RT² Profiler™ PCR Array

PCR cycles	Duration	Temperature	Process
1	10 min	95 °C	Heat activation of HotStart *Taq* DNA polymerase
45	15 sec	95 °C	Denaturation of DNA double strands
	1 min	60 °C	Amplification of DNA + recording fluorescence

4.2.3.3 Melting curve analysis and PCR quality control

After qRT-PCR analysis, a melting curve was recorded to verify specific production of a single PCR product for each individual gene and exclude the formation of primer dimers and other unspecific PCR products. The following melting curve program (Table 11) was immediately run after PCR amplification on the LightCycler® 480 Real-Time PCR instrument (Roche):

Table 11: Melting curve analysis program for the RT² Profiler™ PCR Array

PCR cycles	Duration	Temperature	Process
1	15 sec	60 °C	Hybridization of DNA strands (high fluorescence due to maximal amount of DNA-bound SYBR® Green dye)
	continuous	60 to 95 °C	Denaturation of DNA double strands with intercalated SYBR® Green dye

The melting curve was obtained by slowly increasing a temperature gradient from low to high, thereby denaturating DNA double strands with intercalated SYBR® Green. At low temperatures, fluorescence was high, since SYBR® Green dye intercalated into all DNA molecules. By increasing the temperature, the double strands started to denature, resulting in rapid loss of fluorescence. After the fluorescence was recorded and plotted against the temperature, the first derivative of the melting curve was calculated by the LightCycler® 480 Real-Time PCR software (Roche). At the melting point (T_m), 50% of the DNA is double-stranded, whereas 50% is denatured (single-stranded). At a T_m > 80 °C only a single product peak should appear in the melting curve, whereas peaks at T_m > 90 °C are indicative of gDNA contamination. If peaks occur at T_m << 80 °C, unspecific primer-dimers are present in the sample.

Further quality controls were performed using an excel-based RT² RNA QC PCR Array template (http://www.sabiosciences.com/pcrarraydataanalysis.php) that supports evaluation of C_p-values of specific PCR controls measured with every PCR plate. For quality assurance, all samples should meet the requirements of the control of reverse transcriptase activity (RTC), PCR amplification (PPC for cDNA) and gDNA contamination (GDC for cDNA) summarized in Table 31 (see section 4.2.8.9).

4.2.3.4 Relative quantification of gene expression using the ΔΔC_t-method

For relative quantification of target genes, fold changes of mRNA targets in treated samples relative to controls were calculated using the ΔΔC_t-method. Based on the fluorescence signals recorded during qRT-PCR analysis, the LightCycler® 480 Real-Time PCR software (Roche) calculated the distinct threshold cycles for each gene required to exceed the background fluorescence using the crossing point method. The crossing point values (C_p-values) for each gene are second derivatives calculated from the fluorescence curves of the amplified target gene and similar to the

threshold cycle values (C_t values) frequently used for relative quantification by the $\Delta\Delta C_t$-method.

In the first step, all C_p-values greater than 35 (regarded as negative calls) or not detected (N/A) were set to 35. Then, the C_p values of each gene were normalized to the 5 housekeeping genes Rplp1, Hrpt1, Rpl13a, Ldha and Actb (Table 8). To normalize the expression level, the C_p value of each target gene was subtracted from the average C_p of the HKGs, thereby obtaining the difference (Δ) between both C_p-values (ΔC_p-value):

$$\Delta C_p = C_p \text{ (target gene)} - \text{AVG } C_p \text{ (HKG genes)}$$

Then, the difference between the normalized C_p-values ($\Delta\Delta C_p$) of control and treated samples of a target gene was calculated as follows:

$$\Delta\Delta C_p = \Delta C_p \text{ (treated)} - \Delta C_p \text{ (control)}$$

The relative expression difference of a target gene between treated and control samples normalized to the housekeeping gene (normalized ratio, fold change), resulted from the arithmetic formula:

$$\text{Normalized ratio} = 2^{-\Delta\Delta Cp}$$

In this calculation, a PCR efficiency of 2, which implied a doubling of the amount of PCR product with every cycle, was assumed. Fold changes > 1 indicate upregulation, whereas fold changes < 1 indicate downregulation compared to controls, respectively.

Mean and SD of the fold changes in gene expression were calculated for each control and treatment group (n=4 animals per group). Statistical analysis was performed by one-way analysis of variance (ANOVA) and Dunnett's *post hoc* test using GraphPad Prism® 5 (STATCON) software. Statistically significant changes to controls are indicated by * $p < 0.05$, ** $p < 0.01$ and *** $p < 0.001$.

4.2.4 Quantitative gene expression analysis of PAI-1, Thbs1, and Itga2 using single qRT-PCR assays

To identify organ-specific differences in the expression of selected cancer-related genes (PAI-1, Thbs1 and Itga2) in response to FB_1, mRNA expression of these genes was investigated in both liver and kidney using single qRT-PCR assays.

4.2.4.1 cDNA synthesis using the Verso™ cDNA Kit

For single qRT-PCR assays, cDNA synthesis of the experimental RNA from kidney, liver and cells was performed using the Verso™ cDNA Kit (Thermo Fisher, Scientific) according to the manufacturer's instructions (www.thermoscientific.com). The kit included the following components (Table 12):

Table 12: Components of the Verso™ cDNA Kit

Kit components	Function
Verso™ Enzyme Mix	Includes Verso™ Reverse Transcriptase for DNA strand synthesis and RNAse inhibitor to protect from RNA degradation
5x cDNA synthesis Buffer	Supports reverse transcriptase reaction
Anchored Oligo-dT (500 ng/µl)	RNA priming method I
Random Hexamer (400 ng/µl)	RNA priming method II
dNTP Mix (5mM each)	Deoxynucleotides for DNA strand synthesis
RT Enhancer	Removal of DNA contamination

The volume of each RNA solution corresponding to 3 µg RNA was diluted with DEPC-water to a final volume of 33 µl (1 µg RNA/11 µl concentration). In parallel, a no-enzyme control (NEC) was prepared by pooling the RNA solution of all samples from the respective experiment in a single PCR tube and diluting it to a volume of 11 µl with DEPC-water. Then, 11 µl of each RNA dilution were transferred into a PCR tube and 1 µl of Random Hexamer primer was added to each sample tube or the NEC tube. For the annealing of the Random Hexamer primers to the RNA, samples and NEC were placed in the thermocycler (PTC-200™ Programmable Thermal Controller MJ) for 5 min at 70 °C and then kept on ice. The reaction mix for cDNA synthesis (Table 13) was prepared for all samples and 8 µl of this mixture were added to each sample and gently mixed by pipetting.

Table 13: Composition of cDNA reaction mix for samples and no enzyme control (NEC)

Kit components	1 sample [Volumen in µl]	No enzyme control (NEC) [Volume in µl]
5x cDNA synthesis Buffer	4	4
dNTP Mix	2	2
RT enhancer	1	1
Verso™ Enzyme Mix	1	-
DEPC-water	-	1
Total volume	**8**	**8**

The components of the reaction mix for NEC (Table 13) were directly pipetted into the PCR tube containing the pooled RNA samples. NEC does not contain the Verso™ Enzyme Mix for reverse transcriptase reaction and indicates sample contamination. After adding the reaction mix, samples and the NEC were incubated in the thermocycler (PTC-200™ Programmable Thermal Controller MJ) at 47 °C for 50 min to synthesize the cDNA strands and 95 °C for 2 min to inactivate the RT enhancer. After cooling down to 4 °C, samples were frozen and stored at -20 °C until further analysis.

4.2.4.2 Quantitative analysis of PAI-1, Thbs1 and Itga2 (qRT-PCR)

The cDNA from kidney and liver samples was analyzed for FB_1-mediated changes in the mRNA expression of PAI-1, Thbs1 and Itga2. By diluting cDNA samples 1:2 with DEPC-water, a working concentration of 25 ng/µl was obtained. Then, a serial dilution (1:2 to 1:32) of one cDNA sample was performed with DEPC-water to obtain an internal control for the analysis of PCR efficiency during each run. For subsequent data normalization, the different samples for the amplification of each target gene were measured in parallel with the respective samples for the amplification of the housekeeping gene *Actb*. Accordingly, 2 µl of diluted cDNA or serially diluted internal control was pipetted into the wells of a 96-well PCR plate, which were either assigned to the target or the housekeeping gene. In addition, the no enzyme control (NEC) sample of the cDNA synthesis (see 4.2.4.1), which should not contain any cDNA template, was included by pipetting 2 µl of NEC sample into a single well of the 96-well PCR plate for each the target and the housekeeping gene. The mastermix for qRT-PCR was prepared by mixing the following components (Table 14):

Table 14: Composition of qRT-PCR mastermix for the target genes (PAI-1, Thbs1, Itga2) and the housekeeping gene (beta-Actin)

Components	1 reaction [Volumes in µl]	Final concentration in 20 µl reaction volume
2x LightCycler® 480 SYBR Green I Master	10	1x
14 µM forward primer	0.15	0.105 µM
14 µM reverse primer	0.15	0.105 µM
DEPC-water	7.7	
Total volume	**18**	

18 µl of the qRT-PCR mastermix were transferred into each cDNA or NEC-containing well of the PCR plate and gently resuspended using a pipette. After the PCR plate was carefully sealed with an optical adhesive film, liquids in the wells were briefly spun down at 2,000 rpm for 20 sec (Labofuge GL, Heraeus Sepatech). Then, plates were placed in a LightCycler® 480 Real-Time PCR instrument (Roche) and qRT-PCR reactions were performed using the following program (Pereira *et al.*, 2006) (Table 15):

Table 15: qRT-PCR program for the amplification of PAI-1, Thbs1 and Itga2 (modified from (Pereira *et al.*, 2006)).

PCR cycles	Duration	Temperature	Reaction
1	10 min	95 °C	Heat activation of FastStart *Taq* DNA polymerase
45	20 sec	94 °C	Denaturation of DNA double strands
	20 sec	58 °C (A) 52 °C (B) 55 °C (C)	Annealing of specific primers to single strands (A) = *PAI-1*; (B) = *Thbs1*; (C) = *Itga2*
	20 sec	72 °C	Elongation of single strands

Changes in the mRNA expression of *PAI-1*, *Thbs1* and *Itga2* between control and treated samples were calculated using the $\Delta\Delta C_t$-method as described in section 4.2.3.4.

Mean fold changes and SD were calculated for each control and treatment group (n=4 animals per group). Statistical analysis was performed by one-way analysis of variance (ANOVA) and Dunnett's *post hoc* test using GraphPad Prism® 5 (STATCON)

software. Statistically significant changes to controls are indicated by * $p < 0.05$, ** $p < 0.01$ and *** $p < 0.001$.

4.2.4.3 Melting curve analysis and PCR efficiency control

Unspecific product amplification due to potential gDNA contamination or inappropriate primer design was monitored by melting curve analysis (Table 16):

Table 16: Melting curve analysis program for product specificity determination of PAI-1, Thbs1 and Itga2

PCR cycles	Duration	Temperature	Process
1	5 sec	95 °C	Denaturation of DNA double strands
	1 min	60 °C	Hybridization of DNA strands (high fluorescence of maximal DNA-bound SYBR® Green dye)
	continuous	60 to 95 °C	Denaturation of SYBR® Green intercalating DNA double strands

Correct product amplification of the target gene had occurred, if the melting curves showed only one specific product peak for PAI-1, Thbs1 and Itga2.

The Light Cycler® 480 Real-Time PCR Software (Roche) calculates the PCR efficiency (E) from the slope of a standard dilution curve by plotting the C_p-values of the target or the housekeeping gene of a serially diluted cDNA sample against the logarithmic value of a virtual concentration:

$$E = 10^{(-1/slope)} \text{ or } E\ (\%) = (10^{(-1/slope)} - 1) \times 100$$

For reliable quantification using the $\Delta\Delta C_t$-method, the PCR efficiencies for the target and housekeeping genes need to be similar. In practice, PCR efficiencies between 1.8 and 2.0 are regarded as suitable for data evaluation of qRT-PCR data.

4.2.5 Qualitative and quantitative gene expression analysis of sphingosine 1-phosphate receptors $S1P_{1-3}$ in kidney and liver using classical reverse transcriptase (RT)-PCR and qRT-PCR

To assess which S1P receptors might be predominantly involved in mediating possible sphingoid base 1-phosphate-induced downstream signaling pathways involved in tumor formation and progression, gene expression of the most abundant S1P receptors $S1P_{1-3}$ was performed in kidney and liver of male Sprague Dawley rats and NRK-52E cells.

4.2.5.1 Qualitative analysis of S1P receptors $S1P_{1-3}$ (RT-PCR)

To qualitatively analyze the expression of specific S1P receptors $S1P_{1-3}$, classical RT-PCR was performed. For this, 2.5 µl of each undiluted cDNA sample (50 ng/ml) from kidney, liver and NRK-52E cells obtained with the Verso™ cDNA Kit (see section 4.2.4.1) were mixed with 22.5 µl of RT-PCR mastermix (see Table 17) containing the forward and reverse primers of the respective S1P receptor (see section 4.1.5).

Table 17: Composition of RT-PCR mastermix for amplification of each S1P receptor ($S1P_{1-3}$) mRNA

Components	1 reaction [Volumes in µl]	Final concentration in 25 µl reaction volume
2x FastStart® PCR Master	12.5	1x
3 µM forward primer	2.5	300 nM
3 µM reverse primer	2.5	300 nM
DEPC-water	5.0	
Total volume	**22.5**	

For RT-PCR reaction, the mixture was placed in the thermocycler (PTC-200™ Programmable Thermal Controller MJ) and the following program was run for PCR amplification (Hornuss *et al.*, 2001):

Table 18: qRT-PCR program for the amplification of S1P receptors $S1P_{1-3}$ (modified from (Hornuss *et al.*, 2001))

PCR cycles	Duration	Temperature	Process
1	3 min	94 °C	Heat activation of FastStart *Taq* DNA polymerase
40	45 sec	94 °C	Denaturation of DNA double strands
	30 sec	50 °C	Annealing of specific primers to single strands
	1 min	72 °C	Elongation of single strands
1	10 min	72 °C	Final extension to complete DNA synthesis

The amplified PCR products of the S1P receptors from renal, hepatic and cell cDNA were stored at -20 °C until further use.

4.2.5.2 DNA agarose gel electrophoresis of RT-PCR products

The PCR products of S1P receptors $S1P_{1-3}$ obtained after RT-PCR (see 4.2.5.1) were separated by size using agarose gel electrophoresis.

For the preparation of agarose gels, 0.9 g agarose were dissolved in 75 ml sterile, deionized water under careful microwave heating. After the gel solution was cooled down to 60 °C, it was poured in a horizontal gel cast with inserted 14-well gel comb and allowed to polymerize for approximately 25 min. Then, the gel was placed into the electrophoresis chamber of an Owl Separation Systems Model B1 (Thermo Fisher, Scientific) and covered with 1x TBE electrophoresis buffer. Sample preparation was performed by 1:6 dilutions of the PCR products in 6x DNA loading buffer (Orange G loading buffer, PEQLAB), containing the synthetic dyes Orange G (orange) and xylene cyanol (green) to monitor gel electrophoresis. After removing the combs from the gel, 4 µl of the samples were loaded into the wells of the agarose gel. For determination of DNA fragment size, 4 µl of a commercial marker DNA ladder (peqGOLD 50 bp DNA Ladder Orange G, PEQLAB) were loaded onto the gels. Agarose gel electrophoresis was performed at 80 V for 1 h and 20 min, followed by staining of the gel for 15 min in 100 ml ethidium bromide solution (0.5 µg/ml in TBE electrophoresis buffer). To detect ethidium bromide-stained DNA, fluorescence was visualized under UV light using the transilluminator of the gel documentation system Gel Doc™ 2000 (Biorad).

4.2.5.3 Quantitative analysis of S1P receptors $S1P_{1-3}$ (qRT-PCR)

After qualitative verification, mRNA expression levels of $S1P_{1-3}$ in kidney and liver were quantified by qRT-PCR to determine FB_1-induced expression changes in both target organs.

Sample preparation, loading of the PCR plate and qRT-PCR program was performed as described in section 4.2.4.2 with an annealing temperature of 58 °C for all S1P receptors ($S1P_{1-3}$).

Mean fold change and SD were calculated for each control and treatment group (n=4 animals per group). Statistical analysis was performed by one-way analysis of variance (ANOVA) and Dunnett's *post hoc* test using GraphPad Prism® 5 (STATCON) software. Statistically significant changes to controls are indicated by * $p < 0.05$, ** $p < 0.01$ and *** $p < 0.001$.

4.2.6 Protein expression analysis

4.2.6.1 Protein isolation from tissue

150 mg of frozen tissue samples (kidney or liver) were weighed and transferred into a 2-ml microcentrifuge tube. For protein isolation, 1 ml of ice-cold radio immune-precipitation assay (RIPA) buffer, containing freshly added protease inhibitor cocktail (PIC), sodium orthovanadate (Na_3VO_4) and sodium fluoride (NaF) to inhibit protease and phosphatase activity, were added to the tissue samples and homogenized using an ultra-turrax®. Samples were repeatedly passed through a 26-gauge needle attached to a 2-ml syringe on ice. After centrifugation at 10,000 rpm and 4 °C for 5 min, the sample supernatant was transferred into a 1.5-ml microcentrifuge tube and stored at -20 °C until usage.

4.2.6.2 Protein quantification using the DC™ protein assay (Lowry method)

The protein concentration was measured using the DC™ assay from Biorad®, which is an improved colorimetric assay based on the method of Lowry (Lowry *et al.*, 1951). The determination of the protein concentration is based on the reaction of peptide bonds with an alkaline copper (II) solution, resulting in a blue-violet complex (biuret reaction) and reduction of copper (II) to copper (I) ions. In a second step, Folin-

Ciocalteu reagent is added and reduced by the peptide-bound copper (I) ions leading to color development. The concentration of the reduced Folin-Ciocalteu reagent is measured as a characteristic blue color with maximum absorbance at 750 nm.

For protein quantification with the DC™ assay, tissue protein samples were diluted 1:50 in ice-cold RIPA buffer containing the PIC, Na_3VO_4 and NaF. A calibration curve (ranging from 0 to 1.48 mg/ml protein) was prepared by diluting the BSA standard in the same buffer as for the samples. Using a multipette® (Eppendorf), 100 µl of reagent A' (includes 20 µl of reagent S per 1 ml reagent A) were pipetted into 1.5-ml microcentrifuge tubes containing 20 µl of the standards or samples. After vortexing the tubes, 800 µl of reagent B were added to each tube with a multipette® (Eppendorf). Tubes were immediately vortexed and incubated for 15 min until the maximum color development was achieved, which is stable for at least one hour. Then, absorbance of the blue dye formed in the standards and samples was read at 750 nm using a UV-Vis spectrophotometer. Finally, the protein content of the samples was calculated from the linear equation of the BSA calibration curve, which was obtained by plotting the absorbance of each standard at 750 nm as a linear function of its BSA concentration in µg/ml.

4.2.6.3 Protein separation by sodium dodecyl sulfate-polyacrylamide gel electrophoresis (SDS-PAGE)

SDS-PAGE is a technique to separate proteins according to their specific molecular weight. The anorganic detergent SDS (sodium dodecyl sulfate) serves to denature proteins, and concurrently binds to the unfolded protein chains to negatively charge them. Due to the strong negative charge, proteins migrate from the anode through the polyacrylamide (PA) gel towards the cathode during electrophoresis. Since SDS binds proteins proportional to their molecular weight, the charge to mass ratio for all proteins is nearly the same, so that electrophoretic mobility primarily depends on the size of the protein. Thus, proteins with low molecular weight run faster through the PA gel than larger proteins, which is important for the ability to separate proteins during electrophoresis. Sufficient protein separation is also dependent on the percentage of acrylamide, which influences the polymerization degree of the gel. For instance, the higher the polymerization of the gel, the better is the separation for small proteins. Discontinuous PAGE, consisting of a stacking and resolving gel layer with different pH, is commonly used to separate proteins. Thereby, the resolution of protein bands

is improved by focusing the proteins in the stacking gel at the beginning of electrophoresis.

At first, a 10% resolving gel was prepared by gently mixing the following components (Table 19).

Table 19: Composition of 10% resolving and 6% stacking gels for SDS-PAGE

Components	10% Resolving gel	6% Stacking gel
30% Acrylamide	3.3 ml	400 µl
1.5 M Tris, pH 8.8	2.5 ml	-
0.5 M Tris, pH 6.8	-	62.5 µl
H_2O	4.1 ml	2.0 ml
10% SDS	100 µl	25 µl
10% Ammoniumpersulfate	100 µl	25 µl
TEMED (N,N,N',N'-tetramethyl-ethane-1,2-diamine)	20 µl	2.5 µl

After adding the crosslinker TEMED, the resolving gel solution was rapidly poured between the assembled gel plates and overlaid with isopropanol to avoid drying of the gel. After polymerization was complete (20-30 min), isopropanol was removed and the gel was dried using small stripes of filter paper. Then, a 6% stacking gel was prepared by gently mixing the components listed in Table 19. The stacking gel was rapidly poured on the resolving gel and a comb was gently inserted into the gel (without introducing air bubbles) to form the wells for the protein samples.

After polymerization of the stacking gel (15-20 min), the whole gel was placed into the electrophoresis chamber and filled with 1x electrophoresis running buffer. Sample protein solutions were prepared by dilution with 2x Laemmli buffer, which contains SDS and β-mercaptoethanol for protein denaturation and bromphenol blue for protein staining. Diluted samples were briefly boiled (95 °C for 5 min) in a heating block to completely denature the protein structure. Then, samples were rapidly cooled down on ice, briefly vortexed and spun down in a microcentrifuge. A maximum of 20 µl of the denatured protein sample solution (containing 60 µg of total protein) was loaded in the wells of the stacking gel. For determination of protein weights, 5 µl of a commercial protein molecular weight marker (peqGOLD Protein Marker IV, PEQLAB) was loaded on the gels to run in parallel with the protein samples. Electrophoresis was started at 60 V for 10 min to concentrate the proteins in the stacking gel.

Subsequently, the voltage was increased to 100 V and electrophoresis was run for 1 h and 45 min until the bromphenol blue front reached the bottom of the plates.

4.2.6.4 Western Blot analysis

After electrophoretic separation, negatively charged proteins in the polyacrylamide gel can be transferred to a positively charged membrane (nitrocellulose or polyvinylidene fluoride). In the commonly used wet blotting technique, a blotting cassette containing the gel and the membrane in a sandwich assembly is placed in a buffer-filled blotting tank and an electric current is applied to transfer the SDS-coated proteins from the anode to the membrane at the cathode. After immobilization on the membrane, proteins can be detected using specific antibodies. The immunodetection is performed by primary antibodies with high epitope affinity to the antigen of the target protein (Figure 11).

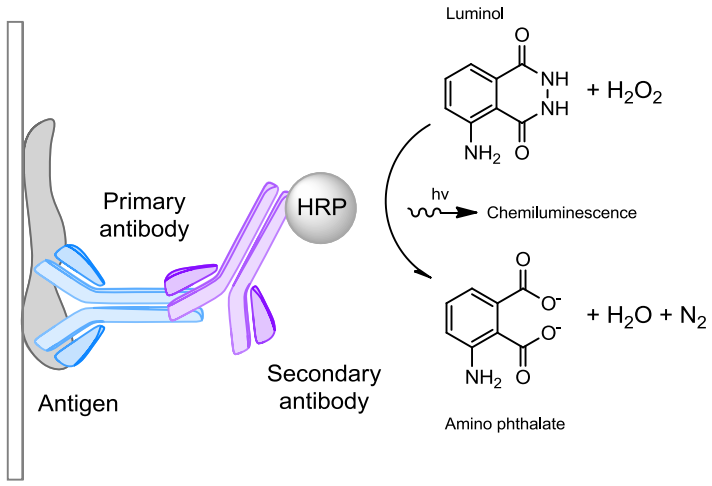

Figure 11: Immunodetection of proteins by chemiluminescence reaction of luminol with the horseradish peroxidase (HRP)-labeled secondary antibody conjugated to the primary, antigen-recognizing antibody.

Then, secondary antibodies, which are chemically coupled to a reporter enzyme, are used to detect and visualize the primary antibody attached to the target protein on the membrane. For western blot detection, secondary antibodies are usually conjugated to horseradish peroxidase (HRP), which catalyzes the oxidation of luminol, thereby producing chemiluminescence, which is characterized by the emission of light (Figure 11).

After electrophoresis, the PA gel together with the nitrocellulose membrane, several filter papers and two fiber pads were soaked for 20 min in the blotting transfer buffer. Then, a blotting sandwich, consisting of 2 sheets of filter paper on a fiber pad, followed by the gel, the membrane, 2 sheets of filter paper, and finally the second fiber pad, was assembled in a blotting cassette, starting on the black perforated fiberglass panel. To avoid air bubbles, which may disrupt the transfer of proteins onto the membrane, each layer of the sandwich was gently rolled using a glass pipette. The sandwich assembly was then placed in the blotting tank containing the transfer buffer, so that the black side of the blotting cassette was towards the cathode. Protein transfer, which is dependent on the protein size, was performed at 100 V and 4 °C for 1 h. To confirm protein transfer, membranes were reversibly stained with Ponceau S dye solution (see 4.1.3) for 3 min. Then, membranes were repeatedly rinsed in deionized water to destain the membrane until red stained protein bands were visible. If the blotting was successful, the red stained protein lanes were uniformly transferred to the membrane and did not show any bubbles, which may disturb immunodetection of the target proteins. After Ponceau S staining, membranes were thoroughly rinsed in deionized water to completely destain the membranes. The blotting membrane was blocked for 1 h at RT in 5% non-fat dried milk powder in a mixture of TBS with 0.1% Tween® 20 detergent (TBST buffer) to prevent non-specific binding of the antibodies and reduce background staining. After blocking, the membrane was briefly rinsed in TBST and incubated with the primary antibody (dilution see 4.1.7) in 5% non-fat dried milk in TBST over night at 4 °C. The next day, membranes were washed 3x in TBST for 15 min using gentle agitation on a rocking platform (Shaker KL-2, Edmund Bühler). Then, the blot was incubated with a dilution of the HRP-conjugated secondary antibody (dilution see 4.1.7) in 5% non-fat dried milk in TBST for 1 h at RT. Before antibody detection was performed, membranes were washed 3x for 15 min under gentle agitation. Then, 750 µl of enhanced chemiluminescence (ECL) reagent were uniformly distributed on the membrane. After incubation for 1 min, excess ECL reagent was drained off and the membrane was covered with a plastic wrap. The membrane was exposed to an X-ray film for different incubation times (30 sec to max. 1 h 30 min), and developed manually using an X-ray film developer and fixer. The film is immersed into the developer until the band signals appear (max. 5 min) and subsequently washed in water. Afterwards, the film is immersed into the fixer for 3 min and washed again with water for 3 min.

Glyceraldehyde-3-phosphate dehydrogenase (GAPDH) was used as a loading control, which equalizes differences in protein amount, sample loading onto the gel and transfer rates during western blotting. Probing with the antibody for the loading control was performed after the western blot had been stripped of the target protein antibody. For this, the membrane was washed twice with 1x TBST to remove the ECL reagent after antibody detection. Then, the membrane was incubated in β-mercaptoethanol-containing stripping buffer (see 4.1.7) at 56 °C for 30 min to unbind the primary antibody from the target protein on the blot. After incubation, the blot was rinsed twice with 1x TBST and the membrane was again blocked in 5% non-fat dried milk in TBST for 1 h at RT. Subsequently, incubation and detection of the loading control GAPDH on the blot was performed as described above.

Signals generated on a western blot were recorded and measured using computerized optical densitometry. The analysis was performed by scanning the target protein bands on the film using the gel documentation system Gel Doc™ 2000 (Biorad). After images were acquired with a camera, bands were selected and the optical density (OD) was determined using the Multi-analyst® software (Biorad). By comparing the ODs, semi-quantitative analysis of protein expression changes in treated samples relative to controls was performed. Densitometric data were expressed as fold change of protein expression in control animals.

Mean and SD were calculated for each control and treatment group (n=4 animals per group). Statistical analysis was performed by one-way analysis of variance (ANOVA) and Dunnett's *post hoc* test using GraphPad Prism® 5 (STATCON) software. Statistically significant changes to controls are indicated by * $p < 0.05$, ** $p < 0.01$ and *** $p < 0.001$.

4.2.7 High pressure liquid chromatography tandem-mass spectrometry (HPLC-MS/MS) for determination of sphingoid bases and sphingolipids

To analyze changes in sphingolipids in response to FB_1 treatment *in vitro* and *in vivo*, HPLC-MS/MS analysis was performed to separate and detect the 18C-D-*erythro*-(2S,3R)-sphingoid bases sphinganine (Sa) and sphingosine (So), their respective 1-phosphate metabolites sphinganine 1-phosphate (Sa1P) and sphingosine 1-

phosphate (So1P), as well as the specific sphingosine-based sphingolipids C16-, C18- and C18:1-ceramide in kidney, liver and NRK-52E cells.

4.2.7.1 Preparation of internal standards

To correct for incomplete extraction efficiencies, differences in chromatographic retention and fragmentation in the mass spectrometer, an internal standard solution was prepared and added to the samples prior to extraction to allow identification and accurate quantification of the analytes. The synthetic 17C-sphingoid bases (not occurring in mammals) with a 17 carbon atom backbone were selected as internal standards for the quantification of the naturally occurring 18C-sphingoid bases, whereas ceramide-based sphingolipids were quantified using an 18C-ceramide internal standard with naturally not occurring amount of carbon atoms (C17) in the fatty acid moiety. The following internal standards (100 µM concentration in methanol) were diluted 1:100 with methanol to achieve an internal standard (IS) mix for the simultaneous quantification of sphingoid bases, their respective 1-phosphates and ceramides (Table 20):

Table 20: Composition of the internal standard (IS) mix

Internal standards	**Abbreviations**
17C-D-*erythro*-sphingosine	17C-So
17C-D-*erythro*-sphinganine (dihydrosphingosine)	17C-Sa
17C-D-*erythro*-sphingosine 1-phosphate	17C-So1P
17C-D-*erythro*-sphinganine 1-phosphate	17C-Sa1P
18C17-ceramide	C17-Cer

4.2.7.2 Preparation of endogenous calibration standards

For identification and absolute quantification of sphingoid bases and ceramides, a calibration standard (CalS) mix containing the following components (each at 100 µM) was prepared by diluting the respective stock solutions of each standard in methanol (see Table 21). Then, the CalS mix was serially diluted in methanol to obtain the working CalS mix solutions required for spiking the calibrator samples with known amounts of each calibration standard. Calibrator samples were extracted in analogy

to analyte samples (see section 4.2.7.3 and 4.2.8.12) by using artificial matrices for the simulation of media/biological fluids/tissue homogenates (serum-free cell culture medium) or cell pellets (BSA).

Table 21: Composition of the calibration standard (CalS) mix

Calibration standards	Abbreviations
18C-D-*erythro*-sphingosine	So
18C-D-*erythro*-sphinganine (dihydrosphingosine)	Sa
18C-D-*erythro*-sphingosine 1-phosphate	So1P
18C-D-*erythro*-sphinganine 1-phosphate	Sa1P
18C16-ceramide	C16-Cer
18C18-ceramide	C18-Cer
18C18:1-ceramide	C18:1-Cer

For generating calibrator samples, artificial matrices (2 ml serum-free medium or 1 mg BSA) were spiked with the respective working CalS mix solution (calibration range between 0.25 and 400 or 2000 pmol for cells or tissue/biological fluids, respectively) and 10 pmol (cells) or 20 pmol (tissues and biological fluids) of IS mix (see section 4.2.7.3 and 4.2.8.12). In addition, a calibrator sample only containing the internal standards (0 pmol calibration standards) and a sample without any standards (blank) was prepared to correct for background signals. Each calibrator sample was generated in triplicate to obtain reliable data sets for the establishment of a calibration curve for each analytical standard.

4.2.7.3 Liquid extraction from serum, urine and tissues

The extraction of sphingoid bases or ceramides from biological fluids or tissues was performed according to the literature (Bielawski *et al.*, 2006; Cai *et al.*, 2007; Bielawski *et al.*, 2009) with slight modifications.

For biological liquids, 500 µl of homogenized urine or 100 µl of serum were mixed with 500 µl 1x PBS, 20 pmol IS mix (see section 4.2.7.1) and 3 ml extraction mixture containing isopropanol:ethyl acetate (15:85; v:v). To enhance extraction of analytes, samples were sonicated for 60 sec at RT and then continuously vortexed at 500 rpm

for 40 min. To improve phase separation, samples were centrifuged at 1,500 x g for 10 min and the upper organic phase was transferred into a 2-ml microcentrifuge tube. For tissues, 20 mg of frozen kidney or liver were weighed and homogenized in a manual tissue homogenizer with 500 µl 0.05 M potassium phosphate buffer (pH 7.4). 50 µl of the homogenate, corresponding to 2 mg of tissue, were mixed with 500 µl 1x PBS and the IS mix (see section 4.2.7.1), and then subjected to the same extraction procedure as described for biological fluids.

4.2.7.4 Sample and calibration standard preparation for HPLC-MS/MS analysis

Extraction solvents from the different biological samples or calibration standards were evaporated to dryness at 40 °C using a Centrivac vaccum centrifuge (Heraeus Instruments). The dried residues containing the analytes were then reconstituted in 100 µl of mobile phase B (see section 4.2.7.5) by vortexing and brief sonication. Then, the total volume of reconstituted sample was transferred into a HPLC autosampler vial with a 300 µl conical insert, closed with a crimp seal (with septum) and subjected to HPLC-MS/MS analysis or stored at -20 °C until analysis.

4.2.7.5 Qualitative and quantitative analysis of sphingoid bases and sphingolipids by HPLC-MS/MS using multiple reaction monitoring (MRM)

HPLC is a suitable tool to separate complex mixtures of biological compounds prior to mass spectrometry analysis. The advantage of HPLC is to separate isomeric and isobaric compounds that would otherwise not be distinguished using mass spectrometry alone. Furthermore, complex biological samples creating undesired background signals in mass spectrometry can be reduced to improve accuracy and sensitivity of the analysis (Merrill *et al.*, 2005).

For the separation of sphingoid bases and ceramides from biological samples, reverse-phase HPLC was performed on a C8 silica membrane column (Phenomenex) with the conditions described in Table 22.

During reverse-phase HPLC, sphingoid bases and ceramides were physically separated due to their differences in hydrophobicity caused by specific structural features such as double bounds, polar residues (phosphorylation) or different chain lengths of the fatty acid moiety. After HPLC separation, eluates were introduced to the interface of the tandem mass spectrometer API 2000 QTRAP™ (Applied

Biosystems) and intact molecular ions were generated by electrospray ionization (ESI) using a Turbo Ion Spray source (Applied Biosystems). The ionization was performed by passing the eluate through a needle with the help of a nebulizer (sheath) gas and applying high voltage that causes the formation of charged droplets (electrospray) from the eluate. In the ion source, the evaporation of the natural solvent of the charged droplets was achieved by a heated (400 °C) nitrogen stream (auxiliary gas) and charged ions released from the droplets were introduced to the mass spectrometer, which was held under high vacuum. In the positive ionization mode, protonated molecular ions $[M+H]^+$ were formed, whereby protonation was assisted by the addition of formic acid to the mobile phase (see Table 22).

Table 22: HPLC-ESI-MS/MS equipment and conditions for analysis of sphingoid bases and ceramides

Tandem mass spectrometer	API 2000 QTRAP™ hybrid triple quadrupole linear ion trap tandem mass spectrometer equipped with Turbo Ion Spray source (Applied Biosystems)
HPLC pump	Agilent Series 1100 LC quaternary pump (Agilent Technologies)
HPLC autosampler	Agilent Series 1100 (Agilent Technologies) Injection volume: 10 µl
Stationary phase	HyperClone™ C8 column with 150 x 2.0 mm dimension and 3 µm pore size (Phenomenex)
Source temperature	400 °C
Ionization mode (polarity)	positive
Scan type	MRM
Sheath and auxiliary gas	nitrogen
Collision gas	argon
Data aquisition	Analyst® software 1.4.2 (Applied Biosystems)
Mobile phase A	2 mM ammonium formiate in water containing 0.2% formic acid (v:v)
Mobile phase B	1 mM ammonium formiate in methanol containing 0.2% formic acid (v:v)
Gradient (sphingoid bases) Binary (%A/B)	0-2 min: 40/60-35/65; 2-4 min: 35/65-30/70; 4-10 min: 30/70-20/80; 10-15 min: 20/80-10/90; 15-17 min: 10/90-5/95; 17-20 min: 5/95; 20-21 min: 5/95-30/70; 21-25 min: 30/70
Gradient (ceramides) Binary (%A/B)	0-3 min: 18/82; 3-4 min: 18/82-10/90; 4-18 min: 10/90-1/99; 18-25 min: 1/99 min; 25-27 min: 1/99-18/82; 27-30 min: 18/82
Flow rate	200 µl/min

Using a triple quadrupole tandem mass spectrometer, consisting of 2 quadrupole mass analyzers in series, molecular (precursor) ions were selected in a first mass analyzer (quadrupole 1, Q1), then fragmented in a collision cell using an inert gas (quadrupole 2, Q2), and the fragments (product ions) were analyzed in the second mass analyzer (quadrupole 3, Q3). Tandem mass spectrometry analysis was performed in the MRM (multiple reaction monitoring) mode, which allowed the simultaneous detection of multiple analytes in one sample by setting the Q1 mass analyzer to pass only a specific m/z (mass-to-charge) precursor ion for each analyte and the Q3 mass analyzer to pass only the particular m/z product ion arising from fragmentation of the selected precursor ion (Bielawski *et al.*, 2009). Since the precursor-to-product ion mass transitions are unique for each analyte, selective and sensitive analysis of complex biological samples such as tissue, urine or blood can be performed.

Acquisition parameters for each individual analyte and internal standard were obtained by direct infusion of the respective compounds using the quantitative optimization function of the Analyst® 1.4.2 software (Applied Biosystems). The transitions were monitored for each analyte and internal standard, and MRMs with the highest relative response and specificities were used for quantification. The analytes and standards were identified by the precursor-to-product ion mass transition and the associated retention time (Table 23).

Specific precursor/product ion mass transitions (*m/z*'s) (see Table 23) were recorded by an ion detector, which detects ions that were deflected in a magnet field depending on their mass and charge. Ions that passed the magnetic field to reach the detector were then transformed into an electric signal, amplified and recorded as electric current. The more ions of a specific mass-to-charge ratio arrive, the greater is the current detected. Using the Analyst® 1.4.2 software (Applied Biosystems), electric signals were processed into total ion current (TICs) chromatograms, summarizing the signal intensity of all selected mass transitions over the time of analysis.

Table 23: Summary of the specific precursor/product ion mass transitions (*m/z*'s), declustering potentials (DP), collision energies (CE), cell exit potentials (CXP) and HPLC retention times used for MRM detection and quantification of analytes and internal standards of sphingoid bases and sphingosine-derived ceramides. Matched pairs of analytes and internal standards for quantification are indicated by similar superscript letters ([a-g]).

Compounds	Mass transition *m/z*	CE [eV]	DP [eV]	CXP [eV]	Retention time [min]
Analytes					
[a]So	300.2/282.3	17	31	6	18.5
[b]Sa	302.2/284.3	17	41	6	19.3
[c]So1P	380.0/264.0	21	41	6	17.3
[d]Sa1P	382.1/284.2	19	56	6	18.1
[e]C16-Cer	538.3/264.2	39	61	6	17.3
[f]C18-Cer	566.3/264.3	39	36	6	19.1
[g]C18:1-Cer	564.3/264.3	35	81	6	17.9
Internal Standards					
[a]17C-So	286.2/268.2	15	26	6	17.1
[b]17C-Sa	288.2/270.3	17	51	6	17.9
[c]17C-So1P	366.0/250.0	21	41	6	15.8
[d]17C-Sa1P	368.1/270.2	19	51	6	16.7
[e-g]C17-Cer	552.3/264.3	39	96	6	18.2

For quantification of specific sphingoid bases and ceramides, extracted ion chromatograms were used, which visualized the signal intensity of a specific mass-to-charge value associated with the selected precursor and product ions as function of the retention time. The obtained signal peaks of each analyte and internal standard were then integrated using the Analyst® 1.4.2 software (Applied Biosystems) and the resulting analyte/internal standard peak area ratios were plotted against the analyte/internal standard concentration ratios using a linear regression model with the 1/x weighing factor to generate specific calibration curves for each analyte. Taken into account the dilution factor of 1:10 for each biological sample, the amount of each analyte in pmol per 100 µl reconstituted sample was calculated based on the calibration curves. For data normalization, amounts of sphingoid bases and ceramides in kidney and liver were related to the amount of extracted tissue (2 mg) and expressed as pmol per mg tissue. The analyte amounts in 100 µl serum sample were related to pmol per ml, whereas the amount in urine samples was normalized to

excreted creatinine (see chapter 5.1.2.2, Table 33) and expressed as pmol per mg creatinine.

The mean and SD of the amount of each sphingoid base or ceramide were calculated for each control and treatment group (n=4 animals per group). Statistical analysis was performed by one-way analysis of variance (ANOVA) and Dunnett's *post hoc* test using GraphPad Prism® 5 (STATCON) software. Statistically significant changes to controls are indicated by * $p < 0.05$, ** $p < 0.01$ and *** $p < 0.001$.

4.2.8 Cell culture experiments in NRK-52E cells

All cell culture work was conducted under a laminar flow clean bench. Before use, the workbench was irradiated with UV light for 15 min and desinfected with 70% ethanol. Cell culture media were autoclaved and prewarmed to 37° C in a water bath before use.

4.2.8.1 Cultivation of NRK-52E cells

NRK-52E cells, which grow as an adherent monolayer in permanent culture, were originally established in 1966 from the proximal tubule epithelium of normal rat kidney tissue by spontaneous immortalization (Huu *et al.*, 1966). In a series of studies, NRK-52E cells were used as a proximal tubule cell model and considered suitable for toxicological investigations (Best *et al.*, 1999). This cells were used because they represent target cells of FB_1 toxicity *in vivo* (NTP, 2001).

NRK-52E cells (purchased from the European Collection of Cell Cultures, ECACC, Salisbury, UK) were cultivated in 75-cm^2 cell culture flasks containing 10 ml Dulbecco's modified Eagle's Medium (DMEM) supplemented with fetal calf serum (FCS), L-glutamine, non essential amino acids (NEAA) and penicillin/streptomycin (Table 24) at 37 °C and 5% CO_2.

Table 24: Composition of NRK-52E cell culture medium

Supplements	Concentration stock solution	Volume stock solution	Final concentration medium [500 ml]
FCS (fetal calf serum)	100%	50 ml	10%
L-glutamine	200 mM	5 ml	2 mM
NEAA (non-essential amino acids)	100x	5 ml	1x
Penicillin/streptomycin	100x	5 ml	1x

4.2.8.2 Subcultivation of NRK-52E cells

When cells reached 70-80% confluence, they were passaged into a new 75-cm^2 culture flask (every 4-5 days). The medium was aspirated using a pipette and cells were washed with 5 ml 1x PBS. After 1x PBS was removed, cells were treated with 2 ml trypsin/EDTA and incubated at 37 °C for 3 min. To inhibit trypsin activity, cells were taken up in serum-containing culture medium, transferred into a 15 ml conical tube and centrifuged at 1,200 rpm for 5 min. The resulting cell pellet was resuspended in approximately 4 ml of culture medium and 20 µl of the cell suspension was collected for cell counting (see section 4.2.8.3). For subcultivation, 2 x 10^6 cells were transferred into a new 75-cm^2 tissue culture flask with 10 ml of culture medium and incubated as described above.

4.2.8.3 Determination of cell number

Cell number was determined using a microscopic counting chamber (improved Neubauer hemocytometer), consisting of nine large squares (each divided into 16 small squares) with a defined area of 1 mm^2 corresponding to a sample volume of 0.1 µl. Cells were trypsinized, washed in culture medium and collected by centrifugation at 1,200 rpm for 5 min. After the cell pellet was taken up in 4 ml culture medium, 20 µl of the cell suspension were mixed with an equal volume of 0.4% (w/v) trypan blue dye and applied to the Neubauer hemocytometer. Vital cells, which remained unstained by trypan blue solution, were counted in four of the large squares of the Neubauer hemocytometer, whereas cells stained blue were excluded from the count, since they represented the proportion of dead cells in suspension. Cell number per ml was calculated using the following equation:

$$\text{Cell number per ml} = \frac{\text{mean number of cells in 4 large squares}}{\text{volume of large square (0.1 µl)}} \times \text{dilution factor} \quad (2)$$

4.2.8.4 Cryopreservation of cells

Cryopreservation in liquid nitrogen was used for long term storage of cells. To freeze cells, medium was aspirated from the cells, which were then gently washed with 1x PBS and removed from the bottom of the cell culture flask by incubation with trypsin/EDTA. After inhibition of trypsinization with serum-containing medium, cells were centrifuged and resuspended with 4 ml of freezing medium, which was freshly prepared by adding 10% FCS and 10% DMSO to the NRK-52E culture medium. The cell suspension was aliquoted (1 ml) into cryovials and stored at -20 °C for 4 hours. Then, cryovials were cooled down to -80 °C for 1 day and placed into a container of liquid nitrogen for long term storage.

4.2.8.5 Thawing of cryopreserved cells

Cryopreserved cells were completely thawed in a 37 °C-tempered water bath within 1-2 min. After decontamination of the cryovial with 70% ethanol, the cell suspension was quickly transferred into a 15-ml conical tube, containing 10 ml of prewarmed culture medium to dilute the cytotoxic DMSO in the freezing medium. Then, cells were sedimented by centrifugation at 1,200 rpm for 5 min, the supernatant was discarded and the cell pellet was taken up in 5 ml culture medium. The entire suspension was seeded into a 75-cm^2 cell culture flask containing 5 ml culture medium. Medium was replaced with 10 ml fresh medium the following day.

4.2.8.6 Treatment of NRK-52E cells

For cell treatment with FB_1, a 1 mM stock solution was prepared by dissolving 1 mg of FB_1 in 1.385 ml of sterile H_2O. Working solutions were obtained by diluting the stock solution of FB_1 in sterile H_2O. For cell treatment, the working solutions were diluted in the respective volumes of culture medium to obtain the desired FB_1 treatment concentrations for each assay (Table 25).

Table 25: Scheme of FB_1-treatment conditions for different endpoints/assays

Endpoint/Assay	Culture dish	Concentrations	Cells/ml	Duration
Cell viability/MTT	96-well plate	0.5, 1, 5, 10, 25, 50, 75 and 100 µM FB_1	5 x 10^3/150 µl	24 + 72 h
Gene expression/ qRT-PCR	21-cm^2 petri dishes	0.5, 5 and 50 µM FB_1	2 x 10^5/5 ml	24 h
Invasion/Modified Boyden chamber	24 transwell inserts in a 24-well plate	0.5, 5 and 50 µM FB_1	1 x 10^4/100 µl	24 h
Sphingolipids/ LC-MS/MS	21-cm^2 petri dishes	0.5, 5 and 50 µM FB_1	2 x 10^5/5 ml	24 h

For experiments with the sphingosine kinase inhibitor 4-[[4-(4-Chlorophenyl)-2-thiazolyl]amino]phenol (SKI II), a 8 mM stock solution was prepared by dissolving 5 mg SKI II in 2.06 ml DMSO. Working solutions were obtained by diluting the stock solutions of SKI II in sterile H_2O. For cell treatment, the working solutions were diluted in the respective volumes of culture medium to obtain the desired FB_1 treatment concentrations for each assay (Table 26).

Table 26: Scheme of treatment conditions of FB_1 in combination with the sphingosine kinase inhibitor SKI II for different endpoints/assays

Endpoint/Assay	Culture dish	Concentrations	Cells/ml	Duration
Cell viability/MTT	96-well plate	0.5, 1.0 or 2.5 µM SKI II; 0.5, 5 and 50 µM FB_1; 0.5, 5 or 50 µM FB_1 + 0.5, 1.0 or 2.5 µM SKI II;	5 x 10^3/150 µl	24 h
Sphingolipids/ LC-MS/MS	21-cm^2 petri dishes	5 µM FB_1 + 0.5, 1.0 or 2.5 µM SKI II	2 x 10^5/5 ml	24 h

For cell invasion experiments using sphingosine 1-phosphate (So1P), a 1.32 mM stock solution was prepared by dissolving 1 mg So1P in 2 ml methanol. Working solutions were obtained by diluting the stock solutions of SKI II in sterile H_2O. For cell treatment, the working solutions were diluted in the respective volumes of culture medium to obtain the desired So1P treatment concentrations Table 27.

Table 27: Scheme of So1P-treatment conditions for the cell invasion assay

Endpoint/Assay	Culture dish	Concentrations	Cells/ml	Duration
Invasion/Modified Boyden chamber	24 transwell inserts in a 24-well plate	0.5, 1.0 and 5.0 µM So1P	1 x 10^4/100 µl	24 h

Cells were seeded at the desired density (see Tables 25-27) and grown to 80-90% confluence. The medium was aspirated and cells were washed with 1x PBS. After careful removal of the washing solution, fresh medium with the respective concentrations of FB_1 and/or SKI II (Table 25 and Table 26) was placed on the cell layer in the culture dish and incubated at 37 °C and 5% CO_2. Control cells were incubated under the same conditions with medium alone or medium containing 0.04% DMSO as vehicle for sphingosine kinase inhibitor experiments, respectively. For invasion experiments with So1P, control cells were treated with medium containing 0.6% methanol as vehicle.

4.2.8.7 Determination of cell viability – MTT assay

The MTT assay was used to determine the time- and dose-dependent effect of FB_1 on cell viability in NRK-52E cells. Cell viability was determined *via* colorimetric measurement of blue formazan crystals formed by metabolic conversion of the yellow tetrazolium salt (3-(4,5-Dimethylthiazol-2-yl)-2,5-diphenyltetrazolium bromide (MTT) by living cells. The reductive conversion of MTT caused by mitochondrial enzymes is thought to depend on the activity of endoplasmic enzymes producing reduction equivalents like nicotinamide adenine dinucleotide (NADH) and nicotinamide adenine dinucleotide phosphate (NADPH) during glycolysis (see Figure 12).

NRK-52E cells were seeded at a density of 5x10^3 cells/well in a 96-well cell culture plate using a multichannel pipette (see chapter 4.2.8.6, Table 25). Additional wells (two rows) of the cell culture plate only contained 150 µl medium without cells to correct for background absorption during measurement. After the cells were allowed to grow over night, the medium was completely removed and cells were washed with 100 µl 1x PBS.

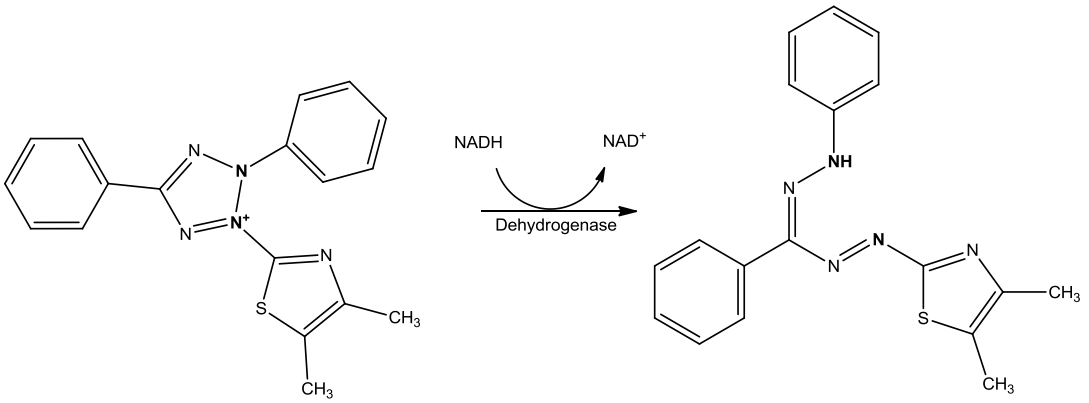

Figure 12: Conversion of the tetrazolium salt MTT (yellow) to formazan crystals (blue) *via* nicotinamide adenine dinucleotide (NADH) reduction equivalents resulting from the metabolic activity of vital cells.

To determine cell viability in response to FB_1, 150 µl fresh medium containing FB_1 (0.5 to 100 µM) or medium alone (control) was added to the cells and cells were incubated at 37 °C and 5% CO_2 for a period of 24 and 72 h (see section 4.2.8.6, Table 25). To assess the effects of a combinatory treatment of the sphingosine kinase inhibitor SKI II and FB_1 on cell viability, cells were either treated with FB_1 (0.5, 5 and 50 µM) and SKI II (0.5, 1.0 and 2.5 µM) alone or a combination of both substances (0.5, 5 or 50 µM FB_1 + 0.5, 1.0 or 2.5 µM SKI II, see section 4.2.8.6, Table 25) for 24 h.

After treatment and microscopic examination of cells, 15 µl of MTT solution (5 mg/ml) were added to the wells and gently mixed with the supernatant medium. Then, the 96-well cell culture plates were incubated for another 2 h at 37 °C to allow for metabolic conversion of the yellow MTT salt to blue formazan crystals (Figure 12). Subsequently, cells were removed from the incubator and homogenized with 100 µl MTT solubilization solution, consisting of acified isopropanol and Triton X-100 to enable the release of the formed blue formazan by permeabilization of cell membranes. The formazan salts were resuspended with a pipette for complete dissolution and measured at a wavelength of 570 nm using a microplate reader. Background absorbance was obtained from the cell-free wells containing medium only at a wavelength of 690 nm. Taking account of the background absorbance at 690 nm, cell viability was calculated using the following equation:

$$\text{Cell viability [\%]} = \frac{\text{Treated cells [Absorbance (570 nm)- Absorbance (690 nm)]}}{\text{Control cells [Absorbance (570 nm)- Absorbance (690 nm)]}} \times 100$$

The mean and SD for each treatment group was calculated from the means of three independent experiments with 3 biological replicates per treatment concentration. Statistical analysis was performed by one-way analysis of variance (ANOVA) and Dunnett's *post hoc* test using GraphPad Prism® 5 (STATCON) software. Statistically significant changes to controls are indicated by * $p < 0.05$, ** $p < 0.01$ and *** $p < 0.001$. Effect concentrations for 50% reduction in cell viability (EC50 values) were calculated from non-linear regression (dose-response curves) by Graph pad prism® (STATCON) software.

After combination of FB_1 and/or SKI II, the mean and SD for each treatment group was calculated from the means of three independent experiments with 3 biological replicates per treatment concentration. Statistical analysis was performed by one-way analysis of variance (ANOVA) and Tukey's *post hoc* test using GraphPad Prism® 5 (STATCON) software. Statistically significant changes between FB_1 treatment alone and the combined treatment with FB_1 and SKI II are indicated by * $p < 0.05$, ** $p < 0.01$ and *** $p < 0.001$. Statistically significant changes between SKI II treatment alone and the combined treatment with FB_1 and SKI II are indicated by $^{\#}$ $p < 0.05$.

4.2.8.8 RNA isolation and quantification for gene expression analysis in NRK-52E cells

The RNA of NRK-52E cells was isolated for subsequent gene expression analysis in response to FB_1 (see section 4.2.8.10). Cells were seeded at a density of 2×10^5 in 21-cm^2 culture dishes containing 5 ml DMEM and grown to 80-90% confluence at 37 °C and 5% CO_2. The medium was removed and cells were washed with 1x PBS. After careful removal of the washing solution, fresh medium with the respective concentrations of FB_1 and/or the sphingosine kinase inhibitor SKI II (see section 4.2.8.6, Table 25 and Table 26) were placed on the cell layer in the culture dish and incubated at 37 °C and 5% CO_2. Control cells were incubated under the same conditions with medium alone or medium containing 0.04% DMSO for sphingosine kinase inhibitor experiments, respectively.

After treatment, cells were washed twice with 1x PBS. Then, wash solution was removed from the cells and 600 µl of the guanidinium-thiocyanate-and β-

mercaptoethanol containing RLT buffer were added to the petri dishes to lyse cells and inactivate RNases. To ensure the complete distribution of lysis buffer on the cell layer, petri dishes were slightly tilted. Then, cells were thoroughly removed from the bottom of the culture dish using a plastic cell scraper and the cell lysate was gently resuspended using a pipette. For homogenization, 600 µl of the cell lysate were placed onto a QIAshredder column inserted into a 2-ml microcentrifuge tube and centrifuged at 14,000 rpm for 2 min. The flow-through was homogenized with 600 µl 70% ethanol and 600 µl of this mixture was applied to an RNeasy mini spin column inserted in a 2-ml microcentrifuge tube. Then, the tube was centrifuged at 11,000 rpm for 15 s to remove undesired high-molecular weight cell components and to bind total RNA to the silica membrane. For complete sample preparation, 600 µl of the remaining cell lysate was applied to the RNeasy mini spin column and the centrifugation steps were repeated as above. The eluate was discarded and total RNA bound to the RNeasy mini spin columns was further purified (see section 4.2.2.1). RNA quantification and determination of purity was performed as described in section 4.2.2.2. The integrity of RNA was assessed by denaturating RNA electrophoresis (see section 4.2.2.3).

4.2.8.9 Optional RNA quality control using the RT² RNA QC PCR Array

For gene expression analysis *in vitro*, optional quality control of RNA and the respective cDNA was performed using the RT^2 RNA QC PCR Array (SABiosciences) according to the manufacturer's instructions (www.sabiosciences.com). In this array, specific PCR controls were used to check:

- RNA integrity,
- presence of inhibitors of reverse transcription and PCR amplification and
- genomic or general DNA contamination

An overview of the function of PCR controls used for quality assessment of RNA and cDNA is given in Table 28. The amplification of RNA/cDNA quality controls was performed by addition of specific PCR mastermixes (see below) to the wells of the PCR array, which contained pre-dispensed forward and reverse primers designed for qRT-PCR of the specific PCR controls.

Table 28: Overview of different PCR controls for RNA and cDNA used in the RT^2 RNA QC PCR Array

Abbreviation	PCR quality control	Function
HK1	Housekeeping gene 1 (Actb)	high expression level gene, estimation of overall RNA integrity
HK2	Housekeeping gene 2 (Hprt1)	low expression level gene, estimation of overall RNA integrity
RTC	Reverse transcriptase control	tests efficiency of cDNA synthesis using the built-in external RNA of the RT^2 First Strand Kit
PPC	Positive PCR control	tests for PCR inhibitors using a pre-dispensed artificial DNA sequence
GDC	Genomic DNA control	detects non-transcribed genomic DNA contamination
NRT	No reverse transcription control	tests for genomic DNA contamination in the RNA sample
NTC	No template control (water control)	tests for general DNA contamination in the PCR system

For PCR analysis, three different PCR mastermixes were prepared for each sample (12 in total) and pipetted into the defined wells of the RT^2 RNA QC PCR Array (Figure 13).

At first, mastermix 1 (PCR control of DNA) was prepared by mixing 6 µl of each diluted First Strand cDNA (see 4.2.3.1) with the following components in sterile, nuclease-free 1.5-ml microcentrifuge tubes (Table 29):

Table 29: Composition of mastermix for each cDNA sample

Mastermix 1 components	**Volume per sample [µl]**
2x RT^2 SYBR® Green qPCR Mastermix (1.4-ml vial)	75
Diluted First Strand cDNA synthesis reaction	6
DEPC-water	69
Total volume	**150**

The 2x RT^2 qPCR SYBR® Green Mastermix (SABioscience) is a ready-to-use composition of HotStart DNA *Taq* polymerase, PCR buffer, dNTP mix (dATP, dCTP, dGTP, dTTP) and SYBR® Green dye. After mixing the diluted cDNA with the SYBR®

Green Mastermix, 25 µl of this mastermix were pipetted into the wells of rows A-E (Figure 13).

Sample		1	2	3	4	5	6	7	8	9	10	11	12
cDNA template	A	HK1	HK1	HK1	HK1	HK1	HK1	HK1	HK1	HK1	HK1	HK1	HK1
	B	HK2	HK2	HK2	HK2	HK2	HK2	HK2	HK2	HK2	HK2	HK2	HK2
	C	RTC	RTC	RTC	RTC	RTC	RTC	RTC	RTC	RTC	RTC	RTC	RTC
	D	PPC	PPC	PPC	PPC	PPC	PPC	PPC	PPC	PPC	PPC	PPC	PPC
	E	GDC	GDC	GDC	GDC	GDC	GDC	GDC	GDC	GDC	GDC	GDC	GDC
RNA	F	NRT	NRT	NRT	NRT	NRT	NRT	NRT	NRT	NRT	NRT	NRT	NRT
H_2O	G	PPC	PPC	PPC	PPC	PPC	PPC	PPC	PPC	PPC	PPC	PPC	PPC
	H	NTC	NTC	NTC	NTC	NTC	NTC	NTC	NTC	NTC	NTC	NTC	NTC

Figure 13: Layout and pipetting scheme of 96-well format RT^2 RNA QC PCR Array. The **green** area (rows A-E) includes the PCR controls for the **cDNA** (**mastermix 1**), the **blue** area (row F) includes the PCR controls for the diluted original **RNA** (**mastermix 2**) and the **red** area includes the PCR controls for the **master mix only** (**mastermix 3**). For explanation of abbreviations see **Table 28**.

Then, mastermix 2 (PCR control of RNA) was prepared by mixing 1 µl of an 1:100 dilution of each original RNA sample with 24 µl of mastermix 2 (1x RT^2 qPCR SYBR® Green Mastermix) and 25 µl of this cocktail were pipetted into the wells of row F (Figure 13).

Finally, mastermix 3 (PCR control of water) was prepared by mixing 45 µl of 2x RT^2 qPCR SYBR® Green Mastermix with 45 µl DEPC-water and 25 µl of this cocktail were pipetted into rows G and H (Figure 13).

After loading the PCR array with all mastermixes, the plate was carefully sealed with an optical adhesive film and liquids in the wells were briefly spun down at 2,000 rpm for 20 sec (Labofuge GL, Heraeus Sepatech). Then, the plate was placed in a LightCycler® 480 Real-Time PCR instrument (Roche) and qRT-PCR detection was performed using the following two-step cycling program:

Table 30: qRT-PCR program for the RT^2 RNA QC PCR Array

PCR cycles	Duration	Temperature	Process
1	10 min	95 °C	Heat activation of HotStart DNA *Taq* polymerase
45	15 sec	95 °C	Denaturation of DNA double strands
	1 min	60 °C	Amplification of DNA + recording fluorescence

Data were evaluated using an excel-based RT^2 RNA QC PCR Array Data Analysis template (http://www.sabiosciences.com/pcrarraydataanalysis.php), which automatically performed the calculation of PCR control values based on the fluorescence signals (C_p values) measured for the PCR products of each well.

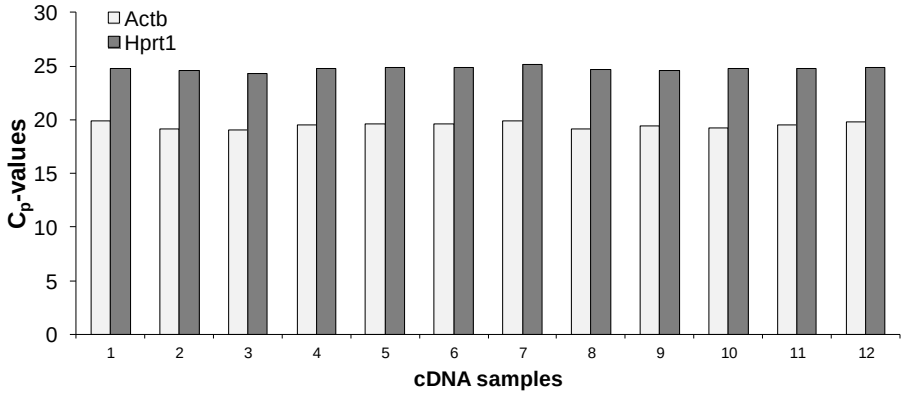

Figure 14: Representative image illustrating C_p-values of the low and high expression housekeeping genes beta-Actin (Actb) and hypoxanthine-guanine phosphoriboyltransferase (Hprt) of cDNA samples analyzed by qRT-PCR using the RT^2 RNA QC PCR Array.

As shown in Figure 14, the levels of the housekeeping genes (HKGs) Actb and Hprt need to be equal for all samples measured to ensure similar cDNA input.

C_p-values greater 35 or N/A (not detected) were set to 35. For quality assurance, all RNA, respective cDNA and water samples need to comply with the following requirements:

Table 31: Interpretation of PCR control values obtained from the RT^2 RNA QC PCR Array

PCR control	Quality criterion	Interpretation
Reverse transcriptase (RTC)	$\Delta C_p = C_p^{RTC} - C_p^{PPC + H_2O}$	$\Delta C_p < 5$: no inhibition $\Delta C_p > 5$: possible inhibition
PCR amplification (PPC)	$C_p^{PPC + H_2O} = 20 \pm 2$ $\Delta C_p = C_p^{PPC + cDNA} - C_p^{PPC + H_2O}$	Proper PCR amplification $\Delta C_p < 3$: no inhibition $\Delta C_p > 3$: possible inhibition
Genomic DNA (in RNA) (NRT)	$C_p^{NRT} \geq 35$ or N/A (n.d.) $C_p^{NRT} < 35$	No genomic DNA Some genomic DNA present, Compare values with GDC
Genomic DNA (in cDNA) (GDC)	$C_p^{GDC} \geq 35$ or N/A (n.d.) $C_p^{GDC} < 30$	No genomic DNA Genomic DNA will affect the results of the PCR
General DNA contamination(NTC)	$C_p^{NTC} \geq 35$ or N/A (n.d.) $C_p^{NTC} \leq 35$	No general contamination Evidence for contamination

4.2.8.10 Gene expression analysis of cancer-related genes in NRK-52E cells

For gene expression analysis, NRK-52E cells were treated with 0.5, 5 and 50 µM FB_1 and RNA was isolated as described in section 4.2.8.8. The isolated RNA was transcribed into cDNA using the RT^2 First Strand Kit (SABiosciences) according to the instructions in section 4.2.3.1. Then, the cDNA/RNA quality for qRT-PCR analysis was assessed by using the RT^2 RNA QC PCR Array (SABiosciences) (see section 4.2.8.9). Changes in the mRNA expression of 84 cancer-related genes in response to FB_1 were analyzed using the RT² Profiler™ PCR Array (SABiosciences) and qRT-PCR (see section 4.2.3.2). After melting curve analysis (see section 4.2.3.3), fold changes in gene expression of FB_1-treated cells relative to controls were calculated using the using the $\Delta\Delta C_t$-method (see section 4.2.3.4).

The mean fold change and SD in gene expression were calculated from the combined data sets (n=6) of two independent experiments with 3 biological replicates per concentration for each control and treatment group. Statistical analysis was performed by one-way analysis of variance (ANOVA) and Dunnett's *post hoc* test using GraphPad Prism® 5 (STATCON) software. Statistically significant changes to controls are indicated by * $p < 0.05$, ** $p < 0.01$ and *** $p < 0.001$.

4.2.8.11 Qualitative gene expression analysis of sphingosine 1-phosphate receptors $S1P_{1-3}$ in NRK-52E cells using classical reverse transcriptase (RT)-PCR

Control RNA samples from the gene expression analysis (see section 4.2.8.8) were used to analyze the expression of sphingosine 1-phosphate receptors $S1P_{1-3}$ in NRK-52E cells by RT-PCR (see section 4.2.5.1). The visualization of RT-PCR products was performed by ethidium bromide staining after DNA agarose gel electrophoresis (see section 4.2.5.2).

4.2.8.12 HPLC-MS/MS for determination of sphingoid bases and sphingolipids in NRK-52E cells

For HPLC-MS/MS analysis of sphingoid bases and sphingolipids, NRK-52E cells were seeded at a density of 2 x 10^5 in 21-cm^2 culture dishes containing 5 ml DMEM and grown to 80-90% confluence at 37 °C and 5% CO_2. The medium was removed and cells were washed with 1x PBS. After careful removal of the washing solution, fresh medium with the respective concentrations of FB_1 and/or the sphingosine kinase inhibitor SKI II (see section 4.2.8.6, Table 25 and Table 26) were placed on the cell layer in the culture dish and incubated at 37 °C and 5% CO_2.

The extraction of sphingoid bases and ceramides from cells and culture media was performed with modifications according to the literature (Bielawski *et al.*, 2006; Bielawski *et al.*, 2009).

After cell treatment, the medium was removed and 2 ml were transferred into a 15-ml conical tube for extraction. Then, cells were washed twice with ice-cold 1x PBS and harvested with 200 µl ice-cold 1x PBS using a cell scraper. The obtained cell suspension was transferred into a 15-ml conical tube on ice. After repeating the harvesting process with further 200 µl ice-cold 1x PBS, the total volume of the cell suspension was gently mixed with a pipette and one aliquot (20 µl) was pipetted into a 0.5-ml microcentrifuge tube on ice for determination of cell number (see section 4.2.8.3). Then, the cell suspension was centrifuged at 1,000 rpm and 4 °C for 10 min and the obtained cell pellets were used for extraction of sphingoid bases and sphingolipids. Before extraction, cell pellets were fortified with 10 pmol of IS mix (see section 4.2.7.1, Table 20). In the next step, 2 ml extraction mixture containing isopropanol:water:ethyl acetate (30:10:60; v:v:v) were added to the cell pellets and the tubes were thoroughly vortexed. After centrifugation at 4,000 rpm for 10 min, the supernatants were collected in a new 10-ml tube and the cell pellets were re-

extracted with 2-ml extraction mixture followed by repeated centrifugation. Then, supernatants were combined in the 10-ml tube to a total volume of 4 ml for each sample.

Subsequently, 2 ml of the collected media from each sample were fortified with 10 pmol IS mix and 2 ml of the medium-extraction mixture containing isopropanol:ethyl acetate (15:85; v:v) were added to the 15-ml tube. For extraction, tubes were thoroughly vortexed, centrifuged at 4,000 rpm for 10 min and the upper, organic phase was transferred into a new 10-ml tube. Before repeating the extraction and centrifugation step, samples were acidified with 100 µl formic acid to improve separation of the aqueous and organic phase. The obtained supernatants from the two extraction steps were combined in the 10-ml tube to a total volume of 4 ml for each sample.

A calibration curve for each sphingolipid analyte was established after analogous extraction of artificial matrices for cells and media spiked with the analytical and internal standard mix solution (see section 0) and subsequent HPLC-MS/MS of extracts.

The samples and calibration standards were prepared for HPLC-MS/MS analysis as described in section 4.2.7.4. HPLC-MS/MS measurement and data evaluation were performed according to the instructions in section 4.2.7.5.

Data from the analysis of NRK-52E cells were normalized by relating the amount of sphingoid bases and ceramides to the amount of counted cells per sample, expressed as pmol per $1x10^6$ cells. The mean and SD of the amounts of sphingoid bases and ceramides was calculated from three biological replicates per concentration for each control and treatment group. Statistical analysis was performed by one-way analysis of variance (ANOVA) and Dunnett's *post hoc* test using GraphPad Prism® 5 (STATCON) software. Statistically significant changes to controls are indicated by * $p < 0.05$, ** $p < 0.01$ and *** $p < 0.001$.

4.2.8.13 Cell invasion assay

To determine if treatment with FB_1 or sphingosine 1-phosphate (So1P) enhances the invasive potential of NRK-52E cells, an invasion assay based on the principle of a Boyden chamber was performed. The modified Boyden chamber is the most

commonly used *in vitro* invasion assay, which was originally derived from the filter assay for studying cell migration (Boyden, 1962).

In this study, transwell inserts with gelatin-coated polyethylene terephthalate membranes were used as modified Boyden chambers for the invasion assay. By inserting these transwells into the wells of a cell culture plate containing 10% FCS as chemoattractant, a migration chamber consisting of an upper and lower chamber separated by the gelatin-coated membrane is formed (Figure 15). Cells that are able to enzymatically degrade the gelatin barrier on the porous membrane in the upper chamber migrate through the pores of the membrane into the lower chamber following a chemotactic gradient (Figure 15).

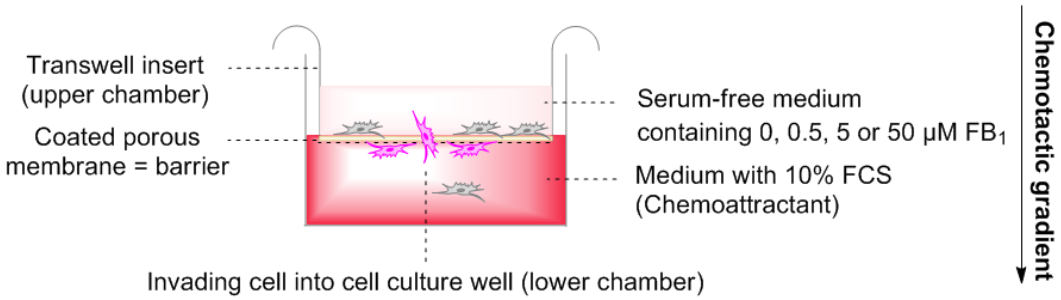

Figure 15: Illustration of cell invasion assay. Cells seeded in serum-free medium in the upper chamber (transwell insert) may migrate through a coated porous membrane (simulating extracellular matrix) into the lower chamber (cell culture well) following a chemotactic gradient. Cells that invade through the coated membranes adhere onto the lower surface of the membrane and are microscopically counted after staining with *e.g.* crystal violet.

The invasive potential can be assessed by counting cells on the lower side of the membrane. The protocol for the cell invasion assay was modified from (Shaw, 2005).

ThinCert™ cell culture transwell inserts with a membrane pore size of 8 µm, which is suitable for the migration of epithelial cells, were coated with 40 µl of an autoclaved 2% gelatin solution (20 mg/ml protein concentration). The transwell inserts (upper chamber) were placed into the wells of a 24-well culture plate (lower chamber) to form a migration chamber. The two-compartment culture plate was gently tipped to evenly cover the surface of the insert membranes with the coating solution and then dried at room temperature (RT) under the laminar flow over night. The following day, the lower chamber was filled with NRK-52E cell culture medium containing 10% FCS as chemoattractant. Then, cells from a 75-cm^2 cell culture flask were harvested using 2

ml trypsin/EDTA followed by incubation at 37 °C and 5% CO_2 for 2 min. To inhibit the trypsinization process, cells were resuspendend in cell culture medium containing 1% BSA and centrifuged at 1,200 rpm for 5 min. The obtained cell pellet was washed with 4 ml serum-free medium containing 0.1% BSA by resuspension with a serological pipette. An aliquot of 20 µl of the cell suspension was used for the determination of cell number in a Neubauer hemocytometer (see section 4.2.8.3). After repeated centrifugation at 1,200 rpm for 5 min, cells were adjusted to a concentration of 1 x 10^5/ml by resuspending the cell pellet in the appropriate volume of serum-free cell culture medium containing 0.1% BSA. Then, 100 µl of the cell suspension (containing 1 x 10^4 cells) were mixed with 25 µl of FB_1 solution (2.5, 25 or 250 µM) or So1P solution (2.5, 5 and 25 µM) in a sterile microcentrifuge tube to obtain the desired concentrations of FB_1 (0.5, 5.0 or 50 µM) or So1P (0.5, 1.0 and 5.0 µM), respectively. For vehicle treatment, 100 µl of cell suspension was suspended with 25 µl sterile water or 2.4% aqueous methanol solution (final concentration of 0.6% methanol). The total volume (125 µl) of premixed FB_1/So1P or vehicle cell suspension was carefully pipetted in the coated inserts (upper chamber) to avoid the formation of bubbles. Then, inserts were placed into the prefilled wells of the lower chamber. After incubation at 37 °C and 5% CO_2 for 24 h, the culture inserts were carefully removed from the wells of the lower chamber and non-invading cells on the upper surface of the membrane were thoroughly wiped off using a cotton swab. The transwell inserts were then placed into the wells of new 24-well cell culture plate, each containing 500 µl of ice-cold methanol for the fixation of invaded cells adherent to the lower surface of the porous membrane. After 15 min fixation in methanol, inserts were removed and transferred to a new 24-well culture plate containing 500 µl crystal violet solution (0.2% in 2% aqueous ethanol) per well. A 15 min incubation period was applied to stain the cells adhering to the lower surface of the membranes of the transwell insert. Then, excess stain was removed from the membranes by immersing the inserts in water. After several washing steps, inserts were inverted and allowed to air dry. To microscopically analyze cell invasion, dried membranes were dissected using a scalpel, transferred to a glass slide and overlaid with a cover slip. Cell invasion was quantified by counting cells that had invaded through the gelatin matrix of the porous membrane. Using an inverted microscope and a grid eyepiece reticule with a defined counting area of 1 mm^2, the number of invading cells was determined in three sections, consisting of 5 adjacent microscopic fields, located in the middle of each

membrane at 200x magnification. After counting, fold changes in cell invasion relative to controls were determined.

The mean fold changes and SD in FB_1-induced cell invasion relative to controls were calculated from the means of three independent experiments with three biological replicates per concentration for each control and treatment group. The mean fold changes and SD in So1P-induced cell invasion relative to controls were calculated from three biological replicates per concentration for each control and treatment group. Statistical analysis was performed by one-way analysis of variance (ANOVA) and Dunnett's *post hoc* test using GraphPad Prism® 5 (STATCON) software. Statistically significant changes to controls are indicated by * $p < 0.05$, ** $p < 0.01$ and *** $p < 0.001$.

5 Results

5.1 Short-term study on the identification of early histopathological, biochemical and transcriptional changes associated with fumonisin B_1 carcinogenicity in rats

This study aimed to identify early molecular changes associated with FB_1 carcinogenicity to provide a more comprehensive understanding of the mechanism of tumor formation by this non-genotoxic carcinogen. A specific objective was to identify early time- and dose-dependent transcriptional alterations of cancer-related genes in kidney and liver of male Sprague Dawley rats following *intraperitoneal* (*i.p.*) administration of 0.25 and 0.75 mg/kg bw/d FB_1 for 1 and 6 days. A further purpose of this study was to link FB_1-induced changes in the transcriptional profile of cancer-related genes to early histopathological alterations (apoptosis and subsequent cell proliferation) as well as biochemical alterations in sphingolipids known to modulate apoptosis, cell proliferation and various other biological processes involved in tumorigenesis. The study design was based on short-term studies demonstrating that *i.p*. administration of FB_1 to male Sprague Dawley rats resulted in increased apoptosis as well as subsequent regenerative proliferation (Bondy *et al.*, 2000) and markedly increased levels of pro-apoptotic sphingoid bases in rat kidney (Domijan *et al.*, 2007b) comparable to those seen in FB_1-treated male Fischer F344N rats administered known carcinogenic doses *via* feed (NTP, 2001).

5.1.1 General toxicity

5.1.1.1 Food and water consumption

Single *i.p.* administration of 0.25 or 0.75 mg/kg bw/d FB_1 had no effect on 24 h food and water consumption in male Sprague Dawley rats (data not shown). However, a small, dose-related decrease in food consumption was observed after ≥ 4 days of exposure (Figure 16). Water consumption was increased in the dose group receiving 0.25 mg/kg bw/d FB_1 for ≥ 3 days (Figure 16).

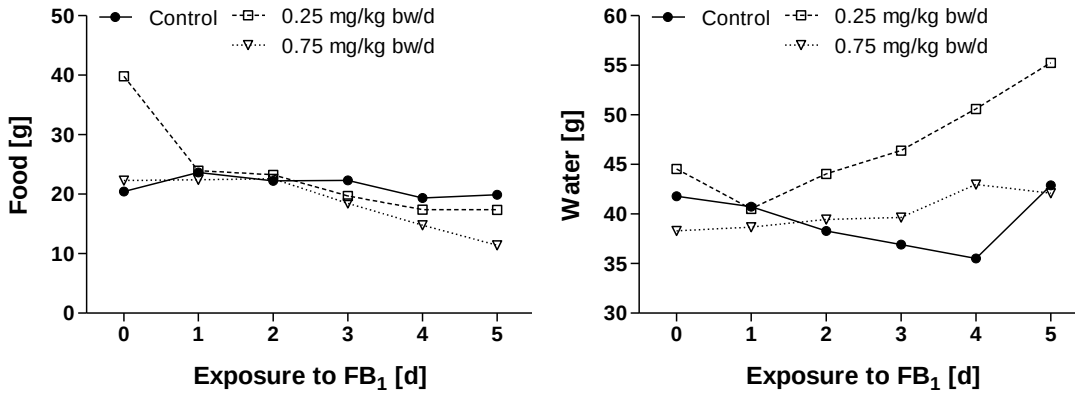

Figure 16: Food and water consumption of male Sprague Dawley rats after treatment with saline (control) or FB_1 (0.25 or 0.75 mg/kg bw/d) for 1 or 6 days. Data are presented as mean daily food and water consumption of n=4 animals per dose group.

5.1.1.2 Body and organ weights

No effects on body weights were observed after a single *i.p.* dose of 0.25 or 0.75 mg/kg bw/d FB_1 (Table 32). In contrast, rats repeatedly treated with *i.p.* doses of 0.25 or 0.75 mg/kg bw/d FB_1 for 6 days showed a statistically significant dose-related decrease in body weights compared to controls (Table 32), consistent with the reduced food consumption in these animals (Figure 16).

Table 32: Body and organ weights (kidney and liver) of male Sprague Dawley rats treated with saline (control) or FB_1 (0.25 or 0.75 mg/kg bw/d) for 1 or 6 days. Data are presented as mean ± standard deviation (n=4). Statistical analysis was performed by one-way analysis of variance (ANOVA) and Dunnett's *post hoc* test. Statistically significant changes to controls are indicated by * $p < 0.05$ and ** $p < 0.01$.

	1-day treatment FB_1 [mg/kg bw/d]			**6-day treatment FB_1 [mg/kg bw/d]**		
	0	0.25	0.75	0	0.25	0.75
Body weight [g]	211 ± 4	206 ± 3	214 ± 4	253 ± 5	235 ± 11 *	225 ± 4 **
Kidney weight [g]						
absolute	1.60 ± 0.10	1.55 ± 0.10	1.66 ± 0.11	1.81 ± 0.13	1.90 ± 0.19	1.74 ± 0.02
relative	0.76 ± 0.05	0.75 ± 0.04	0.78 ± 0.04	0.71 ± 0.04	0.81 ± 0.06 *	0.78 ± 0.02
Liver weight [g]						
absolute	7.56 ± 0.36	7.45 ± 0.41	7.70 ± 0.63	8.37 ± 0.39	7.45 ± 0.64	6.87 ± 0.63 **
relative	3.58 ± 0.13	3.62 ± 0.22	3.60 ± 0.24	3.31 ± 0.13	3.17 ± 0.16	3.05 ± 0.25

Absolute and relative organ weights of kidneys and livers remained unchanged in rats treated with 0.25 or 0.75 mg/kg bw/d FB_1 for 1 day (Table 32). Repeated

administration of FB_1 for 6 days also showed no dose-related effects in kidney (Table 32). Absolute and relative liver weights were decreased in a dose-related manner after 6-day treatment, although statistically significant changes are only seen at 0.75 mg/kg bw/d (Table 32).

5.1.2 Clinical chemistry and urine analysis

5.1.2.1 Serum clinical chemistry parameters

After single *i.p*. administration of 0.25 or 0.75 mg/kg bw/d FB_1, serum levels of potassium and calcium significantly increased (Table 33). Urea, a marker for renal function, was decreased in animals receiving a single *i.p*. dose of 0.75 mg/kg bw/d FB_1. No signs of hepatotoxicity were apparent after single exposure to FB_1.

Exposure to 0.25 or 0.75 mg/kg bw/d FB_1 for 6 days resulted in a dose-dependent increase in creatinine and urea, which are both indicators of nephrotoxicity (Table 33). Signs of hepatotoxicity were indicated by a marked dose-related increase in the activity of the liver enzymes aspartate aminotransferase (ASAT), alanine aminotransferase (ALAT), alkaline phosphatase (ALP) and glutamate dehydrogenase (GLDH). Furthermore, lactate dehydrogenase (LDH), an enzyme indicative of severe tissue damage, was significantly increased at 0.75 mg/kg bw/d FB_1.

5.1.2.2 Urinary clinical chemistry parameters

After single *i.p*. treatment with 0.25 or 0.75 mg/kg bw/d FB_1 no major changes in urinary parameters were observed (Table 33). After *i.p.* administration of FB_1 for 6 days, a dose-related increase in urine volume associated with reduced osmolality was observed, indicating a reduced ability to concentrate urine (Table 33). Urinary excretion rates of creatinine over 12 h were not altered in treated animals (Table 33). Furthermore, urinary pH was decreased in animals receiving FB_1 for 6 days (Table 33).

Table 33: Serum and urinary clinical chemistry parameters in Sprague Dawley rats treated with saline (control) or FB_1 (0.25 or 0.75 mg/kg bw/d) for 1 or 6 days. Data are presented as mean ± standard deviation (n=4). Statistical analysis was performed by one-way analysis of variance (ANOVA) and Dunnett's *post* hoc test. Statistically significant changes to controls are indicated by * $p < 0.05$, ** $p < 0.01$ and *** $p < 0.001$.

Clinical Parameters	1-day FB_1 treatment			6-day FB_1 treatment		
	Control	0.25 mg/kg bw/d	0.75 mg/kg bw/d	Control	0.25 mg/kg bw/d	0.75 mg/kg bw/d
Serum						
Sodium [mmol/l]	143 ± 2	142 ± 1	142 ± 1	144 ± 1	143 ± 2	140 ± 2 *
Potassium [mmol/l]	7.7 ± 0.3	8.9 ± 0.6 *	8.8 ± 0.6 *	7.9 ± 0.5	8.3 ± 1.1	9.7 ± 0.3 *
Calcium [mmol/l]	3.3 ± 0.1	3.5 ± 0.1 *	3.4 ± 0.1 *	3.5 ± 0.2	3.7 ± 0.1	3.6 ± 0.1
Anorganic phosphorus [mmol/l]	4.6 ± 0.2	4.9 ± 0.1 *	4.7 ± 0.1	4.6 ± 0.2	3.9 ± 0.2 **	3.9 ± 0.3 **
Chloride [mmol/l]	100 ± 1	99 ± 2	100 ± 1	101 ± 1	101 ± 2	103 ± 1
Glucose [mg/dl]	128 ± 11	129 ± 21	104 ± 10	223 ± 75	171 ± 35	153 ± 28
Creatinine [mg/dl]	0.20 ± 0.00	0.25 ± 0.06	0.25 ± 0.06	0.38 ± 0.05	0.63 ± 0.13 **	0.60 ± 0.08 *
Urea [mg/dl]	26.5 ± 2.2	28.9 ± 3.9	21.1 ± 1.7 *	41.6 ± 4.4	50.7 ± 5.7	60.6 ± 9.7 **
Total bilirubin [mg/dl]	0.10 ± 0.00	0.10 ± 0.00	0.10 ± 0.00	0.08 ± 0.05	0.15 ± 0.17	0.93 ± 0.85
Aspartate aminotransferase (ASAT) [UI/l]	107 ± 20	166 ± 104	190 ± 110	117 ± 18	265 ± 86	544 ± 124 ***
Alanine aminotransferase (ALAT) [UI/l]	40.1 ± 3.3	53.6 ± 16.8	44.6 ± 6.3	57.3 ± 12.8	126 ± 50	369 ± 189 **
Glutamate dehydrogenase (GLDH) [UI/l]	8.1 ± 2.3	9.1 ± 3.4	7.9 ± 1.8	12.3 ± 6.4	54.0 ± 30.5 *	69.2 ± 15.9 **
γ-Glutamyl transferase (GGT) [UI/l]	0.68 ± 0.59	0.25 ± 0.30	0.50 ± 0.80	1.9 ± 1.4	2.0 ± 0.6	3.1 ± 1.2
Alkaline phosphatase (ALP) [UI/l]	163 ± 29	178 ± 13	176 ± 9	149 ± 19	425 ± 193	822 ± 288 **
Lactate dehydrogenase (LDH) [UI/l]	210 ± 73	412 ± 287	423 ± 327	173 ± 43	381 ± 134	842 ± 304 **
Total creatine kinase (CK) [UI/l]	509 ± 225	1651 ± 2454	1480 ± 1167	508 ± 184	587 ± 421	1284 ± 273 *
Cholesterol [mg/dl]	138 ± 9	171 ± 25 *	182 ± 8 **	125 ± 18	308 ± 26 ***	318 ± 25 ***
Triglycerides [mg/dl]	42.8 ± 8.1	49.8 ± 14.6	61.0 ± 12.5	36.8 ± 5.0	71.3 ± 9.7 ***	72.3 ± 9.7 ***
Total protein [g/dl]	5.7 ± 0.2	6.0 ± 0.2 *	5.9 ± 0.1	6.3 ± 0.1	6.7 ± 0.2	6.5 ± 0.4
Albumin [g/dl]	4.1 ± 0.2	4.2 ± 0.2	4.1 ± 0.1	4.4 ± 0.1	4.7 ± 0.2	4.6 ± 0.3
Urine						
Urine volume [ml]	12.8 ± 2.9	11.6 ± 2.1	12.8 ± 1.3	17.6 ± 3.6	23.5 ± 2.6	25.4 ± 4.0 *
Osmolality [mosmol/kg]	500 ± 163	584 ± 126	468 ± 53	461 ± 97	331 ± 42.9 *	321 ± 45 *
pH	8.0 ± 0.0	8.0 ± 0.8	7.0 ± 0.0 *	8.5 ± 0.6	7.0 ± 0.0 **	7.5 ± 0.6 *
Relative density [g/ml]	1.0 ± 0.0	1.0 ± 0.0	1.0 ± 0.0	1.0 ± 0.0	1.0 ± 0.0	1.0 ± 0.0
Creatinine [mg/12 h]	3.0 ± 0.2	3.1 ± 0.1	3.2 ± 0.3	3.6 ± 0.4	3.4 ± 0.4	3.5 ± 0.5
Calcium [mmol/l]	2.1 ± 1.0	2.8 ± 0.6	2.2 ± 1.0	1.7 ± 1.4	1.6 ± 0.8	1.4 ± 0.5
Potassium [mmol/l]	84.7 ± 27.8	83.9 ± 15.6	75.6 ± 13.1	79.5 ± 18.9	42.8 ± 8.9 **	34.7 ± 6.9 **
Sodium [mmol/l]	75.7 ± 24.6	98.8 ± 24.0	75.1 ± 8.2	62.0 ± 9.1	53.8 ± 9.3	43.6 ± 4.6 *
Anorganic phosphorus [mmol/l]	7.5 ± 3.8	9.6 ± 4.9	13.1 ± 1.4	7.9 ± 2.9	11.8 ± 2.0	14.0 ± 3.1 *
Total protein [mg/mg creatinine]	0.8 ± 0.3	3.1 ± 4.0	0.8 ± 0.1	2.3 ± 0.9	4.4 ± 1.1 *	3.6 ± 0.4

The amount of total urinary protein, indicative of kidney damage, was slightly increased in animals exposed FB_1 (Table 33).

After single exposure to FB_1 a few erythrocytes, but moderate amounts of leukocytes were present in control and treated animals. The number of animals with a positive nitrite test in urine dose-dependently increased after FB_1 exposure. However, urinary nitrite was also present in individual controls.

Table 34: Evaluation of test stripe parameters in urines of male Sprague Dawley rats treated with saline (control) or FB_1 (0.25 or 0.75 mg/kg bw/d) for 1 or 6 days. Each urinary parameter is summarized by - for negative or + for positive results (average of 4 rats per group), whereby positive levels are graded from + (minimal), ++ (mild), +++ (moderate) to ++++ (high).

Test stripes	**1-day treatment FB_1 [mg/kg bw/d]**			**6-day treatment FB_1 [mg/kg bw/d]**		
Parameters	**Control**	**0.25**	**0.75**	**Control**	**0.25**	**0.75**
Protein	(+) (3/4)	+(+) (4/4)	+ (4/4)	+(+) (4/4)	++(+) (4/4)	++ (4/4)
Erythrocytes	-+ (1/4)	(+) (1/4)	-	+++(+) (4/4)	++++ (4/4)	++++ (4/4)
Leukocytes	+(+) (4/4)	++ (4/4)	+ (4/4)	+++ (4/4)	+++ (4/4)	+++ (4/4)
Nitrite	(+) (2/4)	(+) (3/4)	+ (4/4)	-	-	-+ (1/4)
Glucose	-	-	-	+ (3/4)	+ (3/4)	-
Ketones	-+ (1/4)	+ (4/4)	(+) (2/4)	+(+) (4/4)	++ (4/4)	+(+) (4/4)
Bilirubin	-	-	-	-	-	-
Urobilirubin	-	-	-	-	-	-

Compared to the single dose experiment, animals treated for 6 days showed a significant increase in protein, erythrocytes, leukocytes and ketones (Table 34), which may be due to an inflammation or injury of the urinary tract, probably as a result of repeated *i.p.* application. No treatment-related effects were seen, except for a slight increase in urinary protein after treatment with FB_1 at 0.25 and 0.75 mg/kg bw/d.

5.1.3 Histopathology

5.1.3.1 Histopathological alterations in kidney

Administration of 0.25 or 0.75 mg/kg bw/d FB_1 for 1 or 6 consecutive days resulted in time- and dose-dependent histopathological alterations in kidneys of male Sprague Dawley rats compared to controls (Figure 17).

After a single *i.p.* dose, early signs of FB_1-induced nephrotoxicity in the renal cortex and OSOM were evident at both dose levels with increasing severity related to dose. Histopathological alterations included cell degeneration and detachment of tubular cells from the renal epithelium into the tubule lumen (Figure 17). The tubular damage in the cortex and OSOM markedly increased in a dose-dependent manner after 6-day exposure to FB_1 (Figure 17). Dilated and vacuoled tubules, loss of brush border membrane and flattened epithelium along the basement membrane were observed as consequence of substantial tubular cell degeneration and regeneration in response to FB_1. Exfoliation of cellular debris into the tubular lumen was more pronounced than after single dose treatment (Figure 17). Unexpectedly, individual controls of the 6-day study also showed signs of tubular damage in the OSOM, which correlated with the increased excretion of urinary protein compared to controls of the single dose study (see Table 33 and Table 34).

5.1.3.2 Histopathological alterations in liver

Treatment with FB_1 resulted in a time- and dose dependent increase in histopathological lesions in livers of male Sprague Dawley rats compared to controls.

After single exposure to FB_1, histopathological alterations in liver predominantly involved degeneration of hepatocytes as well as enlarged sinusoids with increased numbers of Kupffer cells within centrilobular areas of the hepatic lobules (data not shown). Increased hepatic damage was observed after 6-day treatment and consisted of ongoing disorganization of hepatic cords, sinusoidal dilation and congestion in the centrilobular area (Figure 18).
A significantly increased numbers of Kupffer cells was found in areas of necrosis around the central vein after 6-day exposure to FB_1.

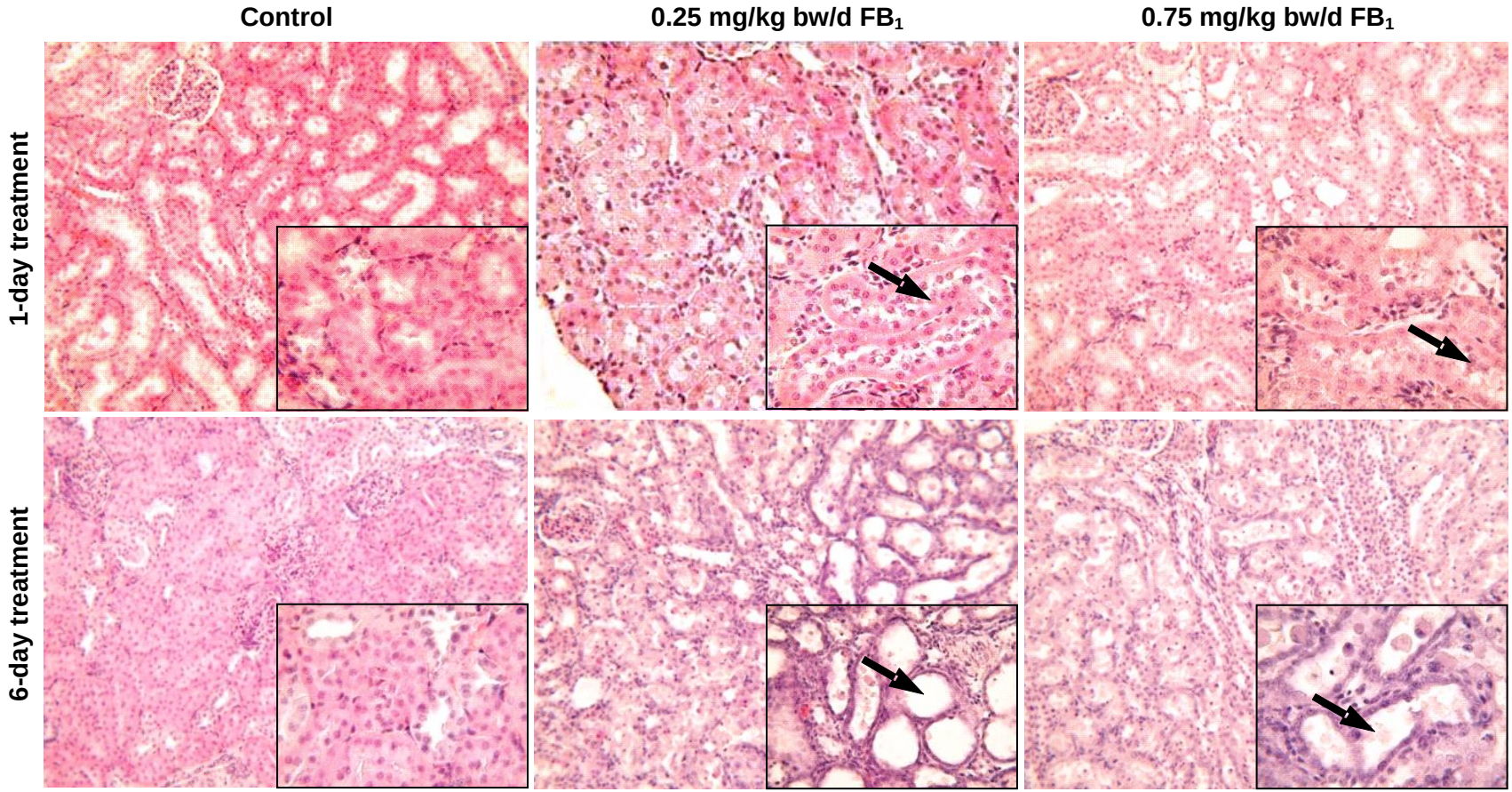

Figure 17: Hematoxylin and eosin (H&E) stained kidney sections of male Sprague Dawley rats after treatment with saline (control) or FB_1 (0.25 and 0.75 mg/kg bw/d) for 1 or 6 days. Representative images from renal cortex and outer stripe of outer medulla (OSOM) of control and treated rats were acquired at 200x and at 400x magnification for zoomed inserts, respectively. After 1-day treatment with 0.25 and 0.75 mg/kg bw/d, FB_1-induced detachment of tubular cells from the renal epithelium into the tubule lumen was observed in the cortical region and OSOM of rat kidneys (arrows). Progressive tubular damage, characterized by dilated and vacuoled tubules with loss of brush border membrane and flattened epithelium (arrows), was prominent in the OSOM and renal cortex after 6-day treatment with 0.25 and 0.75 mg/kg bw/d FB_1.

Single apoptotic hepatocytes with eosinophilic cytoplasm and pyknotic cell nuclei were scattered around the central vein at 0.75 mg/kg bw/d FB_1 (Figure 18).

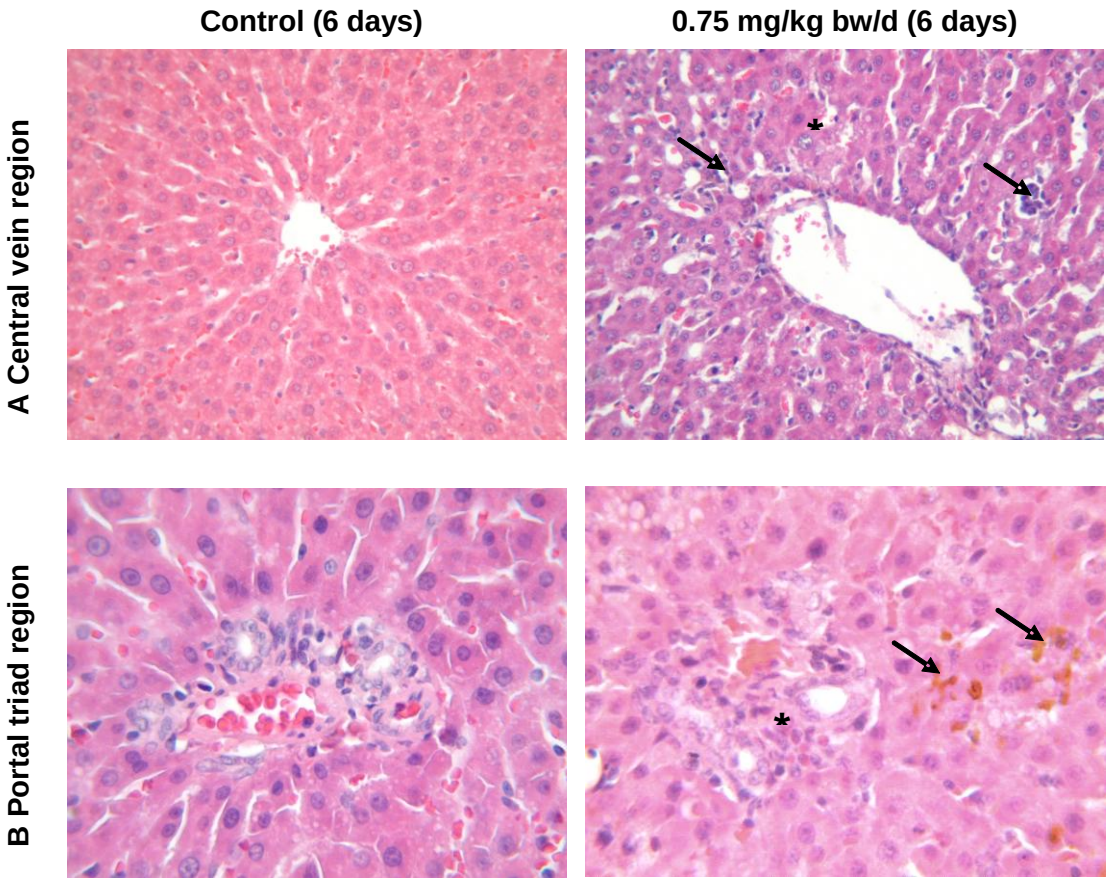

Figure 18: Hematoxylin and eosin (H&E) stained liver sections of male Sprague Dawley rat after treatment with saline (control) or 0.75 mg/kg bw/d FB_1 for 6 days. Representative images from central vein and portal triad of control and treated rats were acquired at 200x and at 400x magnification, respectively. (A) Central vein region: increased numbers of Kupffer cells (arrows) in enlarged sinusoids and single apoptotic hepatocytes (asterisks) were observed. (B) Portal triad region: Bile duct hyperplasia (asterisks) and accumulation of yellow pigment (indicative of cholestasis) within hepatocytes (arrows) were found (B).

In addition, administration of 0.75 mg/kg bw/d FB_1 for 6 days resulted in hyperplasia of the bile duct in livers of male Sprague Dawley rats. Hyperplasia was characterized by increased proliferation of bile duct epithelial cells in the portal triad of the liver (Figure 18). Evidence for hepatic cholestasis was also obtained from histopathological investigation of these animals, showing yellow pigmentation in the liver (Figure 18).

5.1.4 Apoptosis and cell proliferation

5.1.4.1 Assessment of FB_1-induced apoptosis in kidney

To qualitatively assess FB_1-induced renal tubule cell apoptosis in male Sprague Dawley rats, histochemical investigation of DNA fragmentation was performed using the TUNEL assay (Figure 19).

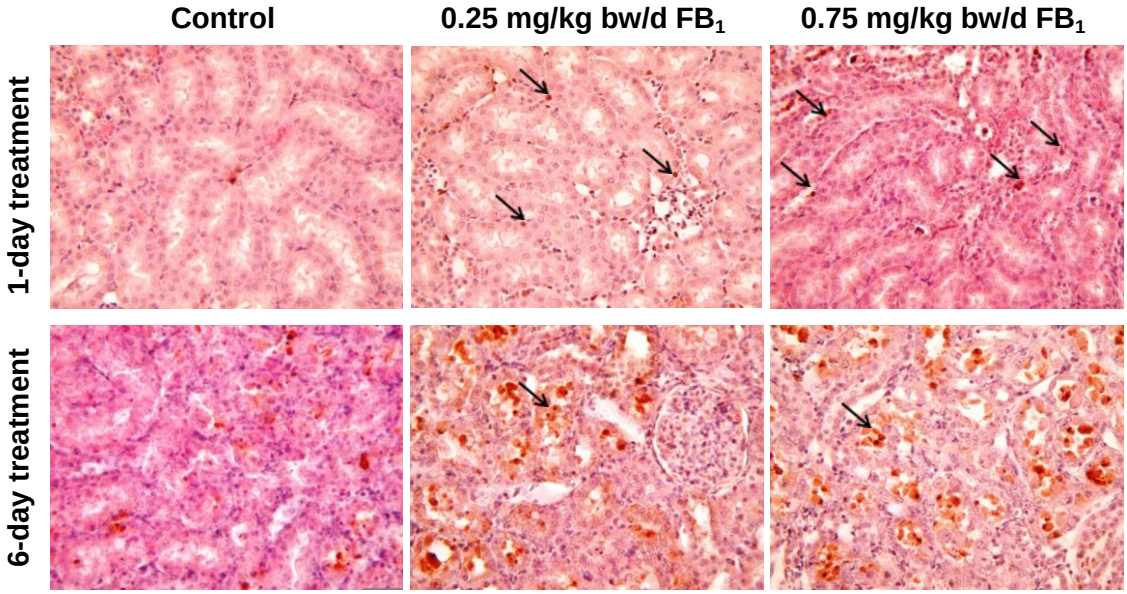

Figure 19: Histochemical assessment of renal apoptosis by TdT-mediated dUTP-biotin nick end labeling (TUNEL) staining of kidney sections of male Sprague Dawley rats treated with saline (control) or FB_1 (0.25 and 0.75 mg/kg bw/d) for 1 or 6 days. Representative images from the renal cortex and the outer stripe of the outer medulla (OSOM) of control and treated rats were acquired at 200x magnification. After 1-day treatment with 0.25 mg/kg bw/d FB_1 only few TUNEL-positive cells were observed in the OSOM and renal cortex of rat kidneys, whereas 0.75 mg/kg bw/d FB_1 enhanced the frequency of apoptotic cells in both regions of the kidney (arrows). Pronounced apoptotic staining in the OSOM as well as the renal cortex was evident in rat kidneys of both dose groups after 6-day treatment with FB_1. At this time point, TUNEL-positive cells were predominantly located in the lumen of the tubular epithelium as a result of cellular detachment from the basal membrane.

After single exposure to FB_1, positively stained apoptotic nuclei were observed in the cortex and OSOM of FB_1-treated animals, whereas controls only showed a few apoptotic cells (Figure 19). However, a statistically significant increase in the percentage of apoptotic cells was only seen in cortex at 0.75 mg/kg bw/d FB_1 (Figure 20).

Marked renal tubular apoptosis within the cortex and OSOM was observed in animals treated with FB_1 for 6 days (Figure 19) with a clear dose-related increase with

increasing dose. However, evidence of apoptosis was also found in the OSOM of controls, which is consistent with the histopathological alterations observed in these animals (see section 5.1.3.1).

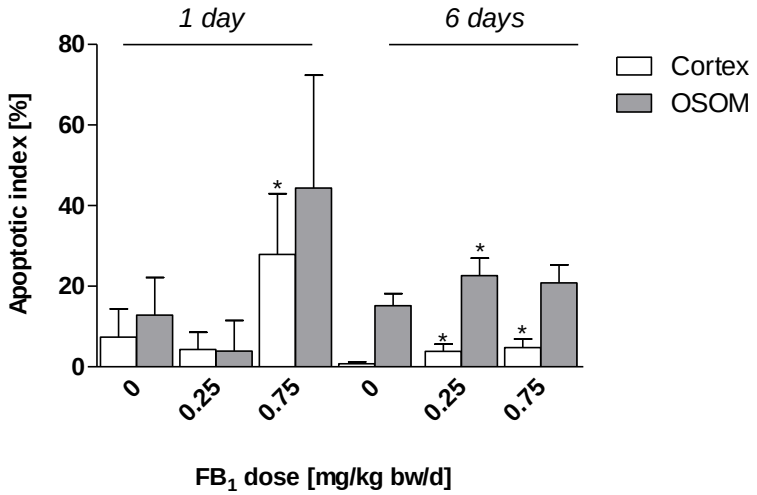

Figure 20: Quantitative assessment of renal cell apoptosis in the cortex and OSOM determined by TdT-mediated dUTP-biotin nick end labeling (TUNEL) of stained kidney sections of male Sprague Dawley rats treated with saline (control) or FB_1 (0.25 and 0.75 mg/kg bw/d) for 1 or 6 days. Apoptotic indices of control and dose groups were calculated as the percentage of the number of TUNEL-stained cell nuclei per total number of cell nuclei per field of view at 400x magnification. Data are presented as mean ± standard deviation (n=4). Statistical analysis was performed by one-way analysis of variance (ANOVA) and Dunnett's post hoc test. Statistically significant changes to controls are indicated by * $p < 0.05$.

5.1.4.2 Assessment of FB_1-induced cell proliferation in kidney

To assess whether FB_1-induced apoptosis in the renal tubular cells of male Sprague Dawley rats was accompanied by regenerative cell proliferation, immunohisto-chemical staining of BrdU-positive cells was performed in kidney tissues of treated and non-treated animals (Figure 21). After a single administration of 0.25 or 0.75 mg/kg bw/d FB_1 no significant increase in BrdU-labeling was seen (Figure 21 and Figure 22). Repeated administration of FB_1 for 6 days led to a marked increase in the number of stained BrdU-positive tubule cells in the renal cortex and OSOM (Figure 21 and Figure 22). Strikingly, the BrdU-labeling index in the OSOM of controls was markedly increased compared to controls after 1-day treatment, which paralleled the observation of an increased apoptotic index in these animals (see section 5.1.4.1, Figure 19).

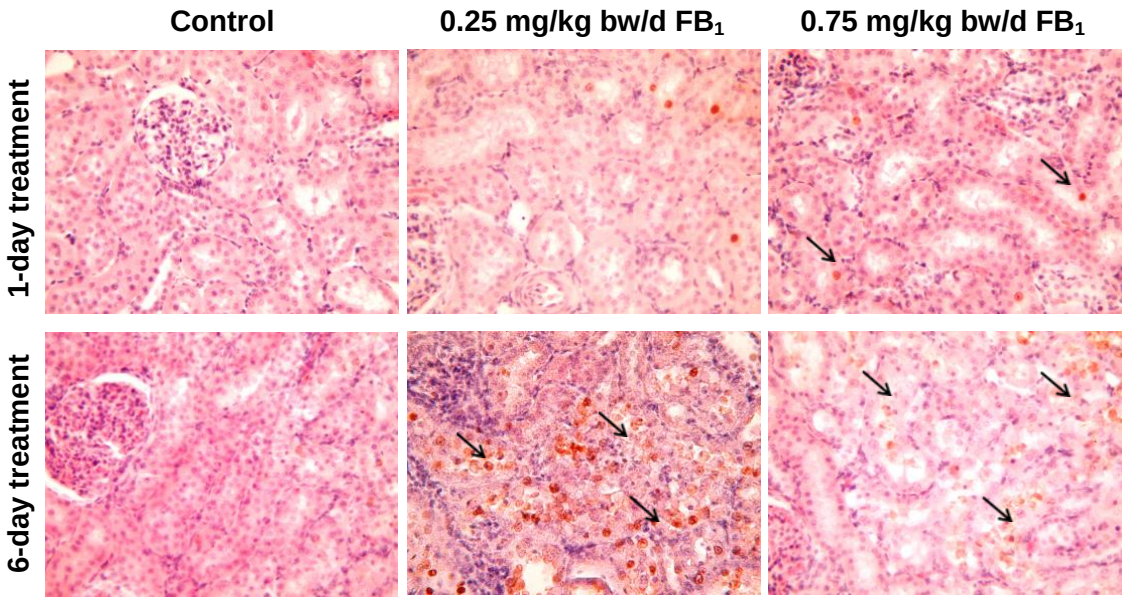

Figure 21: Assessment of renal cell proliferation by BrdU immunohistochemical staining of kidney sections of male Sprague Dawley rats treated with saline (control) or FB_1 (0.25 and 0.75 mg/kg bw/d) for 1 or 6 days. Representative images from renal cortex of control and treated rats were acquired at 200x magnification. A few BrdU positive cells were already present after 1-day treatment with 0.25 and 0.75 mg/kg FB_1 (arrows). In contrast, considerable increases in proliferating cells, which were predominantly located within the tubular epithelium, were observed in renal cortex and OSOM of rats treated with respective doses of FB_1 for 6 consecutive days (arrows).

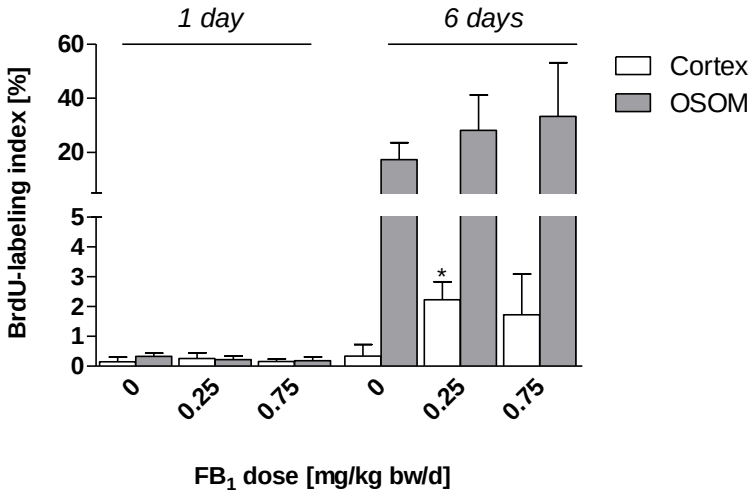

Figure 22: Quantitative assessment of renal cell proliferation in the cortex and OSOM of male Sprague Dawley rats treated with saline (control) or FB_1 (0.25 and 0.75 mg/kg bw/d) for 1 or 6 days. BrdU labeling indices of controls and FB_1 dose groups were calculated as the percentage of the number of proliferating, BrdU-positive cell nuclei per total number of cell nuclei per field of view at 400x magnification. Data are presented as mean ± standard deviation (n=4). Statistical analysis was performed by one-way analysis of variance (ANOVA) and Dunnett's *post hoc* test. Statistically significant changes to controls are indicated by * $p < 0.05$.

5.1.4.3 Assessment of PCNA protein expression in kidney and liver

Complementary evaluation of cell proliferation was performed by western blot analysis of proliferating cell nuclear antigen (PCNA) protein to compare FB_1-mediated cell proliferation in kidneys and livers of male Sprague Dawley rats (Figure 23). Treatment with 0.25 or 0.75 mg/kg bw/d FB_1 for 1 or 6 days resulted in a statistically significant time- and dose-dependent increase in PCNA protein expression in kidneys and livers (Figure 23). In contrast to the BrdU labeling index (see section 5.1.4.2, Figure 21), a statistically significant increase in PCNA expression in kidney was observed after single exposure to FB_1 at both dose levels (Figure 23).

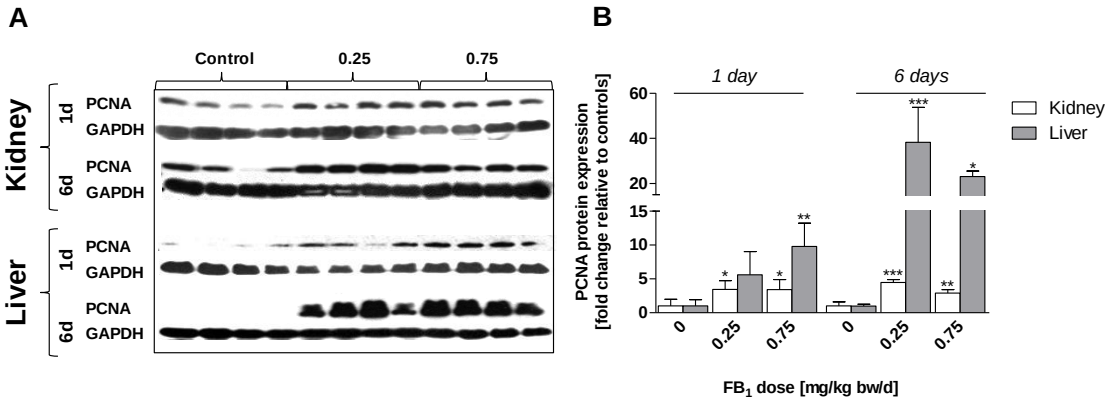

Figure 23: Determination of PCNA protein expression by Western blot and densitometric analysis in kidneys and livers of male Sprague Dawley rats treated with saline (control) or FB_1 (0.25 and 0.75 mg/kg bw/d) for 1 or 6 days. **A** Western Blot bands represent PCNA protein (34 kDa) expression in kidney and liver between control and treated animals (n=4 per group). For normalization of PCNA expression, the expression of GAPDH protein (36 kDa) was determined in parallel. **B** Densitometric analysis of PCNA expression normalized to the expression of GAPDH. Data are represented as mean fold expression changes ± standard deviation (n=4) relative to controls. Statistical analysis was performed by one-way analysis of variance (ANOVA) and Dunnett's *post hoc* test. Statistically significant changes to controls are indicated by * $p < 0.05$, ** $p < 0.01$ and *** $p < 0.001$.

5.1.5 Disruption of sphingolipid metabolism

To characterize biochemical changes in sphingolipid metabolism associated with FB_1 toxicity in our study, liquid chromatography/tandem mass spectrometry (LC-MS/MS) was applied for quantitative assessment of specific sphingolipids, sphingolipid precursors and their metabolites in kidney, liver, serum and urine treated with FB_1.

5.1.5.1 Method performance for identification and quantification of sphingolipids

For the tested calibration range (0.25-2000 pmol) of sphingoid bases, sphingoid base 1-phosphates and ceramides, a linear signal response with correlation coefficients (R^2) ≥ 0.99 was obtained.

In Figure 24, representative HPLC-MS/MS chromatograms of the analytes and internal standards of sphingoid bases (**A**) and ceramides (**B**) are displayed.

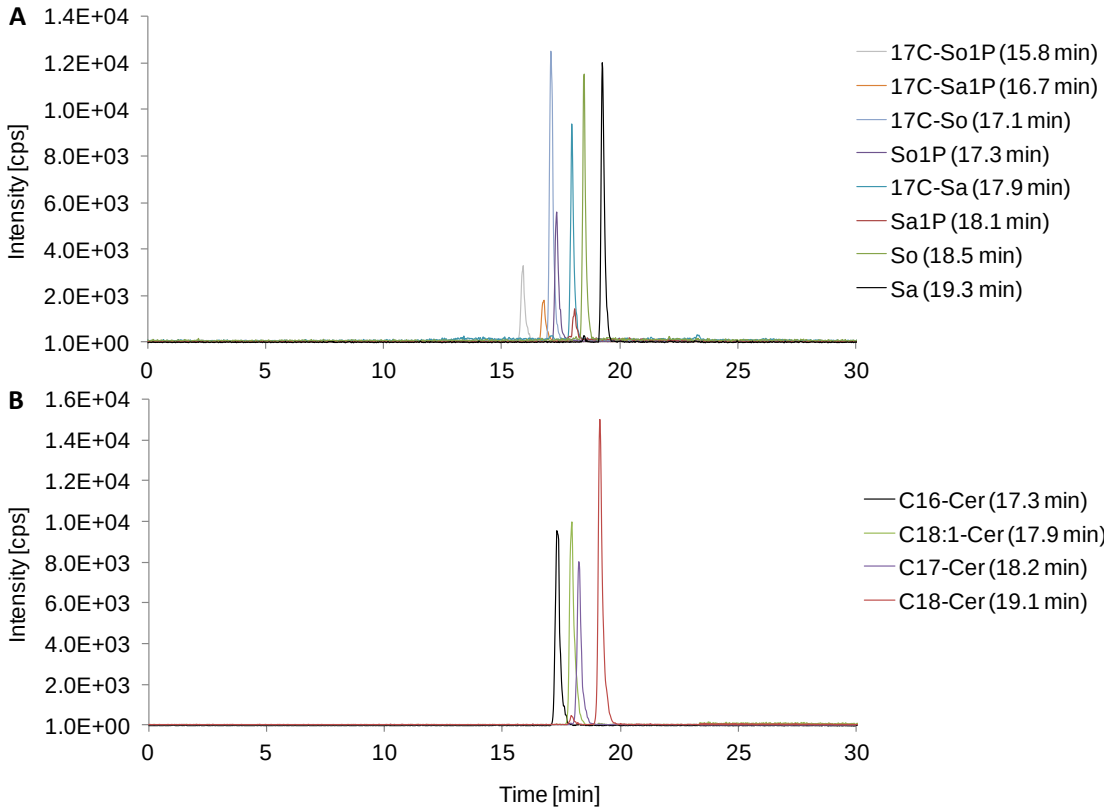

Figure 24: Representative HPLC-ESI_{pos}-MS/MS total ion chromatograms (TICs) showing the analyte and internal standards (17C or C17) of sphingoid bases (**A**) and ceramides (**B**). **So1P** = sphingosine 1-phosphate; **Sa1P** = sphinganine 1-phosphate; **So** = sphingosine; **Sa** = sphinganine; **Cer** = ceramide

As shown for the sphingoid bases Sa, So and their metabolites Sa1P and So1P, all analytes were displayed as separated peaks in their specific mass spectrograms (extracted ion chromatograms) used for integration and quantification (see Figure 25). However, in the extracted ion chromatogram of So, one unidentified peak occurred in all biological samples, but did not affect So quantification.

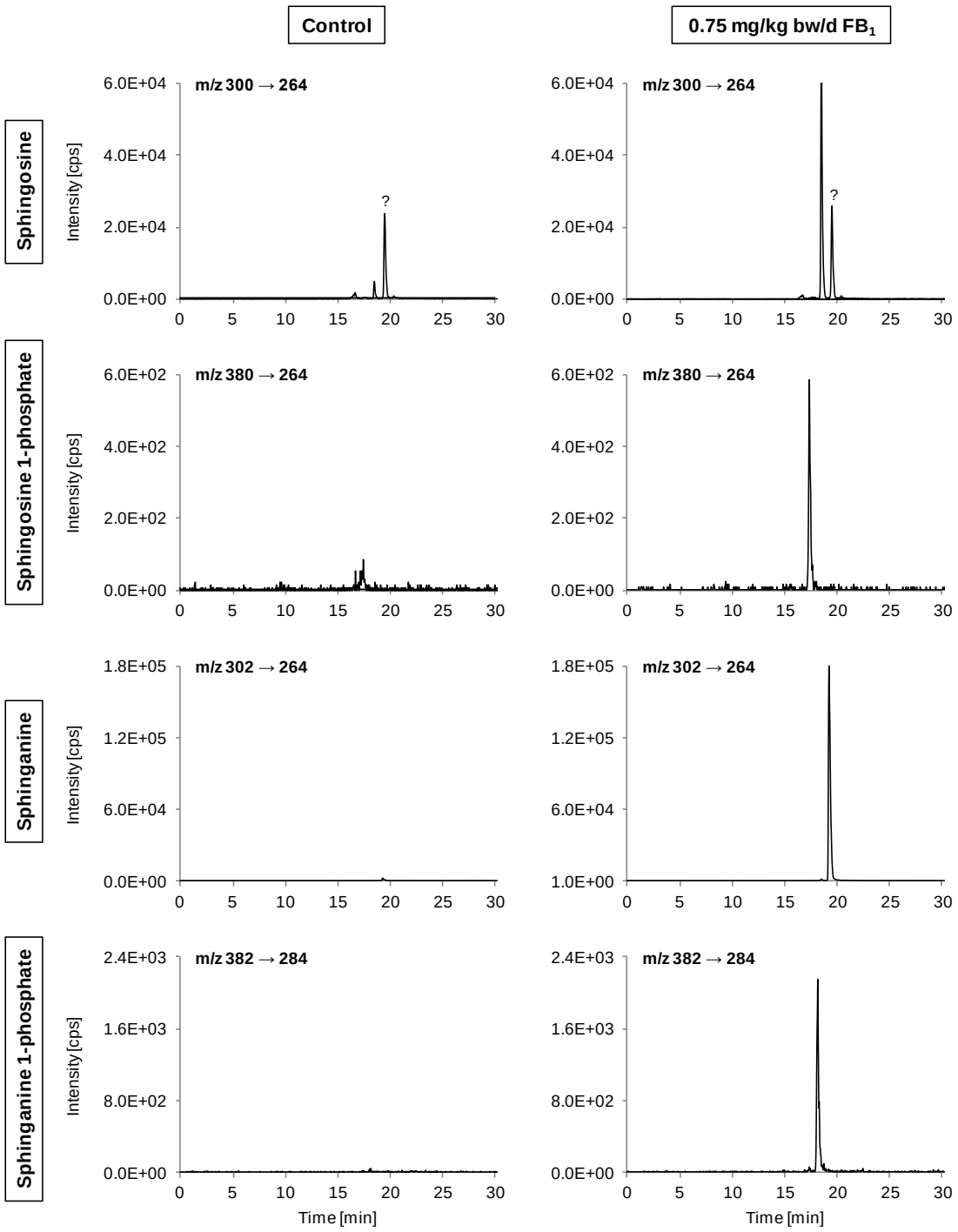

Figure 25: Representative HPLC-ESI_{pos}-MS/MS extracted ion chromatograms (XICs) showing specific mass traces (**m/z**) for sphingosine, sphingosine 1-phosphate, sphinganine and sphinganine 1-phosphate determined in kidneys of a saline-treated (**control**) and a high dose-treated animal (**0.75 mg/kg bw/d FB_1**) after exposure for 1 day. In the mass chromatogram of sphingosine, one unidentified peak (labeled with a question mark) occurs at a retention time of 19.5 min.

5.1.5.2 Alterations in the ceramide precursor sphingoid bases sphinganine and sphingosine and their 1-phosphate metabolites

After treatment with 0.25 and 0.75 mg/kg bw/d FB_1 for 1 or 6 days, a time- and dose-dependent increase in the sphingoid bases sphinganine (Sa), sphingosine (So) and enhanced formation of their respective phosphorylated metabolites sphingosine 1-phosphate (So1P) and sphinganine 1-phosphate (Sa1P) was observed in kidney, liver, serum and urine (see Figure 25 and Table 35). Unexpectedly, increased basal levels of sphingoid bases (Sa and So) and their metabolites (Sa1P and So1P) were found in kidneys and urine of controls after 6-day treatment compared to 1-day treatment, which paralleled the observation of increased renal apoptosis and proliferation in these animals (see section 5.1.4.1 and 5.1.4.2). Strikingly, these effects were only seen in the kidney, but not the liver. Nevertheless, statistically significant effects on the levels of the sphingolipids after treatment with FB_1 for 6 days were seen compared to controls.

Concentrations of the pro-apoptotic *de novo* ceramide precursor Sa were significantly increased in tissues, serum and urine after a single administration of FB_1 compared to the respective controls. At the same time point significant alterations in the amounts of pro-apoptotic So, which is usually formed *via* metabolic degradation of sphingolipids, were only present in liver and kidney, whereas levels in serum and urine were not affected (Table 35). Single exposure to FB_1 also resulted in a significant increase in the ratios of Sa to So, which serves as an important biomarker for the disruption of sphingolipid metabolism in animals studies (Shephard *et al.*, 2007), since it indicates the accumulation of Sa as a result of FB_1-induced inhibition of *de novo* ceramide formation (Table 35).

After 6 days exposure to FB_1, a marked elevation in the serum levels of pro-apoptotic Sa (209-fold), So (2.0-fold) and their respective anti-apoptotic 1-phosphate metabolites Sa1P (3.6-fold) and So1P (1.2-fold) was observed compared to controls (Table 35). In addition, levels of Sa, So, Sa1P and So1P were significantly increased in urine (Table 35).

Table 35: LC-MS/MS determination of sphinganine, sphinganine 1-phosphate, sphingosine and sphingosine 1-phosphate in kidney, liver, serum and urine of male Sprague Dawley rats treated with saline (control) or FB_1 (0.25 or 0.75 mg/kg bw/d) for 1 or 6 days. Data are presented as mean ± standard deviation (n=4). Statistical analysis was performed by one-way analysis of variance (ANOVA) and Dunnett's post hoc test. Statistically significant changes to controls are indicated by * $p < 0.05$, ** $p < 0.01$ and *** $p < 0.001$.

Sphingoid bases	1-day FB_1 treatment			6-day FB_1 treatment		
	Control	0.25 mg/kg bw/d	0.75 mg/kg bw/d	Control	0.25 mg/kg bw/d	0.75 mg/kg bw/d
Sphinganine						
Kidney [pmol/mg]	0.53 ± 0.55	207 ± 24 ***	297 ± 14 ***	307 ± 85	469 ± 85 *	557 ± 62 **
Liver [pmol/mg]	1.9 ± 2.1	8.5 ± 1.8 ***	11.6 ± 1.3 ***	1.0 ± 1.3	39.3 ± 19.9 *	63.6 ± 19.5 ***
Serum [nM]	6.5 ± 4.6	69.1 ± 35.4 *	74.0 ± 25.9 **	1.8 ± 1.3	265 ± 47 ***	376 ± 42 ***
Urine [pmol/mg creatinine]	5.0 ± 10.1	492 ± 280 **	491 ± 81 **	1043 ± 380	3674 ± 1492 **	4073 ± 880 **
Sphinganine 1-phosphate						
Kidney [pmol/mg]	0.34 ± 0.21	51.3 ± 12.6 ***	84.0 ± 8.3 ***	631 ± 95	889 ± 140 *	845 ± 70 *
Liver [pmol/mg]	3.3 ± 1.6	2.4 ± 0.4	2.8 ± 1.1	0.43 ± 0.07	4.8 ± 2.6	10.9 ± 4.3 **
Serum [nM]	2348 ± 425	3073 ± 505	3585 ± 381 **	1853 ± 573	6615 ± 1045 ***	6688 ± 384 ***
Urine [pmol/mg crea]	12.1 ± 5.0	481 ± 125 ***	458 ± 33 ***	3703 ± 443	7627 ± 2954 *	7748 ± 482 *
Sphingosine						
Kidney [pmol/mg]	7.3 ± 0.4	76.1 ± 11.5 ***	99.5 ± 3.9 ***	68.1 ± 15.2	81.5 ± 13.5	92.9 ± 10.0 *
Liver [pmol/mg]	10.1 ± 1.1	14.1 ± 0.8 ***	13.3 ± 0.9 **	10.8 ± 2.9	19.2 ± 4.2 **	19.6 ± 2.0 **
Serum [nM]	126 ± 22	170 ± 55	149 ± 42	90.4 ± 14.5	204 ± 12 ***	182 ± 20 ***
Urine [pmol/mg creatinine]	305 ± 163	224 ± 22	333 ± 203	141 ± 43	366 ± 154 *	464 ± 46 **
Sphingosine 1-phosphate						
Kidney [pmol/mg]	2.1 ± 1.3	13.6 ± 2.4 ***	18.0 ± 4.0 ***	71.1 ± 22.4	71.2 ± 18.1	57.3 ± 5.0
Liver [pmol/mg]	1.6 ± 0.4	2.8 ± 0.9	1.8 ± 0.9	0.67 ± 0.35	2.4 ± 0.9 *	2.1 ± 0.9 *
Serum [nM]	3068 ± 367	3350 ± 187	3220 ± 297	2613 ± 204	3398 ± 387 *	3240 ± 317 *
Urine [pmol/mg creatinine]	1.6 ± 0.5	37.1 ± 8.2 ***	30.3 ± 4.6 ***	123 ± 14	226 ± 105	239 ± 23 *
Sphinganine/sphingosine ratio						
Kidney	0.07 ± 0.08	2.7 ± 0.2 ***	3.0 ± 0.2 ***	4.5 ± 0.5	5.7 ± 0.1 **	6.0 ± 0.5 ***
Liver	0.18 ± 0.19	0.60 ± 0.09 **	0.88 ± 0.10 ***	0.08 ± 0.09	2.0 ± 0.7 **	3.2 ± 0.7 ***
Serum	0.05 ± 0.03	0.40 ± 0.08 ***	0.49 ± 0.04 ***	0.02 ± 0.02	1.3 ± 0.2 ***	2.1 ± 0.2 ***
Urine	0.02 ± 0.04	2.2 ± 1.3 *	2.0 ± 1.1 *	7.3 ± 0.9	10.3 ± 1.6	16.9 ± 2.5 ***

A comparison of the FB_1-induced alterations in sphingolipid metabolism demonstrated that increases in the levels of Sa and So and the formation of the respective 1-phosphates Sa1P and So1P were more pronounced in kidney compared to liver (Figure 26).

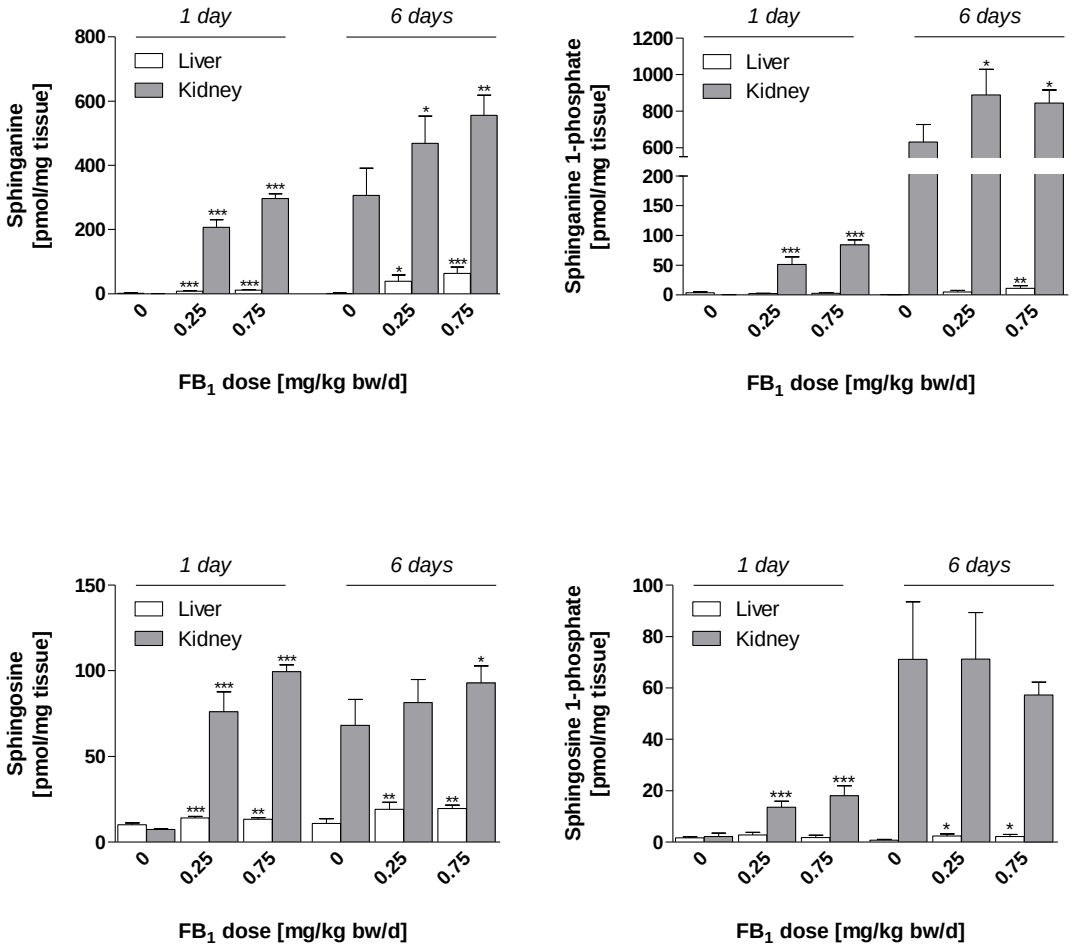

Figure 26: LC-MS/MS determination of alterations in the ceramide precursors sphinganine and sphingosine and their respective phosphorylated metabolites sphingosine- and sphinganine 1-phosphate in kidneys of male Sprague Dawley rats treated with FB_1 (0.25 or 0.75 mg/kg bw/d) for 1 or 6 days. Data are presented as mean ± standard deviation (n=4). Statistical analysis was performed by one-way analysis of variance (ANOVA) and Dunnett's *post hoc* test. Statistically significant changes to controls are indicated by * $p < 0.05$, ** $p < 0.01$ and *** $p < 0.001$.

For instance, single dose treatment with 0.75 mg/kg bw/d FB_1 resulted in a 594 and 13.6-fold increase in the sphingoid bases Sa and So in kidney, whereas in liver Sa and So only increased 6.1 and 1.3-fold compared to control levels (Table 35 and Figure 26). The fold

increase in phosphorylated metabolites after single treatment correlated with the increased concentrations of Sa and So in kidney and showed a 280- and 8.6-fold increase in Sa1P and So1P, respectively. In contrast, no alterations in phosphorylated sphingoid bases were observed in liver after single administration of FB_1.

After 6 days, the amounts of renal So were significantly enhanced at 0.75 mg/kg bw/d FB_1 and exceed the levels of So in liver (Figure 26). However, the levels of the corresponding metabolite So1P were not altered by FB_1 treatment in kidney, but in liver. In contrast, significant alterations in renal Sa and Sa1P were seen at both FB_1 dose levels, whereas levels of Sa and Sa1P in liver were less increased compared to kidney (Figure 26).

5.1.5.3 Alterations in the ceramide-based sphingolipids C16-, C18- and C18:1-ceramide

After single and 6-day administration of 0.25 or 0.75 mg/kg bw/d FB_1, significant alterations in the levels of C16-, C18- and C18:1-ceramide (C16-, C18- and C18:1-Cer) were observed in kidney, liver, serum and urine of male Sprague Dawley rats (Table 36).

In kidney and liver, the pro-apoptotic ceramide-based sphingolipid C16-Cer was slightly decreased after single treatment and significantly reduced after 6-day exposure to FB_1. Furthermore, a significant decrease in C18-Cer was observed in kidney and liver after a single dose of FB_1, and to a lesser extent at the later time point. C18:1-Cer, which is not abundant in kidney and liver, was markedly reduced in response to a single dose of FB_1. In contrast, a slight increase in C18:1-Cer was detected in kidney after 6-day treatment with FB_1 (Table 36).

Serum levels of C18- and C18:1-Cer were significantly reduced after single exposure to FB_1, whereas the amounts of the major ceramide C16-Cer remained unchanged. C18:1-Cer was not detectable in serum of controls and treated animals after 6-day exposure to FB_1. However, 6-day exposure to FB_1 resulted in a statistically significant increase in C18-Cer in serum (Table 36). Similar to serum, C16- and C18:1-Cer levels were significantly increased in urine of rats receiving FB_1 for 6 days, whereas the amount of urinary C18-Cer appeared to be slightly decreased (Table 36).

Table 36: LC-MS/MS determination of the sphingolipids C16-, C18- and C18:1-ceramide (C16-, C18- and C18:1-Cer) in kidney, liver, serum and urine of male Sprague Dawley rats treated with saline (control) or FB_1 (0.25 or 0.75 mg/kg bw/d) for 1 or 6 days. Data are presented as mean ± standard deviation (n=4). Statistical analysis was performed by one-way analysis of variance (ANOVA) and Dunnett's post hoc test. Statistically significant changes to controls are indicated by * $p < 0.05$, ** $p < 0.01$ and *** $p < 0.001$.

Sphingolipids	**1-day FB_1 treatment**			**6-day FB_1 treatment**		
	Control	0.25 mg/kg bw/d	0.75 mg/kg bw/d	Control	0.25 mg/kg bw/d	0.75 mg/kg bw/d
C16-Cer						
Kidney [pmol/mg]	108 ± 26	79.1 ± 3.8	94.6 ± 12.7	60.1 ± 6.7	27.8 ± 6.5 ***	33.7 ± 4.6 ***
Liver [pmol/mg]	83.0 ± 22.7	82.3 ± 8.5	54.4 ± 10.2 *	104 ± 21	38.3 ± 9.3 ***	18.2 ± 4.8 ***
Serum [nM]	2173 ± 868	2408 ± 965	2065 ± 820	2493 ± 338	4000 ± 1242	2935 ± 751
Urine [pmol/mg Crea]	270 ± 97	298 ± 73	281 ± 37	1213 ± 95	1265 ± 331	1702 ± 235 *
C18-Cer						
Kidney [pmol/mg]	2.7 ± 0.2	2.2 ± 0.1 *	2.2 ± 0.4	2.0 ± 0.5	1.7 ± 0.1	1.7 ± 0.1
Liver [pmol/mg]	3.6 ± 0.3	1.9 ± 0.3 ***	1.3 ± 0.1 ***	1.9 ± 0.2	1.5 ± 0.3	1.2 ± 0.3 **
Serum [nM]	24.0 ± 7.2	3.6 ± 0.6 **	5.9 ± 7.5 **	11.6 ± 3.1	52.8 ± 6.8 **	70.8 ± 22.2 ***
Urine [pmol/mg Crea]	35.2 ± 30.6	18.9 ± 10.0	13.3 ± 2.9	49.4 ± 57.4	34.7 ± 19.0	23.2 ± 6.0
C18:1-Cer						
Kidney [pmol/mg]	1.1 ± 0.6	0.21 ± 0.11 **	0.11 ± 0.05 **	0.00 ± 0.00	0.11 ± 0.04	0.13 ± 0.10 *
Liver [pmol/mg]	0.04 ± 0.07	n.d.	n.d.	n.d.	n.d.	n.d.
Serum [nM]	4.4 ± 2.8	n.d.	n.d.	n.d.	n.d.	n.d.
Urine [pmol/mg Crea]	n.d.	n.d.	n.d.	n.d.	n.d.	5.3 ± 2.2

n.d. = not detectable; Crea = Creatinine

5.1.6 Alterations in gene expression of cancer-related genes

To monitor alterations in the gene expression in kidneys of FB_1-treated male Sprague Dawley rats, quantitative real-time polymerase chain reaction (qRT-PCR) was applied for the analysis of 84 cancer-related genes. These target genes were categorized into 6 functional groups, representing genes involved in the most important pathways associated with cancer:

- Cell cycle and DNA damage repair
- Apoptosis and cell senescence
- Signal transduction molecules and transcription factors
- Adhesion
- Angiogenesis
- Invasion and metastasis

An overview of the alterations in mRNA expression of in the kidneys of FB_1-treated rats is given in Figure 27. Gene expression profiling demonstrated early dose-related changes in the expression of cancer-associated genes in kidneys of rats treated with FB_1, whereby the number of deregulated genes increased with time. Of the 84 cancer-related genes analyzed, significant alterations in mRNA expression of treated animals mostly consisted of an upregulation of genes, whereas only few genes were significantly downregulated (Figure 27).

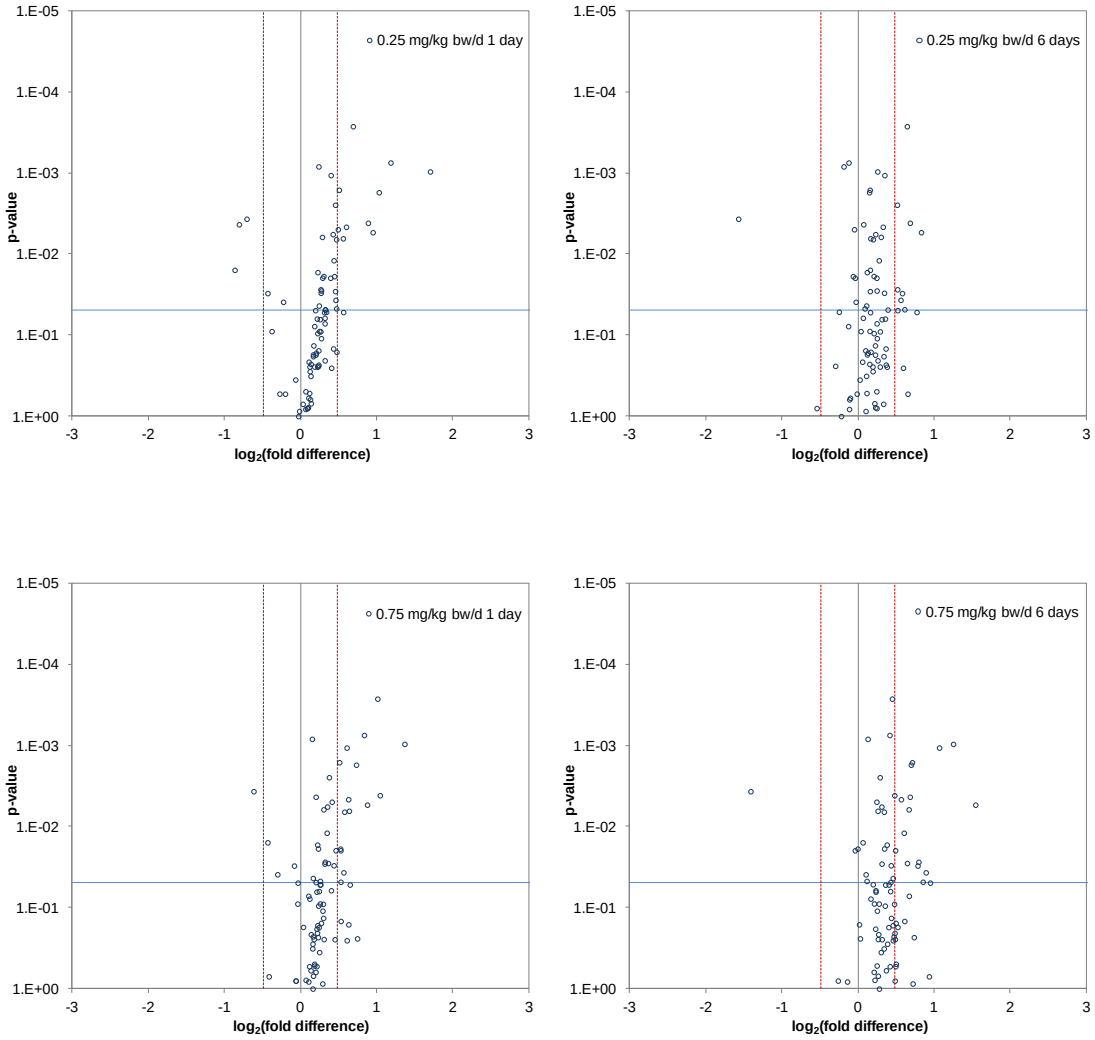

Figure 27: Overview of gene expression changes of cancer-related genes in kidneys of male Sprague Dawley rats after treatment with 0.25 and 0.75 mg/kg bw/d FB_1 for 1 or 6 days. Data (blue dots) are illustrated as volcano plots showing the dual logarithmic fold differences of all 84 genes investigated in relation to their respective *p*-values. The dashed red grids signify gene expression thresholds of ± 1.4-fold compared to control values, whereas gene expression values of 1 (no alterations compared to controls) are represented by a black line. The threshold for statistical significance of alterations in gene expression after FB_1 treatment compared to controls is defined at *p*-values ≤ 0.05 and is indicated by a blue line (right upper corner: significantly upregulated genes; left upper corner: significantly downregulated genes).

FB_1-induced gene expression changes were visualized by a heat map (Eisen *et al.*, 1998) (Figure 28). The comparison between single and repeated administration of FB_1 showed a time- and dose-dependent consistency pattern in genes involved in adhesion (*e.g. Icam1*, *Itga2*, *Itgav*), invasion (*e.g. Serpine1* (*PAI-1)*, *Plaur (uPAR)*, *Hgfr (Met)*, *Muc1*) and angiogenesis (*e.g. Thbs1*, *Egfr*).

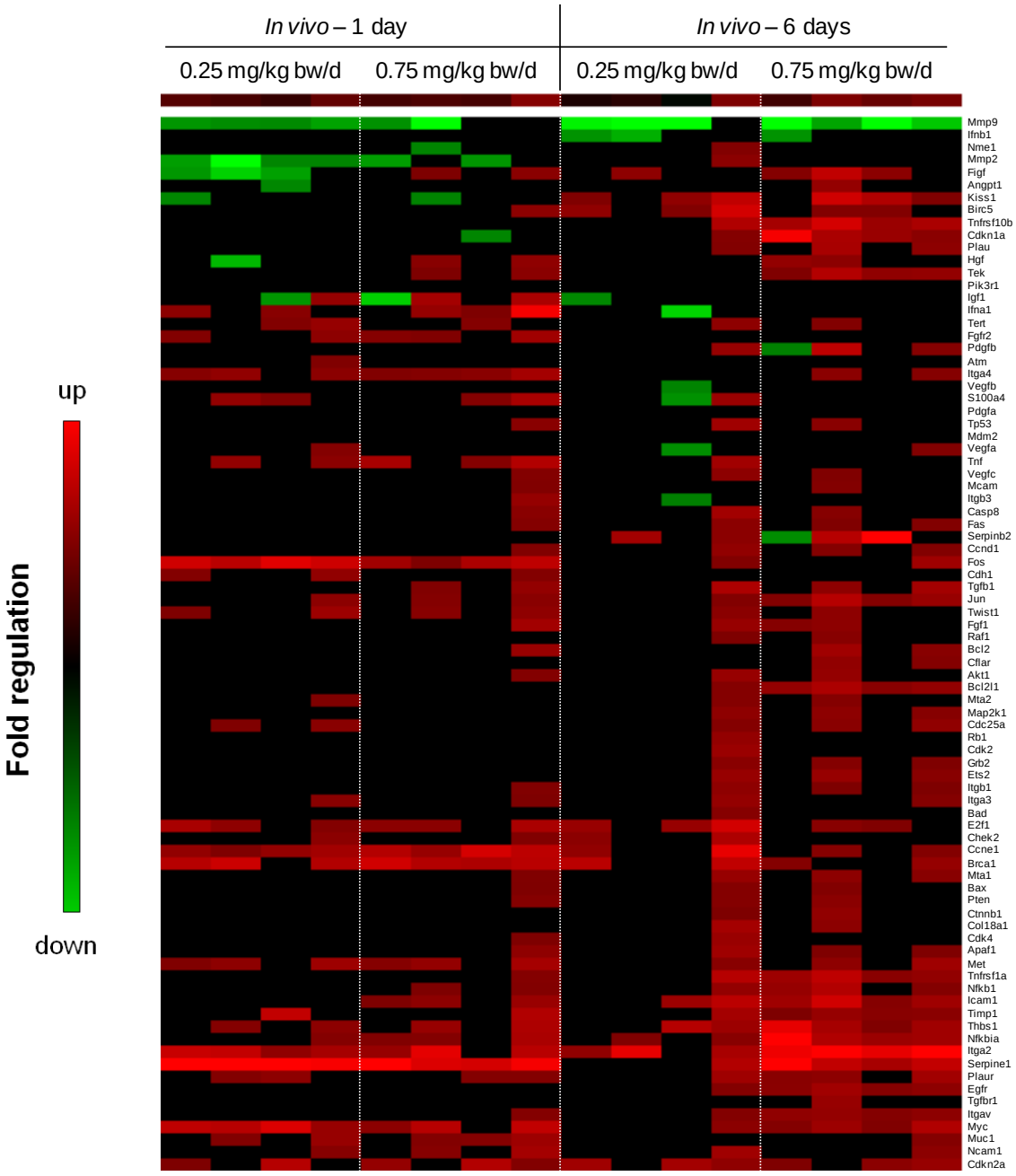

Figure 28: Heat map illustrating the time- and dose-dependent pattern of gene expression in kidneys of male Sprague Dawley rats treated with 0.25 and 0.75 mg/kg bw/d FB_1 for 1 or 6 days. Data for each dose group (with n=4 animals) are presented as individual fold changes (columns of the heat map) relative to the means of respective controls. The heat map was generated using Cluster 2.11 and TreeView 1.6 (Eisen *et al.*, 1998). Threshold values for gene expression changes are set at ± 1.4 relative to controls, whereby up- and downregulated genes are indicated by increased intensity of red and green, respectively.

5.1.6.1 Genes involved in cell cycle control and DNA damage repair

In response to a single dose of FB_1, 5 genes involved in cell cycle regulation (the S-phase-promoting Cyclin *Ccne1*, the cell cycle controlling checkpoint kinase *Chek2*, the S-phase-promoting transcription factor *E2f1*) and DNA damage repair (the DNA damage-induced kinase *Atm* and the DNA-repair-mediating *Brca1*), were significantly upregulated in kidneys of male Sprague Dawley rats in a dose-dependent manner (Table 37).

In contrast, repeated administration of FB_1 for 6 days resulted in significant upregulation of 3 genes involved in cell cycle control (the cyclin-dependent kinase inhibitors *p21 (Cdkn1a)* and *p16 (Cdkn2a)*, the cell cycle regulator and tumor suppressor *Pten*), whereas genes involved in the progression of the cell cycle like *Ccne1* were not as prevalent as after 1 day exposure to FB_1. Consistent with gene expression after single exposure, *Chek2* and *E2f1* were significantly upregulated at the low dose (0.25 mg/kg bw/d FB_1), whereas their expression declined again at the high dose (0.75 mg/kg bw/d FB_1) (Table 37).

5.1.6.2 Genes involved in apoptosis and cell senescence

After a single dose of FB_1 only marginal changes in the expression of apoptosis-related genes were observed in kidneys of male Sprague Dawley rats. Statistically significant upregulation of mRNA expression was obtained for *Tnfrsf1a*, which encodes a receptor involved in the induction of apoptosis, and *Apaf1*, which is part of the cell death-initiating apoptosome (Table 37).

However, 6-day exposure to FB_1 induced a dose-dependent increase in mRNA expression of the TNF receptor subtypes *Tnfrsf1a* and *Tnfrsf10b*, which peaked at relative fold changes of 1.7 and 1.9 after administration of 0.75 mg/kg bw/d FB_1, respectively (Table 37). In parallel, the mRNA expression of anti-apoptotic genes, such as *Bcl-Xl* and *Cflar* was dose-dependently increased after FB_1 treatment. Although not statistically significant, mRNA expression of the apoptosis-inhibiting oncogene *Birc5* (*survivin*) and the anti-apoptotic *Bcl2* was enhanced in kidneys of individual animals (Table 37).

5.1.6.3 Genes involved in signal transduction and transcription factors

Single administration of FB_1 resulted in significant upregulation of 4 genes involved in transcriptional regulation (Table 37). Relative fold changes in mRNA expression of *Jun* and *Fos*, which are both components of the activator protein 1 (*AP-1*) transcription factors and regarded as oncogenes, were dose-dependently increased up to 1.4- or 1.8-fold after treatment with 0.75 mg/kg bw/d FB_1. At the lower dose, changes in mRNA expression of *Fos* were even more pronounced (2.3-fold compared to controls) compared to the high dose. The same phenomenon was also observed for the expression of *Myc*, another oncogenic transcription factor significantly upregulated in response to FB_1. Furthermore, mRNA expression of *Nfκbia*, encoding the inhibitor of the NFκB transcription complex, was upregulated 1.5-fold compared to controls after a single dose of 0.75 mg/kg bw/d FB_1 (Table 37).

Similar to the earlier time-point, increased mRNA expression of the transcription factors *Myc*, *Jun*, but not *Fos*, was observed in kidneys after 6-day treatment with FB_1 (Table 37). Expression of *Nfκbia* was also upregulated 2.2-fold at the high dose. In parallel to *Nfκbia* expression, the corresponding transcription factor *Nfκb1* was found to be statistically significantly upregulated (1.6-fold compared to controls). In addition, mRNA expression of genes involved in signal transduction such as *Map2k1* was significantly increased in kidneys treated with the high dose of FB_1 for 6 days. A slight, but not significant upregulation in gene expression was also found for *Akt*, a gene mediating cell survival, and *Ets2*, a transcription factor involved in the activation of cancer-related genes such as the survival-promoting *Bcl-Xl* and telomerase reverse transcriptase (Xu *et al.*, 2008) (Table 37).

5.1.6.4 Genes involved in cell adhesion

In response to a single dose of FB_1, several genes (6 of 10) involved in adhesion were upregulated in the kidneys of male Sprague Dawley rats (Table 37). In particular, marked alterations were observed in the mRNA expression of alpha integrin subtypes such as *Itga2* and *Itgav*. The mRNA of *Itga3* and *Itga4* was also significantly overexpressed. In contrast, the expression of beta-integrins remained unchanged in response to FB_1. Moreover, members of the immunoglobulin gene superfamily like Icam1, encoding a glycoprotein important for cell adhesion, were up to 1.5-fold overexpressed compared to controls. Also gene expression of *Cdh1*, which

encodes cadherin, a calcium-dependent transmembrane linker glycoprotein with important function in adherens junction, was statistically significantly enhanced in response to single doses of FB_1 (Table 37).

After 6-day treatment with FB_1, fewer mRNA expression changes in renal integrins compared to single FB_1 exposure were seen. However, integrins such as *Itgav* and *Itga2* were dose-dependently increased with maximum fold changes of 1.6 and 2.9 relative to controls, respectively. Likewise, the mRNA expression of *Icam1* increased up to 1.8-fold over control after 6-day treatment (Table 37).

5.1.6.5 Genes involved in angiogenesis

Statistically significant alterations in mRNA expression of 8 genes (of 20 analyzed in total) involved in angiogenesis were observed in kidneys of male Sprague Dawley rats given a single dose of FB_1 (Table 37). Among these, *Thbs1*, encoding an adhesive glycoprotein mediating both pro- and anti-angiogenic functions, and *Tgfb1*, encoding a cytokine involved in tissue repair, were upregulated (1.4 and 1.5-fold) in response to 0.75 mg/kg bw/d FB_1. Furthermore, gene expression of *Fgfr2*, a fibroblast growth factor receptor involved in endothelial proliferation, as well as *Ifna1*, an interferon with anti-angiogenic function, were also significantly upregulated in response to 0.75 mg/kg bw/d FB_1. Minor changes in mRNA expression after exposure to the low dose, but not high dose, were observed for growth factors like *Pdgfb* and *Vegfb*, as well as *Co18a1*, encoding the extracellular matrix (ECM) protein alpha 1 type XVIII collagen (Table 37). Interestingly, a significant downregulation of the c-Fos-induced growth factor *Figf* was only observed at this dose group.

In contrast to the single dose treatment, only 4 of the 20 genes involved in angiogenesis were significantly increased in the kidneys of animals treated for 6 days (Table 37). However, mRNA expression of *Thbs1* was mostly affected by FB_1 treatment, with a 1.9-fold upregulation compared to controls at 0.75 mg/kg bw/d. At the same dose, increased mRNA expression of the growth factor receptors *Egfr* (1.6-fold), *Tek* (1.7-fold) and *Tgfbr1* (1.4-fold) was observed. At 0.75 mg/kg bw/d FB_1, individual animals also showed altered mRNA expression of growth factors like *Pdgfb* (2/4), *Tgfb1* (2/4), *Hgf* (2/4), *Fgf* (3/4), *Figf* (4/4), resulting in an increased, but not statistically significant mean fold change compared to controls (Table 37).

Table 37: qRT-PCR results of gene expression alterations in kidneys of male Sprague Dawley rats treated with saline (control) or FB_1 (0.25 or 0.75 mg/kg bw/d) for 1 or 6 days. Data are presented as mean fold changes ± standard deviation (n=4) of 84 cancer-related genes relative to their respective controls. Statistical analysis was performed by one-way analysis of variance (ANOVA) and Dunnett's *post hoc* test. Statistically significant changes to controls are indicated by * $p < 0.05$, ** $p < 0.01$ and *** $p < 0.001$. Gene expression changes > 1.4 are highlighted in bold black.

Functional gene grouping		**1-day FB_1 treatment [mg/kg bw/d]**		**6-day FB_1 treatment [mg/kg bw/d]**	
Accession No.	**Gene Symbol**	**0.25**	**0.75**	**0.25**	**0.75**
		Cell cycle control and DNA damage repair			
XM_236275	*Atm*	1.3 ± 0.2 *	1.3 ± 0.0 *	1.1 ± 0.1	1.2 ± 0.2
NM_012514	*Brca1*	**1.9** ± 0.4 **	**2.1** ± 0.2 ***	**1.7** ± 0.5	**1.4** ± 0.2
NM_171992	*Ccnd1*	1.1 ± 0.2	1.1 ± 0.3	1.2 ± 0.3	1.2 ± 0.3
XM_574426	*Ccne1*	**1.6** ± 0.2 **	**2.0** ± 0.3 **	**1.6** ± 0.7	**1.4** ± 0.1
NM_133571	*Cdc25a*	1.3 ± 0.3	1.2 ± 0.1	1.2 ± 0.2	**1.4** ± 0.2 *
NM_199501	*Cdk2*	1.1 ± 0.2	1.2 ± 0.1	1.3 ± 0.3	1.2 ± 0.1
NM_053593	*Cdk4*	1.2 ± 0.0	1.2 ± 0.2	1.3 ± 0.3	1.2 ± 0.1
NM_080782	*Cdkn1a (p21)*	1.0 ± 0.2	0.8 ± 0.1	1.3 ± 0.2	**2.0** ± 0.5 **
NM_031550	*Cdkn2a (p16)*	**1.4** ± 0.5	**1.6** ± 0.3	**1.5** ± 0.4 *	**1.4** ± 0.3
NM_053677	*Chek2*	**1.4** ± 0.1 **	1.3 ± 0.1 **	**1.5** ± 0.4 **	1.2 ± 0.1
XM_230765	*E2f1*	**1.5** ± 0.3 *	**1.6** ± 0.2 *	**1.7** ± 0.4 *	1.3 ± 0.2
XM_235169	*Mdm2*	1.1 ± 0.1	1.1 ± 0.1	1.1 ± 0.2	1.2 ± 0.2
NM_031606	*Pten*	1.1 ± 0.1	1.2 ± 0.2	1.2 ± 0.2	**1.4** ± 0.1 *
XM_344434	*Rb1*	1.2 ± 0.2	1.2 ± 0.1	1.2 ± 0.3	1.2 ± 0.1
NM_030989	*Tp53*	1.1 ± 0.1	1.2 ± 0.2	1.2 ± 0.4	1.2 ± 0.2
		Apoptosis and cell senescence			
NM_023979	*Apaf1*	1.2 ± 0.0	**1.4** ± 0.2 **	1.3 ± 0.3	1.4 ± 0.1
NM_022698	*Bad*	1.2 ± 0.1	1.2 ± 0.1	1.1 ± 0.2	1.2 ± 0.1
NM_017059	*Bax*	1.2 ± 0.1	1.2 ± 0.2	1.2 ± 0.2	1.3 ± 0.1
NM_016993	*Bcl2*	1.2 ± 0.2	1.2 ± 0.3	1.1 ± 0.2	**1.4** ± 0.3
NM_031535	*Bcl2l1 (Bcl-Xl)*	1.2 ± 0.2	1.2 ± 0.1	1.3 ± 0.1 *	**1.7** ± 0.2 ***
NM_022274	*Birc5 (survivin)*	0.9 ± 0.1	1.1 ± 0.3	**1.6** ± 0.5	1.3 ± 0.1
NM_022277	*Casp8*	1.1 ± 0.2	1.1 ± 0.3	1.2 ± 0.4	1.2 ± 0.2
NM_057138	*Cflar*	1.2 ± 0.1	1.1 ± 0.1	1.1 ± 0.2	**1.4** ± 0.2 *
NM_053423	*Tert*	**1.4** ± 0.2	1.2 ± 0.2	1.1 ± 0.3	1.1 ± 0.3
XM_344431	*Tnfrsf10b_pred*	1.1 ± 0.1	1.0 ± 0.2	**1.5** ± 0.3	**1.9** ± 0.3 **
NM_013091	*Tnfrsf1a*	1.2 ± 0.1 *	1.3 ± 0.2 *	**1.5** ± 0.4	**1.7** ± 0.3 *
NM_139194	*Fas (Tnfrsf6)*	1.1 ± 0.2	1.2 ± 0.3	1.1 ± 0.3	1.2 ± 0.3

Functional gene grouping		1-day FB_1 treatment [mg/kg bw/d]		6-day FB_1 treatment [mg/kg bw/d]	
Accession No.	**Gene Symbol**	**0.25**	**0.75**	**0.25**	**0.75**
		Signal transduction molecules and transcription factors			
NM_033230	*Akt1*	1.2 ± 0.1	1.2 ± 0.2	1.3 ± 0.3	**1.4** ± 0.2
NM_053357	*Ctnnb1*	1.2 ± 0.1	1.2 ± 0.2	1.2 ± 0.2	1.3 ± 0.2
XM_239510	*Ets2*	1.1 ± 0.2	1.1 ± 0.1	1.2 ± 0.3	**1.4** ± 0.2
NM_022197	*Fos*	**2.3** ± 0.2 ***	**1.8** ± 0.3 **	1.0 ± 0.3	1.4 ± 0.3
NM_030846	*Grb2*	1.1 ± 0.1	1.1 ± 0.1	1.2 ± 0.2	1.3 ± 0.2
NM_021835	*Jun*	**1.4** ± 0.1 ***	**1.4** ± 0.1 ***	1.1 ± 0.2	**1.7** ± 0.3 **
NM_031643	*Map2k1*	1.1 ± 0.1	1.1 ± 0.1	1.2 ± 0.2	**1.4** ± 0.1 *
NM_012603	*Myc*	**2.1** ± 0.3 **	**1.7** ± 0.5 *	1.1 ± 0.3	**1.6** ± 0.3 *
XM_342346	*Nfκb1*	1.2 ± 0.1	1.2 ± 0.2	1.3 ± 0.3	**1.6** ± 0.3 *
XM_343065	*Nfκbia (IκBα)*	1.3 ± 0.1 *	**1.5** ± 0.2 **	1.3 ± 0.2	**2.2** ± 0.7 *
NM_013005	*Pik3r1*	1.1 ± 0.2	1.2 ± 0.2	0.9 ± 0.1	1.2 ± 0.1
NM_012639	*Raf1*	1.1 ± 0.1	1.1 ± 0.2	1.1 ± 0.2	1.3 ± 0.2
		Adhesion			
NM_031334	*Cdh1*	**1.4** ± 0.2 **	1.3 ± 0.1 **	1.0 ± 0.1	1.2 ± 0.1
NM_012967	*Icam1*	1.3 ± 0.1	**1.5** ± 0.2 *	**1.6** ± 0.4	**1.8** ± 0.3 *
XM_345156	*Itga2*	**1.9** ± 0.3 *	**1.9** ± 0.5 *	**1.8** ± 0.5	**2.9** ± 0.4 ***
XM_340884	*Itga3_pred*	1.3 ± 0.1 **	1.3 ± 0.1 *	1.2 ± 0.4	1.2 ± 0.2
XM_230033	*Itga4*	**1.5** ± 0.1 **	**1.6** ± 0.2 ***	1.1 ± 0.1	1.2 ± 0.3
XM_230950	*Itgav_pred*	1.2 ± 0.1 *	1.3 ± 0.1 **	1.2 ± 0.2	**1.6** ± 0.1 **
NM_017022	*Itgb1*	1.2 ± 0.1	1.2 ± 0.2	1.1 ± 0.3	1.3 ± 0.1
NM_153720	*Itgb3*	1.0 ± 0.1	1.2 ± 0.4	0.9 ± 0.2	1.2 ± 0.1
NM_023983	*Mcam*	1.1 ± 0.1	1.1 ± 0.2	1.0 ± 0.3	1.3 ± 0.1
NM_031521	*Ncam1*	1.2 ± 0.3	**1.4** ± 0.3	1.3 ± 0.3	1.3 ± 0.2
		Angiogenesis			
NM_053546	*Angpt1*	0.8 ± 0.1	1.0 ± 0.2	1.0 ± 0.1	1.2 ± 0.3
XM_241632	*Col18a1*	1.3 ± 0.1 *	1.2 ± 0.1	1.3 ± 0.3	**1.4** ± 0.2
NM_031507	*Egfr*	1.2 ± 0.1	1.1 ± 0.1	1.2 ± 0.2	**1.6** ± 0.1 *
NM_012846	*Fgf1*	1.2 ± 0.1	1.2 ± 0.4	1.1 ± 0.4	**1.4** ± 0.1
XM_341940	*Fgfr2*	1.3 ± 0.2	**1.5** ± 0.3 *	1.0 ± 0.2	1.0 ± 0.2
NM_031761	*Figf*	0.6 ± 0.1 *	1.2 ± 0.3	1.1 ± 0.4	**1.6** ± 0.3
NM_017017	*Hgf*	0.9 ± 0.3	1.2 ± 0.4	1.0 ± 0.2	**1.4** ± 0.2
NM_001014786	*Ifna1*	1.2 ± 0.4	**1.8** ± 0.7 *	0.9 ± 0.4	1.1 ± 0.3
NM_019127	*Ifnb1*	1.1 ± 0.1	1.0 ± 0.3	0.7 ± 0.2	0.8 ± 0.2

Functional gene grouping		1-day FB_1 treatment [mg/kg bw/d]		6-day FB_1 treatment [mg/kg bw/d]	
Accession No.	**Gene Symbol**	**0.25**	**0.75**	**0.25**	**0.75**
			Angiogenesis		
NM_178866	*Igf1*	1.1 ± 0.5	1.3 ± 0.7	1.0 ± 0.3	0.9 ± 0.1
NM_012801	*Pdgfa*	1.1 ± 0.1	1.1 ± 0.2	0.9 ± 0.2	1.1 ± 0.2
XM_343293	*Pdgfb*	1.2 ± 0.1 *	1.2 ± 0.1	1.2 ± 0.4	**1.4** ± 0.6
XM_342863	*Tek*	1.0 ± 0.2	1.2 ± 0.3	1.1 ± 0.1	**1.7** ± 0.2 **
NM_021578	*Tgfb1*	1.2 ± 0.1	**1.4** ± 0.2 **	1.2 ± 0.5	**1.4** ± 0.3
NM_012775	*Tgfbr1*	1.1 ± 0.1	1.1 ± 0.1	1.1 ± 0.2	**1.4** ± 0.2 *
NM_001013062	*Thbs1 (TSP-1)*	**1.4** ± 0.2	**1.5** ± 0.4 *	**1.5** ± 0.4	**1.9** ± 0.5 *
NM_012675	*Tnf*	**1.4** ± 0.2	**1.6** ± 0.4	1.2 ± 0.4	1.0 ± 0.2
NM_031836	*Vegfa*	1.3 ± 0.2	1.2 ± 0.1	0.9 ± 0.2	1.2 ± 0.2
NM_053549	*Vegfb*	1.2 ± 0.1 *	1.1 ± 0.1	0.9 ± 0.2	1.1 ± 0.2
NM_053653	*Vegfc*	1.0 ± 0.1	1.2 ± 0.2	1.1 ± 0.3	1.2 ± 0.2
			Invasion and metastasis		
NM_181692	*Kiss1*	0.7 ± 0.1	1.0 ± 0.3	**1.5** ± 0.5	**1.8** ± 0.4
NM_031517	*Met (Hgfr)*	**1.5** ± 0.2 **	**1.6** ± 0.2 **	1.3 ± 0.2	**1.5** ± 0.2 *
NM_031054	*Mmp2*	0.6 ± 0.2 *	0.8 ± 0.3	1.2 ± 0.3	1.1 ± 0.2
NM_031055	*Mmp9*	0.6 ± 0.0	0.7 ± 0.4	0.4 ± 0.2	0.4 ± 0.1
NM_022588	*Mta1*	1.2 ± 0.1	1.2 ± 0.2	1.3 ± 0.3	**1.4** ± 0.2
XM_342015	*Mta2*	1.2 ± 0.2	1.2 ± 0.1	1.2 ± 0.2	1.3 ± 0.1 *
XM_342281	*Muc1*	**1.4** ± 0.2 *	**1.5** ± 0.2 **	1.2 ± 0.1	1.3 ± 0.2 *
NM_138548	*Nme1*	0.9 ± 0.1	0.8 ± 0.2	1.0 ± 0.3	1.1 ± 0.1
NM_013085	*Plau (uPA)*	1.1 ± 0.1	1.0 ± 0.2	1.1 ± 0.3	**1.5** ± 0.3
NM_017350	*Plaur (uPAR)*	**1.4** ± 0.2 *	1.3 ± 0.2	1.3 ± 0.4	**1.5** ± 0.2
NM_012618	*S100a4 (metastasin)*	**1.4** ± 0.2	**1.5** ± 0.3 *	1.0 ± 0.5	1.0 ± 0.2
NM_021696	*Serpinb2 (PAI-2)*	1.1 ± 0.1	1.0 ± 0.3	1.3 ± 0.5	**1.7** ± 1.1
NM_012620	*Serpine1 (PAI-1)*	**3.3** ± 0.9 ***	**2.6** ± 0.2 **	1.3 ± 0.5	**2.5** ± 0.9 *
NM_053819	*Timp1*	**1.4** ± 0.5	**1.5** ± 0.3	1.3 ± 0.3	**1.5** ± 0.1 *
NM_053530	*Twist1*	**1.4** ± 0.3	1.3 ± 0.3	1.1 ± 0.3	1.3 ± 0.2

5.1.6.6 Genes involved in invasion and metastasis

Of the 15 genes involved in invasion and metastasis analyzed, 6 genes were significantly deregulated in kidneys of male Sprague Dawley rats exposed to single FB_1 doses (Table 37). Marked alterations were found in the mRNA expression of *PAI-1*, an important component of the metastasis-associated plasminogen activator system, which was upregulated 3.3 and 2.6-fold in response to 0.25 or 0.75 mg/kg bw/d FB_1, respectively. In addition, mRNA expression of the receptor *Plaur* (*uPAR*), which is also involved in the plasminogen activator system, was significantly enhanced at the low dose (0.25 mg/kg bw/d FB_1), but not at the high dose. Moreover, expression of *Met* (*Hgfr*), encoding a proto-oncogenic growth factor involved in invasive growth, was significantly increased up to 1.6-fold compared to controls after exposure to FB_1 at both dose levels. Single dosing with 0.75 mg/kg bw/d FB_1 resulted in upregulated mRNA expression of *S100A4 (metastasin)*, which encodes a calcium binding protein implicated in motility and invasion. Furthermore, the mRNA of the integral membrane protein Muc1, which regulates cell-adhesion, differentiation and development, was significantly overexpressed after single exposure to FB_1 at both dose levels. Among the genes deregulated in kidneys of treated animals, only mRNA expression of *Mmp2*, a matrix metalloproteinase involved in ECM degradation, was significantly downregulated -1.8-fold (0.6-fold) compared to controls after exposure to the low dose. Similarly, mRNA expression of Mmp9 was decreased -1.6-fold after treatment with the same dose, but failed to reach statistical significance (Table 37).

Genes significantly deregulated in kidneys after 6-day treatment with FB_1 included *Met* (*Hgfr*), *Mta2*, *Muc1*, *PAI-1* and *Timp1* (Table 37). Similar to single dose treatment, most prominent alterations in mRNA expression were observed for *PAI-1*, which was increased up to 2.5-fold compared to controls after treatment with the high dose of FB_1. The mRNA expression of *Met* (*Hgfr*) and *Muc1* was significantly increased in animals receiving this dose. In addition, mRNA expression of *Mta2*, a component of nucleosome remodeling deacetylase complex in nucleus, and *Timp1*, the tissue inhibitor of MMP1 activity, was upregulated in response to the high dose of FB_1. Although not significantly altered, mRNA expressions of several other components of the plasminogen activator system were upregulated in response to 0.75 mg/kg bw/d FB_1, *e.g. Plau* (1.5-fold), *Plaur* (1.5-fold, with t-test p-value < 0.05) and *PAI-2* (1.7-fold), whereas the expression of this genes remained unchanged at

the low dose (0.25 mg/kg bw/d FB_1). In addition, mRNA expression of Kiss1, which is involved in suppression of metastasis, was increased in a dose-dependent manner up to 1.8-fold compared to control, but without statistical significance (Table 37).

5.1.6.7 Biological processes associated with FB_1-induced gene expression changes in cancer-related genes

To confirm biological processes primarily associated with FB_1-induced gene expression changes in kidney, a specific pathway analysis tool (Ingenuity® pathway analysis software, Ingenuity® Systems, Redwood City, USA) was applied. Using Ingenuity® Ontology, the observed expression changes in cancer-related genes were classified with regard to their frequency and statistical significance (enrichment) in particular biological process (Figure 29).

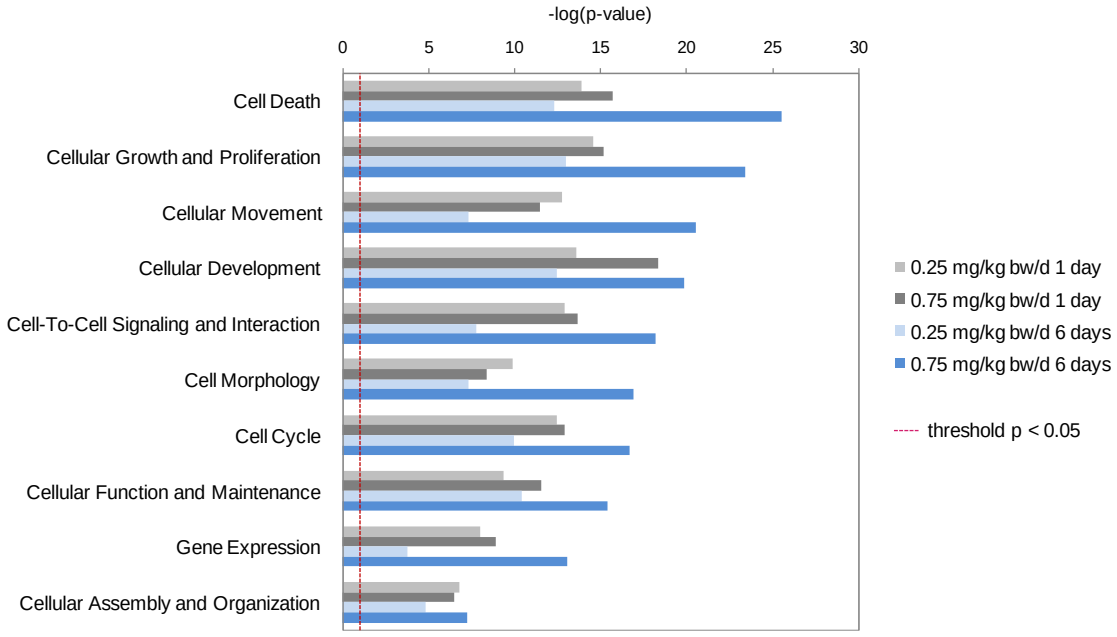

Figure 29: Enrichment of biological processes primarily associated with gene expression changes in kidneys of male Sprague Dawley rats treated with saline (control) or different doses FB_1 (0.25 or 0.75 mg/kg bw/d) for 1 or 6 days. Categorization of gene expression results was performed by Ingenuity pathway analysis software, setting a threshold fold change of ± 1.4 relative to controls and a *p*-value < 0.05 as significance level for Fisher's exact test (red dashed line on the logarithmic scale). Results are displayed as *p*-values for each category to demonstrate whether obtained gene expression changes in kidneys of treated rats were enriched with genes of a particular biological process from Ingenuity® Ontology in the respective dose groups (colored bars).

The most enriched biological processes after treatment with 0.25 or 0.75 mg/kg bw/d FB_1 for 1 or 6 days are displayed in Figure 29. The distribution of bars of each particular biological process reflects a clear time- and dose-dependent response to FB_1 treatment. Consistent with the observed alterations in apoptosis and cell proliferation in kidney (see section 5.1.4.1 and 5.1.4.2), the most significant enrichment was observed among biological processes involved in cell death and cellular growth and proliferation. However, there was also increased occurrence of biological processes mediating cellular movement and development as well as cell-to-cell signaling and interaction.

5.1.7 Comparison of PAI-1, Itga2 and Thbs1 gene expression changes in kidney and liver

Gene expression analysis of cancer-related genes in kidneys of male Sprague Dawley rats revealed that *PAI-1*, *Itga2* and *Thbs1* were the most prominent genes modulated by FB_1 treatment (see chapter 5.1.6). Since these genes are involved in invasion, adhesion and angiogenesis, their specific gene expression in response to FB_1 was compared between kidney and liver to identify possible transcriptional differences that might contribute to the organ susceptibility of kidney to FB_1-induced toxicity and tumor formation.

5.1.7.1 Verification of qRT-PCR array analysis of PAI-1, Itga2 and Thbs1

To verify gene expression changes after qRT-PCR array analysis and to identify appropriate primers for gene expression analysis in liver, single qRT-PCR assays of *PAI-1*, *Itga2* and *Thbs1* were performed using the same RNA samples already used for qRT-PCR array analysis.

As shown in Figure 30, a similar pattern of gene expression was obtained for *PAI-1*, *Itga2* and *Thbs1*, although the increase in mRNA expression was generally more significant in the qRT-PCR array analysis compared to the single qRT-PCR assay. Overall, there was a good correlation between the results of both qRT-PCR analysis, rendering the single qRT-PCR assays suitable to study differences in FB_1-induced gene expression of *PAI-1*, *Itga2* and *Thbs1* in kidney and liver.

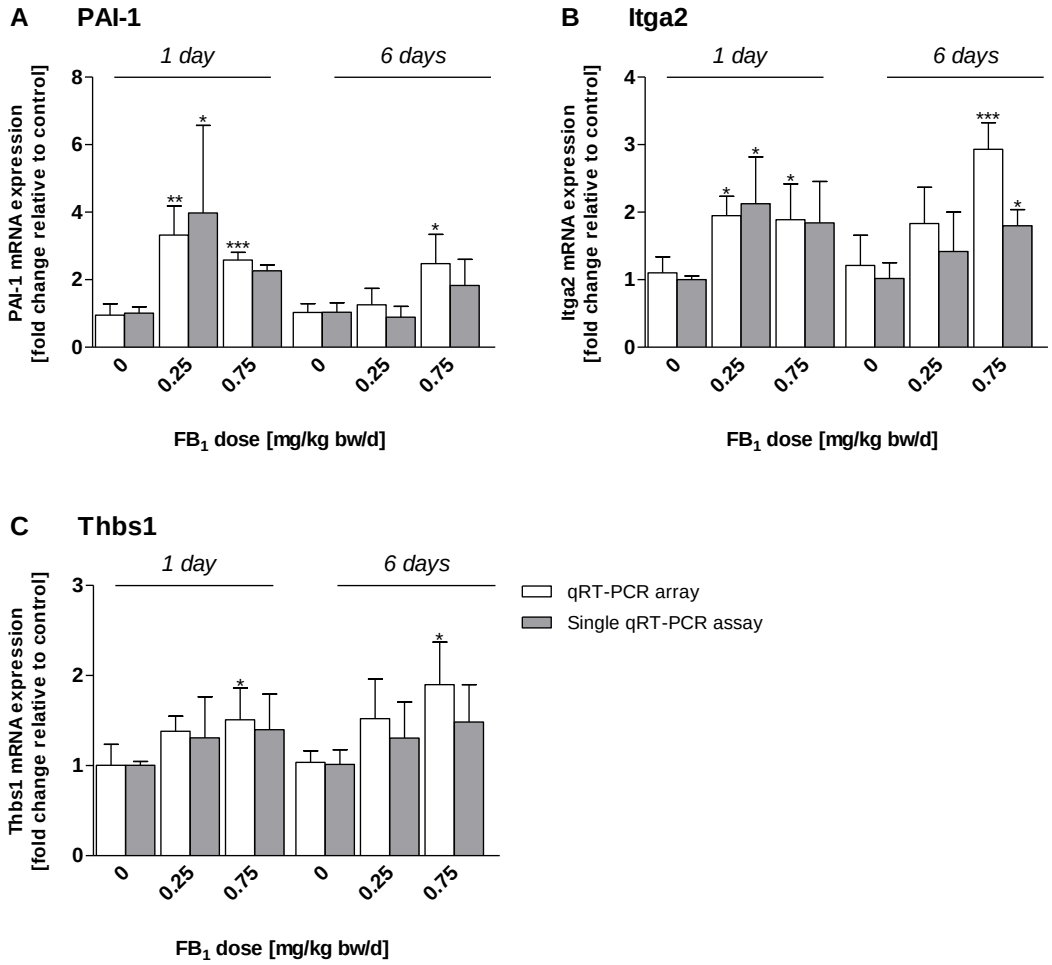

Figure 30: Comparison of mRNA expression changes of PAI-1 (**A**), Itga2 (**B**) and Thbs1 (**C**) obtained with the qRT-PCR array and single qRT-PCR assay in kidneys of male Sprague Dawley rats treated with FB_1 (0.25 or 0.75 mg/kg bw/d) for 1 or 6 days. Data are presented as mean fold change ± standard deviation (n=4 animals per group) relative to controls. Statistical analysis was performed by one-way analysis of variance (ANOVA) and Dunnett's *post hoc* test. Statistically significant changes to controls are indicated by * $p < 0.05$, ** $p < 0.01$ and *** $p < 0.001$.

5.1.7.2 Comparison of PAI-1, Itga2 and Thbs1 gene expression changes in kidney and liver

Single treatment with FB_1 resulted in increased expression of *PAI-1* in kidney compared to liver at both dose levels (Figure 31). In contrast, gene expression of *PAI-1* in liver was more increased compared to kidney after exposure to FB_1 for 6 days. In 2 of 4 animals receiving 0.75 mg/kg bw/d FB_1 for 6 days, mRNA expression of *PAI-1* in liver was increased 10 and 22-fold, whereas the remaining animals only showed a

moderate increase in *PAI-1* mRNA expression (2.2 and 2.5-fold), demonstrating a large interanimals variation on liver.

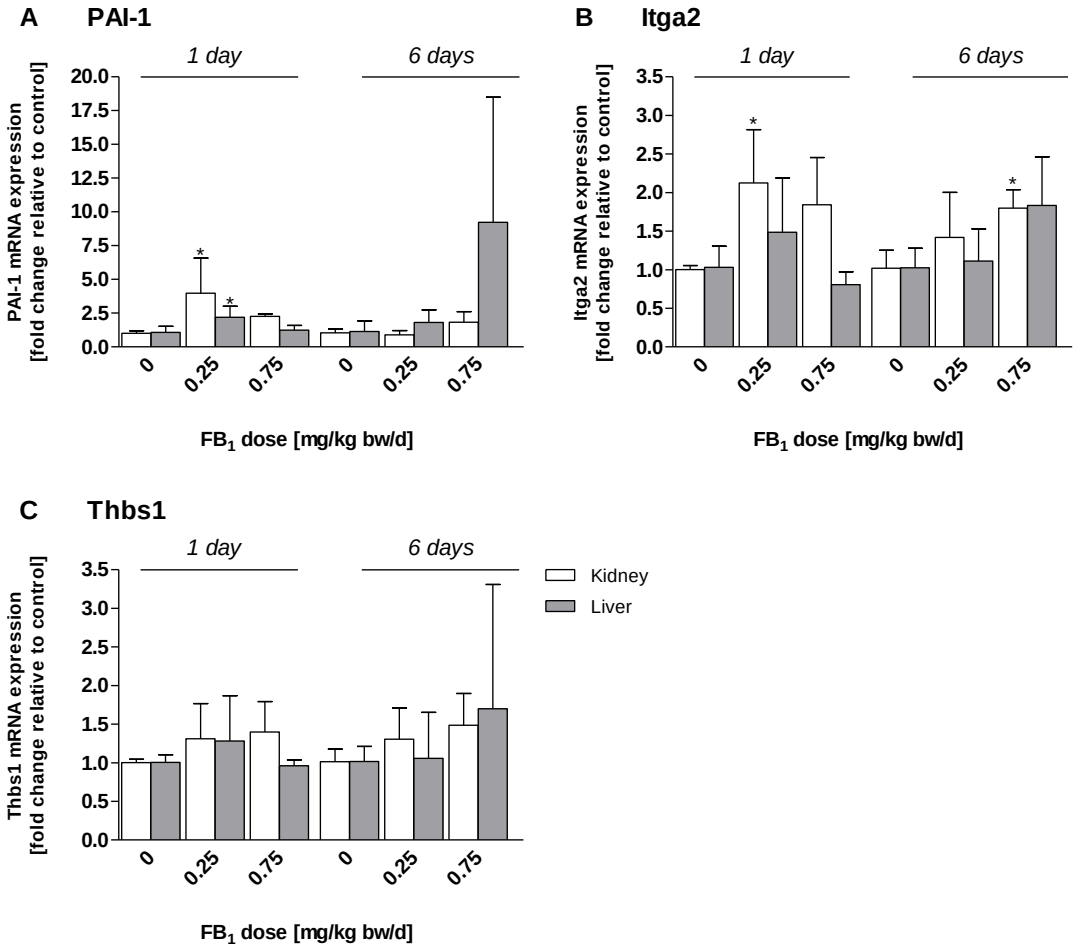

Figure 31: Comparison of **(A)** PAI-1, **(B)** Itga2 and **(C)** Thbs1 mRNA expression in kidneys and livers of male Sprague Dawley rats treated with FB_1 (0.25 or 0.75 mg/kg bw/d) for 1 or 6 days. Data are presented as mean fold change ± standard deviation (n=4 animals per group) relative to controls. Statistical analysis was performed by one-way analysis of variance (ANOVA) and Dunnett's *post hoc* test. Statistically significant changes to controls are indicated by $*p < 0.05$.

Gene expression analysis of *Itga2* showed that fold change in mRNA expression compared to controls was more increased in kidneys than in livers after a single dose of 0.25 and 0.75 mg/kg bw/d FB_1 (Figure 31). After 6 days, *Itga2* gene expression changes were similar in kidney and liver at both dose-levels of FB_1 (Figure 31).

A similar fold change relative to control in *Thbs1* expression was observed in kidneys and livers after single administration of 0.25 mg/kg bw/d FB_1 (Figure 31). At the higher dose, gene expression changes were more enhanced in kidney (1.4-fold) compared

to liver. In animals receiving FB_1 for 6 days, gene expression of *Thbs1* was dose-dependently altered in the kidneys, whereas *Thbs1* expression in liver was only altered in a single animal receiving FB_1.

However, the basal expression of *PAI-1*, *Itga2* and *Thbs1* was significantly lower in liver compared to kidney as shown in Figure 32.

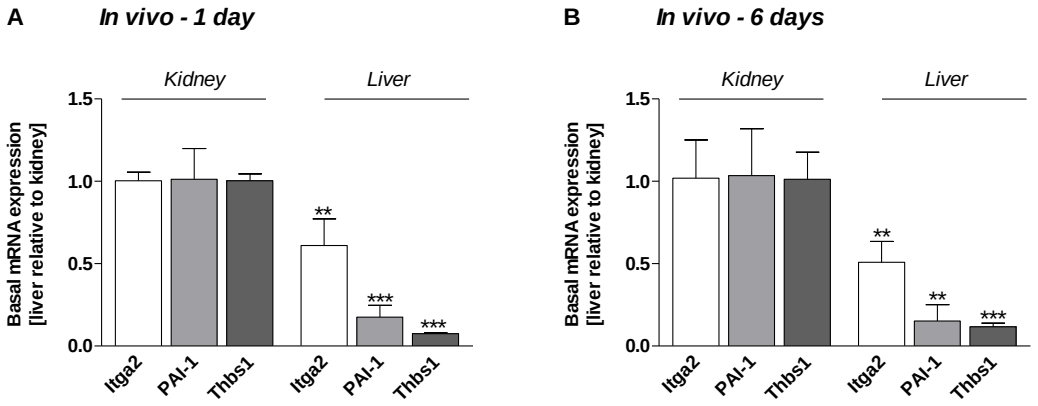

Figure 32: Comparison of basal Itga2, PAI-1 and Thbs1 mRNA expression in kidneys and livers of control animals. Data are expressed as mean fold change ± standard deviation (n=4) in liver relative to kidney**.** Statistical analysis was performed by unpaired t-test and statistically significant changes between basal expression levels of liver and kidney are indicated by ** $p < 0.01$ and *** $p < 0.001$.

5.1.8 Comparison of basal and FB_1-induced expression of Sphk1 in kidney and liver

Since treatment with FB_1 resulted in a different extent of sphingoid base 1-phosphate accumulation in kidney and liver, gene expression of SPHK1, the enzyme which catalyzes the phosphorylation of sphingoid bases, was compared in both organs with regard to basal (control) and FB_1-induced levels.

The analysis of basal *Sphk1* gene expression in kidney and liver of control animals revealed that *Sphk1* is expressed more abundantly in kidney than in liver (Figure 33), which is consistent with the higher formation of sphingoid base 1-phosphates in kidney after FB_1 treatment. The ratio of basal *Sphk1* expression between kidney and liver was more enhanced in control animals after 6-days, consistent with the increased basal levels of sphingoid base-1 phosphates in kidneys at this time-point (see section 5.1.5.2, Table 35).

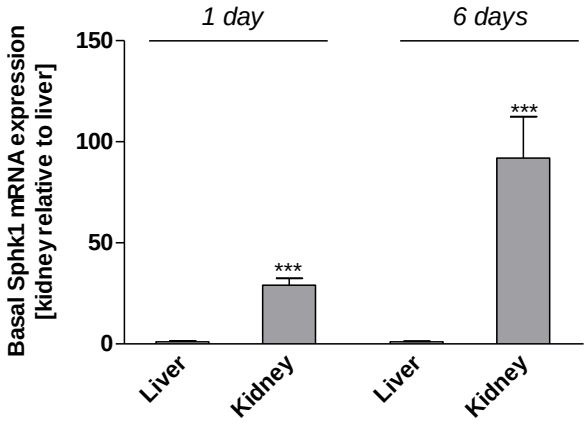

Figure 33: Comparison of basal Sphk1 mRNA expression in kidneys and livers of control animals after 1-day and 6-days. Data are expressed as mean fold changes ± standard deviation (n=4) in kidney relative to liver**.** Statistical analysis was performed by unpaired t-test and statistically significant changes between basal expression levels of liver and kidney are indicated by *** $p < 0.001$.

As shown in Figure 34, no significant treatment-related alterations in renal and hepatic *Sphk1* mRNA expression were observed in response to FB_1 for 1 and 6 days.

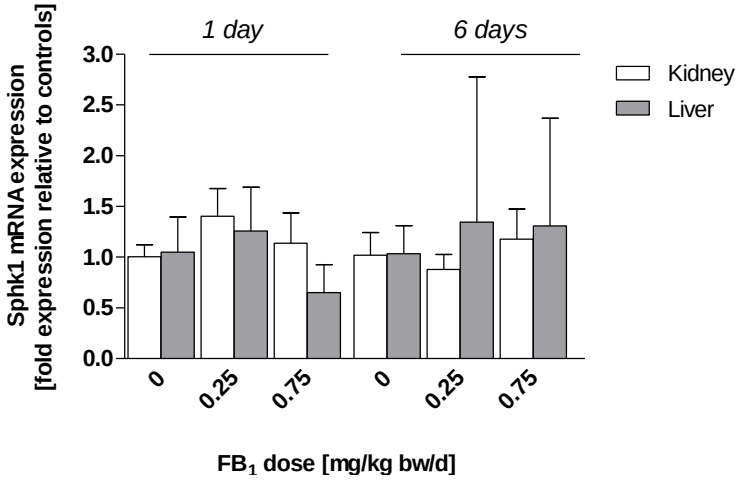

Figure 34: Comparison of Sphk1 mRNA expression in kidneys and livers of male Sprague Dawley rats treated with FB_1 (0.25 or 0.75 mg/kg bw/d) for 1 or 6 days. Data are presented as mean fold changes ± standard deviation (n=4) relative to controls. Statistical analysis was performed by one-way analysis of variance (ANOVA) and Dunnett's *post hoc* test.

5.1.9 Comparison of basal and FB_1-induced expression of sphingosine 1-phosphate receptors (S1PRs) in kidney and liver

Various cancer-related genes and bioactive lipid mediators such as So1P and Sa1P were potently modulated in kidney in response to FB_1 (see chapter 5.1.6 and 5.1.5). To further elucidate reasons for the transcriptional alterations in kidney and to explain the enhanced susceptibility of kidney to FB_1 toxicity, the expression of sphingosine 1-phosphate receptors *S1P*$_{1-3}$ was analyzed in both kidney and liver. As described in section 2.4.4.2, S1P receptors may mediate a range of pathways involved in pathophysiological processes such as tumorigenesis and cancer progression in response to sphingoid base 1-phosphates.

Qualitative analysis of the most common sphingosine 1-phosphate receptors *S1P*$_{1-3}$ by reverse transcriptase polymerase chain reaction (RT-PCR) revealed expression of *S1P*$_{1-3}$ in the kidneys and livers of male Sprague Dawley rats (Figure 35).

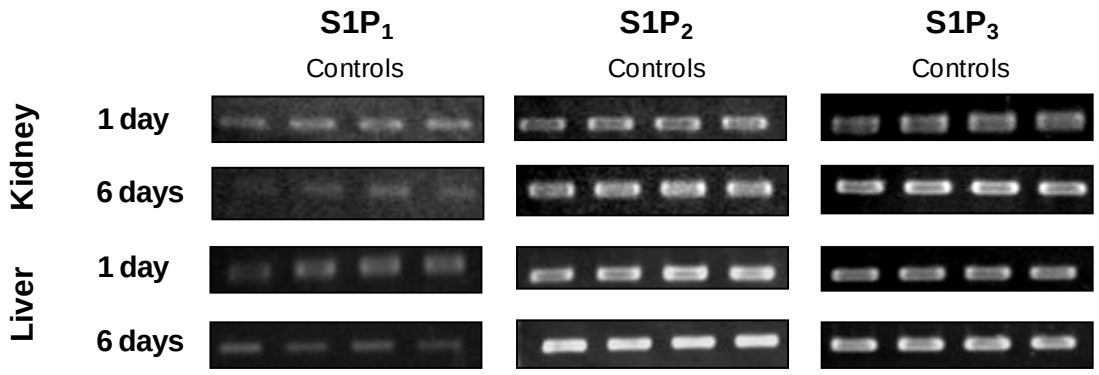

Figure 35: RT-PCR analysis of basal mRNA expression of sphingosine 1-phosphate receptors $S1P_{1-3}$ in kidneys and livers of control animals.

To identify differences in the basal expression of S1PRs between kidney and liver, mRNA expression of each receptor subtype in liver was set in relation to the mRNA expression of the respective receptor in kidney (Figure 36). Basal expression of *S1P$_1$* and *S1P$_2$* was more pronounced in liver compared to kidney, whereas basal expression of *S1P$_3$* was marginally more abundant in kidney after 1 day, but similar to liver after 6 days.

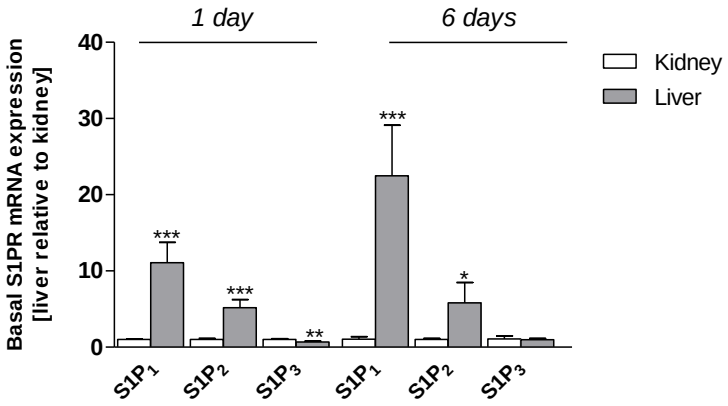

Figure 36: Comparison of basal S1PR ($S1P_2$, $S1P_2$ and $S1P_3$) mRNA expression in kidneys and livers of control animals from the 1- and 6-day study with FB_1. Data are expressed as mean fold changes ± standard deviation (n=4) in liver relative to kidney. Statistical analysis was performed by unpaired t-test and statistically significant changes between basal expression levels of kidney and liver are indicated by * $p < 0.05$, ** $p < 0.01$ and *** $p < 0.001$.

The effect of FB_1 treatment on the mRNA expression of *S1P$_{1-3}$* in liver and kidney is summarized in Figure 37. Gene expression of *S1P$_1$* was significantly reduced in livers but not kidneys of FB_1-treated animals in a time- and dose-dependent manner (Figure 37). Similarly, a treatment-related decrease in the expression of *S1P$_2$* was seen, although effects were not statistically significant. In contrast, FB_1 treatment had no significant effect on *S1P$_{1-3}$* expression in the kidney.

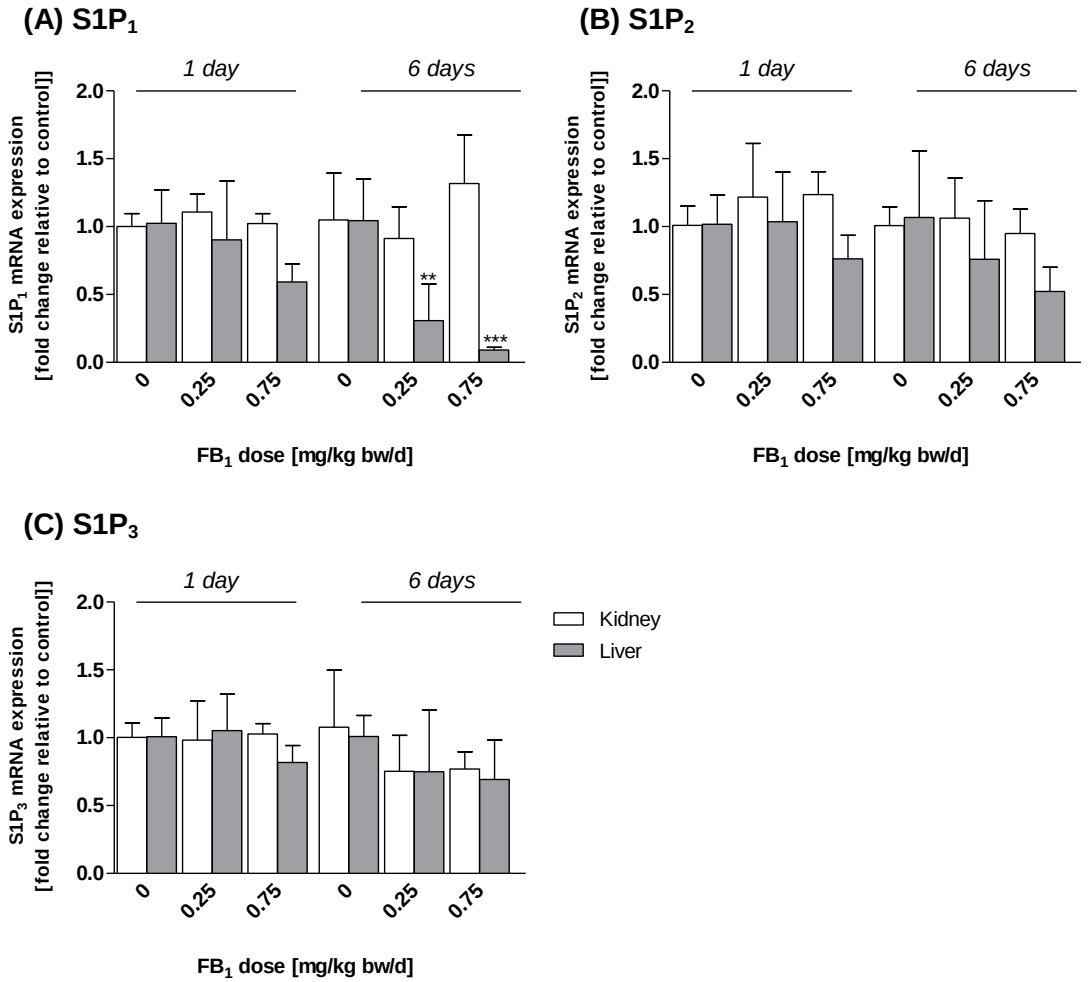

Figure 37: Comparison of $S1P_1$ (**A**), $S1P_2$ (**B**) and $S1P_3$ (**C**) mRNA expression in kidneys and livers of male Sprague Dawley rats treated with FB_1 (0.25 or 0.75 mg/kg bw/d) for 1 or 6 days. Data are presented as mean fold changes ± standard deviation (n=4) relative to controls. Statistical analysis was performed by one-way analysis of variance (ANOVA) and Dunnett's *post hoc* test. Statistically significant changes to controls are indicated by $*p < 0.05$.

5.2 Alterations in biochemical, transcriptional and functional responses associated with fumonisin B_1 carcinogenicity in normal rat kidney epithelial cells

5.2.1 Influence of FB_1 on cell viability in NRK-52E cells (MTT assay)

To determine suitable concentrations for expression profiling of cancer-related genes *in vitro*, cell viability of the renal proximal tubular epithelial cell line NRK-52E in response to different concentrations of FB_1 was determined using the MTT assay.

After treatment of NRK-52E cells with concentrations ranging from 0.5 to 100 µM FB_1 for 24 or 72 h, a statistically significant, time- and concentration-dependent decrease in cell viability was observed (Figure 38).

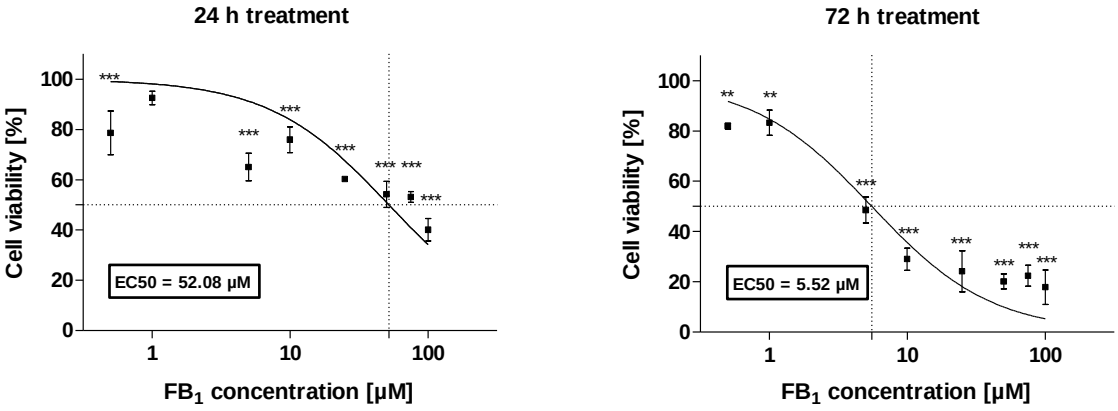

Figure 38: Cell viability (mitochondrial activity) in NRK-52E cells as determined by the MTT assay after treatment with FB_1 (0.5, 1.0, 5.0, 10, 25, 50, 75 and 100 µM) for 24 or 72 h. Data are presented on a logarithmic concentration scale as mean ± standard deviation (n=3) calculated from the means of three independent experiments with 3 biological replicates. Statistical analysis was performed by one-way analysis of variance (ANOVA) and Dunnett's *post hoc* test. Statistically significant changes to controls are indicated by ** $p < 0.01$ and *** $p < 0.001$. Effect concentrations for 50% reduction in cell viability (EC50 values) were calculated from non-linear regression (dose-response curves) using Graph pad prism® software.

After 24 h treatment with FB_1, an effect concentration for 50% reduction in cell viability (EC50 value) of 52.08 µM FB_1 was calculated (Figure 38). In contrast, 72 h treatment with FB_1 resulted in an approximately 10-fold lower EC50 value (5.52 µM) compared to the 24 h treatment. Finally, suitable treatment concentrations of FB_1 for gene expression analysis were derived from the EC50 value (52 µM) obtained after 24 h and set at 0.5, 5.0 and 50 µM FB_1 (Figure 38).

5.2.2 Disruption of sphingolipid metabolism in NRK-52E cells

To link FB_1-induced alterations in sphingolipid metabolism to gene expression changes of cancer-related genes, LC-MS/MS was applied for the determination of specific sphingolipid precursors and metabolites in cells (intracellular) and medium (extracellular) of NRK-52E cells treated with FB_1.

5.2.2.1 Alterations in the ceramide precursor sphingoid bases sphinganine and sphingosine and their 1-phosphate metabolites

After 24 h treatment of NRK-52E cells with 0.5, 5.0 and 50 µM FB_1, a marked increase in the sphingoid bases Sa and So as well as their respective phosphorylated metabolites Sa1P and So1P was observed (Figure 39).

The intracellular levels of Sa and So were low in controls and significantly increased from 5 µM FB_1 onwards (Figure 39A). Treatment with 50 µM FB_1 resulted in a 238-fold increase in Sa, whereas So was only enhanced by 3.9-fold compared to controls. Treatment at 5 and 50 µM FB_1 resulted in formation of the corresponding 1-phosphate metabolites Sa1P and So1P. So1P was not detectable in controls and its formation did not start until 5 µM FB_1. In contrast, Sa1P was also present in untreated cells and already seemed to be slightly increased at the lowest concentration of 0.5 µM FB_1 (Figure 39A).

Analysis of the cell medium (extracellular) revealed that the sphingoid bases Sa and So were dose-dependently increased (Figure 39B). Similar to the intracellular levels of sphingoid bases after 50 µM FB_1 treatment, Sa was more enhanced (146-fold) in medium than So (2.45-fold). The phosphorylated metabolites Sa1P and So1P were detected at very low, but highly significantly elevated levels compared to controls, whereby increased levels of Sa1P were already found at 0.5 µM FB_1. An increase in So1P was only detected at the highest concentration of FB_1 (Figure 39B).

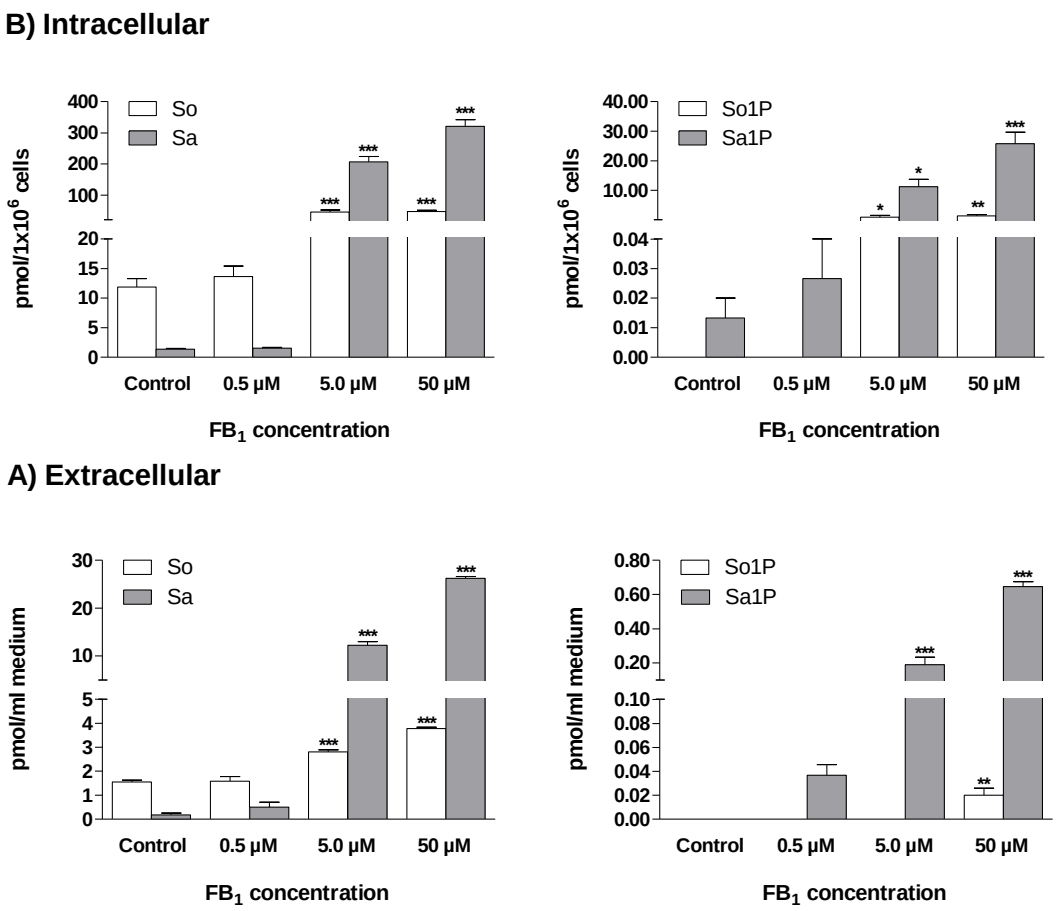

Figure 39: HPLC-MS/MS analysis of sphinganine, sphinganine 1-phosphate, sphingosine and sphingosine 1-phosphate in cell pellets (**A Intracellular**) and medium (**B Extracellular**) of NRK-52E cells treated with different concentrations FB_1 (0.5, 5.0 or 50 µM) for 24 h. Data are presented as mean ± standard deviation of three biological replicates. Statistical analysis was performed by one-way analysis of variance (ANOVA) and Dunnett's *post hoc* test. Statistically significant changes to controls are indicated by * $p < 0.05$, ** $p < 0.01$ and *** $p < 0.001$.

5.2.2.2 Alterations in ceramide-based sphingolipids

Treatment of NRK-52E cells with 50 µM FB_1 for 24 h did not affect the intracellular amounts of the major ceramide-based sphingolipid C16-Cer (Table 38). Intracellular levels of C18-Cer were not consistently altered after FB_1 treatment, but decreased after treatment with FB_1 at 50 µM concentration. However, C18:1-Cer, a less prevalent ceramide in the cells, was significantly increased after 24 h FB_1 treatment in a dose-dependent manner (Table 38).

Table 38: LC-MS/MS analysis of the sphingolipids C16-, C18- and C18:1-ceramide (C16-, C18- and C18:1-Cer) in cell pellets (intracellular) of NRK-52E cells treated with FB_1 (0.5, 5.0 or 50 µM) for 24 h. Data are presented as mean ± standard deviation of three biological replicates. Statistical analysis was performed by one-way analysis of variance (ANOVA) and Dunnett's *post hoc* test. Statistically significant changes to controls are indicated by * $p < 0.05$, ** $p < 0.01$ and *** $p < 0.001$.

Sphingolipids	**24 h treatment FB_1**			
[pmol/1x10^6 cells]	0 µM	0.5 µM	5.0 µM	50 µM
C16-Cer	229 ± 11	246 ± 3	224 ± 34	206 ± 3
C18-Cer	37.5 ± 2.8	42.7 ± 1.6	55.1 ± 7.7	29.4 ± 1.7
C18:1-Cer	1.17 ± 0.06	1.28 ± 0.12	2.20 ± 0.15 ***	4.94 ± 0.32 ***

5.2.3 Alterations in gene expression of cancer-related genes

After treatment of NRK-52E cells with 0.5, 5.0 and 50 µM FB_1 for 24 h, alterations in mRNA expression of 84 cancer-related genes were analyzed by quantitative real-time polymerase chain reaction (qRT-PCR) to compare these results to the gene expression changes obtained after treatment of Sprague Dawley rats. Analogous to the gene expression analysis *in vivo* (see chapter 5.1.6), target genes were categorized into 6 functional groups, representing gene candidates of the most important pathways involved in cancer:

- Cell cycle and DNA damage repair
- Apoptosis and cell senescence
- Signal transduction molecules and transcription factors
- Adhesion
- Angiogenesis
- Invasion and metastasis

5.2.3.1 Comparison of in vitro and in vivo transcription profiles in cancer-related genes

The FB_1-induced expression profiles of cancer-related genes *in vivo* and *in vitro* were compared to identify genes commonly modulated by FB_1.

As illustrated in the heat map (Figure 40), alterations in mRNA expression of several genes *in vitro* corresponded with those found *in vivo*. Among these, the transcription factors *Fos*, *Jun* and *Myc* as well as the cell cycle gene *p21* (*Cdkn1a*) and *Nfκbia*,

which is the inhibitor of the transcription factor NFκB, were identified to be the most prominent genes modulated by FB_1 in *in vivo* and *in vitro*. Furthermore, the mRNA expression of the plasminogen activator system components *Plaur* (*uPAR*) and *Timp1* were significantly increased in response to FB_1 *in vivo* and *in vitro*. In addition, *PAI-1* (*Serpine1*) was found to be markedly increased in kidney as well as in NRK-52E cells after FB_1 exposure.

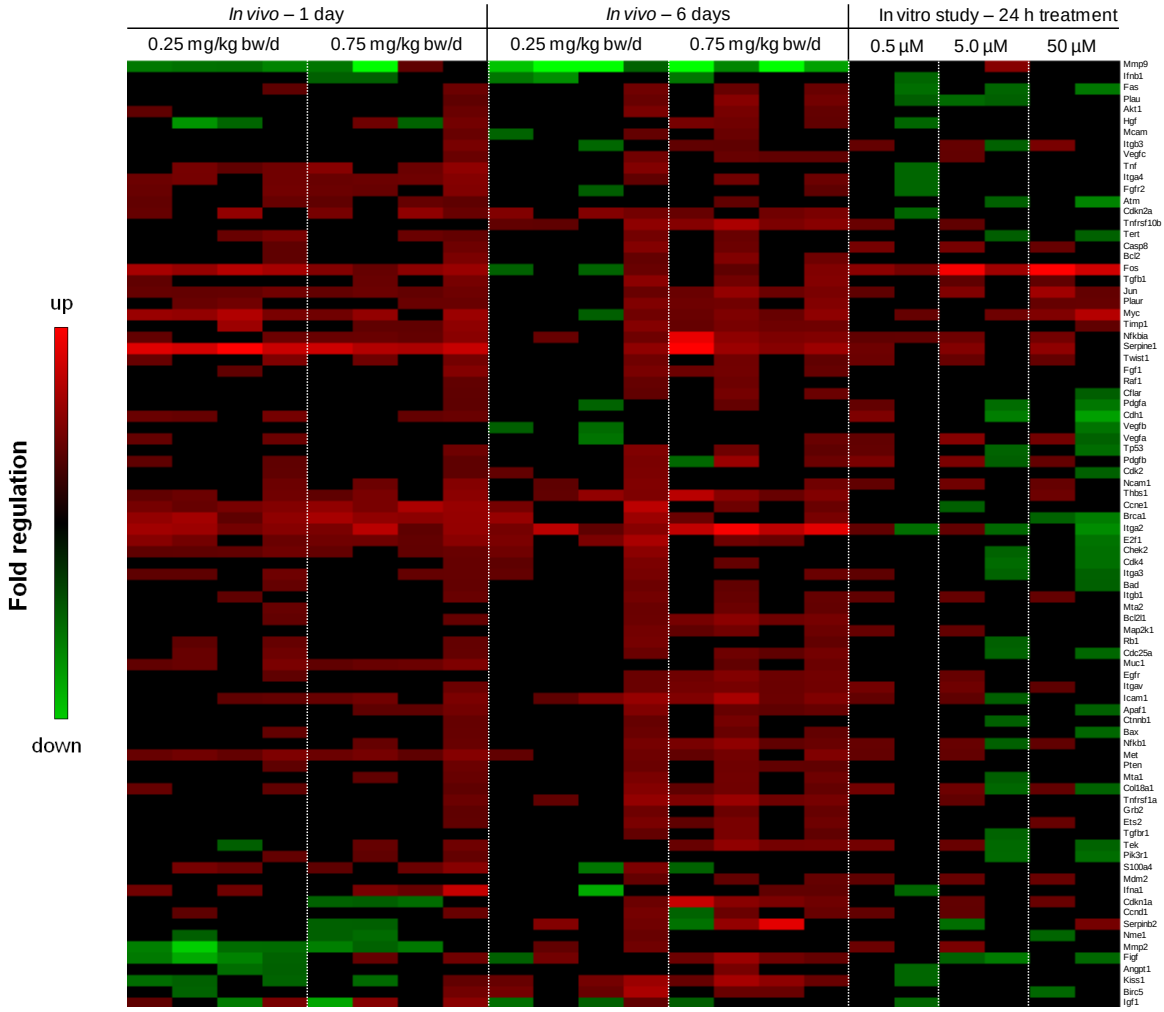

Figure 40: Heat map illustrating time- and dose-dependent patterns of gene expressions in kidneys of male Sprague Dawley rats treated with 0.25 and 0.75 mg/kg bw/d FB_1 for 1 or 6 days in comparison to gene expression changes in NRK-52E cells exposed to 0.5, 5.0 and 50 µM FB_1 for 24 h. Data for each dose group (with n=4 animals) or cell concentration (means of two independent experiments) are presented as individual fold changes (columns of the heat map) relative to the means of respective controls. The heat map was generated using Cluster 2.11 and TreeView 1.6 (Eisen *et al.*, 1998). Threshold values for gene expression changes are set at ± 1.4 relative to controls, whereby increases in up- and downregulated genes are indicated by increased intensity of red and green fields, respectively. The heat map was generated using Cluster 2.11 and TreeView 1.6.

As shown in the heat map, an increased variability was observed between both independent *in vitro* experiments (Figure 40).

An overview of the alterations in mRNA expression in FB_1-treated NRK-52E cells is given in Figure 41.

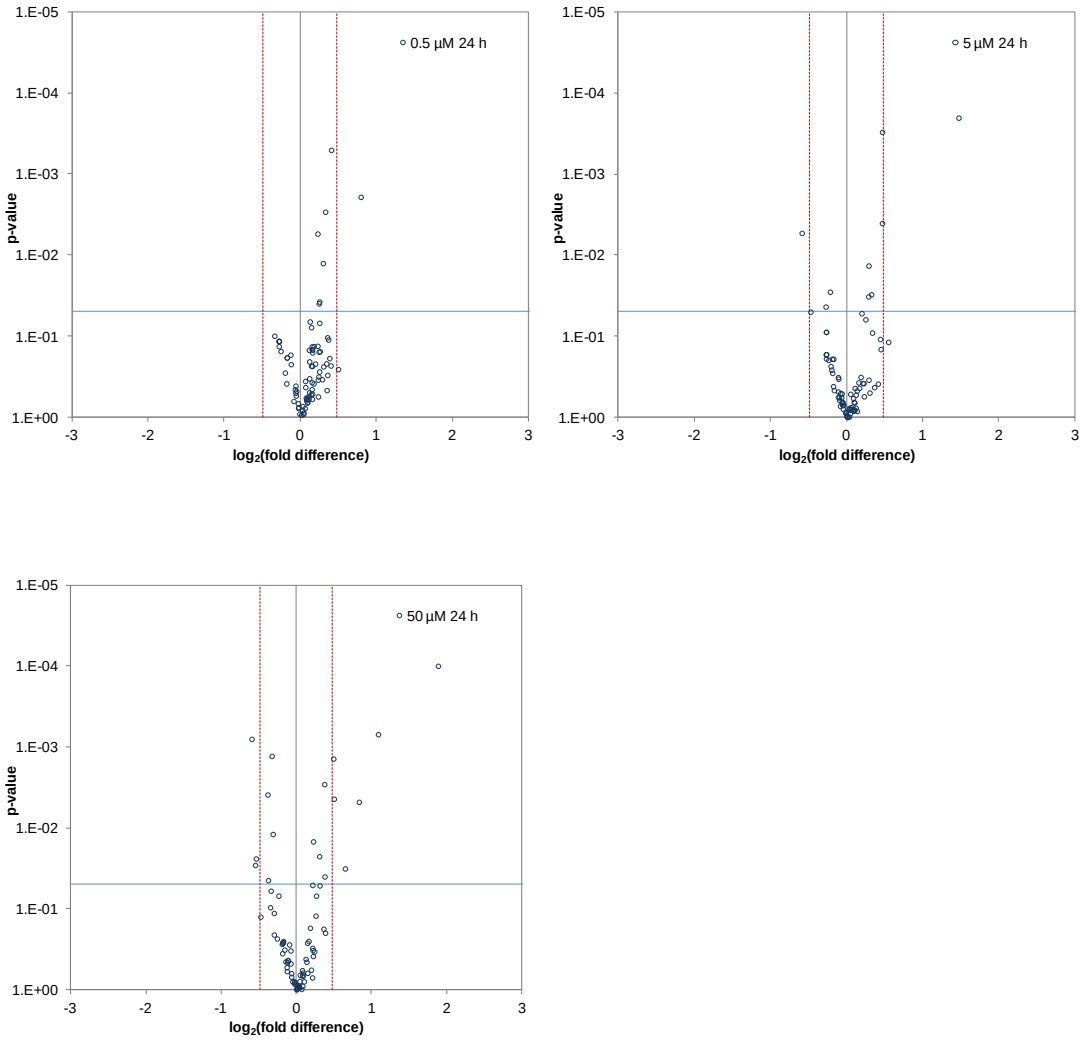

Figure 41: Overview of gene expression changes of cancer-related genes after treatment of NRK-52E cells with FB_1 (0.5, 5.0 or 50 µM) for 24 h. Data (blue dots) are illustrated as volcano blots and presented as mean dual logarithmic fold differences (from combined data of two independent experiments with 3 replicates per concentration for each experiment) of all 84 genes investigated in relation to their respective *p*-values. The dashed red grids signify gene expression thresholds of ± 1.4-fold compared to control values, whereas gene expression values of 1 (no alterations compared to controls) are represented by a black line. The threshold for statistical significance of alterations in gene expression after FB_1 treatment compared to controls is defined at *p*-values ≤ 0.05 and is indicated by a blue line (right upper corner: significantly upregulated genes; left upper corner: significantly downregulated genes).

Consistent with the *in vivo* findings (see section 5.1.6, Figure 27), gene expression profiling demonstrated early dose-related changes in the expression of cancer-associated genes in NRK-52E cells treated with FB_1, whereby the number of deregulated genes increased with time. However, fewer genes were significantly deregulated after *in vitro* than *in vivo* treatment with FB_1.

5.2.3.2 Genes involved in cell cycle control and DNA damage repair

After treatment of NRK-52E cells with FB_1, the mRNA expression of 5 genes involved in cell cycle control (*Ccnd1*, *p21* and *Ccne1*) and DNA damage repair (*Atm*, *Brca1*) was significantly altered (Table 39). Changes in the mRNA expression of *Ccnd1* occurred at 0.5 and 5.0 µM FB_1, but not at 50 µM. Gene expression of *p21* (*Cdkn1a*) was significantly increased at concentrations ≥ 5.0 µM FB_1. In contrast, mRNA expression of *Ccne1*, which similar to *Ccnd1* promotes cell cycle progression, was significantly downregulated at FB_1 concentrations of 5 and 50 µM (Table 39). Furthermore, the expression of *Atm*, which encodes a serine/threonine kinase that activates proteins of the DNA damage checkpoint (*e.g.* p53), and *Brca1*, which is involved in DNA damage repair, were significantly down-regulated at 50 µM FB_1.

5.2.3.3 Genes involved in apoptosis and cell senescence

Among the genes involved in apoptosis and cell senescence, only the mRNA expression of the anti-apoptotic oncogene *Birc5* (*survivin*) was significantly downregulated after treatment with 50 µM FB_1 (Table 39).

5.2.3.4 Genes involved in signal transduction and transcription

Treatment of NRK-52E cells with different concentrations of FB_1 resulted in a dose-dependent increase in mRNA expression of the transcription factors *Fos*, *Jun* and *Myc* and *Nfκbia*, encoding the inhibitor of the transcription factor NFκB (Table 39).

5.2.3.5 Genes involved in cell adhesion

None of the genes involved in cell adhesion were significantly altered in NRK-52E cells in response to FB_1 (Table 39).

5.2.3.6 Genes involved in angiogenesis

A significant, but not dose-related downregulation of mRNA expression was observed for *Figf*, which encodes the c-Fos induced growth factor, whereas the expression of other genes involved in angiogenesis was not significantly altered (Table 39).

5.2.3.7 Genes involved in invasion and metastasis

After treatment with FB_1, 3 genes involved in invasion and metastasis (Plaur, Timp1, and Nme1) were significantly altered in NRK-52E cells (Table 39). Exposure of cells to 50 µM FB_1 resulted in upregulation of the *urokinase-type plasminogen activator receptor* (*Plaur*) and *tissue inhibitor of metalloproteinase 1* (*Timp1*) mRNA expression. At the same concentration, mRNA expression of Nme1, which is thought to be a metastasis suppressor, was significantly decreased (-1.4-fold compared to controls). Although not statistically significant compared to the other treatment groups, PAI-1 gene expression was increased 1.6-fold at 50 µM FB_1 (Table 39).

Table 39: qRT-PCR results of gene expression alterations in NRK-52E cells treated with different concentrations of FB_1 (0.5, 5.0 or 50 µM) for 24 h. Data are combined from two independent experiments and presented as mean fold changes ± standard deviation (with three replicates per concentration for each experiment) of 84 cancer-related genes relative to the means of respective controls. Statistical analysis was performed by one-way analysis of variance (ANOVA) and Dunnett's *post hoc* test. Statistically significant changes to controls are indicated by * $p < 0.05$, ** $p < 0.01$ and *** $p < 0.001$. Gene expression changes > 1.4 are highlighted in bold black.

Functional gene grouping		**24 h FB_1 treatment [µM]**					
Accession No.	**Gene Symbol**	**0.5**		**5.0**		**50**	
		Cell cycle control and DNA damage repair					
XM_236275	*Atm*	1.0 ± 0.1		0.9 ± 0.1		0.7 ± 0.2	*
NM_012514	*Brca1*	1.1 ± 0.1		0.9 ± 0.2		0.7 ± 0.2	***
NM_171992	*Ccnd1*	1.2 ± 0.2	*	1.2 ± 0.2	*	1.2 ± 0.1	
XM_574426	*Ccne1*	1.0 ± 0.1		0.9 ± 0.1	*	0.8 ± 0.1	**
NM_133571	*Cdc25a*	1.1 ± 0.2		0.9 ± 0.2		1.0 ± 0.3	
NM_199501	*Cdk2*	1.1 ± 0.1		1.0 ± 0.1		0.9 ± 0.2	
NM_053593	*Cdk4*	1.0 ± 0.2		0.9 ± 0.2		0.8 ± 0.2	
NM_080782	*Cdkn1a (p21)*	1.1 ± 0.1		1.2 ± 0.1	*	1.3 ± 0.2	**
NM_031550	*Cdkn2a (p16)*	1.0 ± 0.1		1.0 ± 0.2		1.1 ± 0.2	
NM_053677	*Chek2*	1.1 ± 0.2		1.0 ± 0.3		0.8 ± 0.2	
XM_230765	*E2f1*	1.1 ± 0.2		1.0 ± 0.2		0.8 ± 0.2	
XM_235169	*Mdm2*	1.2 ± 0.2		1.3 ± 0.2		1.2 ± 0.2	
NM_031606	*Pten*	1.1 ± 0.1		1.0 ± 0.2		1.1 ± 0.2	
XM_344434	*Rb1*	1.1 ± 0.2		1.0 ± 0.3		1.0 ± 0.2	
NM_030989	*Tp53*	1.1 ± 0.3		1.0 ± 0.3		0.9 ± 0.4	

Functional gene grouping		24 h FB_1 treatment [µM]		
Accession No.	**Gene Symbol**	**0.5**	**5.0**	**50**
		Apoptosis and cell senescence		
NM_023979	*Apaf1*	1.0 ± 0.1	1.0 ± 0.1	0.9 ± 0.2
NM_022698	*Bad*	1.0 ± 0.1	1.0 ± 0.2	1.0 ± 0.3
NM_017059	*Bax*	1.0 ± 0.2	1.0 ± 0.2	0.9 ± 0.2
NM_016993	*Bcl2*	1.1 ± 0.1	1.0 ± 0.1	1.2 ± 0.1
NM_031535	*Bcl2l1 (Bcl-XL)*	1.2 ± 0.1	1.1 ± 0.2	1.1 ± 0.2
NM_022274	*Birc5*	0.9 ± 0.1	0.9 ± 0.2	0.8 ± 0.1 **
NM_022277	*Casp8*	1.3 ± 0.4	1.2 ± 0.5	1.2 ± 0.3
NM_057138	*Cflar*	1.1 ± 0.2	1.0 ± 0.3	1.0 ± 0.3
NM_053423	*Tert*	1.1 ± 0.2	1.0 ± 0.3	0.9 ± 0.2
XM_344431	*Tnfrsf10b_pred*	1.2 ± 0.5	1.1 ± 0.4	1.0 ± 0.2
NM_013091	*Tnfrsf1a*	1.1 ± 0.1	1.1 ± 0.3	1.1 ± 0.3
NM_139194	*Fas*	0.8 ± 0.2	0.9 ± 0.5	0.8 ± 0.3
		Signal transduction molecules and transcription factors		
NM_033230	*Akt1*	1.0 ± 0.1	0.9 ± 0.1	1.0 ± 0.1
NM_053357	*Ctnnb1*	1.1 ± 0.2	1.0 ± 0.3	1.0 ± 0.2
XM_239510	*Ets2*	1.1 ± 0.2	1.1 ± 0.2	1.2 ± 0.4
NM_022197	*Fos*	**1.7** ± 0.3	**2.8** ± 0.7 ***	**3.7** ± 1.0 ***
NM_030846	*Grb2*	1.1 ± 0.1	1.1 ± 0.2	1.0 ± 0.1
NM_021835	*Jun*	1.2 ± 0.2	**1.4** ± 0.5	**1.8** ± 0.5 **
NM_031643	*Map2k1*	1.2 ± 0.3	1.1 ± 0.3	1.0 ± 0.2
NM_012603	*Myc*	1.3 ± 0.2	**1.4** ± 0.2	**2.1** ± 0.6 ***
XM_342346	*Nfκb1*	1.2 ± 0.3	1.1 ± 0.4	1.1 ± 0.3
XM_343065	*Nfκbia (IκBα)*	1.3 ± 0.1 *	**1.4** ± 0.2 **	**1.4** ± 0.3 **
NM_013005	*Pik3r1*	1.0 ± 0.2	0.9 ± 0.3	0.9 ± 0.3
NM_012639	*Raf1*	1.1 ± 0.1	1.0 ± 0.2	1.0 ± 0.2
		Adhesion		
NM_031334	*Cdh1*	1.3 ± 0.6	0.9 ± 0.4	0.7 ± 0.3
NM_012967	*Icam1*	1.1 ± 0.3	1.0 ± 0.3	1.0 ± 0.3
XM_345156	*Itga2*	1.0 ± 0.4	1.0 ± 0.4	0.7 ± 0.2
XM_340884	*Itga3_pred*	1.1 ± 0.2	1.0 ± 0.3	1.0 ± 0.3
XM_230033	*Itga4*	0.8 ± 0.2	0.8 ± 0.2	0.9 ± 0.2
XM_230950	*Itgav_pred*	1.3 ± 0.3	1.2 ± 0.4	1.1 ± 0.3
NM_017022	*Itgb1*	1.2 ± 0.2	1.2 ± 0.3	1.2 ± 0.3
NM_153720	*Itgb3*	1.2 ± 0.3	1.1 ± 0.4	1.3 ± 0.4
NM_023983	*Mcam*	1.1 ± 0.2	1.1 ± 0.2	1.1 ± 0.1
NM_031521	*Ncam1*	1.2 ± 0.2	1.3 ± 0.3	1.2 ± 0.3
		Angiogenesis		
NM_053546	*Angpt1*	0.8 ± 0.2	0.8 ± 0.2	1.0 ± 0.4
XM_241632	*Col18a1*	1.3 ± 0.4	1.1 ± 0.5	1.1 ± 0.4
NM_031507	*Egfr*	1.1 ± 0.2	1.1 ± 0.3	1.0 ± 0.2
NM_012846	*Fgf1*	1.1 ± 0.1	1.0 ± 0.2	1.1 ± 0.2

Functional gene grouping		24 h FB_1 treatment [µM]				
Accession No.	**Gene Symbol**	**0.5**	**5.0**		**50**	
		Angiogenesis				
XM_341940	*Fgfr2*	0.8 ± 0.2	0.9 ± 0.2		0.9 ± 0.2	
NM_031761	*Figf*	0.9 ± 0.1	0.7 ± 0.2	*	0.9 ± 0.3	
NM_017017	*Hgf*	0.9 ± 0.3	0.8 ± 0.2		0.9 ± 0.2	
NM_001014786	*Ifna1*	0.9 ± 0.3	0.8 ± 0.2		1.0 ± 0.2	
NM_019127	*Ifnb1*	0.9 ± 0.3	0.8 ± 0.2		0.9 ± 0.2	
NM_178866	*Igf1*	0.8 ± 0.2	0.8 ± 0.2		0.9 ± 0.2	
NM_012801	*Pdgfa*	1.1 ± 0.3	0.9 ± 0.3		0.8 ± 0.2	
XM_343293	*Pdgfb*	1.3 ± 0.5	1.2 ± 0.7		1.1 ± 0.3	
XM_342863	*Tek*	1.2 ± 0.5	1.1 ± 0.4		1.0 ± 0.3	
NM_021578	*Tgfb1*	1.1 ± 0.1	1.1 ± 0.2		1.2 ± 0.2	
NM_012775	*Tgfbr1*	1.0 ± 0.1	0.8 ± 0.1		0.9 ± 0.2	
NM_001013062	*Thbs1 (TSP-1)*	1.1 ± 0.2	1.0 ± 0.3		1.3 ± 0.3	
NM_012675	*Tnf*	0.8 ± 0.2	0.8 ± 0.2		0.9 ± 0.2	
NM_031836	*Vegfa*	**1.4** ± 0.6	1.3 ± 0.6		1.2 ± 0.5	
NM_053549	*Vegfb*	1.1 ± 0.2	0.9 ± 0.3		0.8 ± 0.3	
NM_053653	*Vegfc*	1.0 ± 0.3	1.1 ± 0.3		1.0 ± 0.2	
		Invasion and metastasis				
NM_181692	*Kiss1*	0.8 ± 0.2	0.9 ± 0.2		0.9 ± 0.2	
NM_031517	*Met*	1.2 ± 0.3	1.1 ± 0.4		1.0 ± 0.3	
NM_031054	*Mmp2*	1.3 ± 0.2	1.3 ± 0.6		1.1 ± 0.1	
NM_031055	*Mmp9*	0.9 ± 0.3	**1.5** ± 0.6		1.1 ± 0.2	
NM_022588	*Mta1*	1.1 ± 0.1	1.0 ± 0.3		1.0 ± 0.3	
XM_342015	*Mta2*	1.1 ± 0.1	1.0 ± 0.2		1.1 ± 0.3	
XM_342281	*Muc1*	1.1 ± 0.2	0.9 ± 0.2		1.0 ± 0.2	
NM_138548	*Nme1*	1.0 ± 0.1	1.0 ± 0.2		0.8 ± 0.1	*
NM_013085	*Plau (uPA)*	0.9 ± 0.2	0.7 ± 0.2		0.9 ± 0.3	
NM_017350	*Plaur (uPar)*	1.2 ± 0.1	1.2 ± 0.1		**1.4** ± 0.1	***
NM_012618	*S100a4*	1.0 ± 0.1	1.0 ± 0.1		1.1 ± 0.2	
NM_021696	*Serpinb2 (PAI-2)*	1.0 ± 0.4	0.9 ± 0.3		1.3 ± 0.4	
NM_012620	*Serpine1 (PAI-1)*	1.3 ± 0.3	**1.4** ± 0.5		**1.6** ± 0.5	
NM_053819	*Timp1*	1.0 ± 0.1	1.1 ± 0.1		1.2 ± 0.2	**
NM_053530	*Twist1*	1.2 ± 0.4	1.2 ± 0.3		1.2 ± 0.3	

5.2.4 Influence of FB_1 and sphingosine 1-phosphate on the invasive potential of NRK-52E cells

A cell invasion assay based on 2% gelatin using a modified Boyden chamber was performed to assess whether treatment with FB_1 or the sphingoid base 1-phosphate So1P may enhance the invasiveness of NRK-52E cells as a result of the observed mRNA expression changes in invasion/metastasis-associated genes.

Treatment of NRK-52E cells with FB_1 concentrations (0, 0.5, 5.0 and 50 µM) induced a significant and concentration-dependent increase in cell invasion into 2% gelatin. The maximum response was a 1.7-fold increase in cell invasion compared to controls at 5 µM FB_1 (Figure 42).

In contrast, treatment of NRK-52E cells with 0.5 and 1.0 µM So1P did not alter cell invasion compared to controls, whereas treatment with 5.0 µM So1P slightly reduced cell invasion into 2% gelatin, but without statistical significance compared to the other treatment groups (Figure 42).

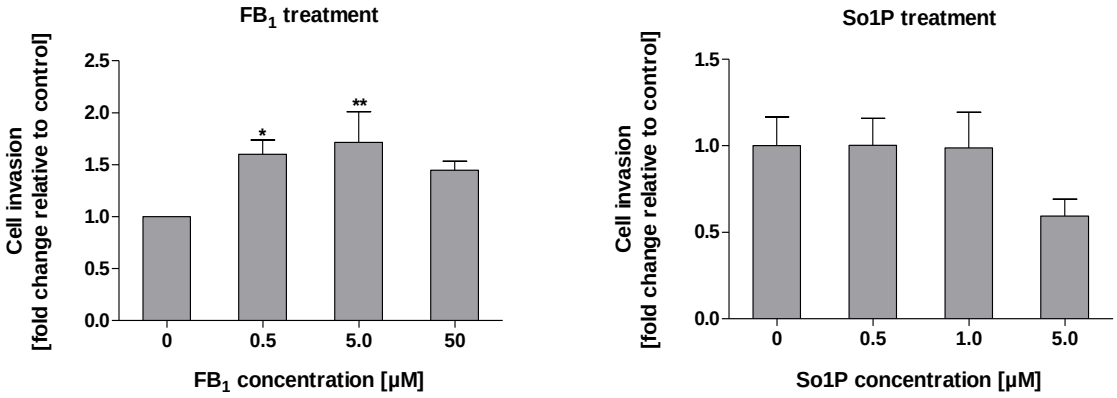

Figure 42: Analysis of cell invasion of NRK-52E cells into 2% gelatin matrix after treatment with 0, 0.5, 5.0 and 50 µM FB_1 or 0, 0.5, 1.0 and 5 µM So1P in a modified Boyden chamber. Data are presented as mean fold change ± standard deviation (calculated from the means of 3 replicates from three independent experiments) relative to the means of controls. Statistical analysis was performed by one-way analysis of variance (ANOVA) and Dunnett's *post hoc* test. Statistically significant changes to controls are indicated by * $p < 0.05$ and ** $p < 0.01$.

5.2.5 Sphingosine 1-phosphate receptor expression in NRK-52E cells

The analysis of S1P receptors *in vitro* was performed to identify receptor subtypes, which might mediate signaling mechanisms of extracellular sphingoid base 1-

phosphates, e.g. migration and invasion, and thus might be crucial for FB_1-induced increase in cell invasion in NRK-52E cells.

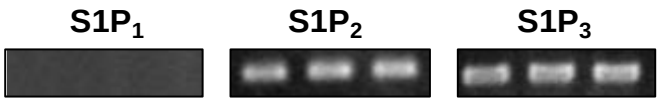

Figure 43: RT-PCR analysis of basal mRNA expression of sphingosine 1-phosphate receptors $S1P_{1-3}$ in untreated (control) NRK-52E cells.

RT-PCR analysis of S1P receptors demonstrated that $S1P_2$ and $S1P_3$ were abundantly expressed in untreated NRK-52E cells, whereas no basal expression was found for $S1P_1$ (Figure 43) in contrast to rat kidney *in vivo* (see chapter 5.1.8, Figure 35).

5.2.6 Role of sphingosine kinase 1 (Sphk1) inhibition in FB_1-mediated toxicity in NRK-52E cells

To confirm that the FB_1-induced formation of phosphorylated sphingoid bases Sa1P and So1P by the enzyme sphingosine kinase 1 (Sphk1) mediates anti-apoptotic and proliferative signaling in NRK-52E cells, the specific inhibitor 4-[[4-(4-Chlorophenyl)-2-thiazolyl]amino]phenol (SKI II) was applied to selectively suppress the activity of sphingosine kinase.

5.2.6.1 Effects of treatment with the sphingosine kinase inhibitor SKI II and FB_1 on cell viability

Treatment with FB_1 (0, 0.5, 5.0 and 50 µM) and SKI II (0, 0.5, 1.0 and 2.5 µM) for 24 h resulted in a significant decrease ($p < 0.001$ compared to controls) in cell viability of NRK-52E cells (Figure 44).

However, a significant decrease in cell viability after treatment with SKI II and FB_1 compared to FB_1 or SKI II treatment alone was only seen at 5 µM FB_1 combined with 0.5 µM SKI II.

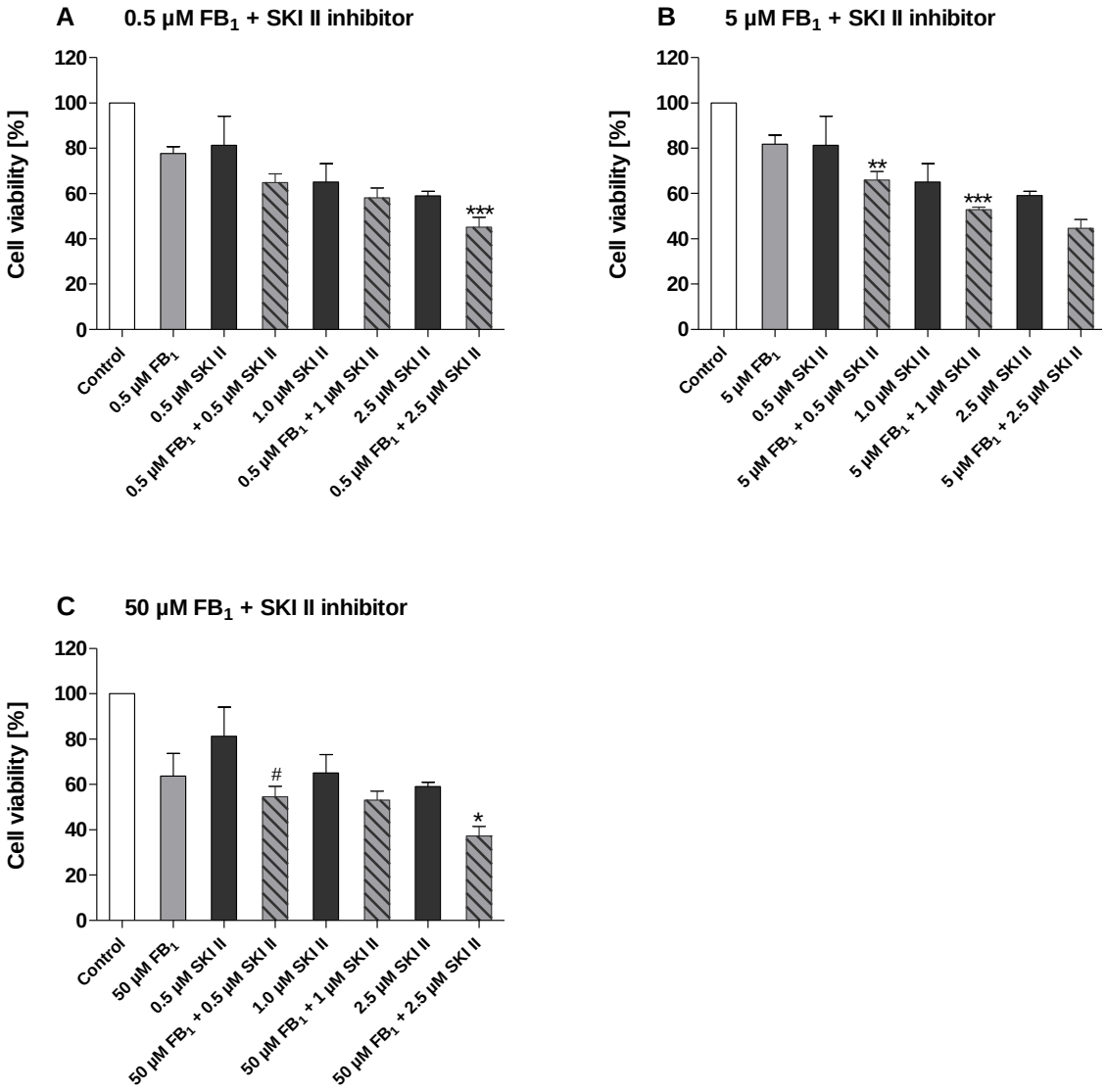

Figure 44: Effect of 24 h treatment with FB_1 ((**A**) 0.5, (**B**) 5.0 and (**C**) 50 µM) and sphingosine kinase inhibitor SKI II (0, 0.5, 1 and 2.5 µM) on cell viability in NRK-52E cells as determined by MTT assay. Data are presented as mean ± standard deviation (n=3) from the means of three independent experiments with 3 biological replicates. Statistical analysis was performed by one-way analysis of variance (ANOVA) and Tukey's *post hoc* test. Statistically significant changes between FB_1 treatment alone (grey bars) and treatment (hatched grey bars) with SKI II are indicated by * $p < 0.05$, ** $p < 0.01$ and *** $p < 0.001$. Statistically significant changes between SKI II treatment alone (dark grey bars) and treatment with FB_1 (hatched grey bars) are indicated by $^{\#}$ $p < 0.05$.

5.2.6.2 Effects of sphingosine kinase inhibition on the intracellular formation of sphingoid base 1-phosphates

To assess whether the observed decrease in cell viability after treatment with FB_1 and SKI II correlated with reduced formation of survival-promoting sphingoid base 1-phosphates, HPLC-MS/MS analysis of intracellular levels of So1P and Sa1P was

performed in NRK-52E cells after treatment with 5 µM and increasing concentrations of SKI II (0.5, 1.0 and 2.5 µM).

After treatment with 5 µM FB_1 and 2.5 µM SKI II, the formation of So1P was decreased compared to FB_1-treatment alone, but without statistical significance compared to the other treatment groups (Figure 45).

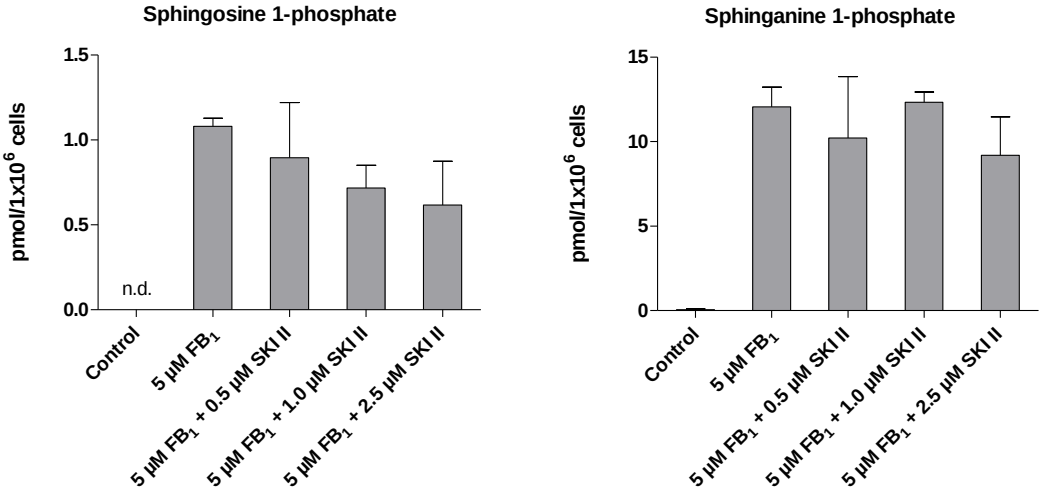

Figure 45: Effect of 24 h treatment with 5 µM FB_1 and different concentrations of sphingosine kinase inhibitor SKI II (0, 0.5, 1.0 and 2.5 µM) on FB_1-mediated intracellular formation of sphingosine- and sphinganine 1-phosphate in NRK-52E cells determined by LC-MS/MS analysis. Data are presented as mean ± standard deviation (n=3) from one experiment. Statistical analysis was performed by unpaired t-test and statistically significant changes between SKI II treatment alone and treatment with FB_1 are indicated by * $p < 0.05$.

Treatment with SKI II resulted in a more pronounced reduction in FB_1-induced levels of So1P compared to Sa1P (Figure 45).

6 Discussion

6.1 FB_1-mediated early pathological and biochemical changes in rat kidney associated with tumorigenesis

6.1.1 Early effects on clinical chemistry and histopathological alterations in the kidney

Clinical markers in serum and urine and histopathological alterations in renal tissue were assessed as classical endpoints for nephrotoxicity in male Sprague Dawley rats after treatment with 0.25 and 0.75 mg/kg bw/d FB_1 for 1 and 6 days. The effects on clinical chemistry parameters and histopathology in kidney were compared to those observed in the study by Bondy *et al.* (Bondy *et al.*, 2000), whose dose regimen and choice of rat strain served as model for the present study design.

The evaluation of clinical markers in serum and urine showed that single *i.p.* administration of FB_1 resulted in early alterations of markers, which are indicative of ongoing renal dysfunction, *e.g.* disturbances in mineral, urea and protein concentrations in serum (see chapter 5.1.2, Table 33). These observations were in line with the elevated protein concentrations in serum of treated animals as reported by Bondy *et al.* (Bondy *et al.*, 2000). After 6-day treatment with FB_1, parameters characteristic for progressive renal dysfunction (creatinine concentrations in serum and protein concentrations in urine) were increased (see chapter 5.1.2, Table 33). In contrast to Bondy *et al.* (Bondy *et al.*, 2000), our results also showed significant alterations in sodium, potassium and anorganic phosphorus after 6-day treatment with 0.75 mg/kg bw/d FB_1.

Early histopathological changes in kidney time- and dose-dependently occurred after administration of different doses FB_1 for the respective treatment durations (see chapter 5.1.3, Figure 17) and correlated with the observed, early alterations in clinical markers of serum and urine (see chapter 5.1.2, Table 33). The degeneration of the tubular epithelium in the cortex and OSOM, characterized by detachment of epithelial cells into the tubular lumen, loss of brush border membrane, flattened epithelium and vacuolized, dilated appearance of tubular cells (see chapter 5.1.3, Figure 17) was also consistent with the observations by Bondy *et al.* (Bondy *et al.*, 2000).

6.1.2 Increased apoptosis and regenerative cell proliferation in kidney correlate with early FB_1-induced alterations in renal sphingolipid metabolism

Sustained tissue injury in form of apoptotic or oncotic cell death followed by stimulation of cell proliferation is well established to promote tumorigenesis. Many non-genotoxic carcinogens are known to induce renal carcinogenesis *via* this mode of action (Hard, 1998). Although it has been assumed that FB_1 may induce tumor formation by direct cytotoxicity (sustained apoptosis) and subsequent compensatory cell regeneration (Dragan *et al.*, 2001; Howard *et al.*, 2001b; Lock and Hard, 2004), the specific molecular events leading to these cellular effects in kidney are still unclear, but strongly correlate with the FB_1-induced disruption of sphingolipid metabolism. Thus, the aim of our study was to link FB_1-induced alterations in the rates of apoptosis and cell proliferation to early time- and dose-dependent changes in the balance between pro-apoptotic or proliferative signaling molecules resulting from the FB_1-mediated disturbance of sphingolipid metabolism.

The present study showed that a single *i.p.* administration of FB_1 (0.25 and 0.75 mg/kg bw/d) was sufficient to induce apoptosis in the cortex and OSOM of male Sprague Dawley rats. Apoptosis resulted in the ongoing degeneration of the tubular epithelium as characterized by detachment of epithelial cells into the tubular lumen. At this early stage, apoptosis was paralleled by proliferation of single tubular epithelial cells in the regions of tubular damage. In contrast, repeated administration of FB_1 for 6 consecutive days resulted in marked tubular apoptosis, predominantly found in the cortex and OSOM of the kidney. As a result of severe renal degeneration, a high number of tubular epithelial cells was detached from the basal membrane and sloughed into the tubule lumen, resulting in the accumulation of cellular debris. This is in line with data from Bondy *et al.*, who had previously shown that 6-day *i.p*. administration of 0.75 mg/kg bw/d FB_1 to male Sprague Dawley rats resulted in occasional to numerous apoptotic tubular cells in the cortex and OSOM of the kidney, respectively (Bondy *et al.*, 2000). In addition to these results, our study also demonstrated increased cell proliferation within the renal tubular epithelium as a consequence of the substantial tubular damage after short-term *i.p.* administration of 0.75 mg/kg bw/d FB_1.

There is strong evidence that both the extent and severity of histopathological changes in rodent kidney correlate with FB_1-induced biochemical alterations in

sphingolipid metabolism (Riley *et al.*, 1994; NTP, 2001; Riley *et al.*, 2001). Persistent alterations in sphingolipid metabolism may cause perturbations in the balance of sphingolipid precursors and metabolites favoring pro-apoptotic (sphingosine and sphinganine) or anti-apoptotic/proliferative (sphingosine- and sphinganine 1-phosphate) signals in FB_1-exposed tissues (Riley *et al.*, 2001). The present study was aimed at analyzing early FB_1-induced changes in pro- and anti-apoptotic/proliferative signaling molecules of sphingolipid metabolism in kidneys of male Sprague Dawley rats.

Although studies demonstrated that FB_1 inhibits ceramide synthase (Wang *et al.*, 1991; Merrill *et al.*, 1993; Mizutani *et al.*, 2005) and decreases ceramide levels in several cell lines *in vitro* (Tolleson *et al.*, 1999; Ogretmen *et al.*, 2002; Mizutani *et al.*, 2005; Lee *et al.*, 2007; Zitomer *et al.*, 2009), levels of specific ceramides have not yet been determined after FB_1-mediated inhibition of ceramide synthase in rat kidney, the major target organ of FB_1 toxicity. Our study, for the first time, showed that single administration of FB_1 (0.25 and 0.75 mg/kg bw/d) resulted in a slight decrease in the main ceramide C16-Cer, which dose-dependently decreased after repeated administration for 6 days in kidney. These data provide evidence for the strong and early inhibitory effect of FB_1 on renal ceramide synthase. Similarly, levels of C18-Cer, a minor ceramide in rat kidney, were dose-dependently decreased after FB_1 treatment, which supports the sensitivity of FB_1-mediated ceramide synthase inhibition in kidney. Ceramides are important constituents of the cell membrane and important precursors of more complex membrane-bound sphingolipids such as sphingomyelin and glycosphingolipids, which are involved in binding to cytoskeletal proteins, cell-cell communication and cell-substratum interactions (Riley *et al.*, 2001). Decreased levels of ceramide and subsequent depletion of complex ceramides may thus result in loss of epithelial cell morphology, reduced rates of cell growth and inhibition of cell-adhesion (Riley *et al.*, 2001; Desai *et al.*, 2002). In this respect, *in vitro* studies revealed that FB_1-induced alterations in sphingolipid metabolism may potently influence membrane structure, as evidenced by a decrease in membrane barrier function in porcine pulmonary artery endothelial cells (Ramasamy *et al.*, 1995) and inhibition of integrin-mediated cell-matrix adhesion in mouse melanoma cells (Pelagalli *et al.*, 1999). Similarly, our histopathological evaluations of FB_1-treated kidneys showed that early degeneration of renal tubules was characterized by detachment of cells from the basement membrane of the renal tubular epithelium in

the tubular lumen. This suggests that FB_1-mediated cell death may in part represent anoikis, a special form of apoptosis that occurs as a consequence of loss of cell anchorage to the ECM, which has also been described in the renal epithelium of FB_1-treated rats from the carcinogenicity study (Hard *et al.*, 2001). Increased apoptosis as a consequence of FB_1-mediated depletion of complex sphingolipids was also observed in the porcine proximal tubule cells LLC-PK_1 (Yoo *et al.*, 1996). Thus, markedly decreased levels in the major ceramide C16-Cer, which consequently reduce the formation of complex sphingolipids involved in cell adhesion, may contribute to FB_1-induced cell detachment and apoptosis observed in the present study.

Due to inhibition of ceramide biosynthesis, reflected by a significant decrease in ceramide levels, a wide range of changes in the intracellular concentration of intermediates originating from sphingolipid metabolism were expected in the present study. Indeed, early alterations in renal sphingolipid metabolism were already observed after single treatment with the low dose FB_1 (0.25 mg/kg bw/d) and increased with the higher dose FB_1 (0.75 mg/kg bw/d). These alterations included a significant increase (594-fold) in the levels of sphinganine, which is an important precursor in the biosynthesis of ceramide and indicative of FB_1-mediated inhibition of ceramide synthase (Wang *et al.*, 1991). Accordingly, levels of the second ceramide precursor sphingosine, which is only formed after metabolic conversion of complex sphingolipids, were also significantly elevated (13.6-fold), but less pronounced as compared to sphinganine.

In previous studies, the ratio of sphinganine to sphingosine in tissue, serum and urine was used as an important biomarker for early exposure to FB_1 (Riley *et al.*, 1993) (Wang *et al.*, 1992; Cai *et al.*, 2007). Alterations in these ratios paralleled FB_1-mediated toxicity in the target organs (Riley *et al.*, 1994; NTP, 2001; Riley and Voss, 2006). In the present study, the Sa/So ratio in kidneys of male Sprague Dawley increased dose-dependently after a single dose of FB_1 and reached a Sa/So ratio of 3.0 after treatment with 0.75 mg/kg bw/d FB_1. In accordance with our results, Domijan *et al.* (Domijan *et al.*, 2007b) showed that *i.p.* administration of 0.5 mg/kg bw/d FB_1 for 2 days resulted in a Sa/So ratio of 4.5 in kidneys of male Wistar rats. These results show a similar extent of early FB_1-mediated alterations in the relative amounts of the renal Sa and So in both rat strains after short-term *i.p.* application of FB_1. Moreover,

our study revealed that ratios of Sa/So in urine strongly reflected the alterations in renal sphingolipid metabolism, since urinary Sa/So was significantly increased (Sa/So: ~2) compared to control (Sa/So: 0.02) after single treatment with FB_1.

After 6-day exposure to FB_1, the levels of pro-apoptotic Sa and So in kidney as well as the renal and urinary ratios of Sa/So further increased and paralleled the histological observations of ongoing cell death and enhanced cell proliferation in the tubules of the renal cortex and OSOM. In this context, it has to be mentioned that control kidneys and urines already contained high basal levels of Sa and So compared to the controls of single FB_1 administration, which was paralleled by marked alterations in urinary parameters such as increased protein levels and enhanced number of leukocytes and erythrocytes. These are normally not present or very low in urine of healthy control animals. However, overall serum parameters (see section 5.1.2.1, Table 33) did not markedly differ from the controls of the 1-day study. Only a slight increase in the basal levels of urea, creatinine and protein was found in serum after 6-day treatment. In the liver, no increases in basal levels of sphingoid bases were observed, assuming a kidney-specific lesion in controls of the 6-day study. The increased occurrence of leukocytes and erythrocytes in control urines may be related to inflammation or injury to the urinary tract, which could be due to repeated *i.p.* application (Gaines Das and North, 2007). As a result, sphingolipid metabolism may be altered, since inflammatory cytokines like TNF-alpha are able to activate sphingomyelinases and ceramidases/SPHK1, which catalyze the enzymatic turnover of complex sphingomyelin into ceramide and So1P, which are both important mediators of inflammation (Hannun and Obeid, 2008; Nixon, 2009). Furthermore, inflammatory cytokines may enhance the activity of SPT, which is the enzyme that catalyzes the formation of the precursor sphingoid base Sa in the *de novo* synthesis of ceramide (Memon *et al.*, 1998). Although basal levels of Sa and So were increased in controls of the 6-day study, treatment with FB_1 significantly and dose-dependently elevated the ratio of Sa/So in kidney compared to controls. In addition, the alterations in the ratio of renal Sa/So were confirmed by a marked increase in urinary Sa/So after exposure to 0.75 mg/kg bw/d FB_1 for 6 days.

The dose-dependent increase in urinary Sa/So in this study was also related to the observed histopathological lesions in the renal tubular epithelium after FB_1 treatment. Importantly, the ratio of Sa/So in kidney and urine under conditions of carcinogenicity has also been closely correlated with increased tubular cell apoptosis and

regenerative proliferation and, more importantly, the induction of renal tubular adenomas and carcinomas (NTP, 2001). In the NTP carcinogenicity study, levels of urinary Sa/So reached 5.3, 14.5 and 26.4 after 26 weeks of exposure to 15, 50 and 150 ppm FB_1 *via* feed (NTP, 2001). Unfortunately, no data regarding the Sa/So ratios in urines of male F344N at the end of the 2-year treatment period were provided. In this regard, our study showed that the ratio of Sa/So in urine of male Sprague Dawley rats was elevated up to 16.9 after 6-day *i.p*. administration of 0.75 mg/kg bw/d FB_1. Thus, our urinary Sa/So ratios from high dose treated animals were similar to those reported by the NTP after 26-week treatment with 50 and 150 ppm, which are the tumor-inducing doses after chronic exposure to FB_1 (NTP, 2001). Our study showed that Sa/So ratio in kidney reached a maximum of 6.0 after 6-day treatment with 0.75 mg/kg bw/d FB_1, which is between the ratios for Sa/So in the kidney of rats treated with 15 ppm (Sa/So: 3.2) and 50 ppm (Sa/So: 15.7) FB_1 in the NTP study (NTP, 2001). Hence, our short-term treatment with FB_1 altered the balance of sphingolipids almost in the same dimension than chronic FB_1 exposure reported by the NTP.

Besides alterations in the sphingoid bases Sa and So in urine and kidney, their respective phosphorylated metabolites Sa1P and So1P were rapidly increased in response to FB_1 – an event indicating enhanced renal SPHK activity. Since changes in Sa levels were more prevalent compared to So, levels of Sa1P in kidney were more increased compared to those of So1P, which is a finding also reported in previous studies (Riley and Voss, 2006; Burns *et al.*, 2008). In line with our results, Riley *et al.* showed that short-term exposure of male Sprague Dawley rats to FB_1 resulted in early alterations in sphingolipid metabolism (Riley and Voss, 2006). These comprised enhanced formation of Sa and Sa1P after exposure to 57.2 ppm FB_1 in the feed - a dietary concentration of FB_1, which also caused tumors in rats (NTP, 2001). Consistent with our study, Riley *et al*. reported a similar extent of alterations in sphingoid bases after 5 days exposure to 57.2 ppm FB_1, where levels of Sa and So, as well as Sa1P and So1P reached a maximum in the kidneys of male Sprague Dawley rats (Riley and Voss, 2006). Interestingly, the authors concluded that these alterations closely correlated with the renal uptake of FB_1 and the associated degree in histopathological lesions in the tubular epithelial cells of the OSOM (Riley and Voss, 2006). Assuming that 57.2 ppm FB_1 in the feed corresponded to an approximate oral intake of 6.5 mg/kg bw/d FB_1 (mean body weight: 177 g; feed consumption: 20 g), an estimated intake of 0.23 mg/kg bw/d (bioavailability: 3.5%) is

calculated. This intake is nearly similar to our low dose (0.25 mg/kg bw/d FB_1). Thus, our study demonstrated that *i.p*. administration of FB_1 was sufficient to induce comparable effects on sphingolipid metabolism in kidney as observed in oral short-term studies with carcinogenic doses of FB_1 (Riley and Voss, 2006).

During our study, FB_1 markedly increased the levels of pro-apoptotic Sa in kidney, which correlated with a higher number of apoptotic cells in the tubular epithelium. This was paralleled by an increase in pro-apoptotic sphingosine after single exposure to FB_1. Although Sa1P and So1P were also significantly increased after single exposure, the pro-apoptotic intermediates Sa and So markedly exceeded the levels of their respective phosphorylated, anti-apoptotic metabolites. Since Sa and So are known to initiate apoptosis (see section 2.4.4.2) their early prevalence in FB_1-exposed kidney may play a pivotal role in the shift towards pro-apoptotic signaling and subsequent degeneration of renal tubular epithelial cells. In particular, sustained accumulation of sphinganine, as observed after 6-day exposure to FB_1, was reflected by progressive renal tubular apoptosis, which is consistent with the strong correlation between the elevation of Sa and the respective pathology scores in treated animals by the study of Riley *et al.* (Riley and Voss, 2006). In contrast to our single dose study, the enhanced levels of Sa in kidney after 6 days were counterbalanced by increased metabolic conversion into Sa1P, which then together with So1P exceeded the levels of the non-phosphorylated sphingoid bases. The prevalence of anti-apoptotic/proliferative Sa1P and So1P, most likely due to a high local enzymatic activity of SPHK1 in the kidney, were strongly correlated with an increased regenerative cell proliferation in renal cortex and OSOM after 6-day exposure to FB_1 (see section 5.1.4.2 and 5.1.4.3).

In rat and mice, enzymatic activity of renal SPHK is much higher compared to other tissues such as liver (Gijsbers *et al.*, 2001; Fukuda *et al.*, 2003). Consistent with this, a strong basal expression of SPHK1 in kidney compared to liver of male Sprague Dawley rats was found in our study (see section 5.1.8). Recently, Facchinetti *et al.* revealed that SPHK1 expression and activity are specifically distributed within the rat kidney with a decreasing gradient of expression from cortex to papilla (Facchinetti *et al.*, 2008). Immunohistochemical localization in the renal tissue showed that SPHK1 was predominantly found in the epithelial cells of the proximal convoluted tubules (Facchinetti *et al.*, 2008). Interestingly, high expression of SPHK1 in the specific kidney zones did not necessarily correlate with high overall enzyme activity, since

SPHK1 activity was found to be more enhanced in medulla than in cortex. Interestingly, the areas of high SPHK1 activity demonstrated by Facchinetti *et al.* (Facchinetti *et al.*, 2008), were in compliance with the FB_1-induced sites of regenerative proliferation in tubular epithelial cells of cortex and OSOM as described in our and the carcinogenicity study of the NTP (NTP, 2001), revealing a pivotal role of SPHK1 activity in organ-specific tumor formation in kidney.

6.1.3 Summary and conclusions

As shown by the results of the present study, FB_1 caused a time- and dose-dependent manifestation of tubular damage in the cortex and OSOM of the kidney, which was followed by the induction of proliferation in the affected areas. Concurrently, FB_1-induced disruption of sphingolipid metabolism caused a marked elevation of pro-apoptotic Sa, which paralleled the time- and dose-dependent increase in renal tubular apoptosis. Over the time of exposure, increased metabolic conversion of the accumulated Sa to phosphorylated Sa1P, a second messenger with anti-apoptotic and proliferative properties, was demonstrated in kidney. This finding was compliant with the increased regenerative cell proliferation in areas of high SPHK1 expression and activity. It thus seems obvious, that early disturbance in sphingolipid metabolism may be crucial to initiate imbalances in the rates of cell death and proliferation, which may consequently lead to conditions favoring the formation of renal tumors as previously postulated by others authors (Howard *et al.*, 2001b; Riley *et al.*, 2001). In addition to the effects on sphingoid bases and their phosphorylated metabolites, this study, for the first time, demonstrated reduced levels of specific ceramides in rat kidney after FB_1 exposure. In particular, C16-Cer, which is a widespread constituent of membrane-bound complex sphingolipids involved in cell to substratum adhesion, was time-and dose-dependently decreased after treatment with FB_1. Besides its role as component of the cell membrane, C16-Cer functions as signaling molecule for the initiation of apoptosis in response to various stress stimuli. Over the time, a reduction in pro-apoptotic C16-Cer together with markedly increased levels of anti-apoptotic and proliferation-promoting sphingoid base 1-phopshates may thus favor resistance to stress-induced apoptosis and facilitate the survival of abnormal cells with potential to initiate tumor formation.

6.2 FB_1 induces early gene expression changes in rat kidney consistent to sphingoid base 1-phosphate signaling

FB_1 has the ability to induce renal cell death and subsequent compensatory cell proliferation, but the mechanisms involved in the invasive growth characteristics and the exceptionally high metastatic potential of FB_1-induced renal tumors are still not elucidated. We thus hypothesized that FB_1-mediated tumor formation is not only a consequence of altered cell death and proliferation, but also involves disruption of specific cell signaling pathways, which govern cell growth, motility, vascular barrier integrity and angiogenesis. As sphingoid base 1-phosphates (So1P and Sa1P) are known to induce a range of these pathways, a specific aim of this study was to identify genes in FB_1-treated kidney that may correspond to transcriptional alterations mediated by So1P and Sa1P signaling.

6.2.1 Alterations in proto-oncogenic transcription factors, cell cycle genes and growth factors may lead to uncontrolled cell growth

In order to maintain tissue homeostasis, cells tightly control the formation and release of growth-promoting signals, which govern the entry into and progression through the cell cycle (Hanahan and Weinberg, 2011). However, both deregulation of cell proliferation characterized by sustained growth signals and concurrent suppression of cell death provide the most common and thus fundamental hallmarks of cancer formation and progression (Evan and Vousden, 2001; Hanahan and Weinberg, 2011). Cancer cells may act in different modes to acquire uncontrolled growth characteristics. These may include autocrine or paracrine stimulation of growth factor secretion, deregulation of respective receptor expression to attain hyperresponsiveness to normally limited growth factor signals, as well as constitutive activation of downstream signaling pathways independent of ligand-stimulated receptor activation (Hanahan and Weinberg, 2011). Cancer cells must also evade and overcome multiple mechanisms that negatively regulate cell proliferation, including the activation of tumor suppressor genes (*e.g. p53* and retinoblastoma gene), inhibition of cell-to-cell contact, initiation of pro-apoptotic signals and cellular senescence (Hanahan and Weinberg, 2011). Consequently, complex biological

events are involved in enabling tumor cells to survive, proliferate and eventually disseminate (Hanahan and Weinberg, 2011).

In the present study, FB_1 treatment resulted in a significant increase in the mRNA expression of proto-oncogenic transcription factors *Myc*, *Fos* and *Jun* (see chapter 5.1.6, Table 37) that are immediate early genes (IEGs) known to be rapidly and transiently activated in response to various stimuli, *e.g.* growth factors, cytokines and pharmacological agonists (Hazzalin and Mahadevan, 2002). Through intracellular signaling pathways, *e.g.* the MAPK cascade, IEGs are directly induced and regulate the transcription of multiple target genes without the need of protein synthesis (Hazzalin and Mahadevan, 2002; Sng *et al.*, 2004).

Role of Myc, survival factors and cell cycle-regulating genes in tumorigenesis

The transcription factor *Myc* is a pleiotropic gene that is estimated to regulate the expression of up to 15% of the whole genome (Zeller *et al.*, 2006), thereby influencing a variety of physiological and pathological processes, including *e.g.* cell proliferation, apoptosis, differentiation and cellular transformation (Pelengaris *et al.*, 2002). Whereas transient mitogen-activated expression of *Myc* is important for cell proliferation in normal cells, upregulation of *Myc* mRNA and protein expression results in rapid transition from G1 to S phase, thereby overriding cell-cycle check points and increasing cell proliferation (Pelengaris *et al.*, 2002). Thus, uncontrolled expression of *Myc* mRNA is frequently related to neoplastic lesions (Evan and Vousden, 2001), as reflected by the high incidence (70%) of deregulated *Myc* in various cancers (Nilsson and Cleveland, 2003). However, the MYC protein bears also controversial roles in cell signaling, since it is also able to induce apoptosis in normal cells, which serves as an innate “fail-safe mechanism” to avoid unintentional MYC-induced transformation and tumorigenesis (Nilsson and Cleveland, 2003; Adhikary and Eilers, 2005). In this regard, MYC can trigger apoptosis *via* multiple pathways, including the activation of pro-apoptotic proteins such as BAX or the induction of ARF/p53 tumor suppressor signaling (Pelengaris *et al.*, 2002; Adhikary and Eilers, 2005). Nevertheless, the increased expression of pro-survival genes/proteins such as BCL2 and BCL-XL has been shown to determine cell fate by inhibiting MYC-induced apoptosis *via* inactivation of the pro-apoptotic protein BAX, thereby promoting the oncogenic activity of MYC (Evan and Vousden, 2001; Pelengaris *et al.*, 2002; Nilsson

and Cleveland, 2003; Adhikary and Eilers, 2005). Besides the pro-apoptotic members of the BCL-familiy, other survival factors such as AKT that are mediated by RAS signaling, may also be implicated in the antagonism of MYC-induced apoptosis (Pelengaris *et al.*, 2002; Adhikary and Eilers, 2005). Considering these apparently contradictory functions, the cellular outcome of deregulated MYC expression primarily seems to depend on the availability of survival factors (Pelengaris *et al.*, 2002).

The results of our study indicate that MYC might at first be involved in the transduction of apoptotic signals through ARF/p53 signaling, since gene expression of *Cdkn2a (p16)*, which also encodes the ARF protein, was increased after single exposure to both FB_1 doses (see chapter 5.1.6, Table 37). This is in line with the innate "fail-safe mechanism" to avoid unintentional MYC-induced transformation and tumorigenesis as reviewed in the literature (Nilsson and Cleveland, 2003; Adhikary and Eilers, 2005) The ARF protein serves to stabilize the function of p53 protein by blocking the p53 inhibitor MDM2 (transformed mouse 3T3 cell double minute 2) (Nilsson and Cleveland, 2003; Adhikary and Eilers, 2005). Interestingly, increased expression of the apoptosis-inhibiting genes *Bcl2*, *Bcl-Xl*, *Cflar* and *survivin* (*Birc5*) has been observed after repeated but not single exposure to FB_1 (see chapter 5.1.6, Table 37), whereas the expression of the cell-cycle-and apoptosis-regulating gene *Cdkn2a (p16)* declined at the high dose of FB_1 (0.75 mg/kg bw/d). This suggests that in the time course of FB_1 treatment pro-survival pathways were activated to counterbalance the prominent apoptotic stress signals probably mediated by ARF/p53 signaling, such as the tumor necrosis factor receptors (*Tnfrsf10b* and *Tnfrsf1a*) and the tumor suppressor genes (*Brca1* and *Pten*) (see chapter 5.1.6, Table 37). As described by Adhikary *et al.*, overexpression of *Bcl2* and *Bcl-Xl* gene and protein exerts a remarkable effect on the oncogenic activity of MYC, since both molecules were shown to promote MYC-induced tumorigenesis by suppressing its pro-apoptotic function *via* inhibition of MYC-induced signaling molecules like BAX (Adhikary and Eilers, 2005).

Cflar (Flip, FADD-like IL-1β converting enzyme (FLICE/caspase-8)-like inhibitory protein) encodes a protein that directly interacts with the death-inducing signaling complex (DISC) and prevents activation of caspase-8 protein and subsequent execution of apoptosis in the death-receptor pathway (Igney and Krammer, 2002).

The *Cflar* gene is a further apoptosis-suppressing survival factor initiated in response to prolonged FB_1 treatment in our study (see chapter 5.1.6, Table 37). As also reported for other survival-associated genes (*e.g. Bcl2* and *Bcl-Xl*), expression of *Cflar* can be induced by the NFκB transcription factors (Karin and Lin, 2002). In this regard, our study provides evidence that NFκB signaling might be involved in the increased expression of pro-survival factors after treatment with high doses of FB_1 (6 days) (see chapter 5.1.6, Table 37). *Nfκb1* gene expression paralleled the increased expression of the anti-apoptotic genes *Cflar*, *Bcl2* and *Bcl-Xl*. In contrast, gene expression of *Nfκbia* (*IκBα*), which inhibits NFκB activity, increased earlier in response to FB_1 treatment than *Nfκb1* gene expression (see chapter 5.1.6, Table 37). This might be an indicator of regulatory mechanisms, which antagonize an increased NFκB activity on the protein level that might result from elevated IκB kinase (IKK)-mediated NFκBIA protein degradation (Nakanishi and Toi, 2005). Another possibility is that increased *Nfκbia* gene expression may be linked to the inhibition of pro-apoptotic functions of NFκB, since this transcription factor is also involved in apoptosis and thus has ambivalent functions in cell signaling (Karin and Lin, 2002). A pro-apoptotic function of NFκB has also been described in the porcine kidney epithelial cell line LLC-PK_1 after short treatment with FB_1 (Gopee and Sharma, 2004). In this study, FB_1 induced the activation of both PKC-alpha and NFκB, which resulted in TNF-alpha expression and subsequent activation of caspase-3 (Gopee and Sharma, 2004).

Furthermore, our data demonstrated that increases in anti-apoptotic genes were accompanied by a deregulation in cell cycle genes, which was observed by increased expression of *Ccne1* (see chapter 5.1.6, Table 37), a transcriptional and functional target of MYC (Roderick and Cook, 2008) that facilitates the entry into S phase by binding and activating its catalytic subunit CDK2 (Moroy and Geisen, 2004) (Figure 46).

To provide full activity of the Cyclin E-CDK2 protein complex, CDC25A phosphatase activity is important (Steiner *et al.*, 1995), because it facilitates dephosphorylation and activation of Cyclin E-CDK2 complexes (Fukasawa, 2007) (Figure 46). However, the regulation of CDC25A activity is tightly controlled *via* CHEK2-mediated phosphorylation and ubiquitin-mediated degradation, which leads to inactivation of Cyclin E-CDK2 complexes, check point control and G1/S cycle arrest in response to

DNA damage and oncogenic stress (Bartek *et al.*, 2001; Fukasawa, 2007) (Figure 46).

Stress-induced activation of CHEK2 is mediated by the tumor suppressor ATM (Bartek *et al.*, 2001) (Figure 46), and both *Chek2* and *Atm* gene were shown to be significantly enhanced after single but not repeated exposure to FB_1 in the present study (see chapter 5.1.6, Table 37). Accordingly, *Cdc25a* gene expression was significantly upregulated after 6-day exposure to the high dose (0.75 mg/kg bw/d) FB_1 (see chapter 5.1.6, Table 37), suggesting an impaired activation of checkpoint pathways with continuing FB_1 treatment (Figure 46). Indeed, *Cdc25a* mRNA and protein levels are frequently overexpressed in cancer and seem to correlate with a continued overactivation of CDC25A-targeted cyclin-CDK complexes. This over-activation has been shown to accelerate the entry of cells in the S phase by circumventing important checkpoint barriers (Boutros *et al.*, 2007) (Figure 46).

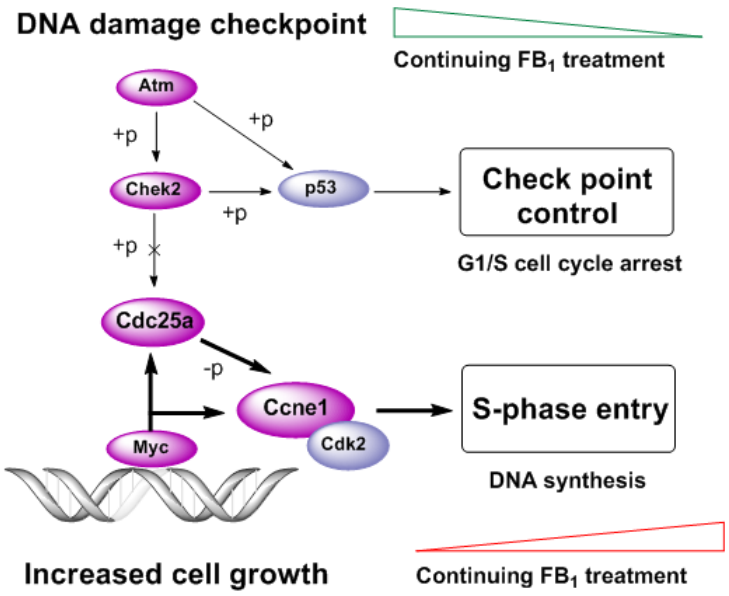

Figure 46: Pathways involved in c-Myc-induced cell cycle progression. Genes analyzed after FB_1 treatment in kidneys of male Sprague Dawley rats were integrated in c-Myc-mediated signaling pathways. Colors indicate: genes **upregulated** in response to FB_1 (**pink**), genes **not regulated** by FB_1 (**light blue**). **+p** = phosphorylation, **-p** = dephosphorylation.

Ultimately, abrogation of checkpoint pathways might facilitate DNA-damaged cells to evade cell cycle arrest and associated DNA repair or apoptosis, which might contribute to tumorigenesis by increasing genomic instability (Boutros *et al.*, 2007; Ray and Kiyokawa, 2008). *Cdc25a* mRNA expression has been reported to be a

direct transcriptional target of MYC oncoprotein (Galaktionov *et al.*, 1996; Boutros *et al.*, 2007). This finding correlated with the parallel increases in *Cdc25a* and *Myc* gene expression after 6-day treatment as shown in chapter 5.1.6 (Table 37). Moreover, increased mRNA expression of *Cdc25a* and *Myc* was also observed in various cancers and correlated with poor prognosis (Aref *et al.*, 2003). Interestingly, pharmacological inhibition of CDC25 phosphatases in human renal epithelial cancer lines was associated with downregulation of CDC25 phosphatases, and resulted in inhibition of cell proliferation and induction of apoptosis by downregulation of anti-apoptotic BCL2 and BCL-XL and upregulation of pro-apoptotic BAX protein (Mizuno *et al.*, 2005). Thus, parallel overexpression of the proto-oncogenes *Cdc25a*, *Bcl2* and *Bcl-Xl* might enhance the pool of survival factors that might counteract (oncogene-induced) apoptotic signaling. Enhanced expression of these survival factors together with oncogenic *Myc* may increase cell proliferation and favor tumor formation in FB_1-exposed kidneys.

AP-1 and its impact on cell proliferation and survival

In compliance with the pleiotropic functions of the transcription factor MYC, the proto-oncoproteins JUN and FOS, which participate in the formation of the transcription factor AP-1, also regulate a variety of cellular processes, including cell proliferation, apoptosis, survival, differentiation and migration (Shaulian, 2010). However, the transcriptional targets mediating these biological effects are yet not fully elucidated (Shaulian and Karin, 2002). Besides their important role in physiological processes, JUN and FOS are also implicated in pathophysiological processes, such as tumor formation, angiogenesis and invasion (Eferl and Wagner, 2003). Regarding cell proliferation, JUN seems to be the most important component of the AP-1 complex, since it may induce the transcription of cell cycle genes that facilitate cell cycle progression (*e.g. Ccnd1*), whereas genes that negatively regulate the cell cycle (*e.g. p53*, *p21* and *p16*) are repressed (Shaulian and Karin, 2001; Eferl and Wagner, 2003). Moreover, JUN has been demonstrated to be required for cellular transformation and malignancy of RAS (Johnson *et al.*, 1996; Shaulian and Karin, 2002). In contrast to its pro-oncogenic function, AP-1 has also been implicated in both apoptotic and proliferative signaling, which seems to be due to cell-type specific transcription of either pro- or anti-apoptotic genes, thus suggesting ambivalent functions of AP-1 in tumorigenesis (Eferl and Wagner, 2003). However, AP-1

primarily is a growth and survival promoter in many cancers, since JUN-containing AP-1 complexes have been shown to induce the expression of pro-survival factors like BCL-XL (Jochum *et al.*, 2001; Jazirehi *et al.*, 2004; Takeuchi *et al.*, 2006), which facilitate survival of tumor cells.

The results of our study demonstrate that genes encoding components of AP-1, including *Fos* and *Jun* were significantly upregulated – even in response to a single dose of FB_1 (see chapter 5.1.6, Table 37), which is consistent with their rapid induction in response to various external stress stimuli or growth factors (Hazzalin and Mahadevan, 2002). After 6-day treatment, *Jun* was more abundant than *Fos*, which was predominantly observed in animals treated with the highest dose of FB_1. These findings are consistent with the literature, reporting that the composition of AP-1 complexes changes in the course of cell cycle progression (Mechta-Grigoriou *et al.*, 2001). This is reflected by the fact that JUN-containing AP-1 complexes mainly contribute to AP-1 DNA-binding activity in highly proliferative tumors, whereas other components such as JUND and JUNB are rather implicated in the anti-proliferative function of AP-1 (Eferl and Wagner, 2003; Lopez-Bergami *et al.*, 2010).

As mentioned before, JUN-containing AP-1 complexes may also enhance tumor survival and apoptosis-resistance by the induction of BCL-XL expression (Jochum *et al.*, 2001; Jazirehi *et al.*, 2004; Takeuchi *et al.*, 2006). This is in line with the results of our study, showing increased *Bcl-Xl* expression together with enhanced *Jun* expression following 6-day exposure to the high dose of FB_1 (see chapter 5.1.6, Table 37). However, the increase in anti-apoptotic *Bcl-Xl* may also be a result of diverse transcriptional inputs resulting from different signaling pathways, since transcriptions factors like NFκB and STAT (Signal transducers and activators of transcription) also have DNA-binding sites for the BCl-XL encoding gene *Bcl-X* (Sevilla *et al.*, 2001). Thus, it is conceivable, that multiple pathways and transcription factors may be involved and cooperate in the expression of anti-apoptotic *Bcl-Xl*.

Activation of RAS/MAPK signaling pathways and its role in FB_1-induced tumor formation

RAS/MAPK signaling is important in cell proliferation and survival. Mutations or aberrant expression/activation of its components or upstream effectors (*e.g.* growth factors/RTKs, GPCRs and integrins) have been frequently found in a variety of

cancers (Radeff-Huang *et al.*, 2004; Sebolt-Leopold and Herrera, 2004; McCubrey *et al.*, 2007). Constitutive activation of the RAS/MAPK cascade has also been demonstrated in renal cell carcinoma (RCC), which included a significant activation of RAF1, MEK and MAPKs that was more frequent in high grade compared to low grade tumors. Interestingly, 50% of the renal tumors show increased protein expression of MEK (Oka *et al.*, 1995).

In the present study, genes encoding components of the RAS/MAPK (RAS/RAF/MEK) cascade, *e.g. Map2k1* (*Mek1*) and *Raf1* (*Raf*) were upregulated in response to prolonged treatment with FB_1 (see chapter 5.1.6, Table 37). Furthermore, FB_1 treatment resulted in increased mRNA expression of growth factors receptors (*e.g. Egfr* and *Hgfr (Met)*) (see chapter 5.1.6, Table 37) that are known to activate MAPK signaling, suggesting an important role of this pathway in the tumorigenesis of FB_1. In view of the chronic exposure to FB_1, it is possible that sustained RAS/MAPK signaling pathways may have a pivotal role in FB_1-induced renal carcinogenesis and tumor malignancy.

Correlation of FB_1-mediated gene expression changes involved in cell proliferation and survival with the biological action of sphingoid base 1-phosphates

Strong evidence is provided that the sustained cell proliferation in response to prolonged FB_1 treatment may be a result of FB_1-mediated disruption of sphingolipid metabolism and the related imbalances in the levels of pro-apoptotic (Sa and So) and anti-apoptotic lipid mediators (Sa1P and So1P) (Kim *et al.*, 2001; Merrill *et al.*, 2001; Riley *et al.*, 2001). As demonstrated in our study, single administration of FB_1 was sufficient to mediate accumulation of pro-apoptotic sphingoid bases accompanied by formation of anti-apoptotic sphingoid base 1-phosphates. Moreover, levels of phosphorylated metabolites exceeded those of the non-phosphorylated precursor after repeated exposure to FB_1, which paralleled the increased regenerative proliferation in the kidney. Thus, these proliferative signaling lipids may largely contribute to uncontrolled cell growth and resistance to apoptosis after chronic exposure to FB_1. Indeed, a variety of studies reported that So1P and Sa1P may both play important roles in cell proliferation and survival, with Sa1P being equally or somewhat less potent than So1P (Wang *et al.*, 1999; Kimura *et al.*, 2000; Tamama *et al.*, 2001; Katsuma *et al.*, 2002; Katsuma *et al.*, 2003; Shi *et al.*, 2007). In particular,

So1P has been widely studied regarding its effects on cell growth, proliferation and survival. These biological processes are often deregulated in the malignant behavior of cancer cells. The increased formation of So1P *via* elevated activity of SPHK has been frequently linked to carcinogenesis (Kohno *et al.*, 2006; Milstien and Spiegel, 2006; Oskouian and Saba, 2007; Shida *et al.*, 2008; Leong and Saba, 2010; Oskouian and Saba, 2010).

Mechanistic studies revealed that So1P as well as Sa1P may exert many of their biological effects *via* extracellular binding to their specific GPCRs (Wang *et al.*, 1999; Kimura *et al.*, 2000; Katsuma *et al.*, 2003). However, dependent on the cell-type specific S1P receptor (S1PR) repertoire, different signaling pathways may be initiated. This of course suggests a complex signaling network of S1P receptors (Taha *et al.*, 2004; Huang *et al.*, 2011). It is well established that $S1P_1$ exclusively couples to G_i-proteins, thereby activating RAS, MAPK, PI3K, AKT, and phospholipase C (PLC) pathways, whereas $S1P_2$ and $S1P_3$ may additionally couple to $G_{12/13}$, which results in the activation of Ras homolog gene family (RHO)-dependent pathways *via* $G_{12/13}$ (Radeff-Huang *et al.*, 2004; Taha *et al.*, 2004). Our data on the expression of S1P receptors revealed that $S1P_2$ and $S1P_3$ were most abundant in kidney, whereas $S1P_1$ was rare (see section 5.1.9, Figure 35). This suggests a possible role of $S1P_2$ and $S1P_3$ in sphingoid base 1-phosphate-mediated extracellular effects involved in cell proliferation in response to FB_1.

A widely studied cell line for So1P-mediated effects on tumorigenesis and malignant progression are glioma cells (Bryan *et al.*, 2008; Paugh *et al.*, 2008). In this cell line, So1P induced cell proliferation predominantly through the receptors $S1P_{1\text{-}3}$ (Figure 47), whereby $S1P_1$ was mainly contributing to these effect (Young and Van Brocklyn, 2007). The authors observed that $S1P_{1\text{-}3}$-induced glioma cell proliferation correlated with activation of ERK, which is a MAPK downstream of RAS/MEK signaling (Young and Van Brocklyn, 2007) (Figure 47). Earlier studies in glioma cells showed that ERK signaling seemed to be activated by G_i-proteins and PI3K signaling, which is in line with the receptor-specific effects of $S1P_{1\text{-}3}$ mentioned above (Van Brocklyn *et al.*, 2002). Interestingly, in rat mesangial cells, both So1P and Sa1P have been demonstrated to potently induce cell proliferation *via* $S1P_2$ and $S1P_3$, which was dependent on the induction of G_i-protein and ERK signaling pathways (Katsuma *et al.*, 2002) (Figure 47). Accordingly, our study showed that repeated FB_1 treatment for

6 days led to slightly increased gene expression of components involved in RAS/MAPK signaling (*i.e. Raf1* and *Mek1*) and PI3K signaling (*i.e. Akt*), which strongly correlated with the elevated formation of the sphingoid base 1-phosphates Sa1P and So1P, the high basal expression of $S1P_2$ and $S1P_3$ and the increase in cell proliferation in kidney (Figure 47). In agreement with our study, activation of MEK1 was also found in the So1P-treated rat embryonic fibroblast cell line Rat-2, resulting in activation of RAS/RAF/MEK/ERK pathways that were dependent on So1P-mediated activation of G_i-protein-coupled receptors and subsequent transactivation of EGFR (Kim *et al.*, 2000) (Figure 47).

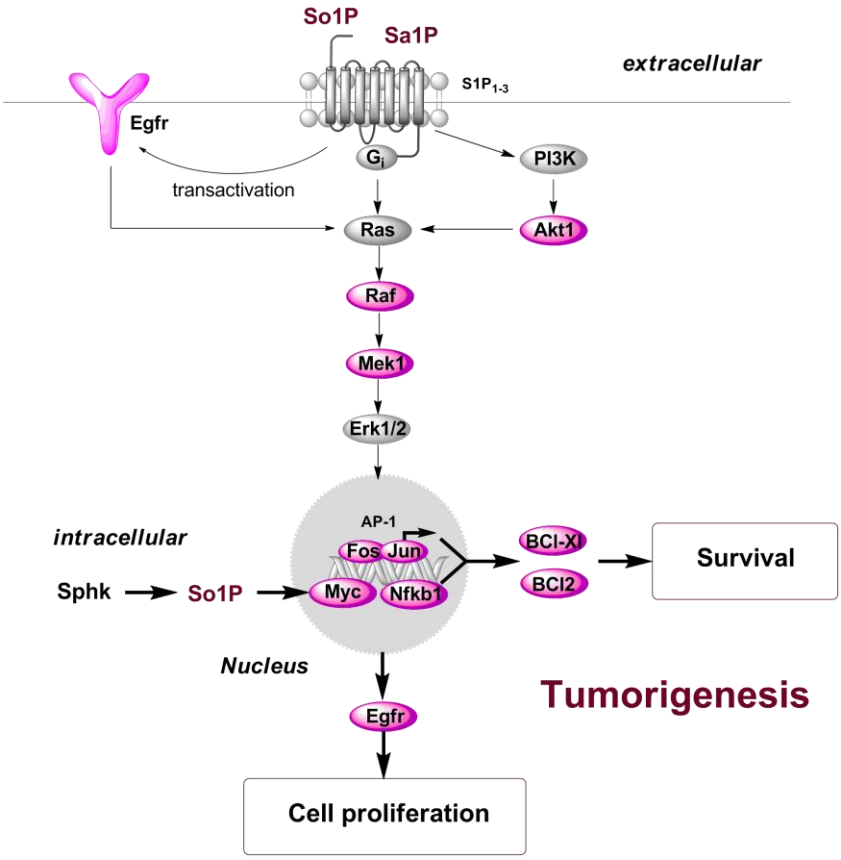

Figure 47: Extra- and intracellular sphingoid base 1-phosphate signaling pathways mediating cell proliferation and survival. Genes analyzed after FB_1 treatment in kidneys of male Sprague Dawley rats were integrated in sphingoid base 1-phosphate-mediated signaling pathways. Colors indicate: genes **upregulated** in response to FB_1 (**pink**), genes **not regulated** by FB_1 (**light blue**), genes involved in pathway but not analyzed in response to FB_1 (**grey**).

The crosstalk with EGFR seems to play a pivotal role in So1P signaling, since So1P has been demonstrated to enhance cell proliferation in rat vascular smooth muscle

cells (VSMC) by increasing *Egfr* gene and protein expression *via* G_i-protein-dependent induction of MEK1/2, ERK1/2 and subsequent increase in the expression of transcription factors like *Jun* and *Fos* (Hsieh *et al.*, 2008) (Figure 47).
This is in agreement with results of our study, which showed increased gene expression of *Jun*, *Fos*, *Mek1* and *Egfr* after prolonged FB_1 treatment (see chapter 5.1.6, Table 37) that correlated with the increased formation of So1P and Sa1P (see chapter 5.1.5, Table 35) and the increase in renal cell proliferation (see chapter 5.1.4, Figure 21) (Figure 47). Furthermore, Hsieh *et al.* (Hsieh *et al.*, 2008) reported that PI3K/AKT signaling was involved in G_i-protein-dependent S1PR signaling, and independently regulated S1P-induced EGFR *via* NFκB expression (Figure 47). Accordingly, our gene expression study showed that prolonged FB_1 treatment resulted in increased expression of *Nfκb1* and *Akt* (see chapter 5.1.6, Table 37), although these effects were less pronounced compared to the alterations in components of the MEK/ERK/AP-1 pathway (Figure 47). However, in view of chronic FB_1 exposure, these pathways may cooperate in the activation of several transcription factors that regulate *Egfr* expression. Thus, the pool of receptors available for growth factor signaling and the associated increase in cell proliferation may be enlarged. Besides upregulation of *Egfr* gene and protein expression, So1P/S1PR signaling has also been shown to transactivate RTKs like EGFR and VEGFR even in the absence of added growth factors (Spiegel and Milstien, 2003) (Figure 47). It is well known that overexpression of EGFR and activation of its pathway results in cell proliferation, migration, invasion and angiogenesis (Adamson and Wiley, 1997; Dancey and Freidlin, 2003). Since high levels of *Egfr* gene have been detected in various human cancers, including kidney tumors (Yoshida *et al.*, 1994), it is thus conceivable that FB_1-induced increase in So1P and also Sa1P may result in continuing overexpression/overactivation of *Egfr*, thereby mediating uncontrolled cell proliferation and subsequent tumorigenesis (Figure 47).

Regarding its impact on cell survival and tumorigenesis, different studies revealed that So1P increases the expression of anti-apoptotic molecules such as BCL2 and BCL-XL (Figure 47), in particular in cells deficient in sphingosine 1-phosphate lyase (SPL) activity (Colie *et al.*, 2009; Colie *et al.*, 2010). This enzyme is important in sphingolipid catabolism and mediates the irreversible degradation of anti-apoptotic So1P and Sa1P, resulting in the formation of ethanolamine 1-phosphate and the

corresponding fatty aldehyde (see section 2.4.4.1, Figure 2) (Hannun and Obeid, 2008). Thus, it is important to maintain cell homeostasis by clearing the formation of undesired bioactive signaling molecules. Interestingly, a previous study by Kim *et al.* (Kim *et al.*, 2007) demonstrated that *i.p*. treatment with FB_1 (10 mg/kg/day for 5 days) in mice modulated sphingolipid-metabolizing and catabolizing enzymes in liver by increasing SPHK1 and decreasing SPL mRNA expression, which led to the accumulation of sphingoid base 1-phosphates. Furthermore, the intracellular formation of So1P by glucocorticoids and its transport to the extracellular space has been shown to increase *Bcl-Xl* gene and protein expression *via* $S1P_3$-mediated AKT signaling, thereby protecting human fibroblasts from apoptosis (Nieuwenhuis *et al.*, 2010) (Figure 47). A direct interaction between So1P and upregulation of BCL2, another important anti-apoptotic protein, has also been demonstrated in human fibroblasts (Sauer *et al.*, 2005). In compliance with these findings, our study showed that *Bcl2* and *Bcl-Xl* were increased after repeated administration of FB_1 (see chapter 5.1.6, Table 37), which again correlated with increased formation of sphingoid base 1-phophates and elevated rates of cell proliferation. In addition, a study in rat mesangial cells demonstrated that both So1P and Sa1P were able to enhance cell survival by inhibiting apoptosis (Katsuma *et al.*, 2002). Under conditions of carcinogenesis, it is thus likely that the FB_1-induced accumulation of Sa1P and So1P and increased expression of anti-apoptotic genes may promote cell survival, resistance to apoptosis, and tumor formation.

Besides its role in activating GPCR-mediated signaling pathways, So1P also mediates receptor-independent intracellular signaling, *e.g.* calcium homeostasis, cell growth, and protection from apoptosis (Spiegel and Milstien, 2003; Huang *et al.*, 2011). Accordingly, Katsuma *et al.* showed that Sa1P also seems to mediate its effects on cell proliferation not exclusively *via* S1PR-depedent G_i-protein signaling, but also *via* mechanisms that might involve other GPCR signaling pathways (*e.g. via* G_q and $G_{12/13}$) or even intracellular signaling (Katsuma *et al.*, 2002). Generally, little is known about intracellular signaling pathways mediated by sphingoid base 1-phosphates (Spiegel and Milstien, 2003). However, in $APC^{min/+}$ mice an intracellular signaling mechanism of So1P was proposed *via* increased SPHK1 expression and activity, resulting in increased expression of the proto-oncogene *Myc* and elevated intestinal adenoma cell proliferation (Kohno *et al.*, 2006) (Figure 47). In contrast, deletion of SPHK1 but not $S1P_{1-3}$ resulted in attenuation of these effects, suggesting a

receptor-independent, intracellular mechanism of So1P that mediates cell proliferation and *Myc* induction (Kohno *et al.*, 2006). Thus, elevation of *Myc* gene expression and the concomitant increase in renal cell proliferation after prolonged FB_1 treatment (see section 5.1.4, Figure 21) may also be related to the intracellular action of accumulated sphingoid base 1-phosphates (Figure 47).

Recently, a further interesting intracellular target of So1P was proposed - the nuclear action of So1P on the promoter regions of genes like *Fos* and *p21* (*Cdkn1a*) *via* inhibition of histone deacetylase 1 and 2 (HDAC1/HDAC2) activities and enhanced acetylation of histone H3, resulting in upregulation of *p21* (*Cdkn1a*) and *Fos* gene expression (Hait *et al.*, 2009). Consequently, FB_1-induced mRNA expression of *Fos* and *p21* (*Cdkn1a*) as reported in this study, may - apart from S1PR-mediated extracellular effects on *Fos* expression - also be related to a nuclear and thus intracellular action of So1P. Although *p21* (*Cdkn1a*) gene and protein expression is primarily associated with inhibition of cell cycle progression by inhibiting the activity of Cyclin-CDK complexes (Besson *et al.*, 2008), there is evidence that this inhibitor is also involved in the positive regulation of the cell cycle *via* promotion of G1 phase progression by promoting the assembly and activation of Cyclin D-Cdk complexes (Sherr and Roberts, 1999; Pruitt and Der, 2001). In addition, a positive role for p21 in the promotion of oncogene-mediated tumor transformation has been established, which might be related to a loss of nuclear tumor suppressor function by phosphorylation-induced cytoplasmatic retention (Rowland and Peeper, 2006; Besson *et al.*, 2008). The cytoplasmatic p21 protein may directly interfere with pro-apoptotic signaling pathways such as JNK/stress-activated protein kinase (SAPK), p38 signaling and caspase-3 activation, resulting in the suppression of cell death (Rowland and Peeper, 2006; Besson *et al.*, 2008). Cytoplasmatic p21 also correlates with poor prognosis in breast cancer and other malignancies (Rowland and Peeper, 2006; Abukhdeir and Park, 2008; Besson *et al.*, 2008), suggesting an important role of the subcellular localization of p21 protein in mediating either tumor-suppressing or tumor-promoting functions in the cell (Rowland and Peeper, 2006; Besson *et al.*, 2008). Whether increased *p21* gene expression in response to repeated FB_1 treatment is associated with increased cytoplasmatic localization of p21 protein exerting anti-apoptotic activity remains to be elucidated.

Collectively, our results show that gene expression changes mediated by FB_1 are strongly associated with both extra- and intracellular signaling pathways of sphingoid base 1-phosphates. These involve cell proliferation, cell survival and tumorigenesis, resulting in upregulation of proto-oncogenes (*e.g. Myc*, *Jun*, *Fos*), cell cycle promoters (*e.g.* Cyclins and Cyclin-dependent kinases), growth factor receptors (*e.g. Egfr*) and anti-apoptotic molecules (*e.g. Bcl-Xl* and *Bcl2*). With regard to its epigenetic functions, So1P (and also Sa1P) may modulate gene transcription through direct interaction with HDACs, whose deregulated activities appear to correlate with aberrant epigenetic changes found in cancer (Hait *et al.*, 2009 38). A variety of gene modulations may arise from the nuclear interaction of So1P (Sa1P) with HDACs, which may also reveal previously unknown targets of So1P. Thus, epigenetic mechanisms might be important functions of sphingoid base 1-phosphates to regulate various changes in cancer-related genes as reported in this study.

6.2.2 Alterations in the plasminogen activator system correlate with sphingosine 1-phosphate-mediated signaling in tumor migration and invasion

The plasminogen activator system, consisting of uPA (PLAU), its receptor uPAR (PLAUR) and the two inhibitory glycoproteins PAI-1 and PAI-2 (SERPINE1 and SERPINB2), plays a major role in migration and invasion. These processes involve the degradation of extracellular matrix (ECM), which is dependent on the targeted activation/inhibition of ECM-digesting proteinases and their inhibitors (Bryan *et al.*, 2008). Since the balance between these constituents is tightly regulated under physiological conditions, deregulated levels have been shown to contribute to numerous disorders (Blasi and Carmeliet, 2002). In tumor cell invasion, controlled degradation of ECM by tumor-cell associated proteases plays a crucial role (Mignatti and Rifkin, 1993). Whereas pericellular proteolysis is important for the initiation of cell invasion, excessive matrix degradation inhibits cell migration and prevents invasion, presumably by destroying the matrix scaffold for tumor adhesion and migration (Krishnamurti and Alving, 1992; Hosokawa *et al.*, 1993; Albo *et al.*, 1994; Albo *et al.*, 1997). In this context, increased levels of PAI-1 have been demonstrated to cease the excessive proteolytic activity of plasmin by inhibiting the serine protease uPA, thereby enhancing tumor invasion in several malignancies (Albo *et al.*, 1997). A variety of

growth factors, cytokines, metabolic factors, hormones and environmental factors that are implicated in kidney diseases have been shown to induce PAI-1 expression (Eddy and Fogo, 2006). Accordingly, uPAR is increased in several renal disease states, including acute tubular necrosis (Zhang *et al.*, 2003). Interestingly, increased levels of PAI-1, uPA and uPAR have also been found in high stage or metastatic RCC and correlate with poor survival (Ohba *et al.*, 2005).

In the present study, gene expression analysis in kidneys of male Sprague Dawley rats showed that *PAI-1* mRNA expression was markedly enhanced after a single dose of FB_1 (chapter 5.1.4, Figure 21). At the low dose (0.25 mg/kg bw/d FB_1), gene expression of *PAI-1* was paralleled by a significant increase in *uPAR* mRNA expression. Repeated administration of high doses of FB_1 for 6 consecutive days resulted in statistically significant upregulation (2.5-fold) of *PAI-1* mRNA expression, which was accompanied by increased mRNA expression of the serine protease *uPA* and its receptor *uPAR* (both 1.5-fold compared to control). Given the importance of increases in *PAI-1*, *uPA* and *uPAR* gene and protein expression as prognostic markers for malignant tumors (Duffy and Duggan, 2004; Dass *et al.*, 2008), including their occurrence in aggressive phenotypes of RCC (Swiercz *et al.*, 1998; Ohba *et al.*, 2005; Zubac *et al.*, 2010), there is strong evidence that FB_1-induced alterations in the regulation of the plasminogen activator system may provide favorable conditions for tumor progression in kidney.

Regulation of the plasminogen activator system in cancer

Physiologically, uPAR binds to inactive uPA to activate it. Activated uPA in turn converts plasminogen to plasmin at the leading edge of cells, and hence facilitates cell migration by degradation of ECM molecules like fibrin and others through its serine protease function. The glycosylphosphatidylinositol (GPI)-anchored uPAR lacks a cytosolic domain for direct signaling function and requires transmembrane proteins like integrins, GPCRs and caveolin as mediators for intracellular signaling (Blasi and Carmeliet, 2002). Moreover, uPAR comprises a binding site for ECM molecules like vitronectin, which is also a ligand for αvβ3 integrin (Blasi and Carmeliet, 2002). This interaction is dependent on the ligation of uPA to uPAR (Waltz and Chapman, 1994), because it increases the affinity of the receptor for both vitronectin and integrins (Czekay *et al.*, 2003). The highest affinity of uPAR for

integrin binding comprises the fibronection receptors α3β1, α5β1, as well as αvβ5 and αvβ3 that bind vitronectin.

Vitronectin attaches the cell either through integrins, uPAR or an interaction of both receptors (Waltz *et al.*, 1997; Deng *et al.*, 2001). Since PAI-1 has a much higher affinity for the somatomedin B (SMB) domain of vitronectin than uPAR, it can competitively inhibit uPAR-dependent attachment of vitronectin to the cells (Deng *et al.*, 1996; Waltz *et al.*, 1997; Deng *et al.*, 2001) and cause cell detachment (Deng *et al.*, 1996) (Figure 48). The regulatory mechanisms of PAI-1 are summarized in Figure 48.

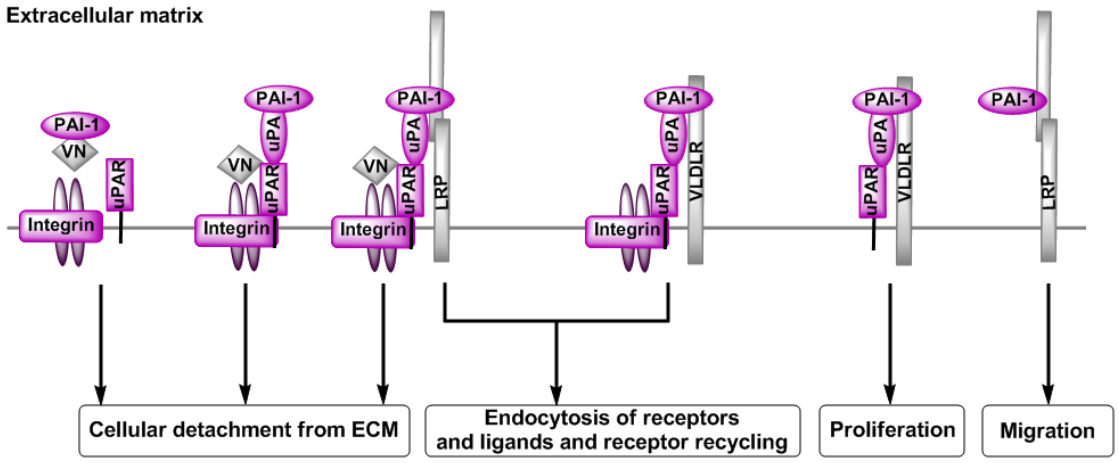

Figure 48: PAI-induced mechanisms involved in cell detachment, migration and proliferation of cancer cells (modified from (Croucher *et al.*, 2008)). Genes analyzed after FB_1 treatment in kidneys of male Sprague Dawley rats were integrated in PAI-mediated mechanisms. Colors indicate: genes upregulated in response to FB_1 (**pink**), genes involved in pathway but not analyzed in response to FB_1 (**grey**). **VN** = vitronectin; **LRP** = low-density lipoprotein-receptor-related protein; **VLDLR** = very low density lipoprotein receptors.

Czekay *et al.* also demonstrated that PAI-1 detaches cells, which are only bound to integrins (Czekay *et al.*, 2003) (Figure 48). It was shown that PAI-1 does not necessarily need vitronectin to detach cells, but it absolutely requires the binding of uPA to form uPA/uPAR/integrin complexes on the cell surface. Moreover, PAI-1 also detached cells connected *via* fibronectin and collagen typ I from the ECM through a mechanism which is similar to that depending on the uPA/uPAR complex (Czekay *et al.*, 2003). Consequently, it is assumed that PAI-1 mediates cell detachment by two separate, but related mechanisms, which depend on the nature and quality of the adhesion receptors actually engaged by the attached cell. If cells bind to vitronectin

through uPAR alone (*e.g.* U937 cells) and without engagement of integrins, PAI-1 detaches the cells by direct competition with uPAR for the SMB binding site in vitronectin (Deng *et al.*, 2001) (Figure 48). This mechanism is specific for cells which only grow on vitronectin. Alternatively, cells can also adhere to their preferred ECM proteins *via* integrins alone, with unoccupied, adjacent uPAR and low-density lipoprotein-receptor-related proteins (LRPs) available on the cell surface (Czekay *et al.*, 2003). If uPA is consequently released from the cells, it specifically binds to surface uPAR and initiates complex formation between the now occupied receptor and integrins. In the case that the ECM contains vitronectin, the uPA/uPAR complexes with integrin will bind to it and enhance cell adhesion. The presence of PAI-1 results in binding of the uPA/uPAR/integrin complex, leading to their deactivation and dissociation from the ECM (Czekay *et al.*, 2003) (Figure 48). After efficiently detaching cells, PAI-1 also mediates binding of these complexes to LRP and thus, the internalization of LRP, uPAR and uPA in early endosomes (Czekay *et al.*, 2001) with subsequent dissociation of uPA/PAI-1 complexes from uPAR and LRP into late endosomes and their final degradation in lysosomes (Figure 48). After dissociation of the unoccupied LRP/uPAR/integrin complexes the single components return to the cell surface *via* recycling vesicles and make uPAR and integrins available for reattachment to the ECM (Czekay *et al.*, 2003).

Furthermore, the interaction of uPA/PAI-1 with very low density lipoprotein receptors (VLDRs) has been described, which stimulated sustained ERK phosphorylation and subsequent cell proliferation (Webb *et al.*, 2001) (Figure 48). The direct interaction of PAI-1 with LPR seems to be a further mechanism for increasing cell motility independently of uPA and vitronectin *via* the JAK/STAT pathway (Degryse *et al.*, 2004; Croucher *et al.*, 2008) (Figure 48).

Induction of the plasminogen activator system by sphingosine 1-phosphate

Up to now, only a single study describes the influence of FB_1 treatment on the expression of PAI protein *in vitro*. The study showed that downregulation of PAI-1 expression in human umbilical vein endothelial cells (HUVECs) by the anthracyclin antibiotic daunorubicin is partially restored *via* decreased *de novo* formation of ceramide by FB_1 (20 µM) (Soeda *et al.*, 2001). These results suggest that alterations in lipid mediators (*e.g.* increases in sphingoid bases and their respective 1-

phosphates) arising from the FB_1-induced inhibition of ceramide synthesis may be involved in the induction of PAI-1 expression.

Indeed, in studies investigating the high invasiveness of human glioblastoma cells So1P has been demonstrated to enhance the mRNA and/or protein expression of PAI-1, uPA and uPAR (Bryan *et al.*, 2008; Paugh *et al.*, 2008; Young *et al.*, 2009) (Figure 49).

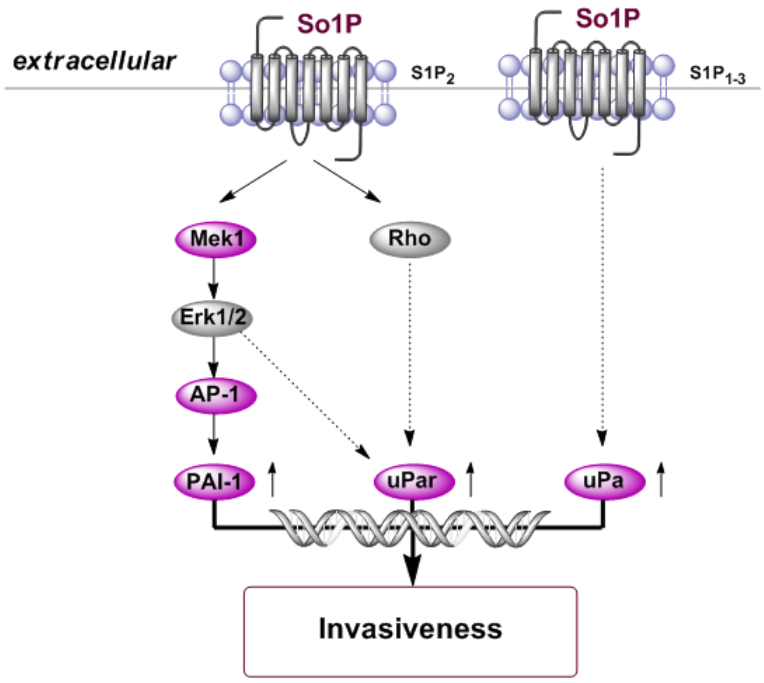

Figure 49: Pathways involved in So1P-mediated invasiveness in cancer cells by regulating the plasminogen activator system. Genes analyzed after FB_1 treatment in kidneys of male Sprague Dawley rats were integrated in sphingoid base 1-phosphate-mediated invasion pathways. Colors indicate: genes **upregulated** in response to FB_1 (**pink**), genes involved in pathway but not analyzed in response to FB_1 (**grey**). Dashed lines indicate unknown downstream pathways involved in gene transcription.

Bryan *et al.* found that S1P efficiently stimulated mRNA and protein expression of PAI-1 and uPAR in a time- and dose-dependent manner in the established glioblastoma cell line U373-MG, whereas mRNA expression of *uPA* remained unchanged (Bryan *et al.*, 2008). In contrast, primary glioblastoma cells also showed a So1P-induced increase in *uPA* mRNA expression, which also correlated with increased invasiveness (Bryan *et al.*, 2008) (Figure 49). The authors demonstrated that So1P may activate *PAI-1* and *uPAR* mRNA expression *via* multiple signaling pathways, such as the rapid phosphorylation of ERK1/2, which does not activate JNK and NFκB transcription factor in established U373-MG cells (Bryan *et al.*, 2008).

Using pharmacological inhibitors for PI3K, p38 kinase, MAPK/ERK1/2 and RHO kinase, So1P-induced expression of PAI-1 and uPAR was down-regulated by the inhibition of MAPK/ERK1/2 and RHO kinase that are described to activate the expression of AP-1, which in turn regulates the expression of both PAI-1 and uPAR in response to various stimuli (Nagamine *et al.*, 2005; Sauer *et al.*, 2005; Abukhdeir and Park, 2008) (Figure 49).

This is in line with our study, which showed significant upregulation of *Jun* and *Map2k1* (*Mek1*) mRNA expression (1.7-and 1.4-fold, respectively) together with an increased mRNA expression of *PAI-1*, *uPA* and *uPAR* after 6–day exposure to 0.75 mg/kg bw/d FB_1 (see chapter 5.1.6, Table 37). Interestingly, mRNA expression of *Jun* and *Fos* as well as *PAI-1* was already markedly upregulated after single exposure to FB_1, suggesting a role for AP-1 transcription factor in the regulation of the plasminogen activator system in response to FB_1 (Figure 49).

In glioblastoma cells, Bryan *et al.* showed AP-1 was involved in the regulation of PAI-1, but not uPAR expression (Bryan *et al.*, 2008). Thus, transcriptional activation of PAI-1 and uPAR was different, although both were induced by So1P treatment. The use of pharmacological antagonists and specific siRNA for $S1P_2$ but not $S1P_1$ resulted in abolished PAI-1 and uPAR mRNA expression after So1P treatment (Bryan *et al.*, 2008) (Figure 49). Furthermore, treatment with So1P enhanced the invasion of glioblastoma cells, whereas downregulation of PAI-1 and uPAR expression abrogated invasiveness. These results indicate that So1P-induced PAI-1 and uPAR upregulation *via* $S1P_2$-mediated activation of RHO kinase and MAPK/ERK signaling with particular regulation of PAI-1 through the transcription factor AP-1, increased the invasiveness of glioblastoma cells by influencing the balance between cell attachment and detachment (Bryan *et al.*, 2008) (Figure 49). In a similar fashion, So1P has been shown to induce PAI-1 protein expression in murine adipocytes through $S1P_2$, which has been demonstrated to activate both PLC-PKC and RHO pathways downstream of $S1P_2$-coupling to the respective G-proteins (Lee *et al.*, 2010). Moreover, another study in glioblastoma cells showed that So1P induced the expression of uPA protein depending on the overexpression of $S1P_{1-3}$ (Young *et al.*, 2009) (Figure 49), which shows that uPA expression seemed to be dependent on the cell-specific expression pattern of S1P receptors.

As shown in our study, S1P receptors were basally expressed in kidneys of male Sprague Dawley rats with $S1P_3$ and $S1P_2$ being most abundant compared to $S1P_1$. Thus, it is conceivable that So1P resulting from FB_1-induced alterations in sphingolipid metabolism may preferably bind to the constitutively higher expressed receptors $S1P_2$ and $S1P_3$, thereby mediating invasion *via* upregulation of the plasminogen activator system (Bryan *et al.*, 2008; Young *et al.*, 2009) as well as migration through interaction with Ras-related C3 botulinum toxin substrate (RAC) and RHO signaling (Taha *et al.*, 2004).
Although data regarding the biochemical function of Sa1P are less comprehensive, some studies showed that Sa1P stimulates cell migration in an equal or less potent manner compared to So1P and *via* binding affinity to the same S1P receptors (Wang *et al.*, 1999; Kimura *et al.*, 2000; Tamama *et al.*, 2001).

In summary, our results revealed that even short-term treatment with FB_1 was sufficient to alter the transcriptional balance between components of the plasminogen activator system, which might be crucial for an environment that favors tumor progression. As described in cancer cells, So1P is an important mediator of PAI, uPA and uPAR gene expression through the activation of S1P receptors that facilitate invasiveness of cells by interaction with RAC and RHO pathways. Importantly, increased formation of So1P and Sa1P as shown in our study occurred even after single exposure to FB_1 and correlated with the So1P-induced alterations in transcription factors and pathways that are known to alter the balance in PAI-1, uPA and uPAR, thereby driving tumor migration and invasion. With regard to continuing exposure to FB_1, it is thus conceivable that alterations in the plasminogen activator system, mediated by sustained formation of So1P and also Sa1P, may largely contribute to FB_1-induced formation of renal tumors with metastatic potential and highly aggressive nature.

6.2.3 Alterations in the expression pattern of adhesive glycoproteins, integrins and growth factor receptors may contribute to renal tumor invasion, angiogenesis and metastasis

Tumor progression, resulting in metastasis, is a multi-step process that involves (1) dissemination of cancer cells from the primary site by migration to and invasion

through the basement membrane into adjacent blood or lymphatic systems (intraversation), (2) acquirement of survival signals to overcome apoptosis by loss of cell contact (anoikis resistance), (3) adhesion to blood and lymphatic systems of foreign tissues, (4) localization into a new environment by migration to and invasion through the basement membrane (extraversation) and, finally, (5) survival and proliferation in the foreign tissue to metastatic (secondary) tumors (Simpson *et al.*, 2008). To overcome all physiological barriers in tumor progression and metastasis, it is assumed that primary tumors need to express a large repertoire of genes that are prerequisites for malignant progression and also include the constant upregulation of genes that are already important during initiation and development of the primary tumor (Nguyen and Massague, 2007; Geiger and Peeper, 2009).

Modulation of migration and invasion by growth factors and adhesive glycoproteins

The initial hallmarks of metastasis are characterized by the ability of tumor cells to locally migrate and invade into their adjacent environment, thereby changing their cell morphology and interaction with the ECM in different ways (van Zijl *et al.*, 2011). Various ECM proteins have been implicated in the modulation of tumor growth and invasion in a paracrine manner, including thrombospondin-1 (THBS1), a large homeotrimeric glycoprotein produced and secreted by various tumors (Sargiannidou *et al.*, 2001; Sid *et al.*, 2004). Under physiological conditions, THBS1 is mainly stored in α granules of blood cell platelets, where it participates in platelet aggregation and clot formation (Lawler, 1986). However, other cell types can also produce THBS1 that is strongly bound to the ECM (Sargiannidou *et al.*, 2001). THBS1 is a multifunctional molecule with various biological activities related to specific domains. Thus, multiple receptors can bind to THBS1, including low density lipoprotein receptor (LRP), αvβ3-integrin and cluster of differentiation (CD) 36 (thrombospondin receptor) (Hugo, 2003).

In our study, *Thbs1* gene expression in kidney was significantly upregulated after FB_1 treatment in a time- and dose-dependent manner. This is in line with literature data showing that *Thbs1* is upregulated in diseases, such as renal failure and fibrosis (Hugo, 2003; Giehl *et al.*, 2008; Hugo and Daniel, 2009). In contrast, THBS1 protein, which is also believed to have anti-angiogenetic functions, has been shown to be downregulated in certain types of progressive cancer, including RCC (Zubac *et al.*,

2009; Zubac *et al.*, 2010). However, a recent study in RCC patients has demonstrated that protein levels of THBS1 were markedly elevated in the interstitial fluid of renal tumors compared to the adjacent normal kidney tissue, suggesting an increased secretion and important role of THBS1 in the microenvironment of tumors (Teng *et al.*, 2011). In this context, it was reported that prolonged exposure to elevated THBS1 may stimulate the expression of pro-angiogenic factors such as VEGF that may counteract the inhibitory action of THBS1 on angiogenesis in tumor cells and shift the effects of THBS1 towards a pro-invasive behavior (Poon *et al.*, 2004; Kazerounian *et al.*, 2008). Indeed, several studies have shown that adhesion and invasion are potentiated by THBS1 through mechanisms leading to upregulation of uPA and PAI-1 expression in epithelial carcinoma cells (Albo *et al.*, 1994; Arnoletti *et al.*, 1995; Albo *et al.*, 1999). Moreover, the expression of transforming growth factor beta1 (TGFB1) seemed to be involved in THBS1-induced cell invasion, since blocking of TGFB1 resulted in the abolishment of uPA/PAI-1 production and THBS1-dependent tumor cell invasion (Albo *et al.*, 1994; Arnoletti *et al.*, 1995). Furthermore, uPAR expression in breast cancer cells was more than 2-fold upregulated by either THBS1 or TGFB1, resulting in a 7-to 8-fold upregulation of tumor cell invasion (Albo *et al.*, 1997). Interestingly, our study showed that *Tgfb1* gene expression was significantly upregulated in response to a single dose of FB_1. In addition, repeated administration of FB_1 resulted in increased expression of the corresponding receptor *Tgfbr1*. Importantly, gene expression of both *Thbs1* and *Tgfb1* correlated well with the increase in *PAI-1*, *uPA* and *uPAR* expression and its involvement in So1P signaling (see chapter 6.2.2). Furthermore, *Tgfb1* has been shown to be transcriptionally regulated by AP-1 (Chen *et al.*, 2010), which is also a target of So1P signaling (Bryan *et al.*, 2008), supporting the possibility of So1P-mediated upregulation of *Tgfb1* in response to FB_1 treatment in our study. In addition, TGFB1 stimulates expression of *Thbs1* (Takekawa *et al.*, 2002; Frangogiannis *et al.*, 2005), which in turn activates latent TGFB1 in the ECM (ten Dijke and Arthur, 2007). Activation of TGFB1 is a prerequisite for receptor binding and signaling (ten Dijke and Arthur, 2007).

Collectively, these results show that although Thbs1 and Tgfb1 both have controversial roles in tumor progression (Sargiannidou *et al.*, 2001; Sid *et al.*, 2004; Bierie and Moses, 2006; Tian *et al.*, 2011), they may play a crucial role in tumor cell adhesion and invasion by regulating the plasminogen/plasmin system and may thus contribute to FB_1-induced tumor formation.

Modulation of angiogenesis by growth factor receptors and integrins

A further important feature of metastatic progression is the ability of cancer cells to create new blood vessels from the pre-existing vasculature to provide sufficient nutrients for optimal growth conditions, to dispose metabolic waste and to facilitate the spread of malignant cells to foreign sites (Geiger and Peeper, 2009; Hanahan and Weinberg, 2011). Angiogenetic factors like growth factors are directly or indirectly upregulated by either oncogenes (*e.g. Myc*, *Ras*) or immune inflammatory cells, respectively (Hanahan and Weinberg, 2011). Thus, the ability to activate neovascularization is strongly dependent on the balance between anti- and pro-angiogenic factors secreted by the tumor or its microenvironment (Geiger and Peeper, 2009; Hanahan and Weinberg, 2011).

Our study showed that treatment with FB_1 resulted in a statistically significant increase in the expression of growth factors like *Tgfb1* and growth factor receptors such as *Egfr*, *Tgfbr1* and *Tek* (*Tie2*), which are all involved in the positive regulation of angiogenesis (De Luca *et al.*, 2008; Thomas and Augustin, 2009; Halper, 2010). For instance, TEK (TIE2), a growth factor receptor almost exclusively expressed on endothelial cells, is mainly activated by angiopoetin-1 and angiopoetin-2 (Jones *et al.*, 2001b; Thomas and Augustin, 2009) and facilitates endothelial cell migration, survival and capillary tube formation (Jones *et al.*, 2001b). In human kidney, TEK (TIE2) protein is strongly expressed by the vascular endothelium of normal tissue and clear cell RCC (Currie *et al.*, 2002). In RCC, TEK expression correlated with the expression of its ligand angiopoietin in the tumor-associated compared to normal vessels (Currie *et al.*, 2002). Besides renal cancer, Tek (Tie2) and angiopoietin expression have also been correlated with tumor angiogenesis and progression in various other malignancies, including gastric carcinoma (Moon *et al.*, 2006), glioblastoma (Brunckhorst *et al.*, 2010) and lung cancer (Hatanaka *et al.*, 2001). In tumor angiogenesis, *Tek (Tie2)* gene expression seems to be primarily regulated *via* members of the ETS family of transcription factors (Huang *et al.*, 2006), which are important downstream targets of oncogenic RAS protein (Sahai and Marshall, 2002).

Interestingly, So1P has been shown to mediate angiogenesis *via* binding to its cell surface receptors S1PR and/or subsequent transactivation of growth factor receptors, such as EGFR (Milstien and Spiegel, 2006; Kim *et al.*, 2009; Leong and Saba, 2010). Furthermore, exogenous So1P has also been shown to induce *Egfr* gene expression

in rat vascular smooth muscle cells *via* pertussis toxin (PTX)-sensitive G_i-protein signaling (Hsieh *et al.*, 2008), supporting an important role of So1P not only in increasing the activation but also elevating the expression of pro-angiogenic receptors. In cancer, overactivation/overexpression of EGFR correlates with increased expression of growth factors, such as vascular endothelial growth factors (VEGFs), which directly stimulate proliferation and spreading of endothelial cells and primarily promote tumor angiogenesis (De Luca *et al.*, 2008). In addition, a study in HUVEC cells has demonstrated that So1P induces *Vegfa* gene expression *via* $G_{\alpha i/o}$-protein mediated downstream signaling and subsequent JUN/AP-1 activation (Heo *et al.*, 2009). Thus, the interaction between So1P/S1PR and growth factor receptors may promote angiogenesis by influencing the induction of pro-angiogenic signaling (Yester *et al.*, 2011). In addition to growth factor receptor transactivation, So1P itself has been demonstrated to directly mediate angiogenic signaling by binding to its high affinity GPCRs $S1P_1$ and $S1P_3$ (Patwardhan and Liu, 2010; Huang *et al.*, 2011; Takuwa *et al.*, 2011; Yester *et al.*, 2011). Moreover, Sa1P, which is the structural analogue of So1P lacking the double bound, has been shown to induce capillary-like tube formation of endothelial cells *in vitro*, which is a model resembling neo-angiogenesis *in vivo* (Wang *et al.*, 1999).

Since Sa1P and So1P markedly accumulated in kidney and serum after 6-day FB_1-treatment in our study, it is conceivable that they may both mediate angiogenic signaling in kidney by stimulation of renal vascular endothelial cells. Under conditions of FB_1-induced carcinogenesis, sustained increases in sphingoid base 1-phosphates and associated upregulation of pro-angiogenic factors may thus facilitate tumor progression and metastasis in the kidney.

Besides the role of growth factors in tumor angiogenesis, integrins and their signaling pathways have been implicated in the regulation of angiogenesis, tumor invasion and metastasis (Guo and Giancotti, 2004). Integrins are important heterodimeric cell surface glycoproteins consisting of two variable transmembrane α- and β-subunits that act as receptors for diverse ECM constituents and mediate various intracellular signals, including cell adhesion, migration and proliferation (Kinbara *et al.*, 2003; Guo and Giancotti, 2004). Moreover, tumor cells often change the expression pattern of integrins during cancer progression to enhance their survival during metastasis. Otherwise, they would undergo programmed cell death due to inadequate or loss of

cell adhesion (anoikis), which serves as a pivotal mechanism to prevent metastasis (Geiger and Peeper, 2009).

The gene expression results of our study revealed that FB_1 treatment induced a significant increase in different integrins depending on duration of exposure. Whereas application of a single dose of FB_1 led to increased expression of *Itga2*, *Itgav* and *Itga3* and *Itga4*, repeated doses of FB_1 exclusively enhanced the expression of *Itga2* and *Itgav*. Increased gene expression of *Itgav*, which encodes the integrin subunit αv, has been shown to be critically involved in the induction of tumor angiogenesis in heterodimers with β3- and β5-integrin subunits (Guo and Giancotti, 2004; Morgan *et al.*, 2007), which are encoded by the *Itgb3* and *Itgb5* genes (Takada *et al.*, 2007). Besides angiogenesis, αv integrins are also implicated in tumor growth, invasion and metastasis, thus making them promising therapeutic targets in many cancers (Nemeth *et al.*, 2007). Interestingly, immunhistochemical investigations showed that αv integrin was increased in high grade tumors of RCC (Markovic-Lipkovski *et al.*, 2001). Similar to *Itgav*, increased expression of the *Itga2* gene has been frequently found in cancer and also seems to play an important role in tumor migration, invasion, angiogenesis and metastasis (Lin *et al.*, 2007; van der Bij *et al.*, 2008; Zhang *et al.*, 2008; Pan *et al.*, 2009; Yoshimura *et al.*, 2009).

Interestingly, integrin-mediated migration of endothelial cells has also been linked to the action of So1P, which has been demonstrated to activate αvβ3 and/or αvβ5 integrin-signaling through $S1P_1$ and/or $S1P_3$-dependent RHO-signaling (Paik *et al.*, 2001; Wang *et al.*, 2008). A further study in endothelial cells showed that So1P increases cell invasion and lumen formation, and stimulates branching morphogenesis by interaction with integrins (α2β1 and αvβ3) as well as activated MMPs (Bayless and Davis, 2003). Moreover, exogenous So1P induced the gene expression of *Itgav* in human embryonic stem cells (hESCs) (Avery *et al.*, 2008). In addition, both *Itgav* and *Itga2* expression were shown to be synergistically elevated in human endothelial cells after combined treatment with So1P and growth factors (*i.e.* Vegf and basic Fgf) (Su *et al.*, 2008). Furthermore, αvβ3 integrin has been shown to enhance survival in endothelial cells in a complex with activated SPHK1, supporting an important linkage between integrin and SPHK1 signaling in mediating cell survival (Gamble *et al.*, 2009).

In summary, these data suggest that So1P/SPHK1 have an important role in increasing migration, invasion, angiogenesis and survival by activation of integrin signaling, which has been shown to correlate with the time- and dose-dependent increase in integrin expression and concomitant accumulation of So1P and Sa1P in kidney and serum after repeated exposure to FB_1 in our study. Thus, it is possible that increased integrin signaling in response to chronic exposure to FB_1 may additionally promote survival, tumor progression and metastasis under conditions of FB_1-mediated renal carcinogenesis.

Modulation of genes enhancing the metastatic potential of tumors

A further gene altered time- and dose-dependently in response to FB_1 was the intercellular adhesion molecule *Icam1*, which is an important cell surface glycoprotein primarily expressed on endothelial cells and ligand of *e.g.* several integrins in the recruitment of leukocytes in response to inflammatory cytokines (Takada *et al.*, 2007). Gene expression of *Icam1* is frequently increased in cancer, *e.g.* breast cancer, where it correlates with metastatic potential (Rosette *et al.*, 2005) and aggressive tumor phenotype (Schroder *et al.*, 2011). Human RCC showed increased *Icam1* expression, which correlated with the degree of monocyte infiltration and increased cytokine levels (Tomita *et al.*, 1990). Furthermore, levels of soluble ICAM1 in serum were shown to correlate with advanced tumor stage or metastasis (Heicappell *et al.*, 1994; Favaro *et al.*, 1997) and shorter survival (Favaro *et al.*, 1997; Kallio *et al.*, 2001) in human RCC. Interestingly, gene expression of *Icam1* is induced by treatment of human endothelial cells with So1P, leading to the activation of G_i-protein and NFκB-signaling (Lee *et al.*, 2004).

In metastasis, ICAM1 protein expression on host endothelial cells has been implicated in binding and recruitment of circulating tumor cells that exhibit membrane-bound MUC1 (Roland *et al.*, 2007). The ligation of MUC1 to ICAM1 in turn upregulates the expression of ICAM1 on tumor cells. This leads to the release of cytokines that attract macrophages to bind the tumor cells *via* specific integrin receptors that facilitate transendothelial tumor cell migration *via* the release of ECM-degrading proteases (Roland *et al.*, 2007). Tumor cells also use MUC1 to detach from the primary tumor and intraversate into blood vessels due to anti-adhesive effects of aberrantly expressed MUC1 (Hollingsworth and Swanson, 2004). Thus, the

interaction of both adhesive and de-adhesive properties of MUC1 may strongly contribute to tumor invasion and metastasis (Hollingsworth and Swanson, 2004). Indeed, aberrant MUC1 expression has been frequently observed in cancer (Hollingsworth and Swanson, 2004) and correlates with poor prognosis, *e.g.* in progressive RCC (Kraus *et al.*, 2002; Leroy *et al.*, 2002; Oudard *et al.*, 2011).

Our study demonstrated that *Muc1* was significantly upregulated in FB_1-treated animals and paralleled the increased expression of *Icam1*. The *Muc1* promoter has been shown to have numerous binding sites for transcription factors like AP-1 (Jonckheere and Van Seuningen, 2010). Thus it is conceivable that sphingoid base 1-phosphate mediated upregulation of AP-1 (An *et al.*, 2000; Hsieh *et al.*, 2008) also promotes expression of *Muc1*.

Considering the implication of both adhesion molecules in cancer progression, FB_1-induced upregulation of Icam1 and Muc1 in tumor cells, which may occur in response to enhanced levels of sphingoid base 1-phosphate, may facilitate the formation of a highly malignant phenotype of tumor cells with increased potential to invade and metastasize.

In addition to MUC1, the receptor tyrosine kinase MET (HGFR) is frequently overexpressed in RCC (Giubellino *et al.*, 2009; Behbahani *et al.*, 2011). MET mediates invasion and metastasis *via* several pathways, including RAS/MAPK, PI3K–AKT, phospholipase Cγ (PLCγ), SRC and STAT (Boccaccio and Comoglio, 2006; Corso *et al.*, 2008). Overexpression of *Met* may be driven by oncogenes such as *Ras* through transcriptional regulation of *Met* (Birchmeier *et al.*, 2003; Boccaccio and Comoglio, 2006). Usually, MET is activated by its ligand HGF, but in cancer cells that express high levels of MET also ligand-independent activation may occur *via* increased cell attachment (Wang *et al.*, 2001; Birchmeier *et al.*, 2003).

Besides overexpression and ligand binding, So1P has been demonstrated to transactivate MET (Shida *et al.*, 2004). In gastric cancer cells, transactivation of MET seemed to be dependent on G_i-protein-independent (PTX-insensitive) $S1P_2$ signaling (Shida *et al.*, 2004). Given the importance of MET in cancer progression (Birchmeier *et al.*, 2003; Boccaccio and Comoglio, 2006), it appears that FB_1-mediated renal carcinogenesis and tumor progression may involve the So1P/S1PR-mediated transactivation of MET, thereby contributing to invasion and metastasis of tumors.

Interestingly, a slight, but significant elevation in gene expression of *Mta2*, which belongs to the group of metastasis-associated genes (MTAs), was found after repeated exposure to the high dose of FB_1. The MTA2 protein has been identified as a component of the nucleosome remodeling and histone deacetylation (NuRD) protein complex, which regulates deacetylation of histones non-histone proteins such as p53 (Toh and Nicolson, 2009). Together with histone deacetylase 1 (HDAC1), a further component of NuRD, MTA2 has been demonstrated to inactivate p53 by deacetylation, which results in degradation of p53 and thus suppression of p53-dependent growth arrest and apoptosis (Toh and Nicolson, 2009). Hence, expression of *Mta2* after repeated FB_1 exposure may facilitate uncontrolled cell proliferation by inhibiting the tumor-suppressor function of p53 protein. Whether *Mta2* gene expression is also regulated by the increased formation of sphingoid base 1-phosphates remains to be determined.

6.2.4 Summary and conclusions

The present study shows that exposure to FB_1 results in increased expression of a plethora of genes involved in tumor initiation as well as tumor progression. While single FB_1 exposure was mainly demonstrated to induce gene expression of proto-oncogenic transcription factors and apoptotic genes, repeated exposure resulted in marked upregulation of genes mediating cell survival and cell proliferation. Moreover, continued exposure to FB_1 initiated increased expression of genes critically involved in tumor migration, adhesion, invasion and metastasis, which may increase the invasive potential of renal cells.

A close correlation was established between gene expression changes in response to FB_1 and known signaling pathways mediated by extracellular or intracellular action of sphingoid base 1-phosphates - bioactive lipids that were markedly increased after FB_1 treatment. In particular, genes encoding components of the plasminogen activator system that mediate invasion and metastasis in response to So1P were abundantly upregulated, and may hence contribute to the formation of highly aggressive and invasive tumors as observed after chronic exposure to FB_1. Thus, it is conceivable that upregulation of a majority of genes in response to FB_1 may be a direct or indirect consequence of increased So1P signaling.

6.3 FB_1-mediated organ-specific effects on kidney and liver of male Sprague Dawley rats

A variety of studies have previously shown that FB_1 may exert different effects in rodents, which strongly depended on the species, strain and gender (NTP, 2001). In different rodent species used for toxicological investigations, FB_1 primarily acted on both kidney and liver as target organs for toxicity (Voss *et al.*, 1993; Bondy *et al.*, 1995; Voss *et al.*, 1995b; NTP, 2001). Since male F344 rats were most susceptible to FB_1-induced nephrotoxicity and tumor formation in the NTP carcinogenicity study (NTP, 2001), human risk assessment was based on the NOAEL for nephrotoxicity in the rat (JECFA, 2001).

Besides Fischer rats, male Sprague Dawley rats have also been demonstrated to be sensitive to FB_1-induced nephrotoxicity (Riley *et al.*, 1994; Bondy *et al.*, 1996; Lim *et al.*, 1996; Riley and Voss, 2006), even though they also exhibited mild to moderate hepatotoxic lesions (Bondy *et al.*, 2000; Riley and Voss, 2006). Thus, an ancillary aim of the present study was to compare early effects on histopathology, sphingolipid metabolism and expression of cancer-related genes in kidneys and livers of male Sprague Dawley rats to elucidate whether these effects were more prevalent in kidneys compared to livers and thus favor renal carcinogenesis.

6.3.1 Early histopathological effects are more pronounced in kidney compared to liver

In the present study, FB_1-induced alterations in histopathology were more pronounced in kidney than in liver, which was evidenced by severe lesions in the renal tubular epithelium in OSOM and cortex. Hepatic damage was primarily restricted to the centrilobular area and consisted of mild to moderate lesions in hepatocytes around the central vein.

Moreover, the higher sensitivity of FB_1-induced effects in kidney was also supported by earlier alterations in clinical chemistry parameters, demonstrating that serum markers indicative of nephrotoxicity were statistically significantly altered after single exposure to FB_1 and correlated with degeneration of renal tubular epithelial cells. After 6 days, statistically significant changes in urinary parameters corresponding to progressive renal tubular damage (*e.g.* decreased osmolality and pH value) as well

as serum clinical parameters indicative of kidney damage (*e.g.* increased creatinine concentration) already occurred at the low FB_1 dose (0.25 mg/kg bw/d). In contrast, classical serum enzymes (*e.g.* ASAT and ALAT) indicative of increased liver toxicity were only statistically significantly altered at the high dose FB_1 (0.75 mg/kg bw/d) and paralleled the increase in histopathological lesions observed in hepatocytes after 6-day treatment.

The effects of FB_1 on histopathology in kidney and liver from our study were consistent with those from Bondy *et al.*, who showed that apoptotic lesions after 6-day *i.p.* administration of 0.75 mg/kg bw/d FB_1 were more pronounced in kidneys compared to livers of male Sprague Dawley rats (Bondy *et al.*, 2000). Independent of the route of application, a variety of short-term studies showed that FB_1-induced effects in male Sprague Dawley rats both included nephro- and hepatotoxicity, although the kidney was more susceptible to FB_1-induced lesions than the liver (Riley *et al.*, 1994; Bondy *et al.*, 1996; Lim *et al.*, 1996).

Riley *et al.* established a link between the increased histopathological effects on kidney and a preferential uptake of FB_1 in kidneys of male Sprague Dawley rats, which was evidenced by an ten-fold higher accumulation of FB_1 in kidney compared to liver (Riley and Voss, 2006). Since it has been shown that FB_1 has a high affinity to rat OAT1 and OAT3 (Kojima *et al.*, 2002), it is conceivable that organ-specific toxic effects in kidney may in part be related to a different expression of OAT subtypes in kidney and liver. Consistent with this, rat OAT1 and OAT3 mRNA were described to be predominantly expressed in kidney and to a lesser extent in liver (Anzai *et al.*, 2006; Sekine *et al.*, 2006). Hence, organ-specific differences in active transporter systems such as the OAT superfamily may probably provide an explanation for the accumulation of toxic FB_1 over the time in rat kidney but not liver.

6.3.2 Alterations in sphingolipid metabolism are more prominent in kidney than in liver and correlate with differences in toxicity

There is strong evidence to suggest that biochemical modulation of sphingolipid metabolism is the initial key event in the FB_1-induced mechanism of carcinogenesis (Riley *et al.*, 2001). Since male Fischer rats chronically exposed to carcinogenic doses of FB_1 were more sensitive to alterations in sphingolipid metabolism in kidney

than in liver (NTP, 2001), it was assumed that this may strongly be related to the increased tumor formation in kidney (Riley *et al.*, 2001). Thus, the present study in male Sprague Dawley rats was performed to elucidate whether FB_1-induced disruption of sphingolipid metabolism may be more pronounced in kidney than in liver and thus correlate with early alterations in the transcriptional profile of cancer-related genes in kidney.

The results of this study demonstrated that FB_1 equally inhibited ceramide synthase in kidney and liver, which was reflected by a similar decrease in C16-Cer levels. However, marked differences occurred with regard to the extent of sphingoid base accumulation in both organs as a consequence of ceramide synthase inhibition. The ceramide precursor Sa was accumulated in kidney up to 25-fold more compared to liver after single administration of the FB_1. At the same time, increased levels of the sphingoid base So were observed in kidney, whereas hepatic levels did not markedly change compared to controls. The extent of renal and hepatic sphingolipid perturbations was reflected by a dose-dependent increase in the ratios of Sa and So. However, the ratios of both sphingoid bases in kidney exceeded those in liver, supporting the fact that the kidney is more susceptible to FB_1-induced effects on sphingolipid metabolism than the liver (NTP, 2001). Primarily, this may be associated with a minor (10-fold less) FB_1 uptake in liver compared to kidney, which has been previously reported in male Sprague Dawley and Wistar rats (Martinez-Larranaga *et al.*, 1999; Riley and Voss, 2006).

In addition, the expression and activity of sphingolipid-metabolizing enzymes may also account for differences in the overall disruption of the sphingolipid rheostat (Merrill *et al.*, 1997; Spiegel and Milstien, 2003). Indeed, comparative gene expression analysis in the present study demonstrated that basal gene expression of *Sphk1*, encoding the enzyme catalyzing the formation of sphingoid base 1-phosphates, was markedly increased (29-fold) in kidney compared to liver. Our results are consistent with data from the literature, showing a substantially higher expression and activity of SPHK1 in renal than hepatic tissue (Melendez *et al.*, 2000; Gijsbers *et al.*, 2001). Accordingly, single exposure to FB_1 resulted in statistically significant alterations in Sa1P and So1P in kidney, while no changes occurred in the livers, indicating increased metabolic activity of SPHK1 in the renal tissue of male Sprague Dawley rats.

In comparison to a single dose, repeated administration of FB_1 for 6 consecutive days further increased the differences in FB_1-induced disruption of sphingolipid metabolism between kidney and liver. This was demonstrated by a considerable accumulation of Sa and high metabolic conversion to Sa1P in renal tissue. Elevation in renal Sa was up to 12-fold increased compared to liver. Considering the total amounts of Sa (Sa + Sa1P) in kidney and urine, which was suggested to constitute the proportion of exfoliated and dead renal tubular epithelial cells (Riley *et al.*, 1994), a strong alteration in sphingolipid metabolism in kidney was demonstrated compared to liver. Correspondingly, increased values of total So (So and So1P) were found in kidney and urine after 6-day exposure, whereas hepatic levels of So and So1P were much less increased. Importantly, the time- and dose-dependent accumulation of sphinganine strongly correlated with the extent of histopathological findings in the respective target organs, showing marked tubular damage and degeneration in kidney and only moderate lesions in liver after repeated exposure to FB_1.

Consistent with our findings, the 2-year carcinogenicity study demonstrated that levels of Sa and So accumulated in FB_1-treated kidney to a greater extent as compared to liver and correlated with increased nephrotoxicity in renal tubular epithelium (NTP, 2001). After chronic administration of carcinogenic doses (50 and 150 ppm FB_1) *via* feed, molar concentrations of Sa in kidney were 216 and 301 µM and corresponded well to those found after single *i.p.* administration in our study (259 and 371 µM after 0.25 and 0.75 mg/kg bw/d). In contrast, molar Sa concentrations in kidney were higher after 6 days exposure to FB_1 (586 and 696 µM after 0.25 and 0.75 mg/kg bw/d, respectively) and might reflect higher mycotoxin uptake caused by parenteral application as well as differences in the metabolic handling and excretion of accumulated Sa after short-term compared to long-term exposure. Indeed, chronic exposure to dietary doses of 50 and 150 ppm, resulted in a higher excretion of sphingoid bases in urine (NTP, 2001) compared to our study and might thus explain differences in Sa and So accumulation in kidney over time.

In the NTP carcinogenicity study, histopathological examination of livers did not reveal marked hepatic lesions in male F344N rats after chronic FB_1 exposure (NTP, 2001), which was different from the histopathological effects in livers of male Sprague Dawley rats found in our study. Similar to our study, Riley *et al.* showed that male Sprague Dawley rats both exhibited renal and hepatic lesions after 5-day exposure to carcinogenic concentrations of FB_1 in feed, which correlated well with the FB_1-induced

accumulation of sphingoid bases as a result of increased FB_1 uptake (Riley and Voss, 2006).

6.3.3 Basal and FB_1-induced expression of S1P receptors in kidney and liver

So1P is an important and widely studied second messenger molecule with both physiological and pathological cell functions, including proliferation, survival, migration, invasion, angiogenesis and lymphocyte trafficking (Spiegel and Milstien, 2003; Leong and Saba, 2010). Although the biological activity of Sa1P is not as well known as that of So1P, both sphingoid base 1-phosphates primarily mediate extracellular signaling through binding to their high affinity GPCRs $S1P_{1-5}$, which transduce intracellular signals *via* specific G-proteins that regulate diverse downstream pathways (Spiegel and Milstien, 2002; Alvarez *et al.*, 2007). Thus, extracellular signaling through S1P receptors in the presence of sphingoid base 1-phosphates can vary greatly between different cell types depending on the expression and abundance of distinct S1P receptors (Taha *et al.*, 2004; Hla and Brinkmann, 2011). Since FB_1-induced perturbations in sphingolipid metabolism were associated with an increased metabolic conversion of sphingoid bases into bioactive sphingoid 1-bases, the present study aimed at elucidating differences in the basal and FB_1-induced expression pattern of S1P receptors in kidney and liver, that may mediate different signaling in both kidney and liver in response to FB_1-mediated elevation of sphingoid base 1-phosphates.

In our study, a similar mRNA expression pattern of S1P receptors in kidney and liver was observed, with $S1P_3$ and $S1P_2$ being most and $S1P_1$ least abundant. Regarding the basal levels of these three S1P receptors, $S1P_1$ and $S1P_2$ mRNA expression seemed to be higher in liver compared to kidney, whereas $S1P_3$ mRNA expression was higher in kidney. Surprisingly, 6-day exposure to FB_1 induced a statistically significant downregulation in the hepatic mRNA expression of $S1P_1$ and a less pronounced reduction in the expression of $S1P_2$ and $S1P_3$. In contrast, renal mRNA expression of $S1P_{1-3}$ was not statistically significantly altered in response to FB_1, albeit expression of $S1P_3$ was slightly reduced after 6-day FB_1 treatment.

Regulation of S1P receptors has been reported in a variety of studies and is primarily involved in lymphocyte trafficking and homing (Goetzl and Rosen, 2004). In this context, downregulation of $S1P_1$ has been shown to retard lymphocytes in lymph

nodes, whereas upregulation facilitates lymphocyte to leave the lymph nodes (von Wenckstern *et al.*, 2006). As lymphocytes are also abundantly present as innate immune cells in liver (Crispe, 2009), it is conceivable that downregulation of $S1P_1$ on lymphocytes may retain these immune cells at sites of hepatic inflammation. A study in knockout mice has demonstrated that T lymphocytes may be involved in mediating the FB_1-induced toxicity in liver (Sharma *et al.*, 2006). However, whether possible downregulation of S1P receptors on lymphocytes in response to FB_1 may promote homing of lymphocytes in liver and thus facilitate hepatotoxicity as result of increased inflammatory response remains to be investigated.

Taken together, these results support the idea of an additional FB_1-mediated immunomodulatory effect in the toxicity of liver compared to kidney, although the mechanisms involved in FB_1-induced immunotoxicity are still not well understood (Stockmann-Juvala and Savolainen, 2008). Considering the differences in receptor expression in response to FB_1, it appears that the kidney might be more sensitive to extracellular sphingoid base 1-phosphate signaling mechanisms than the liver. This may be explained by the fact that FB_1 induces significant downregulation of hepatic $S1P_{1-3}$, which mediate the expression of genes involved in cancer.

6.3.4 Differences in the expression of the cancer-related genes PAI-1, Itga2 and Thbs1

To assess whether FB_1-mediated alterations in gene expression of cancer-related genes may be unique to kidney, and to identify differences in organ susceptibility to FB_1-induced malignancy, selected genes (*PAI-1*, *Itga2* and *Thbs1*) involved in angiogenesis, adhesion, invasion and metastasis were compared regarding their specific expression in kidney and liver in response to FB_1.

The results obtained from our study showed that single administration of FB_1 resulted in a more pronounced expression of *PAI-1* mRNA in kidney than in liver. However, after repeated exposure to FB_1 alterations in gene expression of *PAI-1* in liver were more pronounced compared to kidney. However, only 2 of 4 animals of the high dose group responded markedly to FB_1 by increasing hepatic *PAI-1* expression up to 10- and 22-fold compared to controls, respectively. The increased *PAI-1* expression in these animals correlated with the highest elevation in the levels of the hepatic

enzymes ALAT and GLDH, which are indicative of hepatotoxicity. Indeed, comparison of the liver histopathology of these animals within the high dose group showed that they were mostly affected by FB_1-induced hepatic lesions, which were characterized by ongoing disorganization of hepatic cords, sinusoidal dilation, congestion as well as increased numbers of Kupffer cells in the centrilobular areas of the hepatic lobules. In accordance with the literature, abundant upregulation of PAI-1 expression has been observed in various forms of liver injury and may be potently induced by cytokines and in response to various chemicals (Dimova and Kietzmann, 2008). In immune-mediated hepatotoxicity, TNF-alpha released by Kupffer cells was described to potently induce *PAI-1* gene expression in liver, which decreases fibrinolysis and enhances sinusoidal fibrin deposition, resulting in ischemic hypoxia and hepatic cell death (Roberts *et al.*, 2007). In addition, TNF-alpha may also promote fibrin deposition by activation of sinusoidal endothelial cells and subsequent activation of coagulation (Roberts *et al.*, 2007).

In our study, histopathological findings in liver demonstrated increased numbers of Kupffer cells, which correlated with dilated sinusoids and congestion in the centrilobular area of the hepatic lobules, suggesting a relationship between the FB_1-induced increase in *PAI* expression and increased numbers of Kupffer cells around the central vein that may mediate cytokine production and release in response to FB_1. Indeed, FB_1 has been shown to induce a variety of cytokines like TNF-alpha and pro-inflammatory interleukins such as IL-1, which may be released by Kupffer cells (Bhandari and Sharma, 2002a; Sharma *et al.*, 2006). Furthermore, Sharma *et al.* demonstrated that FB_1-induced hepatotoxicity in mice was dependent on T-lymphocyte-mediated release of cytokines (Sharma *et al.*, 2006). In contrast, depletion of these immune cells in mice resulted in decreased TNF-alpha and IL-1 alpha gene expression and nearly abolished hepatotoxicity in response to FB_1 (Sharma *et al.*, 2006). The authors suggested that activation of T lymphocytes was required to activate Kupffer cells that promote the release of TNF-alpha and IL-1 alpha and thus enhance hepatotoxicity (Sharma *et al.*, 2006). Indeed, depletion of Kupffer cells by gadolinium chloride in mice has been shown to diminish FB_1-induced hepatotoxicity (He *et al.*, 2005a). Furthermore, pharmacological inhibition of sphinganine accumulation in response to FB_1 reduced the expression of cytokines, such as TNF-alpha (He *et al.*, 2005b), suggesting an important role of cytokine signaling in FB_1-mediated hepatotoxicity *via* the increase of sphingoid bases. Since

liver has a high abundance of resident immune cells, such as Kupffer cells (~ 15% of liver cells), that mediate cytokine signaling (Malarkey *et al.*, 2005), it is conceivable that high expression of *PAI-1* is implicated in the acute response to immunomodulatory effects mediated by FB_1. However, as effects of FB_1 on the disruption of sphingolipid metabolism in liver are lower than in kidney, the organ-specificity to FB_1-mediated toxicity may greatly depend on the extent of sphingolipid perturbation in the respective organ.

Comparison of hepatic and renal *Itga2* gene expression in our study showed that alterations in *Itga2* expression in kidney were more pronounced compared to liver after single treatment with FB_1, which strongly correlated with the higher accumulation of sphingoid bases and their 1-phosphates compared to liver. In contrast, repeated exposure to FB_1 resulted in a similar extent of *Itga2* expression in both kidney and liver. However, basal expression of *Itga2* was higher in kidney compared to liver.
In rat liver, high expression of *Itga2* is found in hepatocytes and sinusoidal endothelial cells (SECs) during liver cirrhosis, whereas normal hepatocytes and SECs do not express this integrin (Yuan *et al.*, 2000). Under physiological conditions, *Itga2* expression is mainly found in bile duct epithelial cells (Patsenker and Stickel, 2011). However, periportal hepatocytes have been shown to exhibit elevated *Itga2* expression also during cholestasis, which has been correlated with a “phenotypic switch of hepatocytes towards bile duct epithelium” (Volpes *et al.*, 1991). Indeed, our study demonstrated that serum ALP, which is a diagnostic indicator of hepatic cholestasis due to its increased excretion from bile duct epithelial cells during disturbances of bile flow (Ramaiah, 2007), was markedly elevated in three of four animals of the high dose group that also express high levels of *Itga2* in liver. Furthermore, the same animals also showed elevation in serum bilirubin, which is the yellow pigment of bile and also indicative of bile duct obstruction (Ramaiah, 2007). Evidence for hepatic cholestasis was also obtained from histopathological investigation of these animals, showing yellow pigmentation in the liver (see section 5.1.3.2, Figure 18). Thus, the expression of *Itga2* in liver, which correlated with increased levels of ALP and bilirubin, seemed to be related to FB_1-induced hepatobiliary toxicity, which has also been observed in previous studies (NTP, 2001). The effects on the bile duct epithelium might be related to an increased local FB_1 exposure that results from a predominant elimination route of FB_1 *via* bile (Shephard *et al.*, 1994a).

In our study, male Sprague Dawley rats showed only occasional elevation of *Thbs1* in liver, whereas *Thbs1* gene expression in kidney was mainly elevated in animals of the high dose groups. Basal *Thbs1* gene expression has been demonstrated in Kupffer cells, SECs and hepatic stellate cells (HSCs), whereas normal hepatocytes do not show *Thbs1* mRNA expression (Breitkopf *et al.*, 2005). In HSCs, exogenous TNF-alpha has been shown to potently activate *Thsb1* and subsequent *Tgfb1* expression, which is a known promoter of fibrinogenesis in HSCs (Breitkopf *et al.*, 2005). In liver, increased TNF-alpha is mainly associated with the activation of resident immune cells such as Kupffer cells that mediate hepatotoxicity through the release of this cytokine (Roberts *et al.*, 2007). Since an increased numbers of Kupffer cells was observed in our study, it is conceivable that these macrophages may be activated in response to FB_1 and subsequently secrete TNF-alpha, leading to increased *Thbs1* gene expression and toxicity in the livers of affected animals.

This study demonstrated that changes in *PAI-1*, *Thbs1* and *Itga2* expression were not unique to kidney, but also occurred in liver. It appears that FB_1-induced changes in the expression of these genes in liver may rather be caused by effects on hepatic immune cells that mediate toxicology than being a direct consequence of elevations in sphingoid bases 1-phosphates as proposed in kidney.

6.3.5 Summary and conclusion

Collectively, the present results indicate that kidney and liver showed marked differences in several endpoints of FB_1 toxicity, which seemed to be primarily associated with their different susceptibility to FB_1-mediated alterations in sphingolipid metabolism. In this regard, histopathological observations demonstrated that FB_1 causes earlier and more severe effects in kidney compared to liver that correlated with the higher accumulation of pro-apoptotic sphingoid bases in kidney. Furthermore, the comparison of the expression of S1P receptors, which were hypothesized to mediate pathways involved in proliferation, migration, invasion and metastasis, showed that their gene expression in liver was markedly reduced compared to kidney, suggesting a different mechanism of possible FB_1-induced tumorigenesis in liver compared to kidney. Gene expression analysis of cancer-related genes in kidneys of male Sprague Dawley rats revealed that *PAI-1*, *Itga2* and *Thbs1* were the most prominent genes modulated by FB_1 treatment. Since these genes are involved in

invasion, adhesion and angiogenesis, their specific gene expression in response to FB_1 was compared between kidney and liver to identify possible transcriptional differences that might contribute to the organ susceptibility of kidney to FB_1-induced toxicity and tumor formation. The comparison of FB_1-induced alterations in gene expression showed that these genes were not exclusively deregulated in kidney, but also in liver. Since *PAI-1*, *Itga2* and *Thbs1* are rather associated with immunotoxic effects in liver, different modes of actions for the formation of tumors in kidney and liver are assumed. However, also other genes may account for differences in FB_1-induced susceptibility to tumor formation in kidney and liver that are not analyzed here.

.

6.4 Comparison of *in vitro* and *in vitro*-induced alterations in the expression of cancer-related genes by FB_1

Changes in mRNA expression of cancer-related genes in kidney and the renal tubular epithelial cell line NRK-52E were compared to determine genes commonly altered by FB_1 treatment. The identification of common FB_1-mediated pathways involved in renal tumor formation and progression *in vivo* and *in vitro* was performed to provide novel *in vitro* approaches to mechanistic investigation of FB_1-induced carcinogenesis.

6.4.1 FB_1 induces alterations in the expression of similar genes involved in tumor formation and progression *in vivo* and *in vitro*

The most prominent changes in gene expression of NRK-52E cells after 24 h treatment with FB_1 involved the upregulation of transcription factors such as *Fos*, *Jun* and *Myc*. Furthermore, the gene expression of *p21 (Cdnk1a)* and *Nfκbia* (*Iκbα*) was significantly and dose-dependently increased in response to FB_1 *in vitro*. These observations resembled gene expression changes found in kidneys of FB_1-treated male Sprague Dawley rats, showing marked alterations in the expression of these genes after 1- and/or 6 day treatment. Other genes similarly regulated by FB_1 both *in vivo* and *in vitro* comprised the enhanced mRNA expression of components of the plasminogen activator system such as *uPAR (Plaur)* and *PAI-1 (Serpine1)*.

As discussed in chapter 6.2, all of these genes are involved in signaling pathways mediated by sphingoid base 1-phosphates. These are known to be involved in increasing cell proliferation, migration, invasion and metastasis, and thus may promote renal tumor formation and migration. Similar to the alterations in sphingolipid metabolism in kidneys of male Sprague Dawley rats, treatment of NRK-52E cells with FB_1 led to a significant and dose-dependent increase in intracellular levels of pro-apoptotic sphingoid bases Sa and So as well as their phosphorylated metabolites Sa1P and So1P, which exert anti-apoptotic functions. Importantly, FB_1-induced accumulation of pro-apoptotic sphingoid bases strongly paralleled the concentration-dependent increase in cytotoxicity after 24 h treatment. These observations are in accordance with our findings demonstrating that single exposure to FB_1 resulted in

increased apoptosis together with increased sphingoid base accumulation in kidneys of male Sprague Dawley rats.

Interestingly, a number of genes involved in cell cycle control (*Ccnd1* and *Ccne1*) and DNA damage repair (*Atm* and *Brca1*) were differently regulated by FB_1 *in vitro* compared to *in vivo*. Whereas *Ccnd1*, which encodes the S-phase-promoting Cyclin D1, was significantly increased at 0.5 and 5 µM FB_1, no changes were observed in kidneys of male Sprague Dawley rats after exposure to FB_1 at both treatment durations. In contrast, the gene transcript of the S-phase-promoting Cyclin E1 (*Ccne1*) was significantly upregulated after 24 h FB_1 treatment in vivo, whereas it was downregulated at concentrations ≥ 5 µM *in vitro*. However, this could be a consequence of different cell cycle dynamics in both experimental systems. The gene expression of *Atm*, a kinase involved in the initiation of DNA damage repair, as well as *Brca1*, which is a target of ATM phosphorylation and mediator of DNA damage repair, were significantly down-regulated at 50 µM FB_1 in NRK-52E cells. In contrast, both genes were markedly upregulated in kidney at both FB_1 dose levels after treatment with FB_1. This suggests a different capability to respond to DNA damage in both the *in vitro* and *in vivo* system, and may result in incomplete DNA damage repair *in vitro* through downregulation of *Atm* and *Brca1* expression.

Besides genes involved in cell cycle control and DNA damage repair, the expression of the anti-apoptotic gene *Birc5 (survivin)* was differently regulated *in vivo* and *in vitro*. Whereas FB_1 treatment resulted in a dose-dependent downregulation of *Birc5* (*survivin*) *in vitro*, no treatment-related changes were observed after 24 h *in vivo*. Generally, the observed effects on apoptosis *in vivo* and cytotoxicity *in vitro* were not comprehensively reflected by the gene expression changes in the selected apoptosis-related genes from this qRT-PCR array.

The *tissue inhibitor of metalloproteinase 1 (Timp1)*, a gene associated with invasion and metastasis, was upregulated at the highest concentration/dose of FB_1 *in vitro* and *in vivo*. As multifunctional glycoprotein, TIMP1 is involved in wound healing and tissue remodeling, but has also been associated with apoptosis resistance in several cell lines (Ricca *et al.*, 2009). TIMP1 may mediate cell survival *via* its ability to interact with cluster of differentiation (CD)63/integrins complexes and thus activate focal adhesion kinase (FAK)/PI3K or Src family tyrosine kinases/PI3K pathways, which promote the expression of anti-apoptotic genes such as *Bcl-Xl* (Chirco *et al.*, 2006).

The upregulation of *Timp1* mainly occurs at the transcriptional level and involves transcription factors such as AP-1 and NFκB (Chirco *et al.*, 2006). TIMP-1 was shown to be correlated with a negative prognosis in human cancers including metastatic breast cancer, colorectal cancer, lymphoma, and non-small cell lung carcinoma (Ricca *et al.*, 2009). In several malignancies, TIMP1 expression is associated with increased invasiveness, which may partly be attributed to its ability to enhance cell survival (Kahlert *et al.*, 2008). Interestingly, increased endogenous So1P in human fibroblasts has been shown to upregulate the expression of *Timp1 via* activation of the JUN/AP-1 transcription factor (Yamanaka *et al.*, 2004). Consistent with the increase in So1P after FB_1 treatment *in vivo* and *in vitro*, it is thus conceivable that increased expression of *Timp1* may contribute to pathways involved in FB_1-induced carcinogenesis.

A further gene deregulated and associated with metastasis was Nme1, which was significantly decreased (-1.4-fold) compared to controls after treatment with 50 µM FB_1 in NRK-52E cells. Similar to this finding, a slight downregulation of this gene was also observed in the single dose study with FB_1, but failed to reach statistic significance.

Nme1 (encoding the Nm23 protein) is an isoform of the nucleoside diphosphate kinase and implicated in nucleotide triphosphate metabolism (Marshall *et al.*, 2010). In cancer, it has been identified as a suppressor of metastasis. This was supported by the fact that reduced levels of Nm23 were found in metastatic compared to non-metastatic tumors (Steeg, 2003). The tumor suppressor function of Nm23 has been related to the phosphorylation (activation) of the kinase suppressor of RAS (KSR), which functions to reduce the activation of ERK/MAPK signaling by interaction with ERK1/2 (Steeg, 2003; Marshall *et al.*, 2010). Thus, decreased levels of Nm23 fail to suppress pathways leading to increased migration and invasion, which consequently promotes the metastatic spread of tumors.

None of the genes involved in cell adhesion were significantly deregulated *in vitro*, which contrasts the finding of increased expression of several integrin subunits and other adhesion molecules *in vivo*. This supports the fact that interactions with extracellular matrix proteins and the microenvironment are not adequately reflected in a monolayer system and thus may not be influenced by treatment.

In summary, the comparison of genetic alterations *in vivo* and *in vitro* showed that the renal tubular epithelial cell line NRK-52E was a suitable but limited model to mimic early alterations in genes involved in FB_1-induced nephrotoxicity and carcinogenicity in kidney. As observed in kidneys of male Sprague Dawley rats, several genes involved in tumor formation were observed after FB_1 treatment in the NRK-52E cells that correlated with the increase in sphingoid base 1-phosphates and their biological action. However, the *in vitro* system may not fully resemble the outcome of FB_1-mediated toxicity in kidney, since complex interactions with the ECM, other kidney-specific cell types and blood circulation are not given.

6.4.2 FB_1 enhances the invasive potential of kidney tubular epithelial cells *in vitro*, which correlates with gene expression changes involved in tumor migration and invasion

During tumor invasion, a machinery of proteolytic enzymes is secreted from tumor cells to partially degrade and extensively remodel ECM components, though which tumor cells may break physiological barriers to move towards the vasculature, which facilitates metastatic spread (Geiger and Peeper, 2009). To understand, whether FB_1-induced expression of genes involved in tumor formation may have an impact on the cellular functions of NRK-52E cells, their invasive behavior in an artificial ECM environment consisting of 2% gelatin was investigated after FB_1 treatment. Gelatin, the denaturated form of collagen, was used to resemble the function of a basement membrane that normally surrounds cells to facilitate cell attachment and physiological separation from other tissues.

The present study demonstrated that FB_1 treatment induced the invasion of NRK-52E cell into 2% gelatin, which corresponded well with the observed increase in genes involved in tumor migration and invasion. The effects on the invasive potential of NRK-52E cells were in agreement with the significant upregulation of sphingoid base 1-phosphates that are known to be involved in tumor migration and invasion (Brocklyn, 2010). In this context, the enhanced invasive potential of NRK-52E may be primarily associated with the observed upregulation of genes involved in the plasminogen activator system (*uPA*, *uPAR* and *PAI-1*), which has been shown to be induced through the extracellular action of So1P *via* S1PRs (Bryan *et al.*, 2008; Young *et al.*, 2009) (see 6.2.2).

In the present study, characterization of S1PRs using RT-PCR demonstrated that *S1P$_2$* and *S1P$_3$* were the main receptors expressed in NRK-52E cells, whereas *S1P$_1$* was not detectable. Similar to NRK-52E cells, *S1P$_2$* and *S1P$_3$* were the main receptors identified *in vivo*, but *S1P$_1$* was also found to be slightly expressed in rat kidney. Since a dose-dependent increase in extracellular sphingoid base 1-phosphates was determined after FB_1 treatment *in vitro*, the active transport of these molecules from the intra- to the extracellular compartment may be assumed. Indeed, recent studies identified ABC transporters involved in the active transport of So1P and Sa1P to the extracellular space (Kim *et al.*, 2009; Takabe *et al.*, 2010). Thus, it is conceivable that transport of intracellular sphingoid base 1-phosphates to the extracellular space and their subsequent binding to *S1P$_2$* and *S1P$_3$* might contribute to the increased invasive potential of NRK-52E cells. However, it is also possible that dead cells detached from the cell layer and present in the medium (extracellular) may account for the release of bioactive sphingoid base 1-phosphates that may extracellularly bind to S1PRs *in vitro*.

Interestingly, concentrations of FB_1 (0.5 and 5 µM) that resulted in lower accumulation and release of sphingoid base 1-phosphates, induced an equal or higher capability of invasion than high concentrations of FB_1 (50 µM) that resulted in higher levels of Sa1P and So1P. This corresponded with the observation that exogenous treatment with high nanomolar (500 nM) to micromolar concentrations (1 and 5 µM) of So1P did not induce increased cell invasion of NRK-52E cells, whereas cell invasion was reduced at 5 µM So1P (see section 5.2.4). In this regard it is interesting to note that high levels of exogenous So1P and Sa1P (µM) were shown to rather inhibit or reduce effects on cell migration, whereas nanomolar concentration stimulated cell migration (Wang *et al.*, 1999; Kimura *et al.*, 2000). This may be explained by the fact that high concentrations of sphingoid base 1-phosphates may result in receptor overstimulation, since S1PRs bind sphingoid base 1-phosphates with high affinity in the nanomolar range (Brocklyn, 2010). Furthermore, it is also possible that increased stimulation of $S1P_2$ compared to $S1P_3$ may account for the anti-migratory effect in response to increased sphingosine 1-phosphate levels, since the receptor $S1P_2$ preferably inhibits cell migration through activation of RHO and subsequent inhibition of RAC (Brocklyn, 2010) (see section 2.4.4.2, Figure 8). On the other hand, it is also possible that increased cytotoxicity (50%) at 50 µM FB_1 concentration reduces the

number of cells that may actively invade through the gelatin matrix compared to the lower, less cytotoxic concentrations.

In summary, the present results indicate a good relationship between gene expression changes of metastasis-associated genes in NRK-52E cells and effects on the invasive potential that both paralleled the FB_1-mediated increase in sphingoid base 1-phosphates, which are known mediators of migration and invasion.

6.4.3 Summary and conclusion

The present study demonstrated that alterations in gene expression of FB_1-treated NRK-52E cells strongly correlated with those found after FB_1 treatment in the animal experiment. These changes mainly comprised the upregulation of genes, which are implicated in tumor formation (*e.g.* proto-oncogenes such as *Jun*, *Fos* and *Myc*), cell cycle control (*e.g. cyclins*, *p21*), DNA damage repair (e.g. *Atm* and *Brca1*), invasion (components of the plasminogen activator system, e.g. *uPAR* (*Plaur*) and *PAI-1* (*Serpine1*)) and metastasis (*e.g. Timp1* and *Nme1*). In compliance with the *in vivo* findings, gene expression changes paralleled the marked alterations in sphingolipid metabolism that involved the intracellular and extracellular increase in sphingoid base 1-phosphates. Given the importance of these bioactive lipids in cancer, a good correlation between FB_1-induced gene expression changes obtained *in vivo* and *in vitro* and those known to be mediated by bioactive sphingoid base 1-phosphates was established. Moreover, experiments modeling the invasive behavior of NRK-52E cells showed that FB_1 may enhance cell invasion, which was associated with increases in invasion- and metastasis-associated genes and sphingoid base 1-phophates. Importantly, NRK-52E cells basally expressed the S1P receptors $S1P_2$ and $S1P_3$, which are known mediators of pathways involved in tumor migration and invasion. Since these receptors were also identified as most abundant S1PRs in kidneys of male Sprague Dawley rats, they may present important mediators of gene expression and invasion in response to FB_1 *in vivo*.

6.5 Hypothetical mode of action and proposed pathways involved in FB_1-mediated tumor formation in rat kidney

Based on the early molecular changes in response to FB_1, a hypothetical mode of action for FB_1 toxicity and carcinogenicity was developed from integrating biochemical alterations in sphingolipid metabolism and genetic alterations in cancer-related genes into signaling pathways involved in tumor formation and progression (Figure 50).

After absorption into the blood, FB_1 may be preferentially taken up into renal tubular epithelial cells *via* OAT transporters (1). In renal cells, FB_1 mediates inhibition of ceramide synthase leading to decreased ceramide levels and intracellular accumulation of pro-apoptotic Sa and So (2). The sphingoid bases may intracellularly stimulate apoptosis *via* inhibition of protein kinases that are involved in proliferation and cell survival, *e.g.* ERK1/2, PKC, AKT and stimulation of pro-apoptotic mediators such as cathepsins, BAX and cytochrome c. The release of cytochrome c from the mitochondrion may then result in the activation of caspases that initiate apoptosis in renal tubular cells. To counterbalance the increase in these pro-apoptotic ceramide precursors, the cells may activate the enzyme SPHK1 that results in increased levels of the anti-apoptotic metabolites Sa1P and So1P and intracellular signaling cascades (3). The **intracellular action** of these bioactive lipids may lead to the upregulation of transcription factors such as MYC that are involved in cell proliferation (4). For instance, MYC may induce the gene expression of the cell cycle promoters like *Cyclin E* and *Cdc25a*, which positively regulate cell proliferation (5). Besides its role in intracellular signaling, Sa1P/So1P may also exert **extracellular actions** by binding to their high affinity GPCRs $S1P_{1\text{-}3}$ (6). As shown in our study, the expression of $S1P_2$ and $S1P_3$ was most abundant in kidney and may therefore account for the major biological effects mediated by exogenous sphingoid base 1-phosphates. Coupling of So1P/Sa1P to their receptors may initiate G-protein-dependent (*e.g.* RAS/RAF/MEK) and –independent (e.g. PI3K signaling) S1PR signaling pathways (7). The induction of RAS/RAF/MEK signaling pathways may primarily be involved in the upregulation of oncogenic transcriptions factors, such as *Jun* and *Fos*, which form the AP-1 transcription factor complex (8). Different transcription factors (such as AP-1, ETS-2) may induce the increased expression of pro-angiogenic genes, *e.g. Egfr*, *Tek*, *Hgf* and *Met* (*Hgfr*) (9). Furthermore, S1PR signaling may enhance the expression of

genes that suppress apoptosis and thus promote cell survival, *e.g. Bcl-Xl* and *Bcl2* (10). Importantly, S1PR signaling may increased the expression of invasion- and metastasis-associated genes, such as *PAI-1* and *uPAR*, as well as genes promoting their expression, *e.g. Thbs1* and *Tgfb1* (11). An increase in the metastasis-associated genes *Icam1* and *Muc1* may be crucially involved in tumor intraversation and adhesion (11). In addition to directly mediate cell signaling, S1PR may **transactivate** other receptors (e.g. RTKs and integrins) related to signaling pathways in cancer. The **transactivation of RTKs** like MET (HGFR) and EGFR which are known to be critically involved in renal carcinogenesis may induce RAS signaling and activation of PI3K (12). The activation of PI3K/RAC/FAK pathways may promote cell migration (13). Activation of PI3K may also induce AKT signaling and mediate the suppression of apoptosis *via* multiple pathways. This involves inhibition of NFκBIA, GSK-3B and pro-apoptotic molecules such as BAX to facilitate the pro-survival function of NFκB, beta-catenin and BCL-XL/BCL2 (14). Furthermore, AKT may also mediate RAS/RAF/ERK signaling and thus amplify the S1PR-induced expression of oncogenic transcription factors and their downstream targets (15). The **transactivation of integrins** by $S1P_{1/3}$ may enhance cell migration *via* RAC/FAK pathways (16). The gene expression of integrin subunits such as *Itga2* and *Itgav* may also be increased by exogenous So1P bound to S1PRs (17). A further possibility to influence gene expression is reflected by the **nuclear action** of So1P that results in the inhibition of HDAC1/2 and direct modulation of gene expression of *e.g*. *Fos* and *p21* (18). Cytoplasmatic retention of p21 by *e.g.* AKT (14) may inhibit the nuclear tumor suppressor function of p21. Increased cytoplasmatic p21 may suppress apoptosis and thus facilitate survival. As shown by these pathways, exogenous and endogenous sphingoid base 1-phosphates may reinforce to activation of signals involved in regenerative cell proliferation in response to marked renal tubular damage caused by FB_1. As a result sustained proliferation signals may lead to uncontrolled growth and renal tumor formation in response to FB_1.

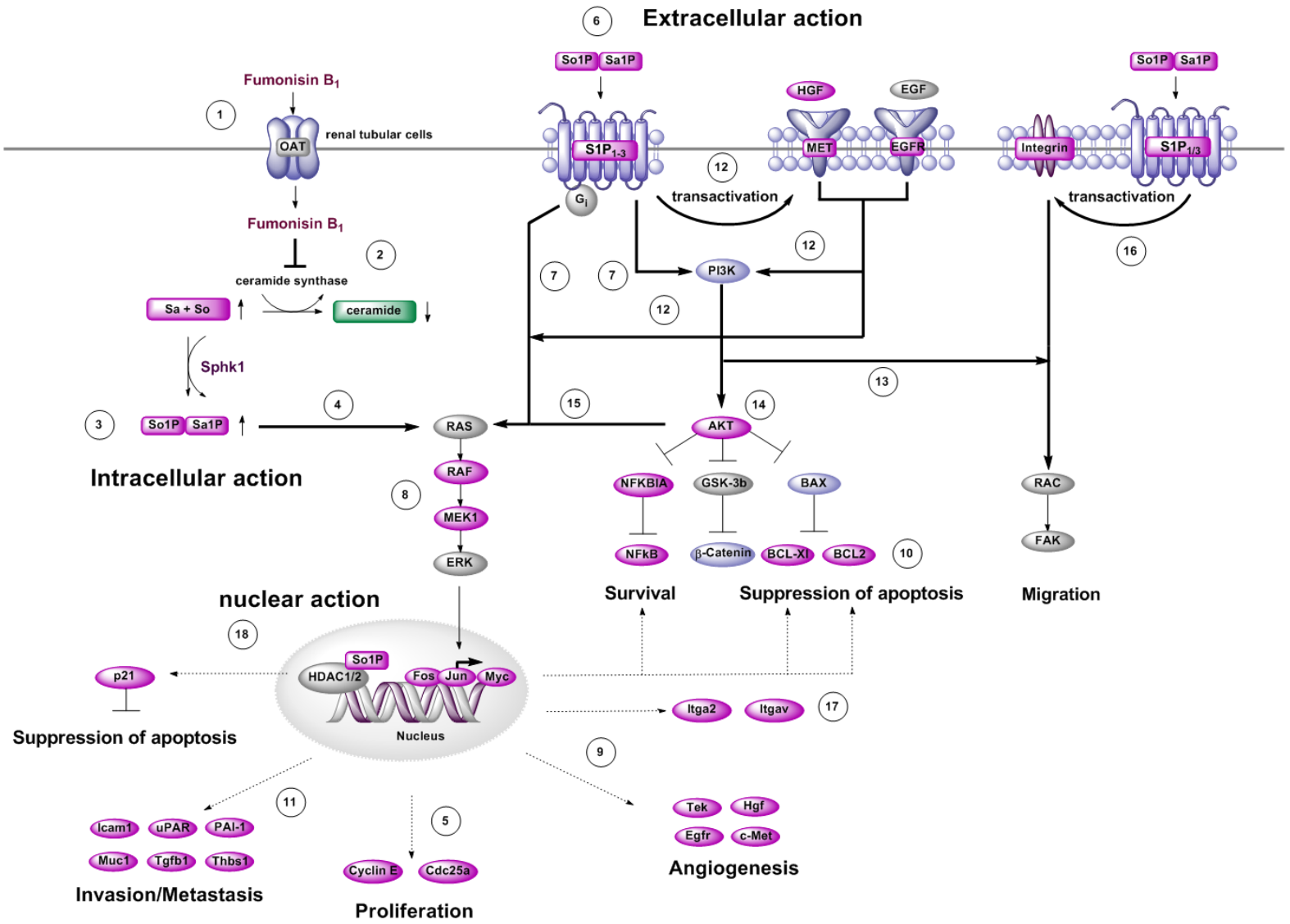

Figure 50: Hypothetical mode of action and proposed pathways involved in early toxicological effects contributing to possible tumor formation in rat kidney. Genes analyzed after FB_1 treatment in kidneys of male Sprague Dawley rats were integrated in sphingoid base 1-phosphate-mediated signaling pathways. Colors indicate: genes/sphingolipids **upregulated** in response to FB_1 (**pink**), genes/sphingolipids downregulated in response to FB_1 (**green**), genes **not regulated** by FB_1 (**light blue**), genes involved in pathway but **not analyzed** in response to FB_1 (**grey**).Number 1-18 are more detailed described in chapter 6.5. The abbreviations of genes analyzed after FB_1 treatment are listed in section 4.2.3.2 in Table 8.

7 Summary

Fumonisin B_1 (FB_1) is a mycotoxin produced by various *Fusarium* species and constitutes a major contaminant of maize worldwide. A 2-year carcinogenicity study of the National Toxicology Program (NTP) in Fischer N344 rats showed that male rats were most susceptible to FB_1-induced tumor formation in the kidney. Histopathologically, a rare and highly malignant tumor type originating from the proximal tubules of rat kidney with increased potential for invasion and metastasis was identified. However, mechanisms underlying the FB_1-induced carcinogenesis in kidneys of male rats are still not clear.

Previous studies have shown that FB_1-mediated disruption of sphingolipid metabolism *via* inhibition of ceramide synthase is a primary key event in FB_1 toxicity. The disruption of sphingolipid metabolism may cause time- and dose-related changes in the relative balance of various bioactive intermediates. Furthermore, the ability of FB_1 to induce renal cell death and subsequent compensatory cell proliferation is well known, but it does not completely explain the invasive growth characteristics and exceptionally high metastatic potential of FB_1-induced tumors. Considering the complexity of sphingolipid metabolism and the fact that various sphingolipids (*e.g.* ceramide, sphingoid bases and their respective 1-phosphates) act on opposing signaling pathways, it is hypothesized that the balance between individual sphingolipids and thus the overall cellular response to FB_1 may shift with time and by continuing FB_1 exposure, resulting in the disruption of specific cell signaling pathways, which may promote tumor formation in kidney.

To identify early FB_1-induced gene expression patterns in the kidney, which may be associated with sphingolipid-mediated signaling pathways in cancer, a short-term *i.p.* study on FB_1 in male Sprague Dawley rats was performed and changes in gene expression were analyzed using a qRT-PCR array that comprises 84 relevant genes of 6 pathways pivotally involved in the formation of cancer. Furthermore, apoptosis and cell proliferation as well as changes in specific sphingolipids were investigated in FB_1-treated kidneys. As shown by classical histopathology (H&E) and (immuno)-histochemical staining (TUNEL and BrdU), FB_1 caused a time- and dose-dependent increase in tubular apoptosis in the cortex and OSOM of the kidney, which was compensated by the induction of proliferation in the affected areas. HPLC-MS/MS

analysis of bioactive sphingolipids demonstrated that FB_1 induced a marked elevation of the pro-apoptotic sphingoid bases sphinganine and sphingosine, which paralleled the time- and dose-dependent increase in renal tubular apoptosis. With prolonged exposure to FB_1, increased metabolic conversion of the accumulated sphinganine to the sphinganine-1-phosphate, a second messenger with anti-apoptotic and proliferative properties, was observed in kidney. This finding was compliant with the increased regenerative cell proliferation in the cortex and OSOM. In addition to effects on sphingoid bases and their 1-phosphate metabolites, this study, for the first time, demonstrated reduced levels of specific ceramides in rat kidney after FB_1 exposure. In particular, C16-ceramide, which is a widespread constituent of membrane-bound complex sphingolipids involved in cell adhesion, was time- and dose-dependently decreased after treatment with FB_1. Besides its role as component of the cell membrane, C16-ceramide functions as a signaling molecule for the initiation of apoptosis in response to various stress stimuli. Under conditions of chronic FB_1 exposure, a significant reduction in pro-apoptotic C16-ceramide together with markedly increased levels of anti-apoptotic and proliferation-promoting sphingoid base 1-phosphates may thus favor resistance to stress-induced apoptosis and facilitate the survival of abnormal cells with potential to initiate tumor formation.

Our study also revealed that early exposure to FB_1 resulted in increased expression of a plethora of genes involved in tumor initiation as well as tumor progression. While single FB_1 exposure was demonstrated to predominately induce gene expression of proto-oncogenic transcription factors (e.g. *Fos*, *Jun*, *Myc*) and apoptotis-related genes (e.g. members of the tumor-necrosis factor family), repeated exposure resulted in marked upregulation of genes mediating cell survival and cell proliferation (e.g. *Bcl-XL*, *Bcl-2*, *Nfκb1* and *Egfr*). Moreover, continued exposure to FB_1 initiated increased expression of genes critically involved in tumor migration, adhesion, invasion and metastasis. A close correlation was established between gene expression changes in response to FB_1 and known signaling pathways mediated by extracellular or intracellular action of sphingoid base 1-phosphates - bioactive lipids that were markedly increased after FB_1 treatment. In particular, genes encoding components of the plasminogen activator system were abundantly upregulated. These mediate invasion and metastasis in response to So1P, and may hence particularly promote the formation of highly aggressive and invasive tumors in kidney as observed after chronic exposure to FB_1. Thus, it is conceivable that upregulation of a majority of

genes in response to FB_1 may be a direct or indirect consequence of increased So1P signaling.

Another aim of this study was to identify differences in the organ-specific susceptibility for tumor formation by comparing FB_1-mediated effects on apoptosis, cell proliferation, sphingolipids, and selected cancer-related genes in kidney and liver. Collectively, the present results revealed that kidney and liver showed marked differences in several endpoints of FB_1 toxicity, which seemed to be primarily associated with their different susceptibility to FB_1-mediated alterations in sphingolipid metabolism. The strong correlation between histopathological lesions and alterations in sphingolipid metabolism as well as sphingoid base 1-phosphate accumulation and concomitant S1P receptor expression suggested that tumor formation and progression to highly malignant carcinomas seems to be rather favored in kidney compared to liver. However, genes mostly deregulated by FB_1 treatment in kidney (*PAI-1*, *Thbs1* and *Itga2*) were also found to be induced in liver.

To verify FB_1-induced gene expression in kidney, normal rat tubular epithelial (NRK-52E) cells were analyzed for FB_1-induced expression changes of the same cancer-related genes as *in vivo*. The results of qRT-PCR analysis revealed that gene expression changes in NRK-52E cells after FB_1 treatment strongly correlated with those found in rat kidney and paralleled the marked alterations in sphingolipid metabolism. Furthermore, a good correlation between FB_1-induced expression changes of cancer-related genes obtained *in vivo* and *in vitro* and those known to be mediated by bioactive sphingoid base 1-phosphates in cancer was established. Moreover, experiments modeling the invasive behavior of NRK-52E cells showed that FB_1 may enhance cell invasion, which also correlated with both the increase in invasion- and metastasis-associated genes and bioactive sphingoid base 1-phophates. Importantly, NRK-52E cells basally expressed the S1P receptors $S1P_2$ and $S1P_3$, which are known to be involved in tumor migration and invasion. Since these receptors were also identified as most abundant S1PRs in kidneys of male Sprague Dawley rats, they may present important mediators of gene expression and invasion in response to FB_1 *in vivo*.

In summary, FB_1-mediated disruption of sphingolipid metabolism and subsequent time- and dose-related increase in intermediates, such as bioactive sphingoid base 1-phosphates, correlate with early changes in genes and signaling pathways that may mediate loss of growth control, replication, evasion of apoptosis, cell motility and

invasion, and thus favor renal tumor formation in response to FB_1. However, to clarify whether the obtained gene expression changes in cancer-related genes in kidney are specific to the biological action of sphingoid base 1-phosphates and their respective receptors, further mechanistic studies are necessary.

8 Zusammenfassung

Fumonisin B_1 ist ein Mykotoxin, das von verschiedenen Spezies der Gattung *Fusarium* produziert wird, und weltweit wesentlich zur Kontamination von Mais beiträgt. Eine zweijährige Kanzerogenitätsstudie des National Toxicology Programs (NTP) zeigte, dass männliche Ratten nach Verabreichung von FB_1 am anfälligsten für die Bildung von Nierentumoren waren. Aus histopathologischer Sicht handelte es sich dabei um sehr seltene und hoch maligne Formen von Tumoren des proximalen Tubulus der Niere, die eine verstärkte Neigung zur Invasion und Metastasierung aufwiesen. Jedoch sind bis heute die genauen Mechanismen nicht hinreichend geklärt, die zu einer FB_1-induzierten Kanzerogenese in der Rattenniere führen können.

Frühere Studien berichteten, dass die durch FB_1 vermittelte Störung des Sphingolipidmetabolismus mittels Inhibierung der Ceramidesynthase ein initiales Ereignis in der Toxizität darstellt und zu zeit- und dosisabhängigen Veränderungen im relativen Gleichgewicht verschiedener bioaktiver Zwischenprodukte des Sphingolipid-metabolismus führen kann. Des Weiteren ist bekannt, dass FB_1 dazu in der Lage ist, in der Niere Zelltod gefolgt von regenerativer Zellproliferation zu induzieren. Dies erklärt jedoch nicht vollständig, wie die durch FB_1 verursachten Tumoren ein invasives Wachstum und außergewöhnlich hohes Metastasierungspotential erlangen. Die Komplexität des Sphingolipidmetabolismus und die Tatsache, dass verschiedene Sphingolipide (z.B. Ceramide, Sphingoidbasen und ihre entsprechenden 1-Phosphate) einen Einfluss auf gegensätzliche Signalwege in der Zelle ausüben können, deuten darauf hin, dass das Gleichgewicht zwischen den einzelnen Sphingolipiden und somit die gesamten zellulären Effekte von FB_1 über die Zeit und mit zunehmender Exposition gegenüber FB_1 zu Störungen spezifischer Signalwegen führen können, die eine Tumorentstehung in der Niere begünstigen.

Um frühere Effekte von FB_1 auf das Expressionsmuster von Genen in der Niere zu ermitteln, die möglicherweise mit den durch Sphingolipide vermittelten Signalwegen und Krebs verbunden sind, wurde eine Kurzzeitstudie mit FB_1 in männlichen Sprague Dawley-Ratten durchgeführt und die Veränderungen der Genexpression von 84 Genen der 6 wichtigsten, krebsrelevanten Signalwege mittels qRT-PCR untersucht. In diesem Zusammenhang wurden in Nieren der FB_1-behandelten Tiere auch

Untersuchungen zu Apoptose, Zellproliferation sowie zu Veränderungen der spezifischen Sphingolipide durchgeführt. Anhand klassischer histopatholgischer sowie (immun)-histologischer Färbungen konnte gezeigt werden, dass FB_1 zu einem zeit- und dosisabhängigen Anstieg von Apoptose in Cortex und OSOM der Niere führte, dem gleichzeitig eine gesteigerte Proliferation in den entsprechenden Bereichen folgte. Die HPLC-MS/MS-Analyse bioaktiver Sphingolipide in der Niere zeigte, dass die Behandlung mit FB_1 zeitgleich zu einem Anstieg der pro-apoptotischen Sphingoidbasen Sphinganin und Sphingosin und verstärkter tubulärer Apoptose führte. Mit anhaltender Exposition gegenüber FB_1 konnte in der Niere eine Zunahme der metabolischen Umwandlung von Sphinganin in Sphinganine-1-Phosphat, einem sekundären Botenstoff mit anti-apoptotischen und wachstumsfördernden Eigenschaften, beobachtet werden. Diese Beobachtung stimmte auch mit der verstärkten regenerativen Zellproliferation in Cortex und OSOM der Niere überein. Weiterhin konnte mittels Sphingolipidanalyse erstmals gezeigt werden, dass die Exposition gegenüber FB_1 zu einer Verminderung spezifischer Zellceramide führte. Insbesondere der Gehalt an C16-Ceramid wurden durch die Behandlung mit FB_1 zeit- und dosishängig in der Niere reduziert. Neben seiner Funktion als Bestandteil der Zellmembran spielt C16-Ceramide eine wichtige Rolle als Grundbaustein von komplexen, Zelladhäsion fördernden Sphingolipiden und ist in Gegenwart verschiedener Stressfaktoren auch ein wichtiges Signalmolekül in der Initiierung von Apoptose. Im Fall einer chronischen Exposition gegenüber FB_1 könnten demnach stark verminderte Gehalte an pro-apoptotischen C16-Ceramid, verbunden mit drastisch erhöhten Gehalten an anti-apoptotischen und wachstumsfördernden Sphingoidbasen-1-Phosphaten, zu einer Resistenz gegenüber stressbedingter Apoptose führen, die das Überleben initiierter Zellen und damit die Tumorentstehung begünstigen.

Weiterhin zeigte unsere Studie, dass bereits eine frühe Exposition gegenüber FB_1 die Expression einer Reihe von Genen in der Niere erhöht, die in der Tumorentstehung- sowie Progression eine Rolle spielen. Während die einmalige Verabreichung von FB_1 hauptsächlich zu einem Anstieg der Expression von Transkriptionsfaktoren (z.B. Protoonkogene wie *Fos*, *Jun* und *Myc*) und apoptotischen Gene (z.B. Mitglieder der Familie der Tumornekrosefaktorrezeptoren) führte, wurde nach mehrmaliger Exposition eine deutliche Heraufregulierung von Genen beobachtet, die das Wachstum und Überleben von Zellen (z.B: *Bcl-XL*, *Bcl-2*, *Nfκb1* und *Egfr*) vermitteln.

Des Weiteren führte die längere Exposition zu einem Anstieg der Expression von Genen, die entscheidend an Migration, Adhäsion, Invasion und Metastasierung von Tumoren beteiligt sind. Dabei konnte ein enger Zusammenhang zwischen den FB_1-induzierten Genexpressionsveränderungen und bereits bekannten extrazellulären und intrazellulären Signalwegen von bioaktiven Sphingoidbasen-1-Phosphaten hergestellt werden. Dazu zählte vor allem die Erhöhung von Genen, die wichtige Komponenten des ‚Plasminogen-Aktivator'-Systems kodieren, und in Gegenwart von Sphingosine-1-Phosphat zu einer Erhöhung der Invasivität und Metastasierung, und somit möglicherweise auch zu einer begünstigten Bildung hochaggressiver und invasiver Tumoren in der Niere nach chronischer Exposition gegenüber FB_1 beitragen können.

Ein weiteres Ziel der Studie war es, mögliche Unterschiede in der organspezifischen Disposition für die Entstehung von Tumoren zu ermitteln, indem die FB_1-vermittelten Effekte auf Apoptose, Zellproliferation, Sphingolipide, und ausgewählte krebsrelevante Gene zwischen Niere und Leber verglichen wurden. Zusammenfassend weisen die Ergebnisse darauf hin, dass zwischen Niere und Leber deutliche Unterschiede in den verschiedenen Endpunkten der FB_1-vermittelten Toxizität existieren, welche hauptsächlich mit der unterschiedlichen Anfälligkeit gegenüber den FB_1-induzierten Veränderungen des Sphingolipidmetabolismus in Zusammenhang gebracht werden. Anhand der starken Korrelation zwischen den beobachteten histopathologischen Läsionen und gleichzeitig starken Veränderungen im Sphingolipidmetabolismus, sowie der Akkumulation von Sphingoidbasen-1-Phosphaten und entsprechender Expression der Sphingosine-1-Phosphatrezeptoren in der Niere, lässt sich vermuten, dass die Tumorentstehung- und Progression zu hoch malignen Karzinomen eher in der Niere als in der Leber begünstigt ist. Die durch die FB_1-Behandlung am stärksten deregulierten Gene (*PAI-1*, *Thbs1* und *Itga2*) in der Niere, wurden jedoch auch in der Leber durch FB_1 induziert.

Um die Genexpressionsveränderungen in der Niere zu verifizieren, wurden Ratten-tubulusepithelzellen (NRK-52E-Zellen) mit FB_1 behandelt und Veränderungen in der Expression der gleichen krebsrelevanter Gene, die zuvor *in vivo* untersucht wurden, analysiert. Die Ergebnisse der qRT-PCR-Analyse zeigten, dass die Genexpressions-veränderungen in NRK-52E-Zellen nach Behandlung mit FB_1 sowie die damit verbundenen Veränderungen im Sphingolipidmetabolismus stark mit denen in der Rattenniere korrelierten. Es konnte zudem sowohl *in vivo* als auch *in vitro* eine gute

Übereinstimmung der FB_1-induzierten Veränderungen in der Expression krebsrelevanter Gene gefunden werden, die auch in Signalwegen von Sphingoidbasen-1-Phosphaten und der damit verbundenen Krebsentstehung eine Rolle spielen. Darüber hinaus zeigten Experimente zur Untersuchung der Invasivität von NRK-52E-Zellen, dass diese nach Behandlung mit FB_1 ein höheres Invasionspotential aufweisen. Dies korrelierte sowohl mit der Beobachtung von Expressionserhöhungen von invasions- und metastasierungsfördernden Genen als auch dem Anstieg bioaktiver Sphingoidbasen-1-Phosphate. Interessanterweise konnte in der vorliegenden Studie festgestellt werden, dass NRK-52E-Zellen die Sphingosine-1-phosphatrezeptoren $S1P_2$ und $S1P_3$ expremieren und über diese Rezeptoren möglicherweise Signalwege zur Migration und Invasion anregen können. Da $S1P_2$ und $S1P_3$ auch als Hauptsphingosine-1-Phosphatrezeptoren in der Rattenniere identifiziert wurden, lässt sich vermuten, dass diese nach FB_1-Behandlung *in vivo* wesentlich zur Expression von Genen, die die Invasivität von Zellen erhöhen, beitragen können.

Zusammenfassend deuten die Ergebnisse darauf hin, dass die FB_1-vermittelte Störung im Sphingolipidmetabolismus und der damit verbundene zeit- und dosisabhängige Anstieg bioaktiver Intermediate wie den Sphingoidbasen-1-Phosphaten, zu frühen Veränderungen in Genen und Signalwegen führen kann. Diese können Zellwachstum, Inhibierung von Apoptose, Migration und Invasion und somit die Bildung von Nierentumoren nach Exposition gegenüber FB_1 fördern. Um jedoch zu klären, ob die ermittelten Genexpressionsveränderungen der untersuchten krebsrelevanten Genen in der Niere spezifisch mit der Wirkung von Sphingoidbasen-1-Phosphaten und deren Rezeptoren zusammenhängen, sind weiterführende mechanistische Studien notwendig.

9 References

Abado-Becognee, K., Mobio, T. A., Ennamany, R., Fleurat-Lessard, F., Shier, W. T., Badria, F., and Creppy, E. E. (1998). Cytotoxicity of fumonisin B1: implication of lipid peroxidation and inhibition of protein and DNA syntheses. *Arch Toxicol* **72**, 233-236.

Abel, S., and Gelderblom, W. C. (1998). Oxidative damage and fumonisin B1-induced toxicity in primary rat hepatocytes and rat liver in vivo. *Toxicology* **131**, 121-131.

Abukhdeir, A. M., and Park, B. H. (2008). P21 and p27: roles in carcinogenesis and drug resistance. *Expert Rev Mol Med* **10**, e19.

Adamson, E. D., and Wiley, L. M. (1997). The EGFR gene family in embryonic cell activities. *Curr Top Dev Biol* **35**, 71-120.

Adhikary, S., and Eilers, M. (2005). Transcriptional regulation and transformation by Myc proteins. *Nat Rev Mol Cell Biol* **6**, 635-645.

Albo, D., Arnoletti, J. P., Castiglioni, A., Granick, M. S., Solomon, M. P., Rothman, V. L., and Tuszynski, G. P. (1994). Thrombospondin (TSP) and transforming growth factor beta 1 (TGF-beta) promote human A549 lung carcinoma cell plasminogen activator inhibitor type 1 (PAI-1) production and stimulate tumor cell attachment in vitro. *Biochem Biophys Res Commun* **203**, 857-865.

Albo, D., Berger, D. H., Vogel, J., and Tuszynski, G. P. (1999). Thrombospondin-1 and transforming growth factor beta-1 upregulate plasminogen activator inhibitor type 1 in pancreatic cancer. *J Gastrointest Surg* **3**, 411-417.

Albo, D., Berger, D. H., Wang, T. N., Hu, X., Rothman, V., and Tuszynski, G. P. (1997). Thrombospondin-1 and transforming growth factor-beta I promote breast tumor cell invasion through up-regulation of the plasminogen/plasmin system. *Surgery* **122**, 493-499; discussion 499-500.

Alvarez, S. E., Milstien, S., and Spiegel, S. (2007). Autocrine and paracrine roles of sphingosine-1-phosphate. *Trends Endocrin Met* **18**, 300-307.

An, S., Zheng, Y., and Bleu, T. (2000). Sphingosine 1-phosphate-induced cell proliferation, survival, and related signaling events mediated by G protein-coupled receptors Edg3 and Edg5. *J Biol Chem* **275**, 288-296.

Anzai, N., Kanai, Y., and Endou, H. (2006). Organic anion transporter family: current knowledge. *J Pharmacol Sci* **100**, 411-426.

Aranda, M., Perez-Alzola, L. P., Ellahuene, M. F., and Sepulveda, C. (2000). Assessment of in vitro mutagenicity in Salmonella and in vivo genotoxicity in mice of the mycotoxin fumonisin B1. *Mutagenesis* **15**, 469-471.

Aref, S., Fouda, M., El-Dosoky, E., Menessy, A., Mabed, M., Saleeb, M., and Zalata, K. (2003). c-Myc oncogene and Cdc25A cell activating phosphatase expression in non-Hodgkin's lymphoma. *Hematology* **8**, 183-190.

Arnoletti, J. P., Albo, D., Granick, M. S., Solomon, M. P., Castiglioni, A., Rothman, V. L., and Tuszynski, G. P. (1995). Thrombospondin and transforming growth factor-beta 1 increase expression of urokinase-type plasminogen activator and plasminogen activator inhibitor-1 in human MDA-MB-231 breast cancer cells. *Cancer* **76**, 998-1005.

Atroshi, F., Rizzo, A., Biese, I., Veijalainen, P., Saloniemi, H., Sankari, S., and Andersson, K. (1999). Fumonisin B1-induced DNA damage in rat liver and spleen: effects of pretreatment with coenzyme Q10, L-carnitine, alpha -tocopherol, and selenium. *Pharmacological Research* **40**, 459-467.

Avery, K., Avery, S., Shepherd, J., Heath, P. R., and Moore, H. (2008). Sphingosine-1-phosphate mediates transcriptional regulation of key targets associated with survival, proliferation, and pluripotency in human embryonic stem cells. *Stem Cells Dev* **17**, 1195-1205.

Barlow, S., and Schlatter, J. (2010). Risk assessment of carcinogens in food. *Toxicol Appl Pharmacol* **243**, 180-190.

Bartek, J., Falck, J., and Lukas, J. (2001). CHK2 kinase--a busy messenger. *Nat Rev Mol Cell Biol* **2**, 877-886.

Bartke, N., and Hannun, Y. A. (2009). Bioactive sphingolipids: metabolism and function. *J Lipid Res* **50 Suppl**, S91-96.

Bayless, K. J., and Davis, G. E. (2003). Sphingosine-1-phosphate markedly induces matrix metalloproteinase and integrin-dependent human endothelial cell invasion and lumen formation in three-dimensional collagen and fibrin matrices. *Biochem Biophys Res Commun* **312**, 903-913.

Behbahani, T. E., Thierse, C., Baumann, C., Holl, D., Bastian, P. J., von Ruecker, A., Muller, S. C., Ellinger, J., and Hauser, S. (2011). Tyrosine kinase expression profile in clear cell renal cell carcinoma. *World J Urol*.

Benford, D., Bolger, P. M., Carthew, P., Coulet, M., DiNovi, M., Leblanc, J. C., Renwick, A. G., Setzer, W., Schlatter, J., Smith, B., Slob, W., Williams, G., and Wildemann, T. (2010). Application of the Margin of Exposure (MOE) approach to substances in food that are genotoxic and carcinogenic. *Food Chem Toxicol* **48 Suppl 1**, S2-24.

Berdyshev, E. V., Gorshkova, I., Skobeleva, A., Bittman, R., Lu, X., Dudek, S. M., Mirzapoiazova, T., Garcia, J. G., and Natarajan, V. (2009). FTY720 inhibits ceramide synthases and up-regulates dihydrosphingosine 1-phosphate formation in human lung endothelial cells. *J Biol Chem* **284**, 5467-5477.

Besson, A., Dowdy, S. F., and Roberts, J. M. (2008). CDK inhibitors: cell cycle regulators and beyond. *Dev Cell* **14**, 159-169.

Best, C. J., Tanzer, L. R., Phelps, P. C., Merriman, R. L., Boder, G. G., Trump, B. F., and Elliget, K. A. (1999). H-ras-transformed NRK-52E renal epithelial cells have altered growth, morphology, and cytoskeletal structure that correlates with renal cell carcinoma in vivo. *In Vitro Cell Dev Biol Anim* **35**, 205-214.

Bhandari, N., and Sharma, R. P. (2002a). Fumonisin B1-induced alterations in cytokine expression and apoptosis signaling genes in mouse liver and kidney after an acute exposure. *Toxicology* **172**, 81-92.

Bhandari, N., and Sharma, R. P. (2002b). Modulation of selected cell signaling genes in mouse liver by fumonisin B1. *Chemico-Biological Interactions* **139**, 317-331.

Bielawski, J., Pierce, J. S., Snider, J., Rembiesa, B., Szulc, Z. M., and Bielawska, A. (2009). Comprehensive quantitative analysis of bioactive sphingolipids by high-performance liquid chromatography-tandem mass spectrometry. *Methods Mol Biol* **579**, 443-467.

Bielawski, J., Szulc, Z. M., Hannun, Y. A., and Bielawska, A. (2006). Simultaneous quantitative analysis of bioactive sphingolipids by high-performance liquid chromatography-tandem mass spectrometry. *Methods* **39**, 82-91.

Bierie, B., and Moses, H. L. (2006). Tumour microenvironment: TGFbeta: the molecular Jekyll and Hyde of cancer. *Nat Rev Cancer* **6**, 506-520.

Birchmeier, C., Birchmeier, W., Gherardi, E., and Vande Woude, G. F. (2003). Met, metastasis, motility and more. *Nat Rev Mol Cell Biol* **4**, 915-925.

Bjorklund, M., and Koivunen, E. (2005). Gelatinase-mediated migration and invasion of cancer cells. *Biochim Biophys Acta* **1755**, 37-69.

Blasi, F., and Carmeliet, P. (2002). uPAR: a versatile signalling orchestrator. *Nat Rev Mol Cell Biol* **3**, 932-943.

Boccaccio, C., and Comoglio, P. M. (2006). Invasive growth: a MET-driven genetic programme for cancer and stem cells. *Nat Rev Cancer* **6**, 637-645.

Bondy, G., Barker, M., Mueller, R., Fernie, S., Miller, J. D., Armstrong, C., Hierlihy, S. L., Rowsell, P., and Suzuki, C. (1996). Fumonisin B1 toxicity in male Sprague-Dawley rats. *Adv Exp Med Biol* **392**, 251-264.

Bondy, G., Suzuki, C., Barker, M., Armstrong, C., Fernie, S., Hierlihy, L., Rowsell, P., and Mueller, R. (1995). Toxicity of fumonisin B1 administered intraperitoneally to male Sprague-Dawley rats. *Food Chem Toxicol* **33**, 653-665.

Bondy, G. S., Barker, M. G., Lombaert, G. A., Armstrong, C. L., Fernie, S. M., Gurofsky, S., Huzel, V., Savard, M. E., and Curran, I. H. A. (2000). A comparison of clinical, histopathological and cell-cycle markers in rats receiving the fungal toxins fumonisin B1 or fumonisin B2 by intraperitoneal injection. *Food and Chemical Toxicology* **38**, 873-886.

Boutros, R., Lobjois, V., and Ducommun, B. (2007). CDC25 phosphatases in cancer cells: key players? Good targets? *Nat Rev Cancer* **7**, 495-507.

Boyden, S. (1962). The chemotactic effect of mixtures of antibody and antigen on polymorphonuclear leucocytes. *J Exp Med* **115**, 453-466.

Brady, R. O., and Koval, G. J. (1958). The enzymatic synthesis of sphingosine. *J Biol Chem* **233**, 26-31.

Breitkopf, K., Sawitza, I., Westhoff, J. H., Wickert, L., Dooley, S., and Gressner, A. M. (2005). Thrombospondin 1 acts as a strong promoter of transforming growth factor beta effects via two distinct mechanisms in hepatic stellate cells. *Gut* **54**, 673-681.

Brocklyn, J. R. (2010). Regulation of cancer cell migration and invasion by sphingosine-1-phosphate. *World J Biol Chem* **1**, 307-312.

Brunckhorst, M. K., Wang, H., Lu, R., and Yu, Q. (2010). Angiopoietin-4 promotes glioblastoma progression by enhancing tumor cell viability and angiogenesis. *Cancer Res* **70**, 7283-7293.

Bryan, L., Paugh, B. S., Kapitonov, D., Wilczynska, K. M., Alvarez, S. M., Singh, S. K., Milstien, S., Spiegel, S., and Kordula, T. (2008). Sphingosine-1-phosphate and interleukin-1 independently regulate plasminogen activator inhibitor-1 and urokinase-type plasminogen activator receptor expression in glioblastoma cells: implications for invasiveness. *Mol Cancer Res* **6**, 1469-1477.

Bu, S., Yamanaka, M., Pei, H., Bielawska, A., Bielawski, J., Hannun, Y. A., Obeid, L., and Trojanowska, M. (2006). Dihydrosphingosine 1-phosphate stimulates MMP1 gene expression via activation of ERK1/2-Ets1 pathway in human fibroblasts. *FASEB J* **20**, 184-186.

Burns, T. D., Snook, M. E., Riley, R. T., and Voss, K. A. (2008). Fumonisin concentrations and in vivo toxicity of nixtamalized Fusarium verticillioides culture material: Evidence for fumonisin-matrix interactions. *Food Chem Toxicol* **46**, 2841-2848.

Cai, Q., Tang, L., and Wang, J. S. (2007). Validation of fumonisin biomarkers in F344 rats. *Toxicol Appl Pharmacol* **225**, 28-39.

Carman, G. M., and Han, G. S. (2009). Phosphatidic acid phosphatase, a key enzyme in the regulation of lipid synthesis. *J Biol Chem* **284**, 2593-2597.

Chen, M., Matsuda, H., Wang, L., Watanabe, T., Kimura, M. T., Igarashi, J., Wang, X., Sakimoto, T., Fukuda, N., Sawa, M., and Nagase, H. (2010). Pretranscriptional regulation of Tgf-beta1 by PI polyamide prevents scarring and accelerates wound healing of the cornea after exposure to alkali. *Mol Ther* **18**, 519-527.

Chirco, R., Liu, X. W., Jung, K. K., and Kim, H. R. (2006). Novel functions of TIMPs in cell signaling. *Cancer Metastasis Rev* **25**, 99-113.

Ciacci-Zanella, J. R., Merrill, A. H., Jr., Wang, E., and Jones, C. (1998). Characterization of cell-cycle arrest by fumonisin B1 in CV-1 cells. *Food Chem Toxicol* **36**, 791-804.

Colie, S., Codogno, P., Levade, T., and Andrieu-Abadie, N. (2010). Regulation of cell death by sphingosine 1-phosphate lyase. *Autophagy* **6**, 426-427.

Colie, S., Van Veldhoven, P. P., Kedjouar, B., Bedia, C., Albinet, V., Sorli, S. C., Garcia, V., Djavaheri-Mergny, M., Bauvy, C., Codogno, P., Levade, T., and Andrieu-Abadie, N. (2009). Disruption of sphingosine 1-phosphate lyase confers resistance to chemotherapy and promotes oncogenesis through Bcl-2/Bcl-xL upregulation. *Cancer Res* **69**, 9346-9353.

Corso, S., Migliore, C., Ghiso, E., De Rosa, G., Comoglio, P. M., and Giordano, S. (2008). Silencing the MET oncogene leads to regression of experimental tumors and metastases. *Oncogene* **27**, 684-693.

Coste, O., Brenneis, C., Linke, B., Pierre, S., Maeurer, C., Becker, W., Schmidt, H., Gao, W., Geisslinger, G., and Scholich, K. (2008). Sphingosine 1-phosphate modulates spinal nociceptive processing. *J Biol Chem* **283**, 32442-32451.

Crispe, I. N. (2009). The liver as a lymphoid organ. *Annu Rev Immunol* **27**, 147-163.

Croucher, D. R., Saunders, D. N., Lobov, S., and Ranson, M. (2008). Revisiting the biological roles of PAI2 (SERPINB2) in cancer. *Nat Rev Cancer* **8**, 535-545.

Currie, M. J., Gunningham, S. P., Turner, K., Han, C., Scott, P. A., Robinson, B. A., Chong, W., Harris, A. L., and Fox, S. B. (2002). Expression of the angiopoietins and their receptor Tie2 in human renal clear cell carcinomas; regulation by the von Hippel-Lindau gene and hypoxia. *J Pathol* **198**, 502-510.

Cuvillier, O. (2002). Sphingosine in apoptosis signaling. *Biochim Biophys Acta* **1585**, 153-162.

Cuvillier, O., Nava, V. E., Murthy, S. K., Edsall, L. C., Levade, T., Milstien, S., and Spiegel, S. (2001). Sphingosine generation, cytochrome c release, and activation of caspase-7 in doxorubicin-induced apoptosis of MCF7 breast adenocarcinoma cells. *Cell Death Differ* **8**, 162-171.

Cuvillier, O., Pirianov, G., Kleuser, B., Vanek, P. G., Coso, O. A., Gutkind, S., and Spiegel, S. (1996). Suppression of ceramide-mediated programmed cell death by sphingosine-1-phosphate. *Nature* **381**, 800-803.

Czekay, R. P., Aertgeerts, K., Curriden, S. A., and Loskutoff, D. J. (2003). Plasminogen activator inhibitor-1 detaches cells from extracellular matrices by inactivating integrins. *J Cell Biol* **160**, 781-791.

Czekay, R. P., Kuemmel, T. A., Orlando, R. A., and Farquhar, M. G. (2001). Direct binding of occupied urokinase receptor (uPAR) to LDL receptor-related protein is required for endocytosis of uPAR and regulation of cell surface urokinase activity. *Mol Biol Cell* **12**, 1467-1479.

Dancey, J. E., and Freidlin, B. (2003). Targeting epidermal growth factor receptor--are we missing the mark? *Lancet* **362**, 62-64.

Dass, K., Ahmad, A., Azmi, A. S., Sarkar, S. H., and Sarkar, F. H. (2008). Evolving role of uPA/uPAR system in human cancers. *Cancer Treat Rev* **34**, 122-136.

De Luca, A., Carotenuto, A., Rachiglio, A., Gallo, M., Maiello, M. R., Aldinucci, D., Pinto, A., and Normanno, N. (2008). The role of the EGFR signaling in tumor microenvironment. *J Cell Physiol* **214**, 559-567.

Degryse, B., Neels, J. G., Czekay, R. P., Aertgeerts, K., Kamikubo, Y., and Loskutoff, D. J. (2004). The low density lipoprotein receptor-related protein is a motogenic receptor for plasminogen activator inhibitor-1. *Journal of Biological Chemistry* **279**, 22595-22604.

Deng, G., Curriden, S. A., Hu, G., Czekay, R. P., and Loskutoff, D. J. (2001). Plasminogen activator inhibitor-1 regulates cell adhesion by binding to the somatomedin B domain of vitronectin. *J Cell Physiol* **189**, 23-33.

Deng, G., Royle, G., Wang, S., Crain, K., and Loskutoff, D. J. (1996). Structural and functional analysis of the plasminogen activator inhibitor-1 binding motif in the somatomedin B domain of vitronectin. *Journal of Biological Chemistry* **271**, 12716-12723.

Depreter, M., Vandesompele, J., Espeel, M., Speleman, F., and Roels, F. (2002). Modulation of the peroxisomal gene expression pattern by dehydroepiandrosterone and vitamin D: therapeutic implications. *J Endocrinol* **175**, 779-792.

Desai, K., Sullards, M. C., Allegood, J., Wang, E., Schmelz, E. M., Hartl, M., Humpf, H.-U., Liotta, D. C., Peng, Q., and Merrill, A. H. (2002). Fumonisins and fumonisin analogs as inhibitors of ceramide synthase and inducers of apoptosis. *Biochimica et Biophysica Acta, Molecular and Cell Biology of Lipids* **1585**, 188-192.

Dimova, E. Y., and Kietzmann, T. (2008). Metabolic, hormonal and environmental regulation of plasminogen activator inhibitor-1 (PAI-1) expression: lessons from the liver. *Thromb Haemost* **100**, 992-1006.

Domijan, A.-M., Peraica, M., Vrdoljak, A. L., Radic, B., Zlender, V., and Fuchs, R. (2007a). The involvement of oxidative stress in ochratoxin A and fumonisin B1 toxicity in rats. *Molecular Nutrition & Food Research* **51**, 1147-1151.

Domijan, A.-M., Zeljezic, D., Kopjar, N., and Peraica, M. (2006). Standard and Fpg-modified comet assay in kidney cells of ochratoxin A- and fumonisin B1-treated rats. *Toxicology* **222**, 53-59.

Domijan, A., Zeljezic, D., Peraica, M., Kovacevic, G., Gregorovic, G., Krstanac, Z., Horvatin, K., and Kalafatic, M. (2008). Early toxic effects of fumonisin B1 in rat liver. *Hum Exp Toxicol* **27**, 895-900.

Domijan, A. M., Zeljezic, D., Milic, M., and Peraica, M. (2007b). Fumonisin B(1): oxidative status and DNA damage in rats. *Toxicology* **232**, 163-169.

Dragan, Y. P., Bidlack, W. R., Cohen, S. M., Goldsworthy, T. L., Hard, G. C., Howard, P. C., Riley, R. T., and Voss, K. A. (2001). Implications of apoptosis for toxicity, carcinogenicity, and risk assessment: fumonisin B1 as an example. *Toxicological Sciences* **61**, 6-17.

Duffy, M. J., and Duggan, C. (2004). The urokinase plasminogen activator system: a rich source of tumour markers for the individualised management of patients with cancer. *Clin Biochem* **37**, 541-548.

Dutton, M. (2009). The African Fusarium/maize disease. *Mycotoxin Research* **25**, 29-39.

EC (2006). Commission Regulation (EC) No. 1881/2006 setting maximum levels for certain contaminants in foodstuffs. *Official Journal of the European Union L 364* **5-24**.

Eddy, A. A., and Fogo, A. B. (2006). Plasminogen activator inhibitor-1 in chronic kidney disease: Evidence and mechanisms of action. *J Am Soc Nephrol* **17**, 2999-3012.

Eferl, R., and Wagner, E. F. (2003). AP-1: a double-edged sword in tumorigenesis. *Nat Rev Cancer* **3**, 859-868.

EFSA (2005). Opinion of the Scientific Committee on a request from EFSA related to a harmonised approach for risk assessment of substances which are both genotoxic and carcinogenic (Request No EFSA-Q-2004-020). Adopted on 18 October 2005. *Available at: http://www.efsa.europa.eu/en/efsajournal/doc/282.pdf*.

Ehrlich, V., Darroudi, F., Uhl, M., Steinkellner, H., Zsivkovits, M., and Knasmueller, S. (2002). Fumonisin B(1) is genotoxic in human derived hepatoma (HepG2) cells. *Mutagenesis* **17**, 257-260.

Eisen, M. B., Spellman, P. T., Brown, P. O., and Botstein, D. (1998). Cluster analysis and display of genome-wide expression patterns. *Proc Natl Acad Sci U S A* **95**, 14863-14868.

Evan, G. I., and Vousden, K. H. (2001). Proliferation, cell cycle and apoptosis in cancer. *Nature* **411**, 342-348.

Facchinetti, M. M., Leocata Nieto, F., Marquez, M. G., and Sterin-Speziale, N. (2008). Stratification of sphingosine kinase-1 expression and activity in rat kidney. *Cells Tissues Organs* **188**, 384-392.

Favaro, D., Santarosa, M., Quaia, M., and Galligioni, E. (1997). Interleukin-6 and soluble intercellular adhesion molecule-1 in renal cancer patients and cultured renal cancer cells. *Urol Oncol* **3**, 51-58.

Frangogiannis, N. G., Ren, G., Dewald, O., Zymek, P., Haudek, S., Koerting, A., Winkelmann, K., Michael, L. H., Lawler, J., and Entman, M. L. (2005). Critical role of endogenous thrombospondin-1 in preventing expansion of healing myocardial infarcts. *Circulation* **111**, 2935-2942.

Fukasawa, K. (2007). Oncogenes and tumour suppressors take on centrosomes. *Nat Rev Cancer* **7**, 911-924.

Fukuda, Y., Kihara, A., and Igarashi, Y. (2003). Distribution of sphingosine kinase activity in mouse tissues: contribution of SPHK1. *Biochem Biophys Res Commun* **309**, 155-160.

Gaines Das, R., and North, D. (2007). Implications of experimental technique for analysis and interpretation of data from animal experiments: outliers and increased variability resulting from failure of intraperitoneal injection procedures. *Lab Anim* **41**, 312-320.

Galaktionov, K., Chen, X., and Beach, D. (1996). Cdc25 cell-cycle phosphatase as a target of c-myc. *Nature* **382**, 511-517.

Galvano, F., Campisi, A., Russo, A., Galvano, G., Palumbo, M., Renis, M., Barcellona, M. L., Perez-Polo, J. R., and Vanella, A. (2002a). DNA damage in astrocytes exposed to fumonisin B1. *Neurochem Res* **27**, 345-351.

Galvano, F., Russo, A., Cardile, V., Galvano, G., Vanella, A., and Renis, M. (2002b). DNA damage in human fibroblasts exposed to fumonisin B(1). *Food Chem Toxicol* **40**, 25-31.

Gamble, J. R., Sun, W. Y., Li, X., Hahn, C. N., Pitson, S. M., Vadas, M. A., and Bonder, C. S. (2009). Sphingosine kinase-1 associates with integrin {alpha}V{beta}3 to mediate endothelial cell survival. *Am J Pathol* **175**, 2217-2225.

Geiger, T. R., and Peeper, D. S. (2009). Metastasis mechanisms. *Biochim Biophys Acta* **1796**, 293-308.

Gelderblom, W. C., Abel, S., Smuts, C. M., Marnewick, J., Marasas, W. F., Lemmer, E. R., and Ramljak, D. (2001a). Fumonisin-induced hepatocarcinogenesis: mechanisms related to cancer initiation and promotion. *Environmental health perspectives* **109 Suppl 2**, 291-300.

Gelderblom, W. C., Jaskiewicz, K., Marasas, W. F., Thiel, P. G., Horak, R. M., Vleggaar, R., and Kriek, N. P. (1988). Fumonisins--novel mycotoxins with cancer-promoting activity produced by Fusarium moniliforme. *Appl Environ Microbiol* **54**, 1806-1811.

Gelderblom, W. C., Kriek, N. P., Marasas, W. F., and Thiel, P. G. (1991). Toxicity and carcinogenicity of the Fusarium moniliforme metabolite, fumonisin B1, in rats. *Carcinogenesis* **12**, 1247-1251.

Gelderblom, W. C., Lebepe-Mazur, S., Snijman, P. W., Abel, S., Swanevelder, S., Kriek, N. P., and Marasas, W. F. (2001b). Toxicological effects in rats chronically fed low dietary levels of fumonisin B(1). *Toxicology* **161**, 39-51.

Gelderblom, W. C., Semple, E., Marasas, W. F., and Farber, E. (1992). The cancer-initiating potential of the fumonisin B mycotoxins. *Carcinogenesis* **13**, 433-437.

Gelderblom, W. C., Smuts, C. M., Abel, S., Snyman, S. D., Van der Westhuizen, L., Huber, W. W., and Swanevelder, S. (1997). Effect of fumonisin B1 on the levels and fatty acid composition of selected lipids in rat liver in vivo. *Food Chem Toxicol* **35**, 647-656.

Gelderblom, W. C., Snyman, S. D., Lebepe-Mazur, S., van der Westhuizen, L., Kriek, N. P., and Marasas, W. F. (1996). The cancer-promoting potential of fumonisin B1 in rat liver using diethylnitrosamine as a cancer initiator. *Cancer Lett* **109**, 101-108.

Gelderblom, W. C. A., and Snyman, S. D. (1991). Mutagenicity of potentially carcinogenic mycotoxins produced by Fusarium moniliforme. *Mycotoxin Research* **7**, 46-52.

Giehl, K., Graness, A., and Goppelt-Struebe, M. (2008). The small GTPase Rac-1 is a regulator of mesangial cell morphology and thrombospondin-1 expression. *Am J Physiol Renal Physiol* **294**, F407-413.

Gijsbers, S., Van der Hoeven, G., and Van Veldhoven, P. P. (2001). Subcellular study of sphingoid base phosphorylation in rat tissues: evidence for multiple sphingosine kinases. *Biochim Biophys Acta* **1532**, 37-50.

Giubellino, A., Linehan, W. M., and Bottaro, D. P. (2009). Targeting the Met signaling pathway in renal cancer. *Expert Rev Anticancer Ther* **9**, 785-793.

Goetzl, E. J., and Rosen, H. (2004). Regulation of immunity by lysosphingolipids and their G protein-coupled receptors. *J Clin Invest* **114**, 1531-1537.

Goldsworthy, T. L., Conolly, R. B., and Fransson-Steen, R. (1996). Apoptosis and cancer risk assessment. *Mutat Res* **365**, 71-90.

Goodman, J. I., and Watson, R. E. (2002). Altered DNA methylation: a secondary mechanism involved in carcinogenesis. *Annu Rev Pharmacol Toxicol* **42**, 501-525.

Gopee Neera, V., and Sharma Raghubir, P. (2004). Selective and transient activation of protein kinase C alpha by fumonisin B1, a ceramide synthase inhibitor mycotoxin, in cultured porcine renal cells. *Life sciences* **74**, 1541-1559.

Gopee, N. V., He, Q., and Sharma, R. P. (2003). Fumonisin B1-induced apoptosis is associated with delayed inhibition of protein kinase C, nuclear factor-kB and tumor necrosis factor alpha in LLC-PK1 cells. *Chemico-Biological Interactions* **146**, 131-145.

Gopee, N. V., and Sharma, R. P. (2004). The mycotoxin fumonisin B1 transiently activates nuclear factor-kB, tumor necrosis factor alpha and caspase 3 via protein kinase Calpha -dependent pathway in porcine renal epithelial cells. *Cell Biology and Toxicology* **20**, 197-212.

Guo, W., and Giancotti, F. G. (2004). Integrin signalling during tumour progression. *Nat Rev Mol Cell Biol* **5**, 816-826.

Hait, N. C., Allegood, J., Maceyka, M., Strub, G. M., Harikumar, K. B., Singh, S. K., Luo, C., Marmorstein, R., Kordula, T., Milstien, S., and Spiegel, S. (2009). Regulation of histone acetylation in the nucleus by sphingosine-1-phosphate. *Science* **325**, 1254-1257.

Hait, N. C., Oskeritzian, C. A., Paugh, S. W., Milstien, S., and Spiegel, S. (2006). Sphingosine kinases, sphingosine 1-phosphate, apoptosis and diseases. *Biochim Biophys Acta* **1758**, 2016-2026.

Halper, J. (2010). Growth factors as active participants in carcinogenesis: a perspective. *Vet Pathol* **47**, 77-97.

Hanahan, D., and Weinberg, R. A. (2011). Hallmarks of cancer: the next generation. *Cell* **144**, 646-674.

Hannun, Y. A., Loomis, C. R., Merrill, A. H., Jr., and Bell, R. M. (1986). Sphingosine inhibition of protein kinase C activity and of phorbol dibutyrate binding in vitro and in human platelets. *J Biol Chem* **261**, 12604-12609.

Hannun, Y. A., and Obeid, L. M. (2008). Principles of bioactive lipid signalling: lessons from sphingolipids. *Nat Rev Mol Cell Biol* **9**, 139-150.

Hard, G. C. (1998). Mechanisms of chemically induced renal carcinogenesis in the laboratory rodent. *Toxicol Pathol* **26**, 104-112.

Hard, G. C., Howard, P. C., Kovatch, R. M., and Bucci, T. J. (2001). Rat kidney pathology induced by chronic exposure to fumonisin B1 includes rare variants of renal tubule tumor. *Toxicologic Pathology* **29**, 379-386.

Harrison, L. R., Colvin, B. M., Greene, J. T., Newman, L. E., and Cole, J. R., Jr. (1990). Pulmonary edema and hydrothorax in swine produced by fumonisin B1, a toxic metabolite of Fusarium moniliforme. *J Vet Diagn Invest* **2**, 217-221.

Hatanaka, H., Abe, Y., Naruke, M., Tokunaga, T., Oshika, Y., Kawakami, T., Osada, H., Nagata, J., Kamochi, J., Tsuchida, T., Kijima, H., Yamazaki, H., Inoue, H., Ueyama, Y., and Nakamura, M. (2001). Significant correlation between interleukin 10 expression and vascularization through angiopoietin/TIE2 networks in non-small cell lung cancer. *Clin Cancer Res* **7**, 1287-1292.

Hazzalin, C. A., and Mahadevan, L. C. (2002). MAPK-regulated transcription: a continuously variable gene switch? *Nat Rev Mol Cell Biol* **3**, 30-40.

He, Q., Kim, J., and Sharma, R. P. (2005a). Fumonisin B1 hepatotoxicity in mice is attenuated by depletion of Kupffer cells by gadolinium chloride. *Toxicology* **207**, 137-147.

He, Q., Riley, R. T., and Sharma, R. P. (2001). Fumonisin-Induced Tumor Necrosis Factor-alpha Expression in a Porcine Kidney Cell Line Is Independent of Sphingoid Base Accumulation Induced by Ceramide Synthase Inhibition. *Toxicology and Applied Pharmacology* **174**, 69-77.

He, Q., Riley, R. T., and Sharma, R. P. (2002). Pharmacological antagonism of fumonisin B1 cytotoxicity in porcine renal epithelial cells (LLC-PK1): A model for reducing fumonisin-induced nephrotoxicity in vivo. *Pharmacology & Toxicology (Oxford, United Kingdom)* **90**, 268-277.

He, Q., Riley, R. T., and Sharma, R. P. (2005b). Myriocin prevents fumonisin B1-induced sphingoid base accumulation in mice liver without ameliorating hepatotoxicity. *Food and Chemical Toxicology* **43**, 969-979.

He, Q., Suzuki, H., Sharma, N., and Sharma, R. P. (2006a). Ceramide synthase inhibition by fumonisin B1 treatment activates sphingolipid-metabolizing systems in mouse liver. *Toxicological Sciences* **94**, 388-397.

He, Q., Suzuki, H., and Sharma, R. P. (2006b). S-adenosylmethionine or 5'-methylthioadenosine are unable to prevent fumonisin B1 hepatotoxicity in mice despite increased oxidation in liver. *Journal of Applied Toxicology* **26**, 509-516.

Heicappell, R., Podlinski, J., Buszello, H., and Ackermann, R. (1994). Cell surface expression and serum levels of intercellular adhesion molecule-1 in renal cell carcinoma. *Urol Res* **22**, 9-15.

Heo, K., Park, K. A., Kim, Y. H., Kim, S. H., Oh, Y. S., Kim, I. H., Ryu, S. H., and Suh, P. G. (2009). Sphingosine 1-phosphate induces vascular endothelial growth factor expression in endothelial cells. *BMB Rep* **42**, 685-690.

Hla, T., and Brinkmann, V. (2011). Sphingosine 1-phosphate (S1P): Physiology and the effects of S1P receptor modulation. *Neurology* **76**, S3-8.

Hoekstra, D., Maier, O., van der Wouden, J. M., Slimane, T. A., and van, I. S. C. (2003). Membrane dynamics and cell polarity: the role of sphingolipids. *J Lipid Res* **44**, 869-877.

Hollingsworth, M. A., and Swanson, B. J. (2004). Mucins in cancer: protection and control of the cell surface. *Nat Rev Cancer* **4**, 45-60.

Hornuss, C., Hammermann, R., Fuhrmann, M., Juergens, U. R., and Racke, K. (2001). Human and rat alveolar macrophages express multiple EDG receptors. *Eur J Pharmacol* **429**, 303-308.

Hosokawa, T., Muraishi, A., Rothman, V. L., Papale, M., and Tuszynski, G. P. (1993). The effect of thrombospondin on invasion of fibrin gels by human A549 lung carcinoma. *Oncol Res* **5**, 183-189.

Howard, P. C., Eppley, R. M., Stack, M. E., Warbritton, A., Voss, K. A., Lorentzen, R. J., Kovach, R. M., and Bucci, T. J. (2001a). Fumonisin b1 carcinogenicity in a two-year feeding study using F344 rats and B6C3F1 mice. *Environmental health perspectives* **109 Suppl 2**, 277-282.

Howard, P. C., Warbritton, A., Voss, K. A., Lorentzen, R. J., Thurman, J. D., Kovach, R. M., and Bucci, T. J. (2001b). Compensatory regeneration as a mechanism for renal tubule carcinogenesis of fumonisin B1 in the F344/N/Nctr BR rat. *Environmental Health Perspectives Supplements* **109**, 309-314.

Hsieh, H. L., Sun, C. C., Wu, C. B., Wu, C. Y., Tung, W. H., Wang, H. H., and Yang, C. M. (2008). Sphingosine 1-phosphate induces EGFR expression via Akt/NF-kappaB and ERK/AP-1 pathways in rat vascular smooth muscle cells. *J Cell Biochem* **103**, 1732-1746.

Hu, W., Xu, R., Zhang, G., Jin, J., Szulc, Z. M., Bielawski, J., Hannun, Y. A., Obeid, L. M., and Mao, C. (2005). Golgi fragmentation is associated with ceramide-induced cellular effects. *Mol Biol Cell* **16**, 1555-1567.

Huang, X., Brown, C., Ni, W., Maynard, E., Rigby, A. C., and Oettgen, P. (2006). Critical role for the Ets transcription factor ELF-1 in the development of tumor angiogenesis. *Blood* **107**, 3153-3160.

Huang, Y. L., Huang, W. P., and Lee, H. (2011). Roles of sphingosine 1-phosphate on tumorigenesis. *World J Biol Chem* **2**, 25-34.

Hugo, C. (2003). The thrombospondin 1-TGF-beta axis in fibrotic renal disease. *Nephrol Dial Transplant* **18**, 1241-1245.

Hugo, C., and Daniel, C. (2009). Thrombospondin in renal disease. *Nephron Exp Nephrol* **111**, e61-66.

Humpf, H. U., Schmelz, E. M., Meredith, F. I., Vesper, H., Vales, T. R., Wang, E., Menaldino, D. S., Liotta, D. C., and Merrill, A. H., Jr. (1998). Acylation of naturally occurring and synthetic 1-deoxysphinganines by ceramide synthase. Formation of N-palmitoyl-aminopentol produces a toxic metabolite of hydrolyzed fumonisin, AP1, and a new category of ceramide synthase inhibitor. *J Biol Chem* **273**, 19060-19064.

Humphreys, S. H., Carrington, C., and Bolger, M. (2001). A quantitative risk assessment for fumonisins B1 and B2 in US corn. *Food Addit Contam* **18**, 211-220.

Huu, D.-N., Rosenblum, E. N., and Zeigel, R. F. (1966). Persistent infection of a rat kidney cell line with Rauscher murine leukemia virus. *J Bacteriol* **92**, 1133-1140.

Igney, F. H., and Krammer, P. H. (2002). Death and anti-death: tumour resistance to apoptosis. *Nat Rev Cancer* **2**, 277-288.

Jazirehi, A. R., Vega, M. I., Chatterjee, D., Goodglick, L., and Bonavida, B. (2004). Inhibition of the Raf-MEK1/2-ERK1/2 signaling pathway, Bcl-xL down-regulation, and chemosensitization of non-Hodgkin's lymphoma B cells by Rituximab. *Cancer Res* **64**, 7117-7126.

JECFA (2001). Safety evaluation of certain mycotoxins in food. Fifty-sixth meeting of the Joint FAO/WHO Expert Committee on Food Additives (JECFA). *WHO Food Additives Series* **47**, 103-279.

Jochum, W., Passegue, E., and Wagner, E. F. (2001). AP-1 in mouse development and tumorigenesis. *Oncogene* **20**, 2401-2412.

Johnson, R., Spiegelman, B., Hanahan, D., and Wisdom, R. (1996). Cellular transformation and malignancy induced by ras require c-jun. *Mol Cell Biol* **16**, 4504-4511.

Johnson, V. J., He, Q., Kim, S. H., Kanti, A., and Sharma, R. P. (2003). Increased susceptibility of renal epithelial cells to TNFalpha -induced apoptosis following treatment with fumonisin B1. *Chemico-Biological Interactions* **145**, 297-309.

Jonckheere, N., and Van Seuningen, I. (2010). The membrane-bound mucins: From cell signalling to transcriptional regulation and expression in epithelial cancers. *Biochimie* **92**, 1-11.

Jones, C., Ciacci-Zanella, J. R., Zhang, Y., Henderson, G., and Dickman, M. (2001a). Analysis of fumonisin B1-induced apoptosis. *Environmental Health Perspectives Supplements* **109**, 315-320.

Jones, N., Iljin, K., Dumont, D. J., and Alitalo, K. (2001b). Tie receptors: new modulators of angiogenic and lymphangiogenic responses. *Nat Rev Mol Cell Biol* **2**, 257-267.

Kagedal, K., Zhao, M., Svensson, I., and Brunk, U. T. (2001). Sphingosine-induced apoptosis is dependent on lysosomal proteases. *Biochem J* **359**, 335-343.

Kahlert, C., Bandapalli, O. R., Schirmacher, P., Weitz, J., and Brand, K. (2008). Invasion front-specific overexpression of tissue inhibitor of metalloproteinase-1 in liver metastases from colorectal cancer. *Anticancer Res* **28**, 1459-1465.

Kallio, J. P., Tammela, T. L., Marttinen, A. T., and Kellokumpu-Lehtinen, P. L. (2001). Soluble immunological parameters and early prognosis of renal cell cancer patients. *J Exp Clin Cancer Res* **20**, 523-528.

Karin, M., and Lin, A. (2002). NF-kappaB at the crossroads of life and death. *Nat Immunol* **3**, 221-227.

Katsuma, S., Hada, Y., Shiojima, S., Hirasawa, A., Tanoue, A., Takagaki, K., Ohgi, T., Yano, J., and Tsujimoto, G. (2003). Transcriptional profiling of gene expression patterns during sphingosine 1-phosphate-induced mesangial cell proliferation. *Biochem Biophys Res Commun* **300**, 577-584.

Katsuma, S., Hada, Y., Ueda, T., Shiojima, S., Hirasawa, A., Tanoue, A., Takagaki, K., Ohgi, T., Yano, J., and Tsujimoto, G. (2002). Signalling mechanisms in sphingosine 1-phosphate-promoted mesangial cell proliferation. *Genes Cells* **7**, 1217-1230.

Kazerounian, S., Yee, K. O., and Lawler, J. (2008). Thrombospondins in cancer. *Cell Mol Life Sci* **65**, 700-712.

Kellerman, T. S., Marasas, W. F., Thiel, P. G., Gelderblom, W. C., Cawood, M., and Coetzer, J. A. (1990). Leukoencephalomalacia in two horses induced by oral dosing of fumonisin B1. *Onderstepoort J Vet Res* **57**, 269-275.

Kim, D.-H., Lee, Y.-S., Lee, Y.-M., Oh, S., Yun, Y.-P., and Yoo, H.-S. (2007). Elevation of sphingoid base 1-phosphate as a potential contributor to hepatotoxicity in fumonisin B1-exposed mice. *Archives of Pharmacal Research* **30**, 962-969.

Kim, J. H., Song, W. K., and Chun, J. S. (2000). Sphingosine 1-phosphate activates Erk-1/-2 by transactivating epidermal growth factor receptor in rat-2 cells. *IUBMB Life* **50**, 119-124.

Kim, M. S., Lee, D.-Y., Wang, T., and Schroeder, J. J. (2001). Fumonisin B1 Induces Apoptosis in LLC-PK1 Renal Epithelial Cells via a Sphinganine- and Calmodulin-Dependent Pathway. *Toxicology and Applied Pharmacology* **176**, 118-126.

Kim, R. H., Takabe, K., Milstien, S., and Spiegel, S. (2009). Export and functions of sphingosine-1-phosphate. *Biochim Biophys Acta* **1791**, 692-696.

Kimura, T., Watanabe, T., Sato, K., Kon, J., Tomura, H., Tamama, K., Kuwabara, A., Kanda, T., Kobayashi, I., Ohta, H., Ui, M., and Okajima, F. (2000). Sphingosine 1-phosphate stimulates proliferation and migration of human endothelial cells possibly through the lipid receptors, Edg-1 and Edg-3. *Biochem J* **348 Pt 1**, 71-76.

Kinbara, K., Goldfinger, L. E., Hansen, M., Chou, F. L., and Ginsberg, M. H. (2003). Ras GTPases: integrins' friends or foes? *Nat Rev Mol Cell Biol* **4**, 767-776.

Kitatani, K., Idkowiak-Baldys, J., and Hannun, Y. A. (2007). The sphingolipid salvage pathway in ceramide metabolism and signaling. *Cell Signal*.

Klaric, M. S., Pepeljnjak, S., Domijan, A.-M., and Petrik, J. (2007). Lipid peroxidation and glutathione levels in porcine kidney PK15 cells after individual and combined treatment with fumonisin B1, beauvericin and ochratoxin A. *Basic & Clinical Pharmacology & Toxicology* **100**, 157-164.

Klaric, M. S., Rumora, L., Ljubanovic, D., and Pepeljnjak, S. (2008). Cytotoxicity and apoptosis induced by fumonisin B(1), beauvericin and ochratoxin A in porcine kidney PK15 cells: effects of individual and combined treatment. *Arch Toxicol* **82**, 247-255.

Knasmueller, S., Bresgen, N., Kassie, F., Mersch-Sundermann, V., Gelderblom, W., Zoehrer, E., and Eckl, P. M. (1997). Genotoxic effects of three Fusarium mycotoxins, fumonisin B1, moniliformin and vomitoxin in bacteria and in primary cultures of rat hepatocytes. *Mutation Research, Genetic Toxicology and Environmental Mutagenesis* **391**, 39-48.

Kohno, M., Momoi, M., Oo, M. L., Paik, J. H., Lee, Y. M., Venkataraman, K., Ai, Y., Ristimaki, A. P., Fyrst, H., Sano, H., Rosenberg, D., Saba, J. D., Proia, R. L., and Hla, T. (2006). Intracellular role for sphingosine kinase 1 in intestinal adenoma cell proliferation. *Mol Cell Biol* **26**, 7211-7223.

Kojima, R., Sekine, T., Kawachi, M., Cha, S. H., Suzuki, Y., and Endou, H. (2002). Immunolocalization of multispecific organic anion transporters, OAT1, OAT2, and OAT3, in rat kidney. *J Am Soc Nephrol* **13**, 848-857.

Kouadio, J. H., Dano, S. D., Moukha, S., Mobio, T. A., and Creppy, E. E. (2007). Effects of combinations of Fusarium mycotoxins on the inhibition of macromolecular synthesis, malondialdehyde levels, DNA methylation and fragmentation, and viability in Caco-2 cells. *Toxicon* **49**, 306-317.

Kraus, S., Abel, P. D., Nachtmann, C., Linsenmann, H. J., Weidner, W., Stamp, G. W., Chaudhary, K. S., Mitchell, S. E., Franke, F. E., and Lalani el, N. (2002). MUC1 mucin and trefoil factor 1 protein expression in renal cell carcinoma: correlation with prognosis. *Hum Pathol* **33**, 60-67.

Krishnamurti, C., and Alving, B. M. (1992). Plasminogen activator inhibitor type 1: biochemistry and evidence for modulation of fibrinolysis in vivo. *Semin Thromb Hemost* **18**, 67-80.

Lawler, J. (1986). The structural and functional properties of thrombospondin. *Blood* **67**, 1197-1209.

Lee, H., Lin, C. I., Liao, J. J., Lee, Y. W., Yang, H. Y., Lee, C. Y., Hsu, H. Y., and Wu, H. L. (2004). Lysophospholipids increase ICAM-1 expression in HUVEC through a Gi- and NF-kappaB-dependent mechanism. *Am J Physiol Cell Physiol* **287**, C1657-1666.

Lee, M. H., Hammad, S. M., Semler, A. J., Luttrell, L. M., Lopes-Virella, M. F., and Klein, R. L. (2010). HDL3, but not HDL2, stimulates plasminogen activator inhibitor-1 release from adipocytes: the role of sphingosine-1-phosphate. *J Lipid Res* **51**, 2619-2628.

Lee, W. K., Torchalski, B., and Thevenod, F. (2007). Cadmium-induced ceramide formation triggers calpain-dependent apoptosis in cultured kidney proximal tubule cells. *Am J Physiol Cell Physiol* **293**, C839-847.

Lemmer, E. R., De la Motte Hall, P., Omori, N., Omori, M., Shephard, E. G., Gelderblom, W. C. A., Cruse, J. P., Barnard, R. A., Marasas, W. F. O., Kirsch, R. E., and Thorgeirsson, S. S. (1999). Histopathology and gene expression changes in rat liver during feeding of fumonisin B1, a carcinogenic mycotoxin produced by Fusarium moniliforme. *Carcinogenesis* **20**, 817-824.

Leonardi-Essmann, F., Emig, M., Kitamura, Y., Spanagel, R., and Gebicke-Haerter, P. J. (2005). Fractalkine-upregulated milk-fat globule EGF factor-8 protein in cultured rat microglia. *J Neuroimmunol* **160**, 92-101.

Leong, W. I., and Saba, J. D. (2010). S1P metabolism in cancer and other pathological conditions. *Biochimie* **92**, 716-723.

Leroy, X., Zerimech, F., Zini, L., Copin, M. C., Buisine, M. P., Gosselin, B., Aubert, J. P., and Porchet, N. (2002). MUC1 expression is correlated with nuclear grade and tumor progression in pT1 renal clear cell carcinoma. *Am J Clin Pathol* **118**, 47-51.

Lim, C. W., Parker, H. M., Vesonder, R. F., and Haschek, W. M. (1996). Intravenous fumonisin B1 induces cell proliferation and apoptosis in the rat. *Nat Toxins* **4**, 34-41.

Lin, M. T., Chang, C. C., Lin, B. R., Yang, H. Y., Chu, C. Y., Wu, M. H., and Kuo, M. L. (2007). Elevated expression of Cyr61 enhances peritoneal dissemination of gastric cancer cells through integrin alpha2beta1. *J Biol Chem* **282**, 34594-34604.

Liu, Y. Y., Han, T. Y., Giuliano, A. E., and Cabot, M. C. (2001). Ceramide glycosylation potentiates cellular multidrug resistance. *FASEB J* **15**, 719-730.

Lock, E. A., and Hard, G. C. (2004). Chemically induced renal tubule tumors in the laboratory rat and mouse: review of the NCI/NTP database and categorization of renal carcinogens based on mechanistic information. *Crit Rev Toxicol* **34**, 211-299.

Lopez-Bergami, P., Lau, E., and Ronai, Z. (2010). Emerging roles of ATF2 and the dynamic AP1 network in cancer. *Nat Rev Cancer* **10**, 65-76.

Lowry, O. H., Rosebrough, N. J., Farr, A. L., and Randall, R. J. (1951). Protein measurement with the Folin phenol reagent. *J Biol Chem* **193**, 265-275.

Malarkey, D. E., Johnson, K., Ryan, L., Boorman, G., and Maronpot, R. R. (2005). New insights into functional aspects of liver morphology. *Toxicol Pathol* **33**, 27-34.

Mao, C., and Obeid, L. M. (2008). Ceramidases: regulators of cellular responses mediated by ceramide, sphingosine, and sphingosine-1-phosphate. *Biochim Biophys Acta* **1781**, 424-434.

Marasas, W. F. (1996). Fumonisins: history, world-wide occurrence and impact. *Adv Exp Med Biol* **392**, 1-17.

Marasas, W. F. (2001). Discovery and occurrence of the fumonisins: a historical perspective. *Environmental health perspectives* **109 Suppl 2**, 239-243.

Marasas, W. F., Kellerman, T. S., Gelderblom, W. C., Coetzer, J. A., Thiel, P. G., and van der Lugt, J. J. (1988). Leukoencephalomalacia in a horse induced by fumonisin B1 isolated from Fusarium moniliforme. *Onderstepoort J Vet Res* **55**, 197-203.

Marasas, W. F., Riley, R. T., Hendricks, K. A., Stevens, V. L., Sadler, T. W., Gelineau-van Waes, J., Missmer, S. A., Cabrera, J., Torres, O., Gelderblom, W. C., Allegood, J., Martinez, C., Maddox, J., Miller, J. D., Starr, L., Sullards, M. C., Roman, A. V., Voss, K. A., Wang, E., and Merrill, A. H., Jr. (2004). Fumonisins disrupt sphingolipid metabolism, folate transport, and neural tube development in embryo culture and in vivo: a potential risk factor for human neural tube defects among populations consuming fumonisin-contaminated maize. *J Nutr* **134**, 711-716.

Markovic-Lipkovski, J., Brasanac, D., Muller, G. A., and Muller, C. A. (2001). Cadherins and integrins in renal cell carcinoma: an immunohistochemical study. *Tumori* **87**, 173-178.

Marshall, J. C., Collins, J., Marino, N., and Steeg, P. (2010). The Nm23-H1 metastasis suppressor as a translational target. *Eur J Cancer* **46**, 1278-1282.

Martinez-Larranaga, M. R., Anadon, A., Diaz, M. J., Fernandez-Cruz, M. L., Martinez, M. A., Frejo, M. T., Martinez, M., Fernandez, R., Anton, R. M., Morales, M. E., and Tafur, M. (1999). Toxicokinetics and oral bioavailability of fumonisin B1. *Vet Hum Toxicol* **41**, 357-362.

McCubrey, J. A., Steelman, L. S., Chappell, W. H., Abrams, S. L., Wong, E. W., Chang, F., Lehmann, B., Terrian, D. M., Milella, M., Tafuri, A., Stivala, F., Libra, M., Basecke, J., Evangelisti, C., Martelli, A. M., and Franklin, R. A. (2007). Roles of the Raf/MEK/ERK pathway in cell growth, malignant transformation and drug resistance. *Biochim Biophys Acta* **1773**, 1263-1284.

Meca, G., Fernandez-Franzon, M., Ritieni, A., Font, G., Ruiz, M. J., and Manes, J. (2010). Formation of fumonisin B(1)-glucose reaction product, in vitro cytotoxicity, and lipid peroxidation on kidney cells. *J Agric Food Chem* **58**, 1359-1365.

Mechta-Grigoriou, F., Gerald, D., and Yaniv, M. (2001). The mammalian Jun proteins: redundancy and specificity. *Oncogene* **20**, 2378-2389.

Melendez, A. J., Carlos-Dias, E., Gosink, M., Allen, J. M., and Takacs, L. (2000). Human sphingosine kinase: molecular cloning, functional characterization and tissue distribution. *Gene* **251**, 19-26.

Memon, R. A., Holleran, W. M., Moser, A. H., Seki, T., Uchida, Y., Fuller, J., Shigenaga, J. K., Grunfeld, C., and Feingold, K. R. (1998). Endotoxin and cytokines increase hepatic sphingolipid biosynthesis and produce lipoproteins enriched in ceramides and sphingomyelin. *Arterioscler Thromb Vasc Biol* **18**, 1257-1265.

Menaldino, D. S., Bushnev, A., Sun, A., Liotta, D. C., Symolon, H., Desai, K., Dillehay, D. L., Peng, Q., Wang, E., Allegood, J., Trotman-Pruett, S., Sullards, M. C., and Merrill, A. H., Jr. (2003). Sphingoid bases and de novo ceramide synthesis: enzymes involved, pharmacology and mechanisms of action. *Pharmacol Res* **47**, 373-381.

Merrill, A. H., Jr. (1991). Cell regulation by sphingosine and more complex sphingolipids. *J Bioenerg Biomembr* **23**, 83-104.

Merrill, A. H., Jr. (2002). De novo sphingolipid biosynthesis: a necessary, but dangerous, pathway. *J Biol Chem* **277**, 25843-25846.

Merrill, A. H., Jr., Morgan, E. T., Nikolova-Karakashian, M., and Stewart, J. (1999). Sphingomyelin hydrolysis and regulation of the expression of the gene for cytochrome P450. *Biochem Soc Trans* **27**, 383-387.

Merrill, A. H., Jr., Schmelz, E. M., Dillehay, D. L., Spiegel, S., Shayman, J. A., Schroeder, J. J., Riley, R. T., Voss, K. A., and Wang, E. (1997). Sphingolipids--the enigmatic lipid class: biochemistry, physiology, and pathophysiology. *Toxicol Appl Pharmacol* **142**, 208-225.

Merrill, A. H., Jr., Sullards, M. C., Allegood, J. C., Kelly, S., and Wang, E. (2005). Sphingolipidomics: high-throughput, structure-specific, and quantitative analysis of sphingolipids by liquid chromatography tandem mass spectrometry. *Methods* **36**, 207-224.

Merrill, A. H., Jr., Sullards, M. C., Wang, E., Voss, K. A., and Riley, R. T. (2001). Sphingolipid metabolism: roles in signal transduction and disruption by fumonisins. *Environmental health perspectives* **109 Suppl 2**, 283-289.

Merrill, A. H., Jr., van Echten, G., Wang, E., and Sandhoff, K. (1993). Fumonisin B1 inhibits sphingosine (sphinganine) N-acyltransferase and de novo sphingolipid biosynthesis in cultured neurons in situ. *J Biol Chem* **268**, 27299-27306.

Meyer zu Heringdorf, D., and Jakobs, K. H. (2007). Lysophospholipid receptors: signalling, pharmacology and regulation by lysophospholipid metabolism. *Biochim Biophys Acta* **1768**, 923-940.

Mignatti, P., and Rifkin, D. B. (1993). Biology and biochemistry of proteinases in tumor invasion. *Physiol Rev* **73**, 161-195.

Milstien, S., and Spiegel, S. (2006). Targeting sphingosine-1-phosphate: a novel avenue for cancer therapeutics. *Cancer Cell* **9**, 148-150.

Min, J. K., Yoo, H. S., Lee, E. Y., Lee, W. J., and Lee, Y. M. (2002). Simultaneous quantitative analysis of sphingoid base 1-phosphates in biological samples by o-phthalaldehyde precolumn derivatization after dephosphorylation with alkaline phosphatase. *Anal Biochem* **303**, 167-175.

Mitra, P., Oskeritzian, C. A., Payne, S. G., Beaven, M. A., Milstien, S., and Spiegel, S. (2006). Role of ABCC1 in export of sphingosine-1-phosphate from mast cells. *Proc Natl Acad Sci U S A* **103**, 16394-16399.

Mizuno, R., Oya, M., Hara, S., Matsumoto, M., Horiguchi, A., Ohigashi, T., Marumo, K., and Murai, M. (2005). Modulation of bcl-2 family proteins in MAPK independent apoptosis induced by a cdc25 phosphatase inhibitor Cpd 5 in renal cancer cells. *Oncol Rep* **14**, 639-644.

Mizutani, Y., Kihara, A., and Igarashi, Y. (2005). Mammalian Lass6 and its related family members regulate synthesis of specific ceramides. *Biochem J* **390**, 263-271.

Mobio, T. A., Baudrimont, I., Sanni, A., Shier, T. W., Saboureau, D., Dano, S. D., Ueno, Y., Steyn, P. S., and Creppy, E. E. (2000). Prevention by vitamin E of DNA fragmentation and apoptosis induced by fumonisin B1 in C6 glioma cells. *Archives of Toxicology* **74**, 112-119.

Mobio, T. A., Tavan, E., Baudrimont, I., Anane, R., Carratu, M.-R., Sanni, A., Gbeassor, M. F., Shier, T. W., Narbonne, J.-F., and Creppy, E. E. (2003). Comparative study of the toxic effects of fumonisin B1 in rat C6 glioma cells and p53-null mouse embryo fibroblasts. *Toxicology* **183**, 65-75.

Moon, W. S., Park, H. S., Yu, K. H., Jang, K. Y., Kang, M. J., Park, H., and Tarnawski, A. S. (2006). Expression of angiopoietin 1, 2 and their common receptor Tie2 in human gastric carcinoma: implication for angiogenesis. *J Korean Med Sci* **21**, 272-278.

Morgan, M. R., Humphries, M. J., and Bass, M. D. (2007). Synergistic control of cell adhesion by integrins and syndecans. *Nat Rev Mol Cell Biol* **8**, 957-969.

Moroy, T., and Geisen, C. (2004). Cyclin E. *Int J Biochem Cell Biol* **36**, 1424-1439.

Nagamine, Y., Medcalf, R. L., and Munoz-Canoves, P. (2005). Transcriptional and posttranscriptional regulation of the plasminogen activator system. *Thromb Haemost* **93**, 661-675.

Nakanishi, C., and Toi, M. (2005). Nuclear factor-kappaB inhibitors as sensitizers to anticancer drugs. *Nat Rev Cancer* **5**, 297-309.

Nemeth, J. A., Nakada, M. T., Trikha, M., Lang, Z., Gordon, M. S., Jayson, G. C., Corringham, R., Prabhakar, U., Davis, H. M., and Beckman, R. A. (2007). Alpha-v integrins as therapeutic targets in oncology. *Cancer Invest* **25**, 632-646.

Nguyen, D. X., and Massague, J. (2007). Genetic determinants of cancer metastasis. *Nat Rev Genet* **8**, 341-352.

Nieuwenhuis, B., Luth, A., and Kleuser, B. (2010). Dexamethasone protects human fibroblasts from apoptosis via an S1P3-receptor subtype dependent activation of PKB/Akt and Bcl XL. *Pharmacol Res* **61**, 449-459.

Nilsson, J. A., and Cleveland, J. L. (2003). Myc pathways provoking cell suicide and cancer. *Oncogene* **22**, 9007-9021.

Nixon, G. F. (2009). Sphingolipids in inflammation: pathological implications and potential therapeutic targets. *Br J Pharmacol* **158**, 982-993.

Norred, W. P., Plattner, R. D., Vesonder, R. F., Bacon, C. W., and Voss, K. A. (1992). Effects of selected secondary metabolites of Fusarium moniliforme on unscheduled synthesis of DNA by rat primary hepatocytes. *Food Chem Toxicol* **30**, 233-237.

Novgorodov, A. S., El-Alwani, M., Bielawski, J., Obeid, L. M., and Gudz, T. I. (2007). Activation of sphingosine-1-phosphate receptor S1P5 inhibits oligodendrocyte progenitor migration. *FASEB J* **21**, 1503-1514.

NTP (2001). Toxicology and Carcinogenesis Studies of Fumonisin B1 (CAS No. 116355-83-0) in F344/N Rats and B6C3F1 mice (Feed Studies). *Natl. Toxicol. Program Tech. Rep. Ser.* , 1-352.

Ogretmen, B., and Hannun, Y. A. (2004). Biologically active sphingolipids in cancer pathogenesis and treatment. *Nat Rev Cancer* **4**, 604-616.

Ogretmen, B., Pettus, B. J., Rossi, M. J., Wood, R., Usta, J., Szulc, Z., Bielawska, A., Obeid, L. M., and Hannun, Y. A. (2002). Biochemical mechanisms of the generation of endogenous long chain ceramide in response to exogenous short chain ceramide in the A549 human lung adenocarcinoma cell line. Role for endogenous ceramide in mediating the action of exogenous ceramide. *J Biol Chem* **277**, 12960-12969.

Ogretmen, B., Schady, D., Usta, J., Wood, R., Kraveka, J. M., Luberto, C., Birbes, H., Hannun, Y. A., and Obeid, L. M. (2001). Role of ceramide in mediating the inhibition of telomerase activity in A549 human lung adenocarcinoma cells. *J Biol Chem* **276**, 24901-24910.

Ohanian, J., and Ohanian, V. (2001). Sphingolipids in mammalian cell signalling. *Cell Mol Life Sci* **58**, 2053-2068.

Ohba, K., Miyata, Y., Kanda, S., Koga, S., Hayashi, T., and Kanetake, H. (2005). Expression of urokinase-type plasminogen activator, urokinase-type plasminogen activator receptor and plasminogen activator inhibitors in patients with renal cell carcinoma: correlation with tumor associated macrophage and prognosis. *J Urol* **174**, 461-465.

Oka, H., Chatani, Y., Hoshino, R., Ogawa, O., Kakehi, Y., Terachi, T., Okada, Y., Kawaichi, M., Kohno, M., and Yoshida, O. (1995). Constitutive activation of mitogen-activated protein (MAP) kinases in human renal cell carcinoma. *Cancer Res* **55**, 4182-4187.

Oskouian, B., and Saba, J. (2007). Sphingosine-1-phosphate metabolism and intestinal tumorigenesis: lipid signaling strikes again. *Cell Cycle* **6**, 522-527.

Oskouian, B., and Saba, J. D. (2010). Cancer treatment strategies targeting sphingolipid metabolism. *Adv Exp Med Biol* **688**, 185-205.

Oudard, S., Rixe, O., Beuselinck, B., Linassier, C., Banu, E., Machiels, J. P., Baudard, M., Ringeisen, F., Velu, T., Lefrere-Belda, M. A., Limacher, J. M., Fridman, W. H., Azizi, M., Acres, B., and Tartour, E. (2011). A phase II study of the cancer vaccine TG4010 alone and in combination with cytokines in patients with metastatic renal clear-cell carcinoma: clinical and immunological findings. *Cancer Immunol Immunother* **60**, 261-271.

Pacella-Norman, R., Urban, M. I., Sitas, F., Carrara, H., Sur, R., Hale, M., Ruff, P., Patel, M., Newton, R., Bull, D., and Beral, V. (2002). Risk factors for oesophageal, lung, oral and laryngeal cancers in black South Africans. *Br J Cancer* **86**, 1751-1756.

Paik, J. H., Chae, S., Lee, M. J., Thangada, S., and Hla, T. (2001). Sphingosine 1-phosphate-induced endothelial cell migration requires the expression of EDG-1 and EDG-3 receptors and Rho-dependent activation of alpha vbeta3- and beta1-containing integrins. *J Biol Chem* **276**, 11830-11837.

Pan, H., Wanami, L. S., Dissanayake, T. R., and Bachelder, R. E. (2009). Autocrine semaphorin3A stimulates alpha2 beta1 integrin expression/function in breast tumor cells. *Breast Cancer Res Treat* **118**, 197-205.

Patsenker, E., and Stickel, F. (2011). Role of integrins in fibrosing liver diseases. *Am J Physiol Gastrointest Liver Physiol* **301**, G425-434.

Patwardhan, G. A., and Liu, Y. Y. (2010). Sphingolipids and expression regulation of genes in cancer. *Prog Lipid Res*.

Paugh, B. S., Paugh, S. W., Bryan, L., Kapitonov, D., Wilczynska, K. M., Gopalan, S. M., Rokita, H., Milstien, S., Spiegel, S., and Kordula, T. (2008). EGF regulates plasminogen activator inhibitor-1 (PAI-1) by a pathway involving c-Src, PKCdelta, and sphingosine kinase 1 in glioblastoma cells. *FASEB J* **22**, 455-465.

Pelagalli, A., Belisario, M. A., Squillacioti, C., Morte, R. D., d'Angelo, D., Tafuri, S., Lucisano, A., and Staiano, N. (1999). The mycotoxin fumonisin B1 inhibits integrin-mediated cell-matrix adhesion. *Biochimie* **81**, 1003-1008.

Pelengaris, S., Khan, M., and Evan, G. (2002). c-MYC: more than just a matter of life and death. *Nat Rev Cancer* **2**, 764-776.

Pereira, M. G., Camara, N. O., Campaholle, G., Cenedeze, M. A., de Paula Antunes Teixeira, V., dos Reis, M. A., and Pacheco-Silva, A. (2006). Pioglitazone limits cyclosporine nephrotoxicity in rats. *Int Immunopharmacol* **6**, 1943-1951.

Perera, F. P. (1996). Molecular epidemiology: insights into cancer susceptibility, risk assessment, and prevention. *J Natl Cancer Inst* **88**, 496-509.

Perry, D. K., Hand, W. L., Edmondson, D. E., and Lambeth, J. D. (1992). Role of phospholipase D-derived diradylglycerol in the activation of the human neutrophil respiratory burst oxidase. Inhibition by phosphatidic acid phosphohydrolase inhibitors. *J Immunol* **149**, 2749-2758.

Poon, R. T., Chung, K. K., Cheung, S. T., Lau, C. P., Tong, S. W., Leung, K. L., Yu, W. C., Tuszynski, G. P., and Fan, S. T. (2004). Clinical significance of thrombospondin 1 expression in hepatocellular carcinoma. *Clin Cancer Res* **10**, 4150-4157.

Pruett, S. T., Bushnev, A., Hagedorn, K., Adiga, M., Haynes, C. A., Sullards, M. C., Liotta, D. C., and Merrill, A. H., Jr. (2008). Thematic Review Series: Sphingolipids. Biodiversity of sphingoid bases ("sphingosines") and related amino alcohols. *J Lipid Res* **49**, 1621-1639.

Pruitt, K., and Der, C. J. (2001). Ras and Rho regulation of the cell cycle and oncogenesis. *Cancer Lett* **171**, 1-10.

Pyne, N. J., and Pyne, S. (2010). Sphingosine 1-phosphate and cancer. *Nat Rev Cancer* **10**, 489-503.

Qiu, M., and Liu, X. (2001). Determination of sphinganine, sphingosine and Sa/So ratio in urine of humans exposed to dietary fumonisin B1. *Food Addit Contam* **18**, 263-269.

Radeff-Huang, J., Seasholtz, T. M., Matteo, R. G., and Brown, J. H. (2004). G protein mediated signaling pathways in lysophospholipid induced cell proliferation and survival. *J Cell Biochem* **92**, 949-966.

Ramaiah, S. K. (2007). A toxicologist guide to the diagnostic interpretation of hepatic biochemical parameters. *Food Chem Toxicol* **45**, 1551-1557.

Ramasamy, S., Wang, E., Hennig, B., and Merrill, A. H., Jr. (1995). Fumonisin B1 alters sphingolipid metabolism and disrupts the barrier function of endothelial cells in culture. *Toxicol Appl Pharmacol* **133**, 343-348.

Ray, D., and Kiyokawa, H. (2008). CDC25A phosphatase: a rate-limiting oncogene that determines genomic stability. *Cancer Res* **68**, 1251-1253.

Rentz, S. S., Showker, J. L., Meredith, F. I., and Riley, R. T. (2005). Inhibition of sphingolipid biosynthesis decreases phosphorylated ERK2 in LLC-PK1 cells. *Food and Chemical Toxicology* **43**, 123-131.

Rheeder, J. P., Marasas, W. F. O., Thiel, P. G., Sydenham, E. W., Shephard, G. S., and Van Schalkwyk, D. J. (1992). Fusarium moniliforme and fumonisins in maize in relation to human eosophageal cancer in Transkei. *Phytopathology* **82**, 353–357.

Ricca, T. I., Liang, G., Suenaga, A. P., Han, S. W., Jones, P. A., and Jasiulionis, M. G. (2009). Tissue inhibitor of metalloproteinase 1 expression associated with gene demethylation confers anoikis resistance in early phases of melanocyte malignant transformation. *Transl Oncol* **2**, 329-340.

Riley, R. T., An, N. H., Showker, J. L., Yoo, H. S., Norred, W. P., Chamberlain, W. J., Wang, E., Merrill, A. H., Jr., Motelin, G., Beasley, V. R., and et al. (1993). Alteration of tissue and serum sphinganine to sphingosine ratio: an early biomarker of exposure to fumonisin-containing feeds in pigs. *Toxicol Appl Pharmacol* **118**, 105-112.

Riley, R. T., Enongene, E., Voss, K. A., Norred, W. P., Meredith, F. I., Sharma, R. P., Spitsbergen, J., Williams, D. E., Carlson, D. B., and Merrill, A. H., Jr. (2001). Sphingolipid perturbations as mechanisms for fumonisin carcinogenesis. *Environmental Health Perspectives Supplements* **109**, 301-308.

Riley, R. T., Hinton, D. M., Chamberlain, W. J., Bacon, C. W., Wang, E., Merrill, A. H., Jr., and Voss, K. A. (1994). Dietary fumonisin B1 induces disruption of sphingolipid metabolism in Sprague-Dawley rats: a new mechanism of nephrotoxicity. *J Nutr* **124**, 594-603.

Riley, R. T., and Voss, K. A. (2006). Differential sensitivity of rat kidney and liver to fumonisin toxicity: Organ specific differences in toxin accumulation and sphingoid base metabolism. *Abstracts of Papers, 232nd ACS National Meeting, San Francisco, CA, United States, Sept. 10-14, 2006*, AGFD-120.

Roberts, R. A., Ganey, P. E., Ju, C., Kamendulis, L. M., Rusyn, I., and Klaunig, J. E. (2007). Role of the Kupffer cell in mediating hepatic toxicity and carcinogenesis. *Toxicol Sci* **96**, 2-15.

Roberts, R. A., Goodman, J. I., Shertzer, H. G., Dalton, T. P., and Farland, W. H. (2003). Rodent toxicity and nongenotoxic carcinogenesis: knowledge-based human risk assessment based on molecular mechanisms. *Toxicol Mech Methods* **13**, 21-29.

Roderick, H. L., and Cook, S. J. (2008). Ca2+ signalling checkpoints in cancer: remodelling Ca2+ for cancer cell proliferation and survival. *Nat Rev Cancer* **8**, 361-375.

Roland, C. L., Harken, A. H., Sarr, M. G., and Barnett, C. C., Jr. (2007). ICAM-1 expression determines malignant potential of cancer. *Surgery* **141**, 705-707.

Rosette, C., Roth, R. B., Oeth, P., Braun, A., Kammerer, S., Ekblom, J., and Denissenko, M. F. (2005). Role of ICAM1 in invasion of human breast cancer cells. *Carcinogenesis* **26**, 943-950.

Rowland, B. D., and Peeper, D. S. (2006). KLF4, p21 and context-dependent opposing forces in cancer. *Nat Rev Cancer* **6**, 11-23.

Rumora, L., Domijan, A.-M., Grubisic, T. Z., and Peraica, M. (2007). Mycotoxin fumonisin B1 alters cellular redox balance and signalling pathways in rat liver and kidney. *Toxicology* **242**, 31-38.

Rumora, L., Kovacic, S., Rozgaj, R., Cepelak, I., Pepeljnjak, S., and Zanic Grubisic, T. (2002). Cytotoxic and genotoxic effects of fumonisin B1 on rabbit kidney RK13 cell line. *Arch Toxicol* **76**, 55-61.

Rylova, S. N., Somova, O. G., and Dyatlovitskaya, E. V. (1998). Comparative investigation of sphingoid bases and fatty acids in ceramides and sphingomyelins from human ovarian malignant tumors and normal ovary. *Biochemistry (Mosc)* **63**, 1057-1060.

Sahai, E., and Marshall, C. J. (2002). RHO-GTPases and cancer. *Nat Rev Cancer* **2**, 133-142.

Santana, P., Pena, L. A., Haimovitz-Friedman, A., Martin, S., Green, D., McLoughlin, M., Cordon-Cardo, C., Schuchman, E. H., Fuks, Z., and Kolesnick, R. (1996). Acid sphingomyelinase-deficient human lymphoblasts and mice are defective in radiation-induced apoptosis. *Cell* **86**, 189-199.

Sargiannidou, I., Zhou, J., and Tuszynski, G. P. (2001). The role of thrombospondin-1 in tumor progression. *Exp Biol Med (Maywood)* **226**, 726-733.

Sato, K., Ui, M., and Okajima, F. (2000). Differential roles of Edg-1 and Edg-5, sphingosine 1-phosphate receptors, in the signaling pathways in C6 glioma cells. *Brain Res Mol Brain Res* **85**, 151-160.

Sauer, B., Gonska, H., Manggau, M., Kim, D. S., Schraut, C., Schafer-Korting, M., and Kleuser, B. (2005). Sphingosine 1-phosphate is involved in cytoprotective actions of calcitriol in human fibroblasts and enhances the intracellular Bcl-2/Bax rheostat. *Pharmazie* **60**, 298-304.

Schmelz, E. M., Dombrink-Kurtzman, M. A., Roberts, P. C., Kozutsumi, Y., Kawasaki, T., and Merrill, A. H., Jr. (1998). Induction of apoptosis by fumonisin B1 in HT29 cells is mediated by the accumulation of endogenous free sphingoid bases. *Toxicol Appl Pharmacol* **148**, 252-260.

Schmelz, E. M., Roberts, P. C., Kustin, E. M., Lemonnier, L. A., Sullards, M. C., Dillehay, D. L., and Merrill, A. H., Jr. (2001). Modulation of intracellular beta-catenin localization and intestinal tumorigenesis in vivo and in vitro by sphingolipids. *Cancer Res* **61**, 6723-6729.

Schroder, C., Witzel, I., Muller, V., Krenkel, S., Wirtz, R. M., Janicke, F., Schumacher, U., and Milde-Langosch, K. (2011). Prognostic value of intercellular adhesion molecule (ICAM)-1 expression in breast cancer. *J Cancer Res Clin Oncol* **137**, 1193-1201.

Schulte-Hermann, R., Bursch, W., Marian, B., and Grasl-Kraupp, B. (1999). Active cell death (apoptosis) and cellular proliferation as indicators of exposure to carcinogens. *IARC Sci Publ*, 273-285.

Schulte-Hermann, R., and Parzefall, W. (2004). Mehrstufenprozess der Kanzerogenese und chemische Kanzerogenese. In *Die Onkologie* (W. Hiddemann, Huber, H., and Bartram, C., Ed.), pp. 181-223. Springer Verlag Berlin, Heidelberg.

Sebolt-Leopold, J. S., and Herrera, R. (2004). Targeting the mitogen-activated protein kinase cascade to treat cancer. *Nat Rev Cancer* **4**, 937-947.

Seefelder, W., Humpf, H. U., Schwerdt, G., Freudinger, R., and Gekle, M. (2003). Induction of apoptosis in cultured human proximal tubule cells by fumonisins and fumonisin metabolites. *Toxicology and Applied Pharmacology* **192**, 146-153.

Seiferlein, M., Humpf, H.-U., Voss, K. A., Sullards, M. C., Allegood, J. C., Wang, E., and Merrill, A. H., Jr. (2007). Hydrolyzed fumonisins HFB1 and HFB2 are acylated in vitro and in vivo by ceramide synthase to form cytotoxic N-acyl-metabolites. *Molecular Nutrition & Food Research* **51**, 1120-1130.

Sekine, T., Miyazaki, H., and Endou, H. (2006). Molecular physiology of renal organic anion transporters. *Am J Physiol Renal Physiol* **290**, F251-261.

Sevilla, L., Zaldumbide, A., Pognonec, P., and Boulukos, K. E. (2001). Transcriptional regulation of the bcl-x gene encoding the anti-apoptotic Bcl-xL protein by Ets, Rel/NFkappaB, STAT and AP1 transcription factor families. *Histol Histopathol* **16**, 595-601.

Sharma, N., He, Q., and Sharma, R. P. (2004). Sphingosine kinase activity confers resistance to apoptosis by fumonisin B1 in human embryonic kidney (HEK-293) cells. *Chemico-Biological Interactions* **151**, 33-42.

Sharma, N., He, Q., and Sharma, R. P. (2006). Amelioration of fumonisin B1 hepatotoxicity in mice by depletion of T cells with anti-Thy-1.2. *Toxicology* **223**, 191-201.

Sharma, R. P., Bhandari, N., He, Q., Riley, R. T., and Voss, K. A. (2001). Decreased fumonisin hepatotoxicity in mice with a targeted deletion of tumor necrosis factor receptor 1. *Toxicology* **159**, 69-79.

Sharma, R. P., Bhandari, N., Riley, R. T., Voss, K. A., and Meredith, F. I. (2000). Tolerance to fumonisin toxicity in a mouse strain lacking the P75 tumor necrosis factor receptor. *Toxicology* **143**, 183-194.

Sharma, R. P., He, Q., Johnson, V. J., and Voss, K. A. (2003). Increased expression of CD95-ligand and other apoptotic signaling factors by fumonisin B1, a hepatotoxic mycotoxin, in livers of mice lacking tumor necrosis factor alpha. *Cytokine* **24**, 226-236.

Shaulian, E. (2010). AP-1--The Jun proteins: Oncogenes or tumor suppressors in disguise? *Cell Signal* **22**, 894-899.

Shaulian, E., and Karin, M. (2001). AP-1 in cell proliferation and survival. *Oncogene* **20**, 2390-2400.

Shaulian, E., and Karin, M. (2002). AP-1 as a regulator of cell life and death. *Nat Cell Biol* **4**, E131-136.

Shaw, L. M. (2005). Tumor cell invasion assays. *Methods Mol Biol* **294**, 97-105.

Shayman, J. A. (2000). Sphingolipids. *Kidney Int* **58**, 11-26.

Shephard, G. S., Thiel, P. G., Sydenham, E. W., and Alberts, J. F. (1994a). Biliary excretion of the mycotoxin fumonisin B1 in rats. *Food Chem Toxicol* **32**, 489-491.

Shephard, G. S., Thiel, P. G., Sydenham, E. W., and Savard, M. E. (1995). Fate of a single dose of 14C-labelled fumonisin B1 in vervet monkeys. *Nat Toxins* **3**, 145-150.

Shephard, G. S., Thiel, P. G., Sydenham, E. W., Vleggaar, R., and Alberts, J. F. (1994b). Determination of the mycotoxin fumonisin B1 and identification of its partially hydrolysed metabolites in the faeces of non-human primates. *Food Chem Toxicol* **32**, 23-29.

Shephard, G. S., Van Der Westhuizen, L., and Sewram, V. (2007). Biomarkers of exposure to fumonisin mycotoxins: a review. *Food Addit Contam* **24**, 1196-1201.

Sherr, C. J., and Roberts, J. M. (1999). CDK inhibitors: positive and negative regulators of G1-phase progression. *Genes Dev* **13**, 1501-1512.

Shi, L., Bielawski, J., Mu, J., Dong, H., Teng, C., Zhang, J., Yang, X., Tomishige, N., Hanada, K., Hannun, Y. A., and Zuo, J. (2007). Involvement of sphingoid bases in mediating reactive oxygen intermediate production and programmed cell death in Arabidopsis. *Cell Res* **17**, 1030-1040.

Shida, D., Kitayama, J., Yamaguchi, H., Yamashita, H., Mori, K., Watanabe, T., Yatomi, Y., and Nagawa, H. (2004). Sphingosine 1-phosphate transactivates c-Met as well as epidermal growth factor receptor (EGFR) in human gastric cancer cells. *FEBS Lett* **577**, 333-338.

Shida, D., Takabe, K., Kapitonov, D., Milstien, S., and Spiegel, S. (2008). Targeting SphK1 as a new strategy against cancer. *Curr Drug Targets* **9**, 662-673.

Sid, B., Sartelet, H., Bellon, G., El Btaouri, H., Rath, G., Delorme, N., Haye, B., and Martiny, L. (2004). Thrombospondin 1: a multifunctional protein implicated in the regulation of tumor growth. *Crit Rev Oncol Hematol* **49**, 245-258.

Simpson, C. D., Anyiwe, K., and Schimmer, A. D. (2008). Anoikis resistance and tumor metastasis. *Cancer Lett* **272**, 177-185.

Smith, E. R., and Merrill, A. H., Jr. (1995). Differential roles of de novo sphingolipid biosynthesis and turnover in the "burst" of free sphingosine and sphinganine, and their 1-phosphates and N-acyl-derivatives, that occurs upon changing the medium of cells in culture. *J Biol Chem* **270**, 18749-18758.

Smith, E. R., Merrill, A. H., Obeid, L. M., and Hannun, Y. A. (2000). Effects of sphingosine and other sphingolipids on protein kinase C. *Methods Enzymol* **312**, 361-373.

Sng, J. C., Taniura, H., and Yoneda, Y. (2004). A tale of early response genes. *Biol Pharm Bull* **27**, 606-612.

Soeda, S., Iwata, K., Hosoda, Y., and Shimeno, H. (2001). Daunorubicin attenuates tumor necrosis factor-alpha -induced biosynthesis of plasminogen activator inhibitor-1 in human umbilical vein endothelial cells. *Biochimica et Biophysica Acta, Molecular Cell Research* **1538**, 234-241.

Solomon, J. C., Sharma, K., Wei, L. X., Fujita, T., and Shi, Y. F. (2003). A novel role for sphingolipid intermediates in activation-induced cell death in T cells. *Cell Death Differ* **10**, 193-202.

Spiegel, S., and Milstien, S. (2002). Sphingosine 1-phosphate, a key cell signaling molecule. *J Biol Chem* **277**, 25851-25854.

Spiegel, S., and Milstien, S. (2003). Sphingosine-1-phosphate: an enigmatic signalling lipid. *Nat Rev Mol Cell Biol* **4**, 397-407.

Spotti, M., Maas, R. F., de Nijs, C. M., and Fink-Gremmels, J. (2000). Effect of fumonisin B(1) on rat hepatic P450 system. *Environ Toxicol Pharmacol* **8**, 197-204.

Steeg, P. S. (2003). Metastasis suppressors alter the signal transduction of cancer cells. *Nat Rev Cancer* **3**, 55-63.

Steiner, P., Philipp, A., Lukas, J., Godden-Kent, D., Pagano, M., Mittnacht, S., Bartek, J., and Eilers, M. (1995). Identification of a Myc-dependent step during the formation of active G1 cyclin-cdk complexes. *EMBO J* **14**, 4814-4826.

Stockmann-Juvala, H., Mikkola, J., Naarala, J., Loikkanen, J., Elovaara, E., and Savolainen, K. (2004). Oxidative stress induced by fumonisin B1 in continuous human and rodent neural cell cultures. *Free Radic Res* **38**, 933-942.

Stockmann-Juvala, H., and Savolainen, K. (2008). A review of the toxic effects and mechanisms of action of fumonisin B1. *Hum Exp Toxicol* **27**, 799-809.

Su, S. C., Mendoza, E. A., Kwak, H. I., and Bayless, K. J. (2008). Molecular profile of endothelial invasion of three-dimensional collagen matrices: insights into angiogenic sprout induction in wound healing. *Am J Physiol Cell Physiol* **295**, C1215-1229.

Sugimoto, N., Takuwa, N., Okamoto, H., Sakurada, S., and Takuwa, Y. (2003). Inhibitory and stimulatory regulation of Rac and cell motility by the G12/13-Rho and Gi pathways integrated downstream of a single G protein-coupled sphingosine-1-phosphate receptor isoform. *Mol Cell Biol* **23**, 1534-1545.

Suzuki, H., Riley, R. T., and Sharma, R. P. (2007). Inducible nitric oxide has protective effect on fumonisin B1 hepatotoxicity in mice via modulation of sphingosine kinase. *Toxicology* **229**, 42-53.

Swiercz, R., Wolfe, J. D., Zaher, A., and Jankun, J. (1998). Expression of the plasminogen activation system in kidney cancer correlates with its aggressive phenotype. *Clin Cancer Res* **4**, 869-877.

Sydenham, E. W., Thiel, P. G., Marasas, W. F. O., Shephard, G. S., Van Schalkwyk, D. J., and Koch, K. R. (1990). Natural occurrence of some Fusarium mycotoxins in corn from low and high esophageal cancer prevalence areas of the Transkei, Southern Africa. *Journal of Agricultural and Food Chemistry* **38**, 1900-1903.

Taha, T. A., Argraves, K. M., and Obeid, L. M. (2004). Sphingosine-1-phosphate receptors: receptor specificity versus functional redundancy. *Biochim Biophys Acta* **1682**, 48-55.

Taha, T. A., Mullen, T. D., and Obeid, L. M. (2006). A house divided: ceramide, sphingosine, and sphingosine-1-phosphate in programmed cell death. *Biochim Biophys Acta* **1758**, 2027-2036.

Takabe, K., Kim, R. H., Allegood, J. C., Mitra, P., Ramachandran, S., Nagahashi, M., Harikumar, K. B., Hait, N. C., Milstien, S., and Spiegel, S. (2010). Estradiol induces export of sphingosine 1-phosphate from breast cancer cells via ABCC1 and ABCG2. *J Biol Chem* **285**, 10477-10486.

Takada, Y., Ye, X., and Simon, S. (2007). The integrins. *Genome Biol* **8**, 215.

Takekawa, M., Tatebayashi, K., Itoh, F., Adachi, M., Imai, K., and Saito, H. (2002). Smad-dependent GADD45beta expression mediates delayed activation of p38 MAP kinase by TGF-beta. *EMBO J* **21**, 6473-6482.

Takeuchi, K., Motoda, Y., and Ito, F. (2006). Role of transcription factor activator protein 1 (AP1) in epidermal growth factor-mediated protection against apoptosis induced by a DNA-damaging agent. *FEBS J* **273**, 3743-3755.

Takuwa, N., Du, W., Kaneko, E., Okamoto, Y., Yoshioka, K., and Takuwa, Y. (2011). Tumor-suppressive sphingosine-1-phosphate receptor-2 counteracting tumor-promoting sphingosine-1-phosphate receptor-1 and sphingosine kinase 1 - Jekyll Hidden behind Hyde. *Am J Cancer Res* **1**, 460-481.

Tamama, K., Kon, J., Sato, K., Tomura, H., Kuwabara, A., Kimura, T., Kanda, T., Ohta, H., Ui, M., Kobayashi, I., and Okajima, F. (2001). Extracellular mechanism through the Edg family of receptors might be responsible for sphingosine-1-phosphate-induced regulation of DNA synthesis and migration of rat aortic smooth-muscle cells. *Biochem J* **353**, 139-146.

Tani, M., Sano, T., Ito, M., and Igarashi, Y. (2005). Mechanisms of sphingosine and sphingosine 1-phosphate generation in human platelets. *J Lipid Res* **46**, 2458-2467.

ten Dijke, P., and Arthur, H. M. (2007). Extracellular control of TGFbeta signalling in vascular development and disease. *Nat Rev Mol Cell Biol* **8**, 857-869.

Teng, P. N., Hood, B. L., Sun, M., Dhir, R., and Conrads, T. P. (2011). Differential proteomic analysis of renal cell carcinoma tissue interstitial fluid. *J Proteome Res* **10**, 1333-1342.

Thomas, M., and Augustin, H. G. (2009). The role of the Angiopoietins in vascular morphogenesis. *Angiogenesis* **12**, 125-137.

Tian, M., Neil, J. R., and Schiemann, W. P. (2011). Transforming growth factor-beta and the hallmarks of cancer. *Cell Signal* **23**, 951-962.

Toh, Y., and Nicolson, G. L. (2009). The role of the MTA family and their encoded proteins in human cancers: molecular functions and clinical implications. *Clin Exp Metastasis* **26**, 215-227.

Tolleson, W. H., Couch, L. H., Melchior, W. B., Jr., Jenkins, G. R., Muskhelishvili, M., Muskhelishvili, L., McGarrity, L. J., Domon, O., Morris, S. M., and Howard, P. C. (1999). Fumonisin B1 induces apoptosis in cultured human keratinocytes through sphinganine accumulation and ceramide depletion. *Int J Oncol* **14**, 833-843.

Tolleson, W. H., Dooley, K. L., Sheldon, W. G., Thurman, J. D., Bucci, T. J., and Howard, P. C. (1996). The mycotoxin fumonisin induces apoptosis in cultured human cells and in livers and kidneys of rats. *Adv Exp Med Biol* **392**, 237-250.

Tomita, Y., Nishiyama, T., Watanabe, H., Fujiwara, M., and Sato, S. (1990). Expression of intercellular adhesion molecule-1 (ICAM-1) on renal-cell cancer: possible significance in host immune responses. *Int J Cancer* **46**, 1001-1006.

Torres, O. A., Palencia, E., Lopez de Pratdesaba, L., Grajeda, R., Fuentes, M., Speer, M. C., Merrill, A. H., Jr., O'Donnell, K., Bacon, C. W., Glenn, A. E., and Riley, R. T. (2007). Estimated fumonisin exposure in Guatemala is greatest in consumers of lowland maize. *J Nutr* **137**, 2723-2729.

Turner, P. C., Nikiema, P., and Wild, C. P. (1999). Fumonisin contamination of food: progress in development of biomarkers to better assess human health risks. *Mutation Research, Genetic Toxicology and Environmental Mutagenesis* **443**, 81-93.

USEPA (2005). Guidelines for Carcinogen Risk Assessment. *US Environmental Protection Agency, Washington, DC*, EPA/630/P-603/001F.

Van Brocklyn, J., Letterle, C., Snyder, P., and Prior, T. (2002). Sphingosine-1-phosphate stimulates human glioma cell proliferation through Gi-coupled receptors: role of ERK MAP kinase and phosphatidylinositol 3-kinase beta. *Cancer Lett* **181**, 195-204.

van der Bij, G. J., Oosterling, S. J., Bogels, M., Bhoelan, F., Fluitsma, D. M., Beelen, R. H., Meijer, S., and van Egmond, M. (2008). Blocking alpha2 integrins on rat CC531s colon carcinoma cells prevents operation-induced augmentation of liver metastases outgrowth. *Hepatology* **47**, 532-543.

van Zijl, F., Krupitza, G., and Mikulits, W. (2011). Initial steps of metastasis: cell invasion and endothelial transmigration. *Mutat Res* **728**, 23-34.

Volpes, R., van den Oord, J. J., and Desmet, V. J. (1991). Distribution of the VLA family of integrins in normal and pathological human liver tissue. *Gastroenterology* **101**, 200-206.

von Wenckstern, H., Zimmermann, K., and Kleuser, B. (2006). The role of the lysophospholipid sphingosine 1-phosphate in immune cell biology. *Arch Immunol Ther Exp (Warsz)* **54**, 239-251.

Voss, K. A., Chamberlain, W. J., Bacon, C. W., Herbert, R. A., Walters, D. B., and Norred, W. P. (1995a). Subchronic feeding study of the mycotoxin fumonisin B1 in B6C3F1 mice and Fischer 344 rats. *Fundam Appl Toxicol* **24**, 102-110.

Voss, K. A., Chamberlain, W. J., Bacon, C. W., and Norred, W. P. (1993). A preliminary investigation on renal and hepatic toxicity in rats fed purified fumonisin B1. *Nat Toxins* **1**, 222-228.

Voss, K. A., Chamberlain, W. J., Bacon, C. W., Riley, R. T., and Norred, W. P. (1995b). Subchronic toxicity of fumonisin B1 to male and female rats. *Food Addit Contam* **12**, 473-478.

Voss, K. A., Riley, R., Dunn, C., and Christopher Corton, J. (2006). The role of tumor necrosis factor alpha and the peroxisome proliferator-activated receptor alpha in modulating the effects of fumonisin in mouse liver. *Toxicology* **222**, 165-174.

Voss, K. A., Riley, R. T., Snook, M. E., and Waes, J. G. (2009). Reproductive and sphingolipid metabolic effects of fumonisin B(1) and its alkaline hydrolysis product in LM/Bc mice: hydrolyzed fumonisin B(1) did not cause neural tube defects. *Toxicol Sci* **112**, 459-467.

Waltz, D. A., and Chapman, H. A. (1994). Reversible cellular adhesion to vitronectin linked to urokinase receptor occupancy. *J Biol Chem* **269**, 14746-14750.

Waltz, D. A., Natkin, L. R., Fujita, R. M., Wei, Y., and Chapman, H. A. (1997). Plasmin and plasminogen activator inhibitor type 1 promote cellular motility by regulating the interaction between the urokinase receptor and vitronectin. *J Clin Invest* **100**, 58-67.

Wang, E., Norred, W. P., Bacon, C. W., Riley, R. T., and Merrill, A. H., Jr. (1991). Inhibition of sphingolipid biosynthesis by fumonisins. Implications for diseases associated with Fusarium moniliforme. *J Biol Chem* **266**, 14486-14490.

Wang, E., Ross, P. F., Wilson, T. M., Riley, R. T., and Merrill, A. H., Jr. (1992). Increases in serum sphingosine and sphinganine and decreases in complex sphingolipids in ponies given feed containing fumonisins, mycotoxins produced by Fusarium moniliforme. *J Nutr* **122**, 1706-1716.

Wang, F., Van Brocklyn, J. R., Hobson, J. P., Movafagh, S., Zukowska-Grojec, Z., Milstien, S., and Spiegel, S. (1999). Sphingosine 1-phosphate stimulates cell migration through a G(i)-coupled cell surface receptor. Potential involvement in angiogenesis. *J Biol Chem* **274**, 35343-35350.

Wang, L., Lee, J. F., Lin, C. Y., and Lee, M. J. (2008). Rho GTPases mediated integrin alpha v beta 3 activation in sphingosine-1-phosphate stimulated chemotaxis of endothelial cells. *Histochem Cell Biol* **129**, 579-588.

Wang, R., Ferrell, L. D., Faouzi, S., Maher, J. J., and Bishop, J. M. (2001). Activation of the Met receptor by cell attachment induces and sustains hepatocellular carcinomas in transgenic mice. *J Cell Biol* **153**, 1023-1034.

Webb, D. J., Thomas, K. S., and Gonias, S. L. (2001). Plasminogen activator inhibitor 1 functions as a urokinase response modifier at the level of cell signaling and thereby promotes MCF-7 cell growth. *J Cell Biol* **152**, 741-752.

Wu, W. T., Chen, C. N., Lin, C. I., Chen, J. H., and Lee, H. (2005). Lysophospholipids enhance matrix metalloproteinase-2 expression in human endothelial cells. *Endocrinology* **146**, 3387-3400.

Xin, M., and Deng, X. (2006). Protein phosphatase 2A enhances the proapoptotic function of Bax through dephosphorylation. *J Biol Chem* **281**, 18859-18867.

Xu, D., Dwyer, J., Li, H., Duan, W., and Liu, J. P. (2008). Ets2 maintains hTERT gene expression and breast cancer cell proliferation by interacting with c-Myc. *J Biol Chem* **283**, 23567-23580.

Yamanaka, M., Shegogue, D., Pei, H., Bu, S., Bielawska, A., Bielawski, J., Pettus, B., Hannun, Y. A., Obeid, L., and Trojanowska, M. (2004). Sphingosine kinase 1 (SPHK1) is induced by transforming growth factor-beta and mediates TIMP-1 up-regulation. *J Biol Chem* **279**, 53994-54001.

Yang, C. S. (1980). Research on esophageal cancer in China: a review. *Cancer Res* **40**, 2633-2644.

Yester, J. W., Tizazu, E., Harikumar, K. B., and Kordula, T. (2011). Extracellular and intracellular sphingosine-1-phosphate in cancer. *Cancer Metastasis Rev*.

Yoo, H. S., Norred, W. P., Showker, J., and Riley, R. T. (1996). Elevated sphingoid bases and complex sphingolipid depletion as contributing factors in fumonisin-induced cytotoxicity. *Toxicol Appl Pharmacol* **138**, 211-218.

Yoshida, K., Tosaka, A., Takeuchi, S., and Kobayashi, N. (1994). Epidermal growth factor receptor content in human renal cell carcinomas. *Cancer* **73**, 1913-1918.

Yoshimura, K., Meckel, K. F., Laird, L. S., Chia, C. Y., Park, J. J., Olino, K. L., Tsunedomi, R., Harada, T., Iizuka, N., Hazama, S., Kato, Y., Keller, J. W., Thompson, J. M., Chang, F., Romer, L. H., Jain, A., Iacobuzio-Donahue, C., Oka, M., Pardoll, D. M., and Schulick, R. D. (2009). Integrin alpha2 mediates selective metastasis to the liver. *Cancer Res* **69**, 7320-7328.

Yoshizawa, T., Yamashita, A., and Luo, Y. (1994). Fumonisin occurrence in corn from high- and low-risk areas for human esophageal cancer in China. *Appl Environ Microbiol* **60**, 1626-1629.

Young, N., Pearl, D. K., and Van Brocklyn, J. R. (2009). Sphingosine-1-phosphate regulates glioblastoma cell invasiveness through the urokinase plasminogen activator system and CCN1/Cyr61. *Mol Cancer Res* **7**, 23-32.

Young, N., and Van Brocklyn, J. R. (2006). Signal transduction of sphingosine-1-phosphate G protein-coupled receptors. *ScientificWorldJournal* **6**, 946-966.

Young, N., and Van Brocklyn, J. R. (2007). Roles of sphingosine-1-phosphate (S1P) receptors in malignant behavior of glioma cells. Differential effects of S1P2 on cell migration and invasiveness. *Exp Cell Res* **313**, 1615-1627.

Yuan, S. T., Hu, X. Q., Lu, J. P., KeiKi, H., Zhai, W. R., and Zhang, Y. E. (2000). Changes of integrin expression in rat hepatocarcinogenesis induced by 3'-Me-DAB. *World J Gastroenterol* **6**, 231-233.

Zeller, K. I., Zhao, X., Lee, C. W., Chiu, K. P., Yao, F., Yustein, J. T., Ooi, H. S., Orlov, Y. L., Shahab, A., Yong, H. C., Fu, Y., Weng, Z., Kuznetsov, V. A., Sung, W. K., Ruan, Y., Dang, C. V., and Wei, C. L. (2006). Global mapping of c-Myc binding sites and target gene networks in human B cells. *Proc Natl Acad Sci U S A* **103**, 17834-17839.

Zhang, G., Kim, H., Cai, X., Lopez-Guisa, J. M., Carmeliet, P., and Eddy, A. A. (2003). Urokinase receptor modulates cellular and angiogenic responses in obstructive nephropathy. *J Am Soc Nephrol* **14**, 1234-1253.

Zhang, Z., Ramirez, N. E., Yankeelov, T. E., Li, Z., Ford, L. E., Qi, Y., Pozzi, A., and Zutter, M. M. (2008). alpha2beta1 integrin expression in the tumor microenvironment enhances tumor angiogenesis in a tumor cell-specific manner. *Blood* **111**, 1980-1988.

Zhou, H. J., Zhang, H. N., Tang, T., Zhong, J. H., Qi, Y., Luo, J. K., Lin, Y., Yang, Q. D., and Li, X. Q. (2010). Alteration of thrombospondin-1 and -2 in rat brains following experimental intracerebral hemorrhage. Laboratory investigation. *J Neurosurg* **113**, 820-825.

Zimmer, I., Usleber, E., Klaffke, H., Weber, R., Majerus, P., Otteneder, H., Gareis, M., Dietrich, R., and Märtlbauer, E. (2008). Fumonisin intake of the German consumer. *Mycotoxin Research* **24**, 40-52.

Zitomer, N. C., Mitchell, T., Voss, K. A., Bondy, G. S., Pruett, S. T., Garnier-Amblard, E. C., Liebeskind, L. S., Park, H., Wang, E., Sullards, M. C., Merrill, A. H., Jr., and Riley, R. T. (2009). Ceramide synthase inhibition by fumonisin B1 causes accumulation of 1-deoxysphinganine: a novel category of bioactive 1-deoxysphingoid bases and 1-deoxydihydroceramides biosynthesized by mammalian cell lines and animals. *J Biol Chem* **284**, 4786-4795.

Zubac, D. P., Bostad, L., Kihl, B., Seidal, T., Wentzel-Larsen, T., and Haukaas, S. A. (2009). The expression of thrombospondin-1 and p53 in clear cell renal cell carcinoma: its relationship to angiogenesis, cell proliferation and cancer specific survival. *J Urol* **182**, 2144-2149.

Zubac, D. P., Wentzel-Larsen, T., Seidal, T., and Bostad, L. (2010). Type 1 plasminogen activator inhibitor (PAI-1) in clear cell renal cell carcinoma (CCRCC) and its impact on angiogenesis, progression and patient survival after radical nephrectomy. *BMC Urol* **10**, 20.

Publications

Poster abstracts

Müller S., Bolzon F., Dekant W., and Mally, A. (2010). Fumonisin B_1 carcinogenicity: Early effects on the expression of genes associated with cell growth and invasion in NRK-52E cells. *Naunyn-Schmiedeberg´s Arch Pharmacol* **381** (Suppl 1), 1-92

Müller S., Bolzon F., Dekant W., and Mally, A. (2010). Fumonisin B_1 mediated alterations in the expression of genes associated with cell growth and invasion in NRK-52E cells. 32nd Mycotoxin Workshop Copenhagen, Denmark, 6/2010

Review article

Müller, S., Dekant, W., and Mally, A. (2012). Mycotoxins and the Kidney: Modes of Action for Renal Tumor Formation by Fumonisin B_1 in Rodents. *Food Chem Toxicol* [submitted].